Modelling of Resistant Infections Between-Host and Within-Host

Dissertation
zur Erlangung des Doktorgrades
der Naturwissenschaften

vorgelegt beim Fachbereich Informatik und Mathematik
der Johann Wolfgang Goethe-Universität
in Frankfurt am Main

von
Josephine Naa Ayeley Tetteh
aus Accra, Ghana

Frankfurt (2022)
(D 30)

vom Fachbereich Mathematik und Informatik (FB 12) der

Johann Wolfgang Goethe-Universität als Dissertation angenommen

Dekan: Prof. Dr. Martin Möller

Gutachter: Dr. Esteban Abelardo Hernandez Vargas
Prof. Dr. Hans Crauel

Datum der Disputation: 11.04.2023

The research herein presented was conducted at the
Frankfurt Institute for Advanced Studies (FIAS)
Systems Medicine of Infectious Diseases Research Group
Frankfurt am Main, Federal Republic of Germany.

Modelling of Resistant Infections Between-Host and Within-Host

A dissertation submitted for the degree of
Doctor of Philosophy

At the Department of Mathematics (FB 12)
of the Johann Wolfgang Goethe-University

Submitted by
Josephine Naa Ayeley Tetteh

July 2022

Abstract

Antimicrobial resistant infections arise as a consequential response to evolutionary mechanisms within microbes which cause them to be protected from the effects of antimicrobials. The frequent occurrence of resistant infections poses a global public health threat as their control has become challenging despite many efforts. The dynamics of such infections are driven by processes at multiple levels. For a long time, mathematical models have proved valuable for unravelling complex mechanisms in the dynamics of infections. In this thesis, we focus on mathematical approaches to modelling the development and spread of resistant infections at between-host (population-wide) and within-host (individual) levels.

Within an individual host, switching between treatments has been identified as one of the methods that can be employed for the gradual eradication of resistant strains on the long term. With this as motivation, we study the problem using dynamical systems and notions from control theory. We present a model based on deterministic logistic differential equations which capture the general dynamics of microbial resistance inside an individual host. Fundamentally, this model describes the spread of resistant infections whilst accounting for evolutionary mutations observed in resistant pathogens and capturing them in mutation matrices. We extend this model to explore the implications of therapy switching from a control theoretic perspective by using switched systems and developing control strategies with the goal of reducing the appearance of drug resistant pathogens within the host.

At the between-host level, we use compartmental models to describe the transmission of infection between multiple individuals in a population. In particular, we make a case study of the evolution and spread of the novel coronavirus (SARS-CoV-2) pandemic. So far, vaccination remains a critical component in the eventual solution to this public health crisis. However, as with many other pathogens, vaccine resistant variants of the virus have been a major concern in control efforts by governments and all stakeholders. Using network theory, we investigate the spread and transmission of the disease on social networks by compartmentalising and studying the progression of the disease in each compartment, considering both the original virus strain and one of its highly transmissible vaccine-resistant mutant strains. We investigate these dynamics in the presence of vaccinations and other interventions. Although vaccinations are of absolute importance during viral outbreaks, resistant variants coupled with population hesitancy towards vaccination can lead to further spread of the virus.

Zusammenfassung

Antibiotikaresistente Infektionen entstehen als Folge von evolutionären Mechanismen in Mikroben, die sie vor der Wirkung von Antibiotika schützen. Das häufige Auftreten resistenter Infektionen stellt eine globale Bedrohung für die öffentliche Gesundheit dar, da ihre Bekämpfung trotz vieler Bemühungen schwierig geworden ist. Die Dynamik solcher Infektionen wird durch Prozesse auf mehreren Ebenen bestimmt. Seit langem haben sich mathematische Modelle als wertvoll erwiesen, um komplexe Mechanismen in der Dynamik von Infektionen zu entschlüsseln. In dieser Arbeit konzentrieren wir uns auf mathematische Ansätze zur Modellierung der Entwicklung und Ausbreitung von resistenten Infektionen auf der Ebene zwischen den Wirten (populationsweit) und innerhalb der Wirte (individuell).

Innerhalb eines individuellen Wirts wurde der Wechsel zwischen Behandlungen als eine der Methoden identifiziert, die zur schrittweisen Ausrottung resistenter Stämme auf lange Sicht eingesetzt werden können. Aus diesem Grund untersuchen wir das Problem mit Hilfe dynamischer Systeme und Begriffen aus der Kontrolltheorie. Wir stellen ein Modell auf der Grundlage deterministischer logistischer Differentialgleichungen vor, das die allgemeine Dynamik der mikrobiellen Resistenz in einem individuellen Wirt erfasst. Im Wesentlichen beschreibt dieses Modell die Ausbreitung resistenter Infektionen und berücksichtigt dabei evolutionäre Mutationen, die bei resistenten Erregern beobachtet werden, und erfasst diese in Mutationsmatrizen. Wir erweitern dieses Modell, um die Auswirkungen von Therapieschaltungen aus einer kontrolltheoretischen Perspektive zu untersuchen, indem wir geschaltete Systeme verwenden und Kontrollstrategien mit dem Ziel entwickeln, das Auftreten von arzneimittelresistenten Erregern innerhalb des Wirts zu reduzieren.

Auf der Ebene zwischen den Wirten verwenden wir Kompartimentmodelle, um die Über–tragung von Infektionen zwischen mehreren Individuen in einer Population zu beschreiben. Insbesondere untersuchen wir die Entwicklung und Ausbreitung des neuen Coronavirus (SARS-CoV-2) als Fallstudie. Bislang ist die Impfung eine entscheidende Komponente bei der Lösung dieser Krise im Bereich der öffentlichen Gesundheit. Wie bei vielen anderen Krank–heitserregern sind auch bei diesem Virus impfstoffresistente Varianten ein Hauptproblem bei den Kontrollbemühungen der Regierungen und aller Beteiligten. Mithilfe von Netzwerktheorie untersuchen wir die Ausbreitung und Übertragung der Krankheit in sozialen Netzwerken, indem wir die einzelnen Kompartimente aufteilen und den Krankheitsverlauf in jedem Kompartiment untersuchen, wobei wir sowohl den ursprünglichen Virusstamm als auch einen der hochgradig übertragbaren impfstoffresistenten Mutantenstämme berücksichtigen. Wir untersuchen diese Dynamik in Gegenwart von Impfungen und anderen Interventionen. Obwohl

Impfungen bei Virusausbrüchen von absoluter Bedeutung sind, können resistente Varianten in Verbindung mit einer zögerlichen Haltung der Bevölkerung gegenüber Impfungen zu einer weiteren Ausbreitung des Virus führen.

Acknowledgements

Firstly, I would like to express my sincere gratitude to my advisor Dr. Esteban Hernandez-Vargas for the continuous support of my Ph.D study and related research, for his patience, motivation, and constructive criticisms. His guidance and insightful feedback helped me throughout my time of research and writing of this thesis to push me to sharpen my thinking and bring my research to a higher level. I am thankful to Prof. Dr. Hans Crauel for his guidance and support during my time as a PhD student.

I would like to thank the Frankfurt Institute for Advanced Studies (FIAS) for supporting my studies with the FIAS Scholarship and also the Alfons und Gertrud Kassel-Stiftung and the Deutsche Forschungsgemeinschaft through the project HE7707/5-1.

My sincere thanks also goes to Prof. Sorin Olaru and Prof. Franziska Matthäus for their insightful comments, encouragement and collaboration. I thank my fellow group members for the stimulating discussions and wonderful collaboration we had during my time as a PhD student.

I would like to thank my family for their prayers and moral support throughout this journey and my life in general. A special thanks to my darling husband, Dr. Sogo Pierre Sanon for his unwavering support, assistance and wonderful moments on this journey. I could not have completed this journey without you all. I am immensely grateful.

Contents

List of Tables

Dedicated to my family

Chapter 1

Introduction

1.1 Motivation

Throughout history, there have been records of human populations being invaded by infectious disease-causing pathogens leading to infectious diseases with varying public health impacts, some more lethal and others frequently recurrent [5]. One of the deadliest natural disasters in human history was caused by a viral infection, the 1918 flu pandemic, which killed approximately 50 million people [6]. Another serious global health threat in recent times is the novel Coronavirus, SARS-CoV-2, which has caused high levels of mortality and morbidity worldwide. According to the World Health Organisation (WHO), as of March 4 2022, there have been more than 440 million confirmed cases of SARS-CoV-2, including over 5 million deaths, reported globally [7].

Generally, infectious diseases can be caused by a variety of microorganisms, most prominently bacteria and viruses. Bacteria are microscopic organisms that can be found everywhere. When found within the human system, they can be either good or bad. In fact, good bacteria helps perform vital functions in the body such as aiding digestion and producing vitamins. On the other hand, harmful bacteria can cause infection when found inside the human body [8, 9, 10]. Viruses are tiny microorganisms that are made up of genetic material inside a protein coating which cause some familiar infectious diseases such as the common cold and flu as well as some severe diseases such as HIV/AIDS, Ebola, SARS and SARS-CoV-2. Viruses invade normal living cells within an individual (the host), multiplying and causing damage to host cells [11, 12]. In general, diseases caused by viruses, such as Influenza, Chicken pox and Measles, confer immunity against reinfection whereas those caused by bacteria, such as Tuberculosis and Gonorrhea, do not.

For most infections, the immune system of the host works to fight the infection. However, the development of drugs and vaccines can help prevent infection and reduce the number of

people infected. Antibiotics and antivirals are powerful weapons to fight against infections. However, many infectious pathogens can evolve and generate successor strains that confer resistance to these drugs owing partly to the misuse and overuse of drugs. This phenomenon where pathogens resist the action of antimicrobial and antivirals thereby reducing the effect of these drugs for treatment is known as *drug resistance* [13, 14, 15]. One characteristic of drug resistance is that it may either be present before the onset of treatment or may occur during or after treatment with a particular drug [16]. Resistance can also occur towards more than one drug, in which case the phenomenon is called *multidrug resistance*.

Thousands of people are killed annually due to the rapid evolution of drug resistant infections [17, 18]. In fact, the World Health Organization (WHO) has reported antimicrobial resistance (AMR) as a global health problem [19]. This has been clearly exposed by a growing list of bacteria that are becoming harder to treat due to antibiotics becoming less effective owing to the evolution of drug resistant strains e.g. pneumococcus, Staphylococcus, aureus, Pseudomonas aeruginosa among others. Resistance to both naturally occurring and synthetic antibiotics have developed in almost all antibiotic classes. Evidence of resistance to fluoroquinolone, a synthetic antibiotic, was found in *Escherichia coli* with about $10-40\%$ of cases occurring in Europe [20]. Other examples of antibiotic resistance infections include multidrug-resistant *mycobacterium tuberculosis* (MDR−MTB), methicillin-resistant *Staphylococcus aureus (S. aureus)* (MRSA), vancomycin-resistant *Enterococci* (VRE) and fluoroquinolone resistant *Neisseria gonorrhoeae* (Gonorrhea). About $490,000$ people were recorded to have developed MDR−TB globally in 2015 [21].

In addition, resistance to antivirals also pose a significant problem to eradicating viral infections globally [22, 1]. Several human viruses have, through their evolutionary process, also developed survival strategies which enable them to resist vaccines. For example influenza A virus (IAV), human immunodeficiency virus (HIV) and hepatitis C virus (HCV)) [1]. Although specific antiviral compounds have been developed for several of those viral infections that have not been adequately controlled by vaccines, resistant infections still persist. For instance, there have been several reports of oseltamivir-resistance influenza virus infections globally. A study by Okomo *et al* [23] found low (about 1%) proportions of oseltamivir-resistant H1N1 influenza in 2006-2007 but then resistance surged rapidly worldwide, reaching as high as about 90% in the United States.

In the past 50 years, the study of infectious diseases has matured into a multidisciplinary field at the intersection of epidemiology, mathematics, ecology, sociology, immunology and public health. Mathematical models for the spread of diseases have played a central role in medicine and epidemics, providing a cost-effective way of assessing disease transmission as well as targets for preventing disease and control [10]. Mathematical modeling has helped to suggest new vaccination strategies to protect against influenza infection [24]; supported

public health strategies for containing an emerging influenza pandemic in southeast Asia [25] and for the use of antiretroviral treatment for HIV-infected patients as a prevention measure [26], among several others. For host infections, mathematical modeling has been used to capture the dynamics of different infectious diseases inside the host to understand the interaction of the pathogen and the immune system, as well as design antivirals [27].

1.2 Overview and Contributions

In this thesis, we aim to explore the problem of resistance at both within-host (progression of infection inside a single individual) and between-host (transmission of infection between multiple individuals of a host population) levels.

Chapter 2, gives a brief overview of the necessary background used in the rest of this thesis. It provides some biological notions important for the subsequent chapters as well as necessary mathematical theories and concepts that appear throughout the thesis.

Chapter 3 introduces the state of the art of drug resistance evolution both within the host and in a given population. We describe mathematical modelling approaches that have been used in the study of resistance development and spread at both between-host and within-host levels. We further explain the various methods commonly used in studies of drug resistance infections such as deterministic, stochastic, individual-based or statistical approaches.

Studying disease dynamics within the host has become necessary mainly due to the increasing rise in resistant infections worldwide. With few new antimicrobial drugs being developed in recent times, it is crucial to be able to rationalise already existing drugs. A key aspect discovered by technological advances in genome sequencing is *collateral sensitivity* - a phenomenon in which a pathogen which has developed resistance to one drug displays increased sensitivity to another drug [28, 29, 30]. These breakthroughs provide the idea of using collateral sensitivity cycling as a sustainable treatment paradigm that may be generally applicable to infectious diseases and cancer [31]. However, to design drug cycling protocols in order to avoid resistance development is a computationally demanding task. To describe how this can be done mathematically, in Chapter 4, we utilise methods from control engineering together with mathematical modelling approaches to describe the dynamics of drug resistance within the host. We then continue further to propose some drug switching strategies which could be helpful in mitigating antimicrobial resistance using existing drugs.

At between-host levels, drug resistance leads to the further spread of infections in a population. This is especially the case for many respiratory tract infections such as measles, influenza and coronavirus diseases (such as MERS-CoV, SARS-CoV and SARS-CoV-2). In

Chapter 5, we present a social network-based compartmental model to describe the dynamics of SARS-CoV-2 using network theory. We further use stochastic simulations to highlight the importance of vaccination towards the prevention of further spread of the SARS-CoV-2 virus for both single and double strains of the virus. We find that there are low infection cases when many people in a given population are vaccinated with a vaccine which is 100% effective.

Chapter 6 concludes the main ideas and results that have been achieved by this thesis and summarizes some open questions for further research. Some of the results of this thesis have led to the following peer-reviewed publications:

1. Tetteh, J. N., & Hernandez-Vargas, E. A. (2021). Network models to evaluate vaccine strategies towards herd immunity in COVID-19. Journal of Theoretical Biology, 531, 110894.

2. Tetteh, J. N., Matthäus, F., & Hernandez-Vargas, E. A. (2020). A survey of within-host and between-hosts modelling for antibiotic resistance. Biosystems, 196, 104182.

3. Tetteh, J. N., Olaru, S., Parra-Rojas, C., & Hernandez-Vargas, E. A. (2020). Lyapunov-based Switching to Mitigate Antimicrobial Resistance. IFAC-PapersOnLine, 53(2), 16049-16054.

4. Hernandez-Vargas, E. A., Alanis, A. Y., & Tetteh, J. (2019). A new view of multiscale stochastic impulsive systems for modeling and control of epidemics. Annual Reviews in Control, 48, 242-249.

Chapter 2

Preliminaries

In this chapter, we give a brief overview of the necessary background used in the rest of this thesis. We provide the necessary mathematical theories that appear throughout the thesis. We also provide some biological notions important for our studies.

2.1 Mathematical preliminaries

The notation used throughout the rest of this thesis is as follows: $\mathbb{Z}$ denotes the set of integers, $\mathbb{N}$ denotes the set of natural numbers and $\mathbb{R}$ denotes the set of real numbers. $\mathbb{R}^n$ denotes the set of $n \times 1$ column vectors of real numbers. $\mathbb{R}^{n\times n}$ denotes the set of $n \times n$ matrices with real number entries. $(\cdot)^T$ denotes matrix transpose. For $x \in \mathbb{R}^n, x_i$ denotes the ith component of x. $\mathbb{R}^n_+ = \{x \in \mathbb{R}^n : x \geq 0\}$ denotes the non-negative orthant in $\mathbb{R}^n$. Given a set φ, a subset of a topological space, we denote by $int\{\varphi\}$ its interior and by $\partial\varphi$ its boundary.

2.2 Dynamical systems

A dynamical system is one whose state changes with time, t. Two main types of dynamical systems are encountered in practice: discrete (when t is discrete, that is $t \in \mathbb{Z}$ or $\mathbb{N}$) and continuous (when t is continuous, that is $t \in \mathbb{R}$). For a state x, discrete dynamical systems can be presented as iterations of a function, that is,

$$x_{t+1} = f(x_t), \qquad t \in \mathbb{Z} \text{ or } \mathbb{N}. \tag{2.1}$$

The dynamics of a continuous dynamical system are usually described by a differential equation, $dx/dt = \dot{x} = f(x)$ and the state space of systems is $\mathbb{R}^n$ allover.

From now on, we refer to dynamical systems as simply systems.

Definition 2.1. Positive System: A system whose states and outputs are always non-negative provided that the initial conditions and the input are non negative.

Consider a general form of an ordinary differential equation given as

$$\dot{x} = f(x, t) \tag{2.2}$$

where the function $f : \mathbb{R}^n \times \mathbb{R} \to \mathbb{R}^n$. Note that the system admits a solution $x(t)$ which is uniquely defined on $\mathbb{R}^n$ for all $x(0) \in \mathbb{R}^n$. The equilibrium points of eq (2.2) are the real roots of the system $f(x, t) = 0$ for all t.

Definition 2.2. Let $\bar{x}$ be an equilibrium point of the system (2.2).

- $\bar{x}$ is stable if for any $\epsilon > 0$ there exists a $\delta > 0$ such that if a solution $x = \phi(t)$ satisfies $||\phi(0) - \bar{x}|| < \delta$, then
$$||\phi(t) - \bar{x}|| < \epsilon$$
for all $t > 0$, where $||x|| = \sqrt{x_1^2 + x_2^2}$ is the Euclidean norm on $\mathbb{R}^2$.
- $\bar{x}$ is unstable if it is not stable as defined above.
- $\bar{x}$ is asymptotically stable if there exists a $\delta > 0$ such that if a solution $x = \phi(t)$ satisfies $||\phi(0) - \bar{x}|| < \delta$, then
$$\lim_{t \to \infty} \phi(t) = \bar{x}.$$

Theorem 2.3. *(Lyapunov stability theorem [32, Theorem 4.1]). Let $\bar{x}$ be an equilibrium point for the system (2.2) and $D \subset \mathbb{R}^n$ be a domain containing $\bar{x}$. Let $V : D \to \mathbb{R}$ be a continuously differentiable function such that*

$$V(\bar{x}) = 0 \text{ and } V(x) > 0 \text{ in } D \setminus \{\bar{x}\} \tag{2.3}$$
$$\dot{V}(x) \leq 0 \text{ in } D \tag{2.4}$$

where $\dot{V}(x) = \sum_{i=1}^{n} \frac{\partial V}{\partial x_i} f_i(x)$.

Then, $\bar{x}$ is stable. Moreover, if

$$\dot{V}(x) < 0 \text{ in } D \setminus \{\bar{x}\} \tag{2.5}$$

then $\bar{x}$ is asymptotically stable. A continuously differentiable function $V(x)$ satisfying these conditions is called a Lyapunov function.

2.2.1 Positive invariance

Definition 2.4. A set $X \in \mathbb{R}^n$ is positively invariant with respect to the system $\dot{x} = f(x,t)$ if $\forall\, x_0 \in X$, the solution $x(t,x_0)$ satisfies $x(t,x_0) \in X\ \forall\, t > 0$.

We introduce here the definition of tangent cone to a set, which will be useful in characterizing positively invariant sets. Consider any norm $||\cdot||$ in $\mathbb{R}^n$. Given a point $x \in \mathbb{R}^n$ and a set φ, we define the distance of x from φ as $dist(x,\varphi) = \inf_{y\in\varphi} ||x-y||$.

Definition 2.5. Let $x \in \mathbb{R}^n$ and $\varphi \subset \mathbb{R}^n$ be a compact set. The tangent cone to φ in x is the set

$$\mathbb{T}_\varphi(x) = \left\{ z \in \mathbb{R}^n : \liminf_{h\to 0} \frac{dist(x+hz,\varphi)}{h} = 0 \right\}.$$

Note that if φ is convex, so is $\mathbb{T}_\varphi(x)$ and lim inf can be replaced by lim. Moreover, if $x \in int\{\varphi\}$, then $\mathbb{T}_\varphi(x) = \mathbb{R}^n$ and if $x \notin \varphi$, then $\mathbb{T}_\varphi(x) = \emptyset$. Hence making the set $\mathbb{T}_\varphi(x)$ non-trivial only on the boundary of φ. So geometrically, the tangent cone for $x \in \partial\varphi$ is a cone with center at the origin and which contains all the vectors whose directions from x are tangent to (or point inside) the set φ.

Theorem 2.6. *(Nagumo's Theorem [33, Theorem 3.1]). Consider the system $\dot{x} = f(x,t)$ and assume that, for each initial condition in a set $X \in \mathbb{R}^n$, it admits a globally unique solution. Let $\varphi \subseteq X$ be a closed and convex set. Then the set φ is positively invariant for the system if and only if*

$$f(x) \in \mathbb{T}\varphi(x) \quad \textit{for all } x \in \varphi. \tag{2.6}$$

The condition in eq.(2.6) is known as the sub-tangentiality condition which has meaning only for $x \in \partial\varphi$ since for $x \in int\{\varphi\}, \mathbb{T}_\varphi(x) = \mathbb{R}^n$. Thus, this condition can be replaced by

$$f(x) \in \mathbb{T}\varphi(x) \quad \text{for all } x \in \partial\varphi.$$

2.2.2 Control theory

Control theory is a discipline whose objective deals with the behaviour of dynamical systems. Broadly, it involves developing models and algorithms governing the application of inputs to a dynamical system to drive it to a desired state, ensuring a level of control stability, often to achieve a degree of optimality.

2.2.2.1 Switched systems

Many systems are made up of interactions which are continuous and discrete in nature. Dynamical systems described by an interaction between continuous and discrete dynamics

are usually called *hybrid systems* [34]. Several researchers in systems and control theory, tend to regard hybrid systems as continuous systems with switching and place a greater emphasis on properties of the continuous state. These continuous-time systems considered without details of their discrete behaviour are known as *switched systems*.

Throughout this thesis, we are interested in positive systems. These types of systems can be found in chemical processes, stochastic models, biology and economics. To a large extent, several models representing biological processes, such as compartmental models, are positive systems.

Definition 2.7. Switched positive system: Generally refers to a positive hybrid dynamical system consisting of a family of subsystems and a rule which brings about the switching between them. Mathematically, these subsystems are usually described by a collection of indexed differential equations.

Classification of switched systems is based on the dynamics of their subsystems, for example; continuous-time or discrete-time, linear or nonlinear. In addition, switched systems can be classified as state-dependent, time-dependent, autonomous or controlled switching. In this thesis, we focus on time-dependent switching.

Time-dependent switching

Suppose we have a family f_p , $p \in \mathcal{P}$ of functions from $\mathbb{R}^n$ to $\mathbb{R}^n$, where $\mathcal{P}$ is some index set (typically, $\mathcal{P}$ is a subset of a finite-dimensional linear vector space). This gives rise to a family of systems

$$\dot{x} = f_p(x), \quad p \in \mathcal{P} \tag{2.7}$$

evolving on $\mathbb{R}^n$. The functions f_p are assumed to be sufficiently regular (at least locally Lipschitz). The easiest case to think about is when all these systems are linear:

$$f_p(x) = A_p x, \quad A_p \in \mathbb{R}^{n\times n}, \quad p \in \mathcal{P} \tag{2.8}$$

and the index set $\mathcal{P}$ is finite: $\mathcal{P} = \{1, 2, \cdots, m\}$.

To define a switched system generated by the above family, we need the notion of a switching signal. This is a piecewise constant function $\sigma : [0, \infty) \to \mathcal{P}$. Such a function σ has a finite number of discontinuities - which we call the switching times - on every bounded time interval and takes a constant value on every interval between two consecutive switching times. The role of σ is to specify, at each time instant t, the index $\sigma(t) \in \mathcal{P}$ of the active subsystem, i.e., the system from the family (2.7) that is currently being followed. We assume for concreteness that σ is continuous from the right everywhere: $\sigma(t) = \lim_{\tau\to t+} \sigma(\tau)$ for each $\tau \geq 0$.

Thus, a switched system with time-dependent switching can be described by the equation

$$\dot{x}(t) = f_{\sigma(t)}(x, t) \tag{2.9}$$

where $x(t) \in \mathbb{R}^n$ is the state vector at time t. $f_{\sigma(t)} : \mathbb{R}^n \to \mathbb{R}^n$ is called a switching vector field.

A particular case is a switched linear system

$$\dot{x}(t) = A_{\sigma(t)}x(t) \tag{2.10}$$

2.2.3 Network theory

Network theory is the study of graphs as a representation of either symmetric relations or asymmetric relations between discrete objects. A graph is made up of vertices (also called nodes or points) which are connected by edges (also called links or lines). A graph is an ordered pair $G = (V(G), E(G))$, where $V(G)$ is a finite set of vertices of G and $E(G)$ is a set of 2-element subsets of $V(G) \times V(G)$ called edges of G. For the sake of simplicity, an edge (v_1, v_2) will be denoted by v_1v_2. Suppose $v_1, v_2 \in V(G)$ and $v_1v_2 \in E(G)$. Then we say v_1 and v_2 are adjacent.

The degree of a vertex v of G is the number of edges incident with v and the degree of a graph is the maximum of the degrees of the vertices of a network. The probability distribution of the all node degrees over the network is the degree distribution. Vertices that have highest degree are called hubs.

Definition 2.8. Suppose G is a graph with $V(G) = v_1, ..., v_n$ and $d(v_i)$ denotes the degree of vertex v_i, $1 \leq i \leq n$. Then we call $(d(v_1), \ldots, d(v_n))$ the degree sequence of G and the average degree, denoted by $\langle k \rangle$, is given by

$$\langle k \rangle = \frac{1}{n} \sum_{i=1}^{n} d(v_i)$$

Definition 2.9. Connected Graph: A graph G is connected if there exists a path between any pair of its vertices. Otherwise, G is disconnected. When a graph is connected and undirected, we call it an epidemiological network.

Definition 2.10. Bipartite Graph: A bipartite graph G is a graph whose vertex set $V(G)$ can be divided into two disjoint subsets V_1 and V_2 such that every edge joins a vertex in V_1 to a vertex in V_2.

Definition 2.11. Adjacency Matrix: The connections between nodes can be expressed by the adjacency matrix $A = (a_{ij})$. For a given graph G with vertex set $V(G) = v_1, ..., v_n$,

the adjacency matrix $A \in \mathbb{R}^{n \times n}$ of the graph is defined component-wise as $a_{i,j} = 1$ if $(v_i, v_j) \in E(G)$ and 0 otherwise. In addition, the graph and its adjacency matrix determine each other up to enumeration.

In networks, clustering involves grouping nodes into classes based on some characteristics of the nodes.

2.3 Explanations of notions from biology

In the previous sections, we discussed some of the key mathematical concepts that are necessary for the rest of the thesis. In this section, we will provide explanations of some of the key notions from biology that are relevant to this thesis. By providing a foundation in both mathematical and biological concepts, we hope to offer a comprehensive understanding of the mathematical models used to describe biological phenomena.

Definition 2.12. Genome: It is the complete set of genetic information in an organism. It provides all of the information the organism requires to function. In living organisms, the genome is stored in long molecules of DNA called chromosomes.

Definition 2.13. Deoxyribonucleic acid (DNA) and Ribonucleic acid (RNA):

DNA is a molecule that carries genetic information in all living organisms. It consists of two complementary strands that form a double helix structure.

RNA is a molecule that is involved in protein synthesis and other cellular processes. It is similar to DNA but typically consists of a single strand, and the sugar molecule in its nucleotides is ribose instead of deoxyribose.

A single strand, in the context of DNA or RNA, refers to a nucleic acid molecule that consists of only one chain of nucleotides, rather than the two complementary chains that make up a double-stranded molecule.

Definition 2.14. Variant (or strain): In virology, a variant is a term used to describe a subtype of a microorganism that is genetically distinct from a main strain, but not sufficiently different to be termed a distinct strain. Variants might be caused by mistakes during cell division.

Definition 2.15. The mutation rate of a virus has been described as the probability that during a single replication of the virus genome a particular nucleotide position is altered.

Definition 2.16. Epidemic: An epidemic is the rapid spread of disease to a large number of hosts in a given population within a short period of time.

Definition 2.17. Pandemic: A pandemic is an epidemic that has spread over several countries or continents, usually affecting a large number of people.

Definition 2.18. Herd immunity: This is a form of indirect protection from an infectious disease which occurs when a large part of the population of an area is immune to a specific disease.

Definition 2.19. Mass vaccination: This is a vaccination strategy which involves immunization of a large number of people at one or more locations in a short interval of time. Mass vaccinations are useful in increasing herd immunity during a disease outbreak.

Definition 2.20. Ring vaccination: This is a vaccination strategy in which infected cases and contacts of cases are identified and vaccinated. This strategy is especially efficient in controlling rare pathogens and has been successful in the eradication of Smallpox and the Ebola virus disease.

Chapter 3

Modelling Drug Resistance

This chapter describes the state of the art of resistance evolution in bacteria and viruses. Resistant mechanisms, optimality of treatment strategies and overview of mathematical modelling techniques used in the study of resistance development and spread at both between-host and within-host levels are presented. The methodology employed in studies of drug resistance infections such as deterministic, stochastic, individual-based or statistical approaches is also discussed.

3.1 Introduction

Drug resistance can be caused by various physiological and biochemical processes. The paucity of knowledge about these mechanistic processes is primarily one of the reasons very little has been achieved for effective prevention and control [35, 36]. The increasing need to find lasting solutions makes many international, national and local agencies recognise drug resistance as a major threat to public health [37, 38, 39, 40, 8]. The sixty-eighth World Health Assembly in May 2015 endorsed a global action plan to address antimicrobial resistance, especially antibiotic resistance [41]. The United Nations General Assembly in 2016, called upon the World Health Organization (WHO) and the Food and Agriculture Organization (FAO) to finalize a framework with the aims of developing, conserving and ensuring affordable access to antimicrobials in relation to the Global Action Plan on antimicrobial resistance [42].

The rapid spread of resistance over the years can be associated with the misuse of antimicrobials as well as bad prescription by medical practitioners. Nowadays, antibiotics are by far the most common drugs frequently prescribed by physicians and in some cases prescribed for other non-bacterial infections. This situation becomes more complicated as there are numerous pathways of transmission between animals and humans, coupled with weakened

immune systems. However, this transfer process cannot be easily identified due to enormous interactions between humans and animals. Studies in existing literature have established that intervention strategies that restrict antibiotic use are associated with reduction in antibiotic resistance in food-producing animals and in humans [43]. Furthermore, the European ban on the use of antibiotics for livestock production in Europe in 2006 [44] led to a decline in resistance to antibiotics in both humans and animals [45, 46].

We have witnessed enormous advances in the field of antiviral drug discovery including the introduction of therapies capable of preventing human immunodeficiency virus (HIV) replication, or cure hepatitis C virus infections in people suffering from liver disease [47]. However, there are other viral diseases without effective treatments and the emergence of drug resistance threatens the efficacy of successful therapies used today. For instance, development of resistance to two classes of drugs, adamantanes and neuraminidase inhibitors (NAIs), currently used for treatment of influenza has increased, thereby threatening the ability of clinicians to effectively treat influenza.

Mathematical models have played a central role in medicine, epidemics, and public health. They provide a cost-effective way of assessing transmission as well as targets for prevention and control of infections. Many mathematical models on spread and control of drug resistance can be found in literature, for instance, comprehensive systematic reviews of these models have been conducted by [48, 49, 50, 51, 52, 53] and [54] among several others. In this chapter, we explore modelling techniques for drug resistance in bacteria and in viruses.

3.2 Drug resistance in bacteria

Bacteria are broadly classified as either Gram-positive or Gram-negative based on differences in the thickness of their cell wall (peptidoglycan). Gram-positive bacteria are composed of thick cell walls (about $20 - 80$nm) whereas Gram-negative bacteria have thin cell walls (< 10nm) [9]. Though Gram-positive bacteria have thicker cell walls than Gram-negative bacteria, antibiotics can easily get access to the cell wall (peptidoglycan). This is however not feasible for Gram-negative bacteria because unlike Gram-positive bacteria, Gram-negative bacteria have an outer membrane which serves as a protective layer and is essential for survival. Gram-negative bacteria are a major cause of morbidity and mortality in both humans and animals. Gram-negatives have been identified to be more inclined to antibiotic resistance [55, 56, 10] and hence result in the evolution of many 'resistant-related' infections [57]. Examples of Gram-positive bacteria are *S. aureus* (most popular Gram-positive pathogen), *Clostridium difficile*, *Proteus vulgaris* and *Proteus mirabilis*. Examples of Gram-negatives include *E. coli*, *Klebsiella pneumoniae*, *Pseudomonas aeruginosa*, *Salmonella enterica* and more recently, *Acinetobacter baumannii*.

The most serious bacterial infections occur in health care settings and are most commonly caused by Enterobacteriaceae (mostly *K. pneumoniae*), *Enterococcus faecium*, *P. aeruginosa*, *S. aureus* and *Acinetobacter* [58, 59, 60, 35, 61, 10], a group collectively known as ESCAPE pathogens [62]. Infections caused by these pathogens are particularly difficult to treat due to increasing levels of resistance and paucity of therapeutic strategies [63, 64]. *P. aeruginosa* is a major threat related to hospital-acquired infection and effectively treated with $\beta-$lactams (such as penicillin and carbapenems) and aminoglycosides. However, resistance to relevant antibiotics for this pathogen evolved as a concomitant consequence of introduction of new derivatives of antibiotics for treatment. Patients with cystic fibrosis infection are at higher risk of developing resistance due to the use of these antibiotics over a long period of time [57, 31]. *Acinetobacter baumannii* infections have rapidly evolved in recent times to be problematic and highly difficult to treat due to resistance to last-line antibiotics such as colistin and carbapenem [65, 61].

An antibiotic effectively inhibits bacterial growth if it recognizes its target and has enough concentration at the target site to effectively impede its activity. Thus, resistance mechanisms can either be due to target modification or antibiotic concentration reduction. Resistance mechanisms vary depending on the type of bacteria and class of antibiotic used. Yet, resistance to the same antibiotic can be caused by more than one resistance mechanism.

Antibiotic resistance can also be caused by modifications due to antibiotic-inactivating enzymes - a mechanism found in several antibiotic classes. It leads to a reduction in the amount of active antibiotics reaching the target [66]. For instance, in the $\beta-$lactam class of antibiotics, resistance arises due to hydrolitic inactivation of $\beta-$lactamases. That is, the substrate specificity of the enzyme changes with even a single base change in a $\beta-$lactamase gene. In addition, for the aminoglycoside class of antibiotics, it has been found that introduction of new variants of aminoglycosides leads to acquisition of new resistance genes [67]. For example, a new type of antibiotic inactivating enzyme was discovered in gentamicin-resistant strains when gentamacin was used as a replacement of kanamycin. A similar mechanism is found for chloramphenicol-resistance [57].

Intracellular alterations and modifications of antibiotic targets, such as ribosomes and DNA proteins, is another resistance mechanism. Such a mechanism inhibits action of the drug in the microbial cell. This mechanism has generated resistance in macrolide antibiotics which are widely used for treatment of Gram-positive infections. Another resistant mechanism is to target the means of transportation of the drugs to action sites; for example, resistance to tetracyclines and fluroquinolones is caused by drug efflux from the cell [8, 68].

3.2.1 Treatment strategies employed to prevent antibiotic resistance

Discovery and designing of new antibiotics have been given a lot of effort [69, 70] but unfortunately with not much success achieved. Several intervention strategies have been proposed and implemented for prevention and control of resistance; ranging from personal hygiene, a combination of different antibiotics, and rational prescription and use of antibiotics in hospitals and by the public [71, 20]. There have also been recommendations for appropriate use of antibiotics in other areas such as animal husbandry, fish farming, and agriculture [20]. Implementation of these strategies have however been slow and have also encountered more challenges as resistance still persists [72, 73]. Thus, intervention strategies that are capable of predicting resistance evolution should be developed and implemented at international, national and local levels [74].

One way to reduce the development and spread of antibiotic resistance is by lowering selection pressure based on the assumption that susceptible strains will outnumber resistant strains [75]. This is however not always the case as it has been identified that some resistant strains persist in the human immune system even after treatment [76, 77, 78, 79, 74] or on human and animal skins for many years at low levels without detection. This is because the fitness cost of resistance is often not large enough to be selected against. Even when the cost of resistance is high, it can easily be compensated for by mutations that cause resistance when an antibiotic is used. Thus, making complete eradication of antibiotic resistance non-trivial.

Treatment strategies involving more than one or a combination of antibiotics have been found to be a good strategy against developing resistance. Two treatment methods which involve a heterogeneous use of antibiotics, antibiotic mixing and antibiotic cycling were proposed by clinicians to curb the evolution of resistance [71]. *Antibiotic mixing* refers to the use of different antibiotics by different hosts at any given time whereas *antibiotic cycling* refers to the use of different antibiotics in a sequence. Simultaneous administration of antibiotics to each infected host, a treatment strategy known as *combination treatment* has also been used. These strategies have been the subject of a number of mathematical modelling evaluations with the consistent conclusion that antibiotic cycling is less likely to be effective compared to antibiotic mixing [71, 80, 81].

3.2.2 Between-host models

Mathematical models have been used to improve knowledge of the epidemiology and spread of resistance [48] between multiple individuals of a host population. Compartmental models describing the dynamics of an antibacterial treatment have been considered for single and multiple antibiotic treatment regimens. These models have been simplified with assumptions

of the availability of either one or two drugs in a population. Most of these models are formulated based on resistance transmission dynamics in the hospital [71, 82, 81, 83, 84] with very few based on the community [76]. Early between-host models of antibiotic resistance can be considered as basic models. These models, for single and multiple treatments, proposed by Bonhoeffer *et al* [71] and Lipsitch *et al* [82] (Figure 3.1) have been widely used in other studies with several other models being variants and/or modifications of these two models. Modelling analysis of [71] were done by other authors [85, 86] and for [82] by [87, 88, 89, 83, 80, 90].

Assuming that only one drug is used for treatment in the entire population, three compartments are considered. These are the uninfected hosts, patients infected with bacteria sensitive to the drug and patients infected with bacteria resistant to the drug. In the case when two antibiotics are used for treatment, say drug A and drug B, the model considers additional compartments for patients resistant to either drug A or drug B. Resistance to a combination of both, that is AB, is also considered in some models. Bonhoeffer *et al* [71] modelled antibiotic resistance to both treatments with one drug and treatment with two drugs using a simple compartmental model.

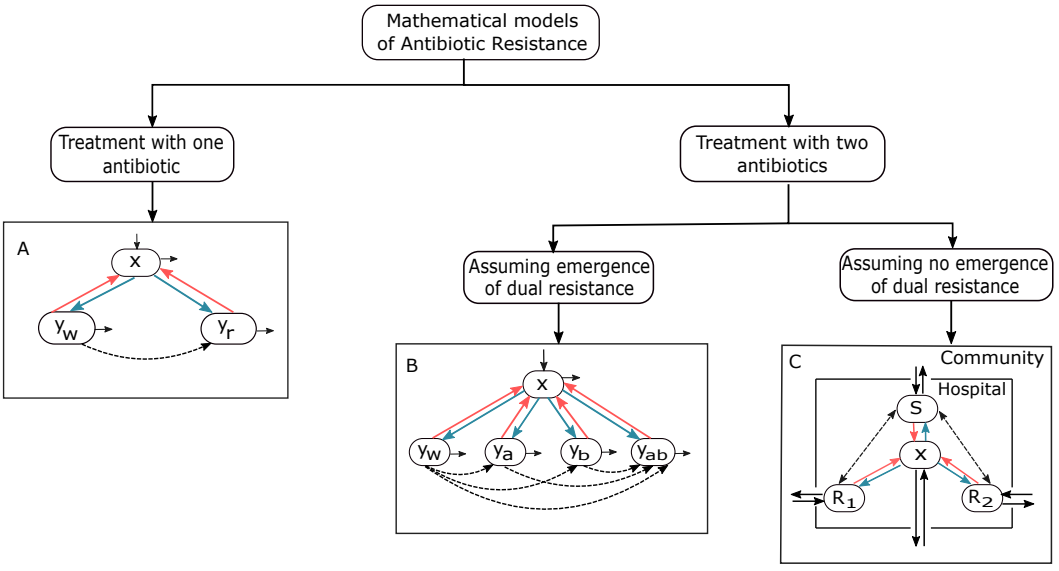

FIGURE 3.1: The most basic mathematical models for one and two antibiotic treatment regimen. (A): Basic model for single drug treatment of bacterial infection [71]. Uninfected hosts (X) entering the population can be infected with either sensitive (y_w) or resistant (y_r) bacteria strains (shown by blue arrows). It is assumed that in the absence of treatment infected patients recover from the infection and that infected patients become susceptible again after treatment (shown by red arrows). (B),(C): Basic models for multiple antibiotic treatments. Unlike in (B) [71] where there is resistance to drug A (y_a), B (y_b) and AB (y_{ab}), there is only resistance to drug A and B in (C) [91]. In (C), hosts colonized by susceptible strains of the bacteria of interest are represented in the S compartment.

3.2.2.1 Treatment with one antibiotic

Mathematical models for single antibiotic treatment describe the transmission and spread of resistance. Some models of this kind consider the interaction between the hospital and the community [91] while others do not [71]. Generally, such mathematical models comprise interactions between three compartments, namely the uninfected, infected and sensitives. These models are appropriate for the transmission dynamics of resistant bacteria to a single antibiotic and can be used to study bacteria frequently transmitted in the hospital like the Gram-positive cocci such as *S. aureus* species and *Enterococcus* species. The model proposed by [71] is illustrated in box A of Figure 3.1.

For this model ([71], Figure 3.1 box A), uninfected hosts enter the population at a rate, λ, and leave at the rate d. Uninfected hosts can become infected by bacteria that are either sensitive or resistant to the treating antibiotic. The densities of hosts infected with sensitive and resistant bacteria are y_w and y_r respectively. Uninfected hosts become infected at a transmission parameter rate b and infected hosts die at a rate c. Rates of recovery from infections are r_w and r_r for sensitive and resistant patients respectively. The fraction of patients treated is represented as f and the maximum rate of treatment is h. A fraction, s, of uninfected become infected with sensitive strains of bacteria and another fraction $(1-s)$ become infected with resistant strains. The model equations are as in eq (3.1).

$$\frac{dx}{dt} = \lambda - dx - bx(y_w + y_r) + r_w y_w + r_r y_r + fh(1-s)y_w, \tag{3.1a}$$

$$\frac{dy_w}{dt} = (bx - c - r_w - fh)y_w, \tag{3.1b}$$

$$\frac{dy_r}{dt} = (bx - c - r_r)y_r + fhsy_w. \tag{3.1c}$$

The model assumes that the fitness cost of resistance is characterized by a higher rate of recovery of hosts with resistant bacteria relative to recovery in hosts with sensitive bacteria. It disregards temporary immunity, in that, treated patients become susceptible again after treatment. The model also assumes that there is a small proportion of resistant bacteria pre-existing in a fraction of sensitive infected patients. Thus, resistant populations can outgrow the sensitive bacteria and dominate the infection. Superinfection of sensitive infected by resistant bacteria is however not considered. The model predicts that if the rate of treatment of sensitive infected, fh, outweighs the cost of resistance, $\Delta r = r_r - r_w$, that is if $fh > r_r - r_w$, then resistant infections will prevail for longer time periods and there will be no sensitive infections (Figure 3.2b). However, if $fh < r_r - r_w$, sensitive infections will prevail and resistant infections will coexist at low levels. Qualitative analysis of this model was done by [85] with solution trajectories as shown in Figure 3.2c.

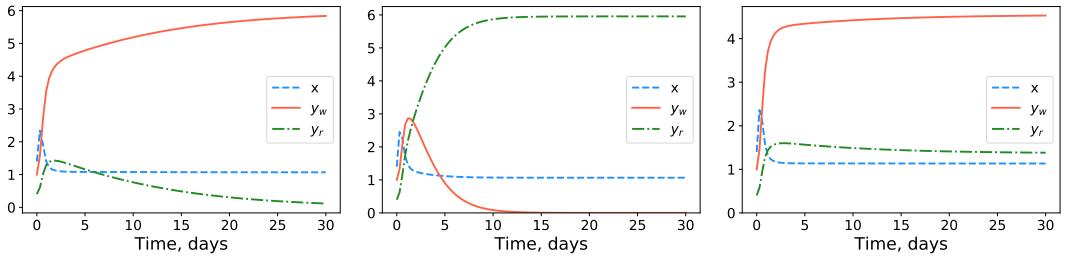

(A) $r_r > r_w, fh = 0$ (B) $r_r < r_w + fh, fh > 0$ (C) $r_r > r_w + fh, fh > 0$

FIGURE 3.2: Simulation of single antibiotic treatment model with $\lambda = 10, d = 1, b = 1.5, s = 0.3, c = 1.5$ and initial values $x_0 = 1.4, y_{w0} = 1.0, y_{r0} = 0.4$. Parameter values are obtained from [85]. (a) Absence of antibiotic treatment with cost of resistance. With antibiotic treatment, (b) resistant infections (y_r) prevail at longer time periods and there is no sensitive infections when cost of resistance outweighs selection pressure; (c) sensitive infections (y_w) prevail while resistant infections (y_r) coexist at low levels when selection pressure outweighs cost of resistance.

The model proposed by [82, 91] is as in eq (3.2a) and illustrated in box C of Figure 3.1.

$$\frac{dS}{dt} = m\mu - \beta SX - (\tau_1 + \tau_2 + \gamma + \mu)S \tag{3.2a}$$

$$\frac{dR}{dt} = \beta(1-c)RX - (\mu + \tau_2 + \gamma)R \tag{3.2b}$$

$$\frac{dX}{dt} = (1-m)\mu + (\tau_1 + \tau_2 + \gamma + \mu)S + (\tau + \gamma)R - \beta SX - \beta(1-c)RX - \mu X \tag{3.2c}$$

This model outlines the transmission dynamics of hospital-transmitted bacterial infections. It is assumed that a fraction of patients entering the hospital is already colonized with the bacteria. Thus, individuals entering the hospital may carry either sensitive or resistant bacterial strains or be uncolonized and free of the bacteria (X). For simplicity, it is assumed that there is no frequent entry of hosts with resistant strains. The fraction m represents the fraction of sensitive individuals whilst the fraction $(1 - m)$ represents the fraction of uncolonized individuals entering the hospital. Rate of treatment with drug 1 per day is τ_1 and for drug 2 is τ_2. Sensitive and resistant bacteria are cleared at the rate γ. Uncolonized individuals are colonized with sensitive bacteria at the rate β and with resistant bacteria at the rate $\beta(1 - c)$, where c is the fitness cost of resistance to drug 1. The average duration of stay in the hospital is given as $1/\mu$, where μ is the rate of admission per day.

Three main predictions were made based on the model in [82]. Firstly, the model predicts that using antibiotic for which there is no resistance in the hospital is positively associated with carriage of resistance to other antibiotics in patients but is negatively associated with the prevalence of resistance to another drug in the population. In other words, when there is no resistance to an antibiotic in the hospital, resistance to other antibiotics is more likely in patients. However, on the population level, the prevalence of resistance to another drug is less likely. Secondly, the prevalence of colonization with resistant bacteria can be reduced

by interventions that reduce transmission of bacteria within a hospital. Thirdly, changes in the prevalence resistance after treatment is faster in hospital-acquired infections than in community-acquired infection.

3.2.2.2 Multiple antibiotic treatment

Generally, treatment protocols involving the use of two or more antibiotics give rise to antibiotic cycling and mixing. Mathematical models have been used to investigate the effectiveness of these treatment protocols either in the hospital setting or in individual patients. Theoretical models describing treatment with two antibiotics broadly consider assumptions of the emergence of dual resistance. Bonhoeffer *et al* [71] proposed a model which assumes the emergence of dual resistance whilst the model proposed by Bergstrom *et al* [81] assumes non emergence of dual resistance.

Bonhoeffer *et al* [71] raised questions about the best strategy to employ when using more than one antibiotic. By assuming that the cost of resistance to each drug is equal, a multiple antibiotics treatment strategy is proposed to address the issue concerning optimal treatment protocols by considering three scenarios of resistance transmission with regards to cycling, $50-50$ treatment (a kind of antibiotic mixing strategy in which equal fractions of the population receive different antibiotics at any given point) and combination therapy. First, the transmission of resistance is by infectious patients with resistant bacteria. For this case, as long as initial appearance of primary resistance is considerably greater than the appearance of acquired resistance, treatment is of equal benefit irrespective of the treatment strategy used. Second, is resistance acquired in the course of treatment. Cost to resistance determines the performance of the treatment protocol. If there is no cost to resistance then cycling and $50-50$ treatment yield the same total gain of infected. However, if there is cost to resistance then the $50-50$ treatment is superior to the cycling of antibiotics; this is affirmed with numerical simulations. This scenario does not hold true when resistance to both drugs is carried by the same plasmid. In this case, the probabilities of acquiring single and multiple resistance are equal. The last scenario is the case when there is no or small amount of bacteria with multiple resistance. In this case, cycling of antibiotics is worse than $50-50$ treatment.

The model proposed by Bergstrom *et al* [81] is an extension of their previous models [82, 91] to account for cycling of antibiotics as a way of controlling resistance. This new model assumes that two drugs are used and that resistant strains to each of the two drugs are present but with no dual resistance yet. Cycling is important for limiting the spread of resistant strains currently present in the population and also for inhibiting the formation of new resistant strains. Resistant strains currently present in the population will be expected to abound in

higher quantities in a slowly changing environment than in a rapidly changing environment. Antibiotic mixing provides a more heterogeneous environment at the individual level whilst cycling offers greater heterogeneity at the level of the ward. This is because selection pressure experienced by resistant strains of the bacteria occurs consistently in a cycling protocol than in a mixing protocol where these selection pressures alternate at much shorter time periods between patients under different drug treatments. The authors found that cycling can be an effective approach for reducing the evolution of multiple resistance, relative to mixing. If more of the drug is used, the cost of resistance decreases, patients arriving with resistance decreases and finally, there is an equal fraction of patients arriving with strains resistant to drug one and drug 2. However, cycling fails if this fraction is unequal.

Empirical and clinical studies have examined various multiple antibiotic treatment strategies, but the question of which approach is optimal remains unclear. This uncertainty raises concerns about the effectiveness of proposed treatment strategies for resistance development and control, as noted by Beardmore et al. [92]. To address this question, optimal control theories and computational tools must be considered. These strategies have been utilized to describe the dynamics of resistance evolution to antibiotics.

Empirical and clinical studies have examined various multiple antibiotic treatment strategies, but the question of which approach is optimal remains unclear. This uncertainty raises concerns about the effectiveness of proposed treatment strategies for resistance development and control, as noted by Beardmore *et al* [92]. To address this question, optimal control theories and computational tools must be considered. These strategies have been utilized to describe the dynamics of resistance evolution to antibiotics. Beardmore *et al* [92] made some realistic predictions using optimal control theory and computational tools used for dynamic programming problems. These optimal control strategies were applied to the already existing models by [81] and [71] to compare cycling and mixing based on synthetic data presented from both models. The criterion used in these mathematical explorations is to maximize the probability that patients in a cohort will receive appropriate treatment.

For the model by Bergstrom *et al* [81] which assumes all patients are treated with either one of the drugs, the constraint, $\tau_1 + \tau_2 = \tau$, where τ is a fixed constant representing the rate at which each drug, is used. In this model, x represents uninfected hosts, y_w represents the number of individuals infected with the wild type, y_a denotes the number of patients with drug A resistant strain and y_b denotes the number of patients with drug B resistant strain. The optimal control problem in this case is to find a function that minimizes the total fraction of days within which a patient is observed with a drug-resistant infection. That is, to find a function $f_a(t)$ such that

$$\int_0^T y_w + y_a + y_b \, dt,$$

where T is the observation time, is minimized. For the lack of better strategies, the authors [92] applied an optimal control law to the model by Bergstrom *et al* to compare the performance of cycling and mixing using control strategies.

Stochastic versions of the models were used to determine the performance of cycling and mixing. Stochasticity is achieved by introducing a random process into the model so that τ_1 represents a noisy protocol which varies with time such that the expectation $\mathbb{E}(\tau_1(t)) = \alpha(t)$ for each $t > 0$ where $\alpha(t)$ is some treatment protocol. The authors [92] found that deterministic and stochastic variations of the same model can yield different optimal strategies, hence making it difficult to establish which protocol is better. For instance, deterministic models yield mixing strategies whereas stochastic models yield switching strategies. Their findings are also consistent with previous studies suggesting that it is not possible to distinguish the impacts of cycling and mixing therapies.

Prior studies [81, 71] concluded that antibiotic mixing was optimal using exemplar simulations, but many of these ignore the perspective of individual patients. Since it is possible for resistance to evolve at the patient level, individualised treatment strategies should be considered when optimizing antibiotic resistance. Beardmore [92] predict that mixing might not be an optimal strategy after all. This prediction has gained support from other studies ([93]) which consider treatment on the individual and population levels. These studies found that antibiotic treatment strategies differ on individual-based and population-based levels and neither cycling nor mixing is an optimal strategy. On the other hand, combination therapy has been found to perform better than cycling and mixing [94].

3.2.3 Within-host models

Within-host mathematical models of antibiotic resistance evolution and development are useful for understanding bacteria dynamics within a single individual. These models describe how antibiotic treatment strategies affect resistance evolution and how resistance can be prevented within the host. Within-host models capture the effect of the immune system cells on the bacteria of interest and vice versa. Development of resistance is recognised to begin within the host [95] and that within-host competition shapes resistance evolution [96]. These models have explained the theoretical framework for studying multiply resistant bacteria [95], described the effect of antibiotics in a heterogeneous bacterial population [97], tried to understand factors that determine the fraction of resistant strains in a bacterial population [98], describe the interplay of host immune responses [99, 100, 101] and antibiotic treatment as well as optimality of drug dosage [102, 103, 104].

Antibiotic resistance evolution is also impacted by the existence of competing sensitive and resistant strains within the host. The dynamics of various forms of competition have been

addressed in some theoretical as well as empirical studies [105, 106, 13, 96, 107, 108, 109]. In a simple two-strain (sensitive and resistant) logistic model, Garber [110] describes the selection pressure for resistance in the presence of an antibiotic.

In this model (as depicted in Figure 3.3), x_s and x_r represent sensitive and resistant strains respectively and $X = x_s + x_r$. The growth rate of the sensitive strain is μ and the rate at which resistance is lost is δ. Competition between the two strains is represented by β and the antibiotic concentration is a. The inhibitory strength of the antibiotic is considered as being quantitative and is represented by γ. This model was used to identify conditions which lead to the survival or existence of sensitive or resistant strains as well as coexistence of both strains (see Figure 3.4). In particular, the sensitive strain survives if $a < \delta/\gamma$ whereas the resistant strains survive if a is much larger. Furthermore, this model predicts that antibiotics can minimize bacterial population while selecting resistant strains.

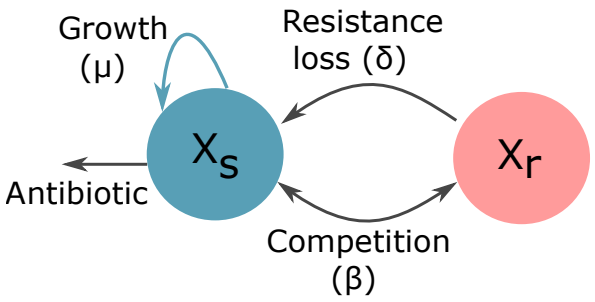

FIGURE 3.3: Schematic illustration of within-host model by Garber [110]. μ is the growth rate of sensitive strain X_s, δ represents loss of resistance and β represents competition between sensitive X_s and resistant X_r strains.

A simulation of this model is shown in Figure 3.4.

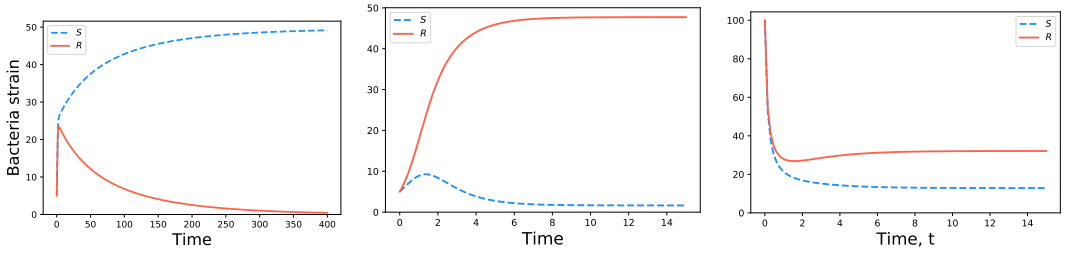

(A) Susceptible or sensitive strain survives.

(B) Resistant strain survives

(C) Co-existence of both strains

FIGURE 3.4: Within-host antibiotic resistance. Due to paucity of biologically meaningful parameter values, arbitrary values have been used to generate these plots. For all simulations, $\beta = 0.04$ and $\mu = 2$. Other parameter values: (a) $\gamma = 0.3, a = 0.055, \delta = 0.025$; (b) $\gamma = 0.3, a = 2.5, \delta = 0.025$; (c) $\gamma = 0.7, a = 1.0, \delta = 0.2$

Davies *et al* [96] identified competition between sensitive and resistant strains within the host to promote coexistence and shape resistance evolution and spread. This study was conducted using an individual-based model (IBM) which describes within-host competition of sensitive and resistant bacterial strains. Using empirical data, the authors argue that competition between resistant and sensitive pathogens within hosts gives resistant pathogens a relative fitness benefit when they are rare, promoting coexistence between strains at the population level.

One important factor assumed to facilitate infection clearance time and resistance control is host immunity. A strong immune system can necessitate shorter duration of treatment [100]. The interaction between host immune response and antibiotic treatment has been the focus of some mathematical models. Previous studies have shown that the presence of a strong immune response can reduce the *mutant selection window* (MSW) despite a considerable decrease in bacteria population [99, 111]. The MSW is defined as the range of drug concentrations for which the drug is strong enough to remove the sensitive population but not strong enough to remove the partially resistant pathogen population.

The century-old chemotherapy principle of "hit hard and hit early" introduced by Paul Ehrlich has been supported by numerous studies [101]. The original basis for the use of this principle was to gradually eradicate bacterial populations in order to increase efficacy of drugs. However, it has been used to understand the evolution of antibiotic resistance [101] and to guide rational development of treatment. "Hitting hard" has been justified by the following reasons: (1) higher doses of antibiotics supplement immune response by rapidly decreasing the density of infecting bacteria and thereby ensuring a decline in the amount of resistant bacteria in the host and (2) lower doses create a pathway for intermediately resistant strains to increase resistance due to mutations. This protocol might however not be the best because a high antibiotic dose increases selection for resistance even though it restricts the appearance of a resistant enough strain [72]. On the other hand, "hitting early" is supported with the notion that an early high dose can drive resistant strains to extinction. Administering a high dose earlier has the advantage of limiting the emergence of resistance in the presence of intermediate resistant strains. Thus, the dichotomy of antibiotic dose administration lies between low dosages efficient to clear the bacteria and high dosages which will be safe for the host.

Using a within-host mathematical model, Ankomah and Levin [101] investigated the relationship between antibiotics and immune response in acute infections. Their model is shown in eq (3.3) below

$$\frac{dB_i}{dt} = \psi_i(A_i R)B_i - k_P B_i P - k_I B_i I + f_{PS} BP_i - f_{SP} B_i \tag{3.3a}$$

$$\frac{dBP_i}{dt} = \psi_{Pi}(R)BP_i - j_P BP_i P - j_I BP_i I - f_{PS} BP_i + f_{SP} B_i \tag{3.3b}$$

where B_i and BP_i represent the population of bacterial cells and their mutants respectively. ψ_i and ψ_{P_i} represent the rate of growth or death of bacterial cells of either a B_i and BP_i population respectively. The probability that a mutant cell BP_i will be produced from the B_i population is $f_{SP}B_i$. Antibiotic concentration for each bacteria cell is denoted as A_i and limiting resource is denoted as R. k is the resource concentration at which the population is growing at half its maximum rate.

Results from this study suggest that the net bactericidal effect of antibiotics can be affected by the intensity of the immune response and the amount of pathogens. So that if the efficacy of the immune response is dependent on the bacterial load, antibiotics can reduce immune response stimulation by reducing the density of bacteria. This is evident at lower antibiotic doses which trigger low immune response due to relatively low bactericidal effect of drug.

A within-host model by Gjini *et al* [100] studies the interplay between host immune response and antibiotic treatment. The model equations can be found in eq (3.4) below.

$$\frac{dN}{dt} = -\sigma N \frac{B}{k+B} \tag{3.4a}$$

$$\frac{dB_s}{dt} = r_0 B_s - dB_s I - \delta_0 B_s \eta(t) A_m \tag{3.4b}$$

$$\frac{dB_r}{dt} = r_1 B_r - dB_r I - \delta_0 B_r \eta(t) A_m \tag{3.4c}$$

$$\frac{dE}{dt} = (2\sigma N + \sigma E)\frac{B}{k+B} - hE(1 - \frac{B}{k+B}) \tag{3.4d}$$

$$\frac{dM}{dt} = fEh(1 - \frac{B}{k+B}), \tag{3.4e}$$

where $I(t) = N(t) + E(t) + M(t)$ is the total number of immune cells activated to clear the pathogen and $B(t) = B_s(t) + B_r(t)$ is the total pathogen load at time t. They found that in the absence of antibiotics, drug-sensitive strains, B_s, grow exponentially in the absence of immune response whereas in comparison, drug-resistant strain grow more slowly. As immunity builds up, naive precursor cells, N, differentiate into effector cells, E, which initiate clearance of the bacteria and differentiate into persistent memory cells, M, as the pathogen decreases (see Figure 3.5). Analysis of this model emphasises that better treatment outcomes can be achieved when there exists a balance between antibiotic therapy and the natural defence system of the host. Exploring two dosing regimes, classical regime (fixed drug dose and treatment duration) and adaptive regime (follows infection outcomes and patient symptoms), the authors also found that successful antibiotic treatment is influenced by the timing of therapy in both cases. Furthermore, this optimal timing is affected by bacterial load and host immunity.

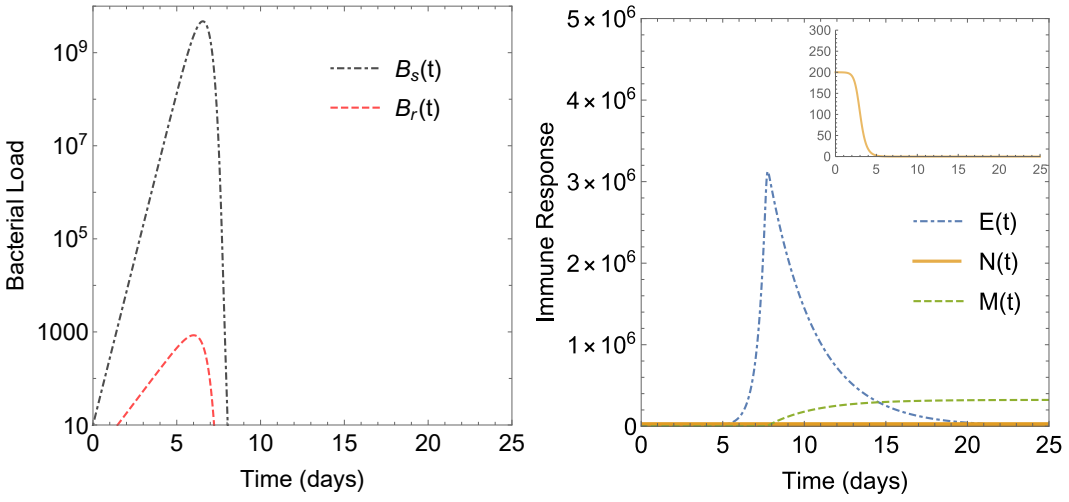

(A) Bacteria dynamics.

(B) Immune response dynamics.

FIGURE 3.5: Illustration of the model by Gjini *et al* for dynamics of the model in the absence of antibiotics. Parameters used are same as in [100]. In the absence of antibiotics and immune response, sensitive B_s and resistant B_r bacteria grow exponentially and reach a peak with the density of B_s higher than B_r. When immune response accumulates, naive cells N transform into effector cells E which initiate bacteria clearance. As bacteria density decreases, effector cells differentiate into persistent memory cells M.

Alavez-Ramirez *et al* [112] developed models of TB infection which address drug administration based on strength of the immune system. Results from this study indicate that administering a single drug can be effective against low bacteria population and an immune system with reduced immune response. On the other hand, using two drugs prolongs the time for the appearance of resistance for an immune system with severe immune deficiency.

3.2.3.1 PK/PD modelling

Another way suggested to combat antibiotic resistance is finding novel techniques of using the already extant drugs [113, 114]. Thus, instead of developing new drugs, optimizing the present ones [115] and understanding their action on the human body is crucial to the success of treatment [116, 117]. Pharmacokinetic and pharmacodynamic properties of drugs are considered in this regard. *Pharmacodynamics (PD)* describes the functional relationship between drug concentrations and the change in bacteria population whereas *Pharmacokinetics (PK)* encapsulates the body's reaction to drugs during absorption, distribution, metabolism and excretion [118, 113]. PK/PD analysis can be employed in optimizing dosing of both new and old antibiotics, leading to an increased probability of therapy success [103]. Hence, such models are likely to minimize the risk of within-host resistance development thereby, minimizing endemic levels of resistant bacterial strains in the community at large [119].

3.2.3.2 Treatment duration and dosage

The dynamics of an infection can greatly influence the optimal duration and dosing of antibiotic treatment. Optimising treatment duration and dose in order to minimize infection duration and reduce selection for resistance can be used as a protocol to extend the efficacy of drugs. The effect of the length of treatment may be similar to the amount of dose administered. Some studies have found that more bacteria can be annihilated if a given amount of antibiotic is administered frequently in small doses instead of few large doses [99].

Current traditional treatment regimens involve fixed daily doses of drugs over a set period of time. These protocols remain largely unchanged and there is little evidence about their optimality. Considering a baseline current antibiotic treatment regimen of 23 $\mu g/ml$ per day for 8 days, Paterson *et al* [104] in a nouveau study approach involving the use of genetic algorithms, identified that an optimal antibiotic dosage consists of an initial high dose followed by tapering lower doses. They found that with a comparable success rate, the baseline treatment uses 20% more antibiotics and longer days than the alternative treatment identified by the genetic algorithm. This tapered treatment approach has been found to be effective in treating *Clostridium difficile*.

Using within-host models, Geli *et al* [103] determined optimal antibiotic dosing strategies that are capable of simultaneously minimizing morbidity and selection for resistance. In this model, it is assumed that there is competition between drug sensitive and drug-resistant bacteria with population sizes of S and R, respectively. It is also assumed that bacteria grow at the rate λ, but a fraction, μ, of the sensitive bacteria become resistant through mutations. Sensitive and resistant bacteria die at the rates ζ_s and ζ_r respectively. The bacteria populations are limited by immune response I and their growth is also limited by the population size K. The functions f_R and f_S describe the relation between antibiotic concentration and antibiotic effect on bacteria. a is the maximum per capita proliferation rate, b is the bacterial population that gives half the maximum rate, and $1/\delta$ is the average duration of the immune response. Their model is represented as in eq (3.5).

$$\begin{aligned}
\frac{dS(t)}{dt} &= (1-\mu)\lambda\left(1-\frac{S(t)+R(t)}{K}\right)S(t) - (\zeta_s + f_s)S(t) - \gamma I(t)S(t) && \text{(3.5a)}\\
\frac{dI(t)}{dt} &= \frac{aI(t)(S(t)+R(t))}{b+S(t)+R(t)} - \delta I(t) && \text{(3.5b)}\\
\frac{dR(t)}{dt} &= (\mu\lambda S(t) + \lambda R(t)\left(1-\frac{S(t)+R(t)}{K}\right)S(t) - (\zeta_r + f_r)S(t) && \text{(3.5c)}\\
&- \gamma I(t)R(t).
\end{aligned}$$

Their findings concur with other studies that shorter treatment duration is more likely when there is a functional immune response in which case the successful treatment of infected

patients is not compromised. In addition, for infections caused by commensal pathogens, they found that short and aggressive treatment at early stages of the infection could be the best treatment strategy. In general, shorter duration of treatments could limit the emergence of resistance, but might not always be optimal.

3.2.3.3 Fitting models to data (Data-driven models)

Regoes *et al* [113] used a mathematical PK/PD model to describe the relationship between growth rates of bacteria and antibiotic concentration. Using pharmacodynamic data from previous studies in conjunction with pharmacokinetic data, they investigated the efficacy of antibiotics going beyond the use of only the MIC of the drug. The pharmacodynamic function used in this study is the functional relationship between growth or death of bacteria and antibiotic concentration. Treatment efficiency can be determined by combining this pharmacodynamic function (Ψ) with pharmacokinetic data. The pharmacodynamic function from Regoes *et al* [113] is as follows:

$$\Psi(a) = \Psi_{max} - \frac{(\Psi_{max} - \Psi_{min})(a/zMIC)^{\kappa}}{(a/zMIC)^{\kappa} - \Psi_{min}/\Psi_{max}} \tag{3.6}$$

where a is antibiotic concentration, Ψ_{max} is the maximum growth rate of bacteria in the absence of antibiotic, Ψ_{min} is the minimum net growth rate of bacteria at high antibiotic concentrations, κ is the Hill coefficient which determines how strongly the bacterial growth or death rate responds to changes in the antibiotic concentration and $zMIC$ is the pharmacodynamic minimum inhibitory concentration (MIC). This model is similar to a four-parameter E_{max} model where these four parameters, $\Psi_{max}, \Psi_{min}, zMIC$ and κ characterise the pharmacodynamic function. A plot of the relationship between bacteria growth and antibiotic concentration is shown in Figure 3.6.

Regoes *et al* found that when only one bacterial strain is used, the three parameters, Ψ_{max}, $zMIC$ and κ, vary across antibiotic classes except the parameter Ψ_{max} . However, incorporating Ψ_{max} as a model parameter is essential if the effect of antibiotics on bacterial strains that differ in their growth rates is considered. For the development of new antibiotics and novel treatment strategies, Regoes *et al* [113] perceive that the shape of the pharmacodynamic function is important as these contain information about the effect of antibiotics on bacterial growth that are not captured by MICs or other single pharmacodynamic parameters. Therefore, they recommended a multi-parameter approach involving the consideration of the entire pharmacodynamic function rather than relying solely on MICs or other single parameters as representatives of pharmacodynamics of antibiotics.

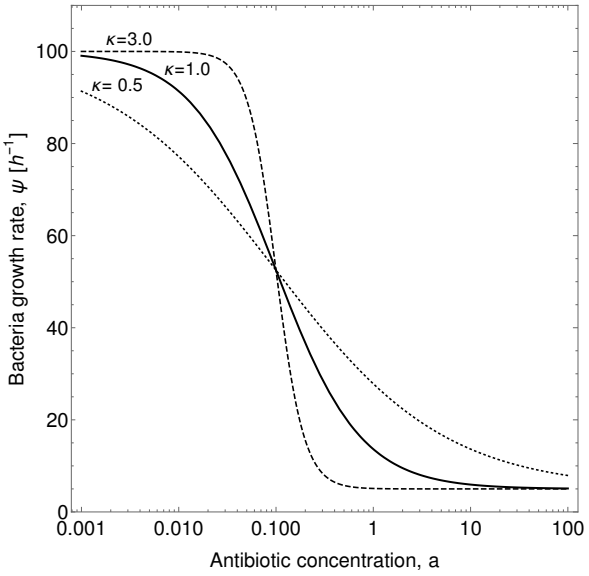

FIGURE 3.6: Relationship between bacteria growth rate (Ψ) and antibiotic concentration (a) for different values of the Hill coefficient, $\kappa = 0.5, 1.0, 3.0$. The following parameter values were used: $\Psi_{max} = 100, \Psi_{min} = 5, zMIC = 0.1$

Furthermore, a mathematical model for antibiotic cycling is proposed by Udekwu *et al* [114] to test the plausibility of optimisation of antibiotic cycling based on collateral sensitivities of drug pairs. This model not only incorporates PK/PD approaches but also accounts for collateral sensitivity to study the efficacy of the antibiotic cycling treatment regimen. The pharmacodynamic function defined by Regoes *et al* [113], above, is used together with computer simulations. This function was applied to each antibiotic considered and simulations were performed to cycle two antibiotics with varying pharmacodynamic properties and different cycling times. For easy understanding, pharmacodynamic properties of antibiotics are described broadly as bactericidal (cidal), killing bacteria, or bacteriostatic (static), inhibiting bacterial growth [120]. The model equations are shown in the system (3.7) and (3.8). For antibiotic 1, the parameters are: $MIC_S = 1, MIC_1 = 15, MIC_{12} = 0.5, MIC_2 = 15$ and the model equations are as follows:

$$\frac{dR}{dt} = Cw - eH(R)(v_{max_s}S + v_{max_{M_1}}M_1 + v_{max_{M_2}}M_2 + v_{max_{M_{12}}}M_{12}) - wR \tag{3.7a}$$

$$\frac{dS}{dt} = v_{max}H(R)\psi_1(Ab_1, MIC_s)S - \mu_1 S - \mu_2 S - \mu_1\mu_2 S - wS \tag{3.7b}$$

$$\frac{dAb_1}{dt} = c\ hsf(t) - wAb_1 \tag{3.7c}$$

$$\frac{dM_1}{dt} = v_{max_{M_1}}H(R)\psi_1(Ab_1, MIC_{M_1})M_1 - \mu_2 M_1 + \mu_1 S - wM_1 \tag{3.7d}$$

$$\frac{dM_2}{dt} = v_{max_{M2}}H(R)\psi_1(Ab_1, MIC_{M_2})M_2 - \mu_1 M_2 + \mu_2 S - wM_2 \tag{3.7e}$$

$$\frac{dM_{12}}{dt} = v_{max_{M_{12}}}H(R)\psi_1(Ab_1, MIC_{M_{12}})M_{12} + \mu_1 M_2 + \mu_2 M_1 + \mu_1\mu_2 S - wM_{12} \tag{3.7f}$$

$$\frac{dAb_2}{dt} = -wAb_2 \tag{3.7g}$$

For antibiotic 2, the parameters are: $MIC_S = 1, MIC_1 = 0.5, MIC_{12} = 15, MIC_2 = 15$ and the model equations are as follows:

$$\frac{dR}{dt} = Cw - eH(R)(v_{max_s}S + v_{max_{M_1}}M_1 + v_{max_{M_2}}M_2 + v_{max_{M_{12}}}M_{12}) - wR \tag{3.8a}$$

$$\frac{dS}{dt} = v_{max_s}H(R)\psi_2(Ab_2, MIC_s)S - \mu_1 S - \mu_2 S - \mu_1\mu_2 S - wS \tag{3.8b}$$

$$\frac{dAb_1}{dt} = -wAb_1 \tag{3.8c}$$

$$\frac{dM_1}{dt} = v_{max_{M_1}}H(R)\psi_2(Ab_2, MIC_1)M_1 - \mu_2 M_1 + \mu_1 S - wM_1 \tag{3.8d}$$

$$\frac{dM_2}{dt} = v_{max_{M_2}}H(R)\psi_2(Ab_2, MIC_2)M_2 - \mu_1 M2 + \mu_2 S - wM_2 \tag{3.8e}$$

$$\frac{dM_{12}}{dt} = v_{max_{m_{12}}}H(R)\psi_2(Ab_2, MIC_{12})M_{12} + \mu_2 M_1 + \mu_1 M_2 + \mu_1\mu_2 S - wM_{12} \tag{3.8f}$$

$$\frac{dAb_2}{dt} = c\ hsf(t) - wAb_2 \tag{3.8g}$$

In the above model, Ab_1 = Antibiotic 1 concentration, Ab_2 = Antibiotic 2 concentration, S = Sensitive cells, M_1 = Resistant mutants to Ab_1, M_2 = Resistant mutants to Ab_2, $M_{12=}$ Double-resistant mutants, μ_1 = Mutation rate (to Ab_1), μ_2 = Mutation rate (to Ab_2), w = flow rate, v_{max} = maximum growth rate of cells. Computer simulations from this model show that in exploiting mutual collateral sensitivity, static antibiotics prevent resistance evolution and are more superior to cidal ones as they prevent the growth of resistant strains.

The proposed model is similar to other models [71, 81] considered above. It is made up of four compartments representing dynamics of sensitive bacteria, and cells resulting from mutation due to drug 1, drug 2 or both drugs. PK/PD is incorporated into the model by modulating the minimum growth rates relative to each strain's respective MICs. Collateral sensitivity is assumed to be instantaneous and is accounted for by switching the MIC of the pre-exposed strain at periods corresponding to when the drug is cycled. It was observed that resistance to both antibiotics occurred quickly for low doses of the drug. However, cycling a combination of moderate to high concentrations of cidal and static antibiotics prevented resistance development. The most suitable strategy from their *in silico* simulations to prevent resistance was cycling static antibiotics that have low Hill's constant every 3 days.

A summary of mathematical models describing within-host dynamics within the host are presented in Table 3.1 according to questions addressed by these models and the approaches used.

TABLE 3.1: Overview of different within-host mathematical models for antibiotic resistance.

Questions	**Methods**				
	Deterministic	Stochastic	IBM	Statistical	PK/PD
Optimality of treatment regimes	[112],[121]			[122]	[121], [114]
Interaction with Immune response	[112],[123],[100]	[99], [101]			[95]
Strain Competition	[96],[110],[124]	[96]	[96]	[96]	
Optimal treatment duration	[103]	[102]			
Optimal drug dosage					[95],[113]
Evolution and spread of resistance	[125], [126] [98], [122]		[127]	[126]	[128]

3.3 Drug resistance in viruses

Mammalian viruses represent a diverse group of tiny infectious agents and have been classified to be the most abundant species on the planet [12, 11]. Viruses can exist as particles called virions when not inside an infected cell [129]. These virions are very small to be seen and are made up of long molecules of DNA or RNA that encode the structure of the proteins by which the virus acts (making up the genetic material), a protein coat which surrounds and protects the genetic material and in some cases, an outside envelope of lipids [130, 129]. Viruses can be found in a wide variety of sizes and shapes, ranging from simple helical forms to more complex structures. When a host cell is infected with a virus, these viruses rapidly replicate, producing thousands of copies of the original virus [12].

The viruses that cause diseases commonly found in human populations comprise approximately 25 known families, which fall into groups according to their genome and replication strategies (see [1] for a full list of all these families). For instance, double-stranded DNA viruses include the poxviruses, adenovirus, the herpesvirus groups and double stranded RNA viruses include reoviruses and rotavirus. Viruses such as west nile virus, yellow fever virus, dengue, hepatitis A, rubella virus and rhinovirus are all made up of single strand RNA genomes [1, 131]. Table 3.2 summarises some human viruses and their genome structures.

The discovery of antivirals to combat virus infection dates back to the 1970s when the first antiviral compound, aciclovir, was found to inhibit DNA replication of herpes simplex virus at concentrations lower than those affecting the production of cellular DNA [132]. This

discovery was a beacon of hope to both academics and clinicians as this meant that there was a possibility of counteracting the adverse effects of viruses. Today, there are more than 50 antiviral drugs [133, 134] that have been proven for treatment of several viral infections such as amantadine for influenza A infection, enfuvirtide for HIV infection, entecavir for hepatitis B virus (HBV) infection [134] and in more recent years, remdesivir for SARS-CoV-2 [135].

TABLE 3.2: Examples of human viruses and their genome structures

Genome	**Genome structure**	**Virus**
DNA	Double strand	Adenoviruses Herpesviruses HSV Cytomegalovirus VZV Papillomaviruses Poxviruses
	Single strand	Parvoviruses
	Partial double strand, replicating via RNA	Hepadnavirus HBV
RNA	Double strand, segmented	Reoviruses Rotavirus
	Single strand, positive strand	Flaviviruses HCV West Nile virus Yellow fever virus Dengue virus Picornaviruses hepatitis A or HAV Rhinovirus Togaviruses Rubella virus
	Single strand, negative strand, segmented	Orthomyxoviruses Influenza virus
	Single strand, negative strand, nonsegmented	Rabies virus Paramyxoviruses Mumps, measles, RSV
	Replicating via DNA	Retroviruses HIV

Drug resistance in viruses is usually discussed in the context of antiviral therapy. Through the process of evolution, viruses have acquired various attributes that enable them exacerbate infections and increase their burden on public health. Similar to many other antimicrobial resistant mechanisms, antiviral drug resistance depends on the viral mutation frequency,

intrinsic mutability of the antiviral target site, the selective pressure exerted by the drug, and the magnitude and rate of virus replication [136, 137]. In viruses, the process of random mutation combined with the ability to replicate quickly results in the selection of resistant strains with altered antiviral targets or antiviral activators [137]. In addition, in the absence of mechanisms to prevent rapid viral replication at greater rates, resistance to antiviral therapy develops quickly [136].

Generally, all viruses have one main mechanism for development of resistance to antivirals and vaccines. This is the evolutionary process that leads to selection of random mutations. In many instances, mutation leads to increased resistance of viruses to the antiviral drug. For example in the treatment of influenza infections using amantadine and rimantadine, resistant variants are selected so quickly in such a way that it is still possible for a treated person to pass on resistant virus to contacts [136, 138]. This mechanism has severely limited the clinical usefulness of these drugs. Table 3.3 summarises the resistance rate of some viruses and their corresponding clinical implications.

TABLE 3.3: Clinical consequences due to varying resistance rates. Adapted from [1]

Virus	**Resistance rate**	**Clinical outcome**
Vaccinia (DNA)	Very slow	Vaccine has eliminated virus from human population. Selective antiviral agents (e.g., ST 246) being developed as anti-bioterrorism agent. Resistance can be obtained in the laboratory but no clinical data available.
Polio (RNA)	Very slow	Vaccine has eliminated virus in most countries.
Varicella zoster (DNA)	Moderately slow	Vaccine expected to be effective for decades; antiviral slow therapy has not led to an increase ($< 1\%$) of resistant isolates among the immunocompetent patients (no increase in three decades) but some increase in immunocompromised patients.
Herpes simplex types 1 and 2 (DNA)	Moderately slow	No efficacious vaccine yet available but resistance to slow antiviral therapy similar to that with VZV.
Rubella, mumps, measles, HAV(RNA viruses) and HBV	Slow	Vaccines have remained clinically effective for years; antiviral resistance to therapy of HBV with single antiviral agents may occur (within one or a few years).
Influenza (RNA)	Fast	Vaccine needs to be updated at least annually. Resistance to antiviral compounds occurs in the population at various rates for different compounds (days to years).
HIV (RNA)	Very fast	No vaccine successful. Monotherapy leads quickly to resistance in individual patients. Combination therapy (3 or 4) gives low resistance rate.

In the particular case of SARS-CoV-2, the increase in emerging SARS-CoV-2 variants is promoted by two complementary pathways: infectivity and vaccine resistance [139, 140]. In the early stages of evolution of the virus, mutation leading to severe infections was dominant. However, since March 2021 when vaccination programmes were being rolled out [141, 3, 142]

and vaccines had provided protection to vaccinated populations, several vaccine-resistant mutations have been observed relatively frequently. Considering that a good portion of the population is still not vaccinated, mutations which cause severe infections and are resistant to vaccines still dominate among the prevailing and future variants [139].

3.3.1 Mathematical models for drug resistance in viruses

In the literature, it is possible to find several mathematical approaches to describe the transmission dynamics of viruses in a population during an epidemic [143]. Modelling the emergence of drug resistance in other viruses has been overshadowed by epidemic models relating to drug resistance in HIV. A few models of antiviral resistance have also been developed for HSV-2 and influenza [144, 145].

To predict (with a degree of uncertainty) the effectiveness of Antiretroviral therapy (ART) in San Francisco, Blower *et al* [146] developed and analyzed a mathematical model which includes the potential effects of ART on the transmission dynamics of both drug-sensitive and drug-resistant HIV strains. Their model keeps track of the infection dynamics of five groups: susceptible individuals (X), untreated individuals infected with either drug-sensitive (Y_S^U) or drug-resistant strains (Y_R^U), and ART-treated individuals infected with either drug-sensitive (Y_S^T) or drug-resistant strains (Y_R^T). The model equations are shown in the system (3.9) and illustrated in Figure 3.7.

$$\begin{aligned}
\frac{dX}{dt} &= \pi - X[c(\lambda_s + \lambda_R) + \mu] && \text{(3.9a)}\\
\frac{dY_s^U}{dt} &= Xc\lambda_s + Y_R^U q + Y_S^T - g_S - Y_S^U(\sigma_S + v_S^U + \mu) && \text{(3.9b)}\\
\frac{dY_S^T}{dt} &= Y_S^U\sigma_S - Y_S^T(g_S + r + v_S^T + \mu) && \text{(3.9c)}\\
\frac{dY_S^U}{dt} &= Xc\lambda_R + Y_R^T g_R - Y_R^U(q + e\sigma_R + v_R^U + \mu) && \text{(3.9d)}\\
\frac{dY_R^T}{dt} &= Y_R^U e\sigma_R + Y_S^T r - Y_R^T(g_R + v_R^T + \mu) && \text{(3.9e)}
\end{aligned}$$

In system 3.9, π is the rate at which gay men join the sexually active community; $1/\mu$ is the average time during which a gay man acquires new sex partners; c is the average number of new receptive anal sex partners per year; $1/q$ is the average time for an untreated drug-resistant infection to revert to a drug-sensitive infection; σ is the per capita effective treatment rate; e is the relative efficacy of ART in treating drug-resistant infections; r is the rate of emergence of resistance due to acquired resistance; g is the proportion of cases that give up ART per year; and v is the average disease progression rate. λ specifies the per capita force of infection for drug-sensitive (λ_S) and drug-resistant (λ_R) HIV. The total population size is $N(t) = X + Y_S^U + Y_R^U + Y_S^T + Y_R^T$.

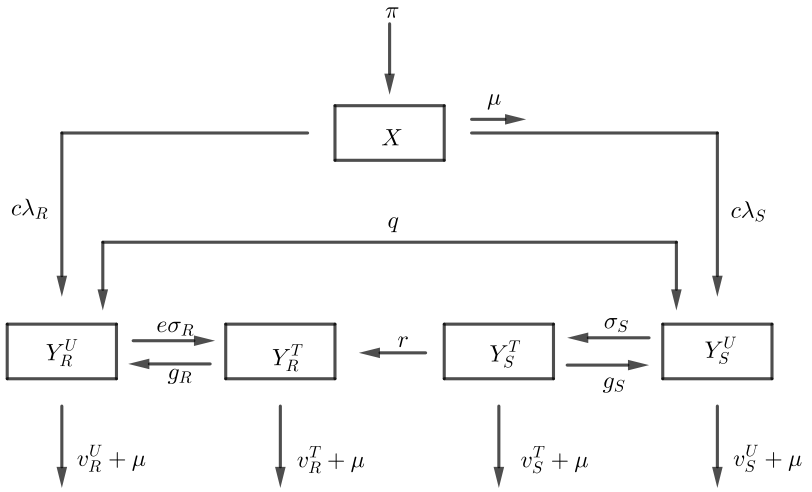

FIGURE 3.7: Schematic illustration of the transmission dynamics of an HIV epidemic in the presence of combination antiretroviral therapy (ART) by Blower *et al* [145]. Model equations are given in eq (3.9).

In this study, it was assumed that none of the possible ART-resistant HIV strains that could possibly evolve could be as transmissible as the wild type. The study also assumed that individuals infected with ART-sensitive virus undergoing treatment cannot be co-infected or superinfected by an ART-resistant strain. From their model, Blower *et al* predicted that acquired resistance will continue to be on the rise, but transmitted resistance is likely to increase only gradually, with a doubling time of around four years and a predicted median of 15.6% new HIV infections likely to be resistant to antiretroviral drugs by 2005. Although their analysis predicts a stabilisation of transmitted ART resistance at low levels, the predicted range around the 15.6% is very wide (0.05% to 73.21%). With this, the authors argue that the higher values in the range generated from their sensitivity analysis have a very low probability.

Another virus of concern relating to drug resistance is influenza. The emergence of influenza drug resistance has become of particular interest as current planning for an influenza pandemic involves using massive amounts of antiviral drugs. Dobrovolny *et al* [22] developed stochastic models to simulate the emergence of drug resistant strains in the course of infection within a host patient in the presence and absence of antiviral therapy. The antiviral used in this study is adamatanes. Specifically, this model examines the effects of antiviral mechanism, immune response, and surface proteins on the emergence of drug resistant strains

in the host. Their model equations are as follows (see eq (3.10)):

$$\frac{dT}{dt} = -T\sum_i \beta_i V_i \tag{3.10a}$$

$$\frac{dE_i}{dt} = (1-m_i)\beta_i T V_i - \frac{E_i}{\tau_E} \tag{3.10b}$$

$$\frac{dI_i}{dt} = \frac{E_i}{\tau_E} - \frac{I_i}{\tau_i} \tag{3.10c}$$

$$\frac{dV_i}{dt} = (1-n_i)p_i\sum_j \rho_{ij} I_j - cV_i, \tag{3.10d}$$

where T is the pool of uninfected, susceptible target cells. When a target cell is infected, it enters the eclipse phase, E_i, where the cell is infected with viral strain i but is not yet producing virions. Cells remain in the eclipse phase for an average time τ_E before becoming infectious. Infectious cells, I_i, are cells infected with viral strain i, releasing virions of strain i at constant rate p_i with probability ρ_i, and of strain j at constant rate p_j with probability ρ_{ij}. Infectious cells die after producing virus continuously for an average time τ_I. Infection rate is β_i.

From their study, Dobrovolny *et al* [22] found that adamantanes, because they act at the start of the replication cycle to prevent infection, are less likely to produce drug-resistant mutants than other drugs, which act at the end of the replication cycle. They also found that immune response subdues slow growing infections thereby further decreasing the probability that a drug resistant mutant will arise and lead to drug-resistant infection. Even in the absence of any drug treatment, their model predicts that drug-resistant mutants will be present during an infection, potentially in large enough numbers and can be transmitted to other individuals. This finding is in agreement with other previous studies in bacteria [16].

Furthermore, investigating the spread of influenza infections in a closed population, Stilianakis *et al* [143] developed a model to determine the effects of different treatment strategies on the spread of the infection. Using a complex SIR model, the authors consider the effect of treatment either before infection or after infection. The model is given as in eq (3.11) where S represents susceptible persons, S_{pr} represents susceptible persons taking drug before infection, I = infected untreated persons, I_s shows infected untreated persons who develop clinical symptoms, I_r shows infected untreated asymptomatic persons who shed drug-resistant virus, $I_{s,r}$ shows infected untreated persons with clinical symptoms who shed drug to the resistant virus, I_{tr} shows infected treated persons, $I_{s,tr}$ shows infected treated persons who develop clinical symptoms, $I_{r,tr}$ represents infected treated asymptomatic persons who shed drug-resistant virus, and $I_{s,s,tr}$ represents infected treated persons with clinical symptoms who

shed drug-resistant virus.

$$\frac{dS}{dt} = -(\beta_1 I + \beta_2 I_s + \beta_{1,r} I_r + \beta_{2,r} I_{s,r} + p_1\beta_1 I_t r + p_2\beta_2 I_{s,tr} + \beta_{1,r} I_{r,tr} + \beta_{2,r} I_{s,r,tr})S - \theta_1 S \tag{3.11a}$$

$$\frac{dS_{pr}}{dt} = -(p_3\beta_1 I + p_4\beta_2 I_s + \beta_{1,r} I_r + \beta_{2,r} I_{s,r} + p_5\beta_1 I_t r + p_6\beta_2 I_{s,tr} + \beta_{1,r} I_{r,tr} + \beta_{2,r} I_{s,r,tr})S_{pr} + \theta_1 S \tag{3.11b}$$

$$\frac{dI}{dt} = (\beta_1 I + \beta_2 I_s + p_1\beta_1 I_{tr} + p_2\beta_2 I_{s,tr})S - (\gamma_1 + \delta_1 + \theta_2)I \tag{3.11c}$$

$$\frac{dI_s}{dt} = \delta_1 I - (\gamma_2 + \theta_3)I_s \tag{3.11d}$$

$$\frac{dI_r}{dt} = (\beta_{1,r} I_r + \beta_{2,r} I_{s,r} + \beta_{1,r} I_{r,tr} + \beta_{2,r} I_{s,r,tr})S + (\beta_{1,r} I_r + \beta_{2,r} I_{s,r})S_{pr} - (\gamma_1 + \delta_2 + \theta_2)I_r \tag{3.11e}$$

$$\frac{dI_{s,r}}{dt} = \delta_2 I_r - (\gamma_2 + \theta_3)I_{s,r} \tag{3.11f}$$

$$\frac{dI_{tr}}{dt} = (p_3\beta_1 I + p_4\beta_2 I_s + p_5\beta_1 I_{tr} + p_6\beta_2 I_{s,tr})S_{pr} - (r_1\gamma_1 + \delta_3 + q_1\kappa)I_{tr} + \theta_2 I \tag{3.11g}$$

$$\frac{dI_{s,tr}}{dt} = \delta_3 I_{tr} - (r_2\gamma_2 + q_2\kappa)I_{s,tr} + \theta_3 I_s \tag{3.11h}$$

$$\frac{dI_{r,tr}}{dt} = (\beta_{1,r} I_{r,tr} + \beta_{2,r} I_{s,r,tr})S_{pr} - (\gamma_1 + \delta_4)I_{r,tr} + q_1\kappa I_{tr} + \theta_2 I_r \tag{3.11i}$$

$$\frac{dI_{s,r,tr}}{dt} = \delta_4 I_{r,tr} - \gamma_2 I_{s,r,tr} + q_2\kappa I_{s,tr} + \theta_3 I_{s,r} \tag{3.11j}$$

In their model, eq (3.11), transmission of infection from infected individuals to susceptible individuals occurs with a rate β. Transition from the asymptomatic infected to the symptomatic infected stage occurs with a rate δ and the rate of development of drug resistance is κ. Infected persons recover and become immune with a rate γ (infectivity period is $1/\gamma$). The rate at which treatment is given before infection is given is denoted as μ and the rate at which treatment is given is denoted as σ. p_i represents the relative infectivity of wild type virus during treatment compared with that of wild type virus without drug intervention, q_1 and q_2 correspond to the likelihood of developing drug resistance from I_{tr} and $I_{s,r,tr}$ respectively.

In this model, it was assumed that drug treatment has no effect on viral replication and

that the reduction of transmissibility in susceptibles is about one-third that of an encounter with an I or I_s person. It is also assumed that there is no difference in transmission for contacts of susceptible and infected persons with clinical symptoms shedding resistant virus whether treated or not. Figure 3.8 illustrates the epidemic curves as predicted by the model in (3.11-3.11j).

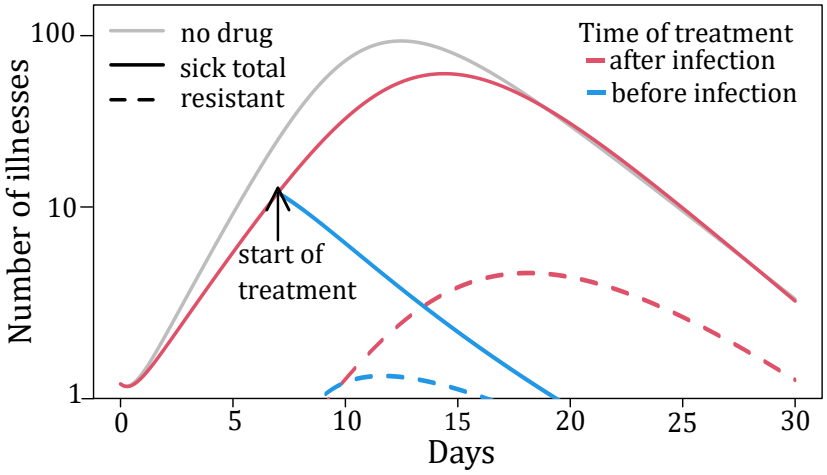

FIGURE 3.8: Epidemic curves as predicted by eq (3.8). Number of infected individuals using treatment only (red) or using prophylaxis in addition to treatment(blue) over the first 30 days of the epidemic. The gray line shows the course of the epidemic without any intervention. The solid lines depict the total number of infected individuals, whereas the dashed lines depict the number of individuals infected with resistant virus.

Comparing different strategies in their analysis, the researchers found that the optimal strategy (in their study) which leads to low infection levels during an epidemic involves drug treatment before infection. With this strategy, a considerable high number of people remain susceptible to infection. Thus, there is low emergence of drug resistance as a strong blocking of the epidemic occurs and the epidemic is shorter than without any intervention. In a pandemic, this approach moderately reduces the number of symptomatic infected individuals. They also found that both treatment before and after infection strongly suppress the epidemic with low emergence of drug-resistant virus. However, this depends heavily on the relative transmissibility of resistant and wild type virus.

3.4 Epidemic burden of SARS-CoV-2

The novel Coronavirus SARS-CoV-2 epidemic first emerged in December 2019 [147, 148, 149, 150]. It was considered to have originally started via a zoonotic transmission associated with a seafood market in Wuhan, China. Later, it was discovered that human to human transmission was possible with this virus and that such transmission significantly contributed

to the subsequent viral outbreak. The disease caused by this virus was called Coronavirus Disease 19 (COVID-19). It has also been shown that this novel Coronavirus is structurally related to the virus that causes severe acute respiratory syndrome (SARS, 2002 and 2003) and Middle East respiratory syndrome (MERS, 2012 to the present) [149, 151]. Since its discovery, SARS-CoV-2, has spread globally, causing high levels of mortality and morbidity worldwide and poses as a critical challenge for public health, research, and medical communities. On January 30, 2020, the W.H.O. Emergency Committee declared a global health emergency based on increasing case notification rates of the disease globally [147].

Coronaviruses are enveloped, positive single-stranded large RNA viruses that not only infect humans, but also a variety of animals including birds and bats [150, 152]. For a long time, human coronaviruses circulate in the population and have been known to cause seasonal and usually mild respiratory tract infections associated with symptoms of the common cold. In contrast, SARS, MERS and SARS-CoV-2, which have emerged in the human population over the past 20 years, are highly pathogenic and may potentially cause severe disease and fatalities. By infecting bronchial epithelial cells and the upper respiratory tract cells in humans, SARS, MERS and SARS-CoV-2 infections can develop into severe, life-threatening respiratory infections and lung injuries for which no definite therapy has been approved to date [153].

Since its inception, COVID-19 has impacted a large number of people worldwide, being reported in approximately 200 countries and territories. As of August 3rd, 2021, around 200 million cases and 4 million deaths have been recorded worldwide according to the Center for Systems Science and Engineering (CSSE) at John Hopkins University [154]. Though prevalent in all age groups, epidemiological studies have shown that mortalities are much higher in elder population than in children [155, 156, 157].

The symptom of patients infected with SARS-CoV-2 ranges from minimal symptoms to severe failure of respiratory organs with a large portion of the population being asymptomatic carriers. The most common reported symptoms include fever (83%), cough (82%) and shortness of breath (31%) [158, 159, 160, 153]. Gastrointestinal symptoms such as vomiting, diarrhea, and abdominal pain are described in 2–10% of the patients with COVID-19, and in 10% of patients, diarrhea and nausea precede the development of fever and respiratory symptoms [161, 162, 151].

As with other respiratory viruses, SARS-CoV-2 transmission occurs with high efficacy mainly through the respiratory route. The main recognized route of transmission of the virus is through droplets and aerosols although the oral-fecal route may be another route of transmission of the virus. In the course of the outbreak of the virus, viral particles have been

detected on inanimate surfaces such as door handles and the surface of cell phones in residential sites of patients with confirmed COVID-19. Thus, individuals who come into contact with infected surfaces could be infected if they touch their eyes, mouth or nose [153, 158].

To curb the spread, the WHO recommends standard precautions for all patients, which are also appropriate for public prevention, including hand and respiratory hygiene, the use of appropriate personal protective equipment, safe waste management, environmental cleaning and sterilization of patient-care equipment. Governments across the world have implemented these measures ranging from quarantining, social distancing, wearing of face masks among others. Amidst this crisis, national health care systems such as in Italy and the United States of America have been overwhelmed by the ever-increasing number of infection cases [163].

At the start of the epidemic, pharmaceutical companies have been in a race to produce safe and highly effective vaccines to counter transmission of the disease. As of December 2020, there were 52 vaccine candidates in clinical trials in humans, 13 of which were in Phase 3 trials [2]. In November 2020, some pharmaceutical companies and institutes, including Pfizer Inc and BioNTech, Moderna, the University of Oxford (in collaboration with AstraZeneca), announced positive results from the first interim analyses of their Phase 3 vaccine trials [164, 165, 166]. Initial data released from these trials report that the vaccines manufactured by Pfizer Inc/BioNTech and Moderna both yielded 95% efficacy whereas that by University of Oxford (in collaboration with AstraZeneca) yielded 70% efficacy. On 2 December 2020, the UK medicines regulator MHRA granted a temporary regulatory approval for the Pfizer-BioNTech vaccine [142] which was under evaluation for emergency use authorization (EUA) status by the United States Food and Drug Administration [167] and approved for use on 11 December 2020 [142] in the United States.

Although the Pfizer, Moderna and University of Oxford/AstraZeneca vaccines are being used worldwide, in other countries such as China and Russia, other vaccines (from Sinovac in China and Gameleya Research Institute in Russia) have been developed and are currently in limited use. Table 3.4 summarizes candidate vaccines currently in use as well as their manufacturers and vaccine platform (that is, a system which uses certain basic components as the backbone but is relatively flexible and can be adapted quickly to be used against different pathogens [168]).

3.4.1 Mathematical modelling of SARS-COV-2

To understand and curb the spread of the disease, COVID-19 epidemiological models have been formulated. Many of these models follow an SIR framework [169, 170] either in the deterministic or stochastic form or both [171, 172, 173, 174, 175, 176]. Other variations and modifications to this general model have been considered including SEIR [177, 178, 179]

TABLE 3.4: List of candidate vaccines currently in use. Adapted from [2] and [3]

SARS-CoV-2 Vaccine Manufacturer / Developer	**Vaccine platform**	**Timing of doses**	**Overall Efficacy (from [3])**
University of Oxford/AstraZeneca	Non-replicating viral vector	0, 28 days	74%
Sinovac	Inactivated	0, 14 days	50%
Janssen Pharmaceutical Companies	Non-replicating viral vector	0 or 0, 56 days	72%
Moderna/NIAID	RNA	0, 28 days	92%
CanSino Biological Inc./Beijing Institute of Biotechnology	Non-replicating viral vector		66%
BioNTech/Fosun Pharma/Pfizer	RNA	0, 21 days	95%
Beijing Institute of Biological Products/Sinopharm	Inactivated	0, 21 days	73%
Novavax	Protein subunit	0, 21 days	89%
Gameleya Research Institute / Sputnik	Non-replicating viral vector	0, 21 days	91%
Medicago Inc.	Virus-like particle (VLP)	0, 21 days	–

and SIRD [180] compartmental models. Some models also include parameters such as age-heterogeneity [181], guiding the flow of users in supermarkets [182], and governmental policies [179, 183, 184]. In addition, a few studies incorporate the dynamics of the disease within an individual host [185, 186]. However, only a few of these models consider the structure of the population and the underlying interactions between individuals [187, 188, 189]

Fitting a stochastic model to publicly available data in Wuhan, Kucharski *et al* estimated the early dynamics of SARS-COV-2 transmission in Wuhan [178]. Their model follows an SEIR formulation and accounts for delays in symptom onset. In this model, a Poisson distribution is used to model newly symptomatic cases, reported onsets of new cases and reported confirmation of cases. Furthermore, transmission was modelled as a geometric random walk process and sequential Monte Carlo simulations were used to infer the transmission rate over time and the resulting number of cases as well as the basic reproduction number.

In their study, Kucharski*et al* [178] estimated that the median daily reproduction number in Wuhan decreased from 2.35 one week before travel restrictions were introduced on Jan 23, 2020, to 1.05 one week after indicating the effect of travel control measures on the transmission of the disease. Their findings also suggest a 50% probability of infection spread in places where there are at least four new cases in the population. Thus, as more cases are reported, there is a likelihood of the incidence of new outbreaks in the population.

Using ordinary differential equations (ODEs) and data from patients in Germany, Hernandez-Vargas *et al* [185] modelled the viral kinetics of SARS-COV-2 within the host [185]. In their work, they presented different mathematical models in an attempt to adjust viral kinetics in patients in the data. The mathematical models considered include a so-called target cell-limited model which divides the cell population into susceptible, infected and viral cells and an immune response model for SARS-CoV-2 which is based on T-cell response to infection from the virus.

From their findings, the best model that fits the data is the one which includes immune cell response. This model is a minimalistic viral replication model for influenza infection and is utilised in this study owing to the role of T-cells in clearing Influenza infections within the host. This model assumes that the virus (V) level induces the proliferation of T-cells (T) and is represented with a logistic function with maximum carrying capacity K, growth rate ρ and viral clearance rate c. The model also assumes that the activation of T cell proliferation by the virus follows a log-sigmoidal form with half saturation constant kT and width m. The terms s_T and δ_T in eq (3.12-3.13) represent cell homoeostasis and half-life of T-cells respectively and the term $c_T VT$ represents the rate of killing infected cells by the immune response [185]. This formulation is as follows:

$$\frac{dV}{dt} = \rho V\left(1-\frac{V}{K}\right) - c_t VT - cV \tag{3.12}$$

$$\frac{dT}{dt} = s_T + rT\left(\frac{V^m}{V^m + k_T^m}\right) \tag{3.13}$$

Although limited to data collected at the beginning of infection, analysis of the model (3.12-3.13) suggests that T-cell response slowly mounts up against the virus peaking between 5 to 10 days post infection. These findings also agree with the data and act as evidence to support the slow rate of replication by the SARS-CoV-2 virus.

3.5 Chapter summary

In the absence of the development of new drugs and success of treatment strategies, mathematical models can be used to understand the problem of drug resistance. Several mathematical models describing the problem of drug resistance evolution exist and can provide some insights for public health policies. These models vary in structure, methodology and aim. From deterministic ordinary differential equations to mechanistic individual-based models, models for resistance aim to explore some biologically relevant foci ranging from evolution and spread of resistance to immune response to resistance.

In this chapter, we have discussed the biological underpinnings of resistance and provided analysis of studies pertaining to the evolution of drug resistance in bacteria and viruses at within and between host levels. We have seen how mathematical modelling is crucial to understanding the problem of drug resistance in microorganisms in the absence of the development of new drugs and success of treatment strategies. Mathematical models describing the problem of resistance evolution and capable of providing some insights for public health policies have been discussed.

Deterministic models are popular at both between-host and within-host levels for drug resistance infections in bacteria. These epidemiological models have been used to study various groups of a population with emphasis on treatment with single or multiple antibiotics, emergence of dual resistance and interplay with immune response. Though not extensively used, models involving stochastic processes can be used to provide simplified solutions to questions posed by these deterministic models. Pharmacodynamic properties of antibiotics are also considered by PK/PD models which give insight into immune response to drug resistance.

Appropriate dosing regimens and therapy duration have also been questionable. For within-host models, a high antibiotic dose eliminates resistant strains whilst a low antibiotic dose subdues the less fit resistant strain. An intermediate antibiotic dose however, leads to the emergence of resistance [72]. Though verified by experimental studies, these model predictions should be fitted to *in vivo* data for validation. Some studies validate that prolonged antibiotic treatment can lead to the emergence and spread of resistance in the host whereas frequent antibiotic doses in small fractions can lead to the clearance of more resistant strains.

Chapter 4

Within-Host Resistance

Therapy switching has been identified as one of the methods that can be used for the gradual eradication of resistant strains on the long term. This chapter explores the use of positive switched systems to describe the dynamics of resistance infections within the host. We provide a background on the notion of collateral sensitivity and cross resistance and discuss how this notion can be exploited to mitigate antimicrobial resistant infections within a host patient, using notions from control engineering. Using numerical simulations, we compare different drug switching strategies and explore their performance in eradicating resistant strains within the host.

4.1 The phenomenon of collateral sensitivity

Biochemical or phenotypic resistance may arise in cells spontaneously or be acquired as a result of exposure to a drug. This kind of resistance is thought of to be as a result of the modification of cellular phenotype due to genetic factors which causes these phenotypes to have varying resistance properties [16, 190]. In cancer patients for example, exposure to cancer therapy causes the development of resistance to drugs [191]. Although treatment with appropriate curative therapy decreases tumor burden in some cases, in other cases, a relapse can occur after the commencement of treatment [192].

The survival of a resistant strain depends on the environment and population characteristics. In the absence of antibiotics, the growth of resistant cells is often slower than that of sensitive cells [16, 191]. The presence of antibiotics causes the production of enzymes which can lead to the expression of resistance thereby preventing the growth of sensitive cells. With the use of antibiotics, it is possible for a strain susceptible to one drug to generate resistant cells which are susceptible to another drug. Over time, the newly developed susceptible cells

can also generate cells which are resistant to the current drug but susceptible to a different drug. This continuous occurrence of resistant and susceptible cells can eventually lead to the appearance of resistant cells susceptible to the initial drug used. This phenomenon is known as *Collateral Sensitivity* (CS) [30, 193] and its converse is known as *Cross Resistance* (CR) (see Figure 4.1).

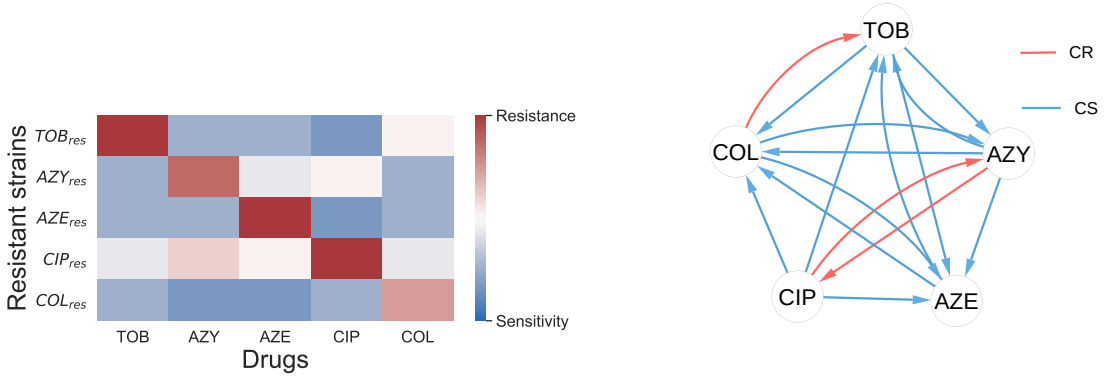

(A) (B)

FIGURE 4.1: Evolution of antibiotic resistance in five drugs commonly used for the treatment of *P.aeruginosa* infections in cystic fibrosis. TOB: Tobramycin, AZY: Azithromycin, AZE: Aztreonam, CIP: Ciprofloxacin, COL: Colistin. (a) Heatmap of collateral sensitivity and cross resistance of evolved resistant strains of antibiotics. It represents the collateral sensitivity matrix for evolved resistant cell lines (columns) tested against another drug (rows). (b) Network of collateral interactions from (a). Blue arrows represent CS and red arrows represent CR. The directed path of each arrow represents the collateral susceptibility or cross resistance of a drug-resistant strain on the drug. Adapted from [31].

Several studies have suggested the use of collateral sensitivity as a new treatment strategy for combating drug resistance infections through a drug scheduling protocol called *Collateral Sensitivity Cycling* (CSC) [31, 192, 193, 29, 114]. In general, collateral sensitivity cycling is a treatment framework in which traditional antibiotic cycling is done using drugs which have compatible collateral sensitivity profiles. By cycling between drugs which are collaterally sensitive, resistance cells can always be targeted and the life span of drugs can be extended as drugs are reintroduced. Experimental analysis of drug-resistant strains of *E. coli* have shown collateral interactions between Aminoglycosides, such as tombramcyin and kanamycin, and other classes of antibiotics [194]. In drug-resistant strains of *P. aeruginosa*, Imamovic *et al* found that about 75% of resistant strains exhibited collateral sensitivity to at least one antibiotic and 78% of these could be possible candidates for collateral sensitivity cycling.

Modeling of infectious diseases has been developed at different scales [195]. At the epidemiological level, models have helped to propose new vaccination strategies or support public health strategies [196, 197]. At within-host level, mathematical modeling has been used to capture the dynamics of different infectious diseases inside the host (patient) to understand

the interaction of the pathogen and the immune system, as well as scheduling of therapies [198, 199, 200].

Most mathematical models to represent microbe dynamics are shown to be based on variations of the classical Verhulst logistic growth equation. In a general form, this model is given by

$$\frac{dP}{dt} = rP\left(1 - \frac{P}{K}\right) \tag{4.1}$$

where P is the population at time t, r is the growth rate and K is the carrying capacity of the population (that is the maximum value that P can reach). This model has served as a key mathematical tool in representing the growth of tumors [201] and microbes [202]. Although other models, including exponential growth models [203] and stochastic growth models [191, 16, 204] have been used to study drug resistance in microbes, such models are often limited by the assumption of a constant growth rate which oversimplifies cell growth and development of resistance. The logistic model however, considers that a population will proliferate and reach a limiting saturation level of resources of the human body, known as the carrying capacity [205, 203].

In the literature, infections have been studied using the notion of switched positive dynamical systems [206, 207]. A switched positive system generally refers to a hybrid dynamical system consisting of a family of continuous-time subsystems and a rule which brings about the switching between them. Interest in switched systems has increased recently due to their applications in diverse areas such as economics, engineering and biology, to mention a few [34, 208, 209, 210]. The feedback stabilization of such systems has received a lot of attention and numerous tools have been developed to make such analysis. In particular, the use of control Lyapunov functions have gained wide popularity in studying the stabilization of both linear and nonlinear switched systems [211, 212]. Studies show that for switched systems, control Lyapunov functions provide a robust feedback solution for achieving stability [213]. Though widely used in engineering and biology, these types of systems have also been applied in studying infectious diseases [207, 206].

While theoretical approaches to mitigate drug resistance have been mainly developed at between-host level [48][111], too little has been directed to investigate within-host strategies against antimicrobial resistance [207]. Our goal is to abstract the concept of collateral sensitivity in relation to drug-resistant infections as studied by the clinical investigations of Imamovic *et al* [31] and develop examples of tailored therapy cycling strategies towards the eradication of drug-resistant microbes within the host.

In this chapter, we develop a mathematical abstraction of the dynamics of antimicrobial resistance in the form of non-linear switched systems. We make use of dynamical systems based on logistic equations. We then develop different switching control techniques designed

to minimize the appearance of drug resistant bacteria within the host. Using numerical simulations, we present and compare these techniques for the mitigation of drug resistance.

4.2 Logistic switching maps to model drug resistance

Mathematical modelling of antimicrobial resistance can be done using logistic equations. Logistic equations are well-known differential equations used to model population growth and interactions between two or more populations. When using these equations, it is assumed that the growth rate of the population is proportional to the existing population and the amount of resources available. With numerous applications in other scientific fields, logistic equations are used to explore dynamical systems which exhibit bifurcations and chaos.

The dynamics of antibiotic resistance can be described using the following general switched logistic system as proposed by [214]. This model describes the interaction between genetic bacterial strains and helps tailor appropriate interventions. The model equation is as follows:

$$\dot{x}_i(t) = \rho_{i,\sigma(t)} x_i(t) \left(1 - \tfrac{x_i(t)}{K}\right) - \delta_{\sigma(t)} x_i(t) + \mu \sum_{j=1}^{n} m_{ij,\sigma(t)} x_j(t) \tag{4.2}$$

defined for all $t \geq 0$, and where $x_i : i = 1, 2, 3, ..., n$ with n representing different bacterial strains. Each state x_i denotes a strain of bacteria which is either sensitive or resistant to any particular drug used. μ is the mutation rate. $\delta_{\sigma(t)}$ is the bacterial clearance depending on the drug used. $\rho_{i,\sigma(t)}$ is the proliferation rate of the strain i under therapy σ at any time t. $m_{ij,\sigma(t)}$ represents the mutation from strain i to strain j under therapy σ at any time t. K defines the maximum carrying capacity and $\sigma(t)$ denotes the switching signal (see Section 2.2.2.1) based on the treatment policy such that $\sigma(t)$ takes values in $\{\sigma_1, \sigma_2, \ldots, \sigma_N\}$ with N representing the number of drugs. All parameters and initial conditions are assumed to be non-negative so that $x_i(0) \geq 0$ for $i \in \{1, 2, \ldots, n\}$. A description of all parameters used can be found in Table 4.1.

By setting K equal to 1, we can express eq (4.2) in matrix notation as follows:

$$\dot{x}(t) = \text{diag}\{x\}[P_{\sigma(t)} - \text{diag}\{R_{\sigma(t)}\}x^T] + \mu M_{\sigma(t)} x(t) \tag{4.3}$$

where $x = (x_1, x_2, \ldots, x_n) \in \mathbb{R}^n$, $R_{\sigma(t)} = (\rho_{1,\sigma(t)}, \rho_{2,\sigma(t)}, \ldots, \rho_{n,\sigma(t)}) \in \mathbb{R}^n$ and $P_{\sigma(t)} = (R^T_{\sigma(t)} - \delta_{\sigma(t)}) \in \mathbb{R}^n$. The mutation matrix $M_{\sigma(t)} := [m_{ij,\sigma(t)}] \in \mathbb{R}^{n \times n}$ defines the observed mutations based on the therapy, σ, in use at time t.

Remark. The mutation matrix, $M_{\sigma(t)}$ describes how strains gain or lose sensitivity or resistance, thereby, altering the bacterial composition of the system without changing the total

number of bacteria. The main diagonal of this matrix should be non-positive, as a positive diagonal implies that a strain can mutate into itself, which is not biologically feasible.

TABLE 4.1: Description of parameters used.

Parameter	Description
K	carrying capacity
n	number of bacterial strains
t	time variable
N	number of drugs or therapy
$\sigma(t)$	switching signal dependent on therapy.
$\rho_{i,\sigma(t)}$	proliferation rate of strain i under drug σ at time t
μ	mutation rate
$\delta_{\sigma(t)}$	clearance rate depending on drug σ at time t
$M_{\sigma(t)}$	mutation matrix describing observed mutations based on $\sigma(t)$. $M_{\sigma(t)} := [m_{ij,\sigma(t)}] \in \mathbb{R}^{n\times n}$

In the subsequent sections, we employ notions in control engineering and positive switched systems, to develop control techniques based on Lyapunov functions to minimize the appearance of drug resistant bacteria within the host. We begin with a model of two strains of a pathogen and with two treatment options and continue with a more general form of this model with several treatment strategies. We analyse each of these models and carry out numerical simulations to explore therapy switching strategies towards eradication of resistant strains.

4.3 Two strain model for antimicrobial resistance

With the use of therapy, it is possible for a strain susceptible to one drug to generate resistant strains which are susceptible to another drug by a phenomenon known as collateral sensitivity [30]. Over time, the newly developed susceptible strains can also generate strains which are resistant to the current drug but susceptible to a different drug. This continuous occurrence of resistant and susceptible strains can eventually lead to the appearance of resistant strains susceptible to the initial drug used.

4.3.1 Model analysis without switch between therapies for two pathogen strains

Our aim is to illustrate a hypothetical scenario of collateral sensitivity using a two-strain bacterial population, x_1 and x_2, where each strain represents a family of strains sharing the same susceptibility to a given drug. Assuming that each mutation changes the susceptibility

of the bacteria from one family to the other, the connection between the families can be written by the following symmetric matrix:

$$M = \begin{bmatrix} -1 & 1 \\ 1 & -1 \end{bmatrix}.$$

For this two-strain system, we can express eq (4.2) based on the aforementioned assumptions, where $M_{\sigma(t)} := [m_{ij,\sigma(t)}] \in \mathbb{R}^{2\times 2}$ and $\sigma(t) \in \{\sigma_1, \sigma_2\}$ as:

$$\dot{x}_1 = [-\delta + \rho_1 (1 - x_1)] x_1 + \mu(-x_1 + x_2) \tag{4.4a}$$

$$\dot{x}_2 = [-\delta + \rho_2 (1 - x_2)] x_2 + \mu(x_1 - x_2). \tag{4.4b}$$

All parameters and initial conditions are assumed to be non-negative so that $x_1(0) \geq 0$ and $x_2(0) \geq 0$.

A schematic illustration of this model is shown in Figure 4.2

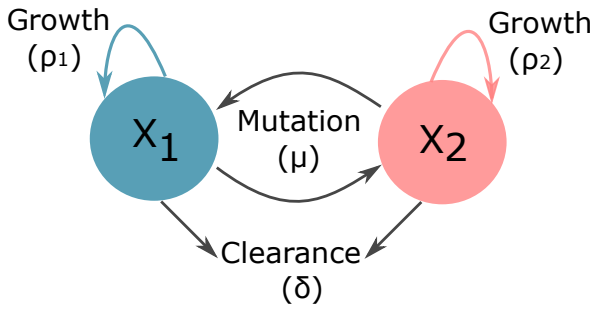

FIGURE 4.2: Schematic illustration of the model (4.4). x_1 and x_2 are two bacterial strains with proliferation (growth) rates ρ_1 and ρ_2 respectively, mutation rate μ and clearance rate δ.

Further qualitative characterisation of the model with and without switching is considered in the subsequent sections.

4.3.1.1 Equilibrium points and stability

Equilibrium points

The substitution method is used to find the equilibrium points of the system. Equating the right hand side of eqn (4.4) to zero, an expression for x_2 in terms of x_1 is obtained from eq (4.4b) which is substituted into eq (4.4a) to obtain a quartic polynomial, $H(x_1)$ described explicitly as :

$$H(x_1) = \frac{x_1\left(-\mu\rho_1 x_1(\delta+\mu)\right)}{\mu^2} + \frac{x_1\left(\rho_1\left(\delta+\mu-\rho_2\right)+\rho_2(\delta+\mu)-\delta(\delta-2\mu)\right)}{\mu} - \frac{x_1\left(\rho_2\left(\rho_1\left(x_1-1\right)\left(2x_1(\delta+\mu)-\mu\right)+x_1(\delta+\mu)^2+\rho_1^2\left(x_1-1\right)^2 x_1\right)\right)}{\mu^2}$$

and

$$x_2(x_1) = \frac{\delta x_1 + \mu x_1 + \rho_1 x_1^2 - \rho_1 x_1}{\mu}.$$

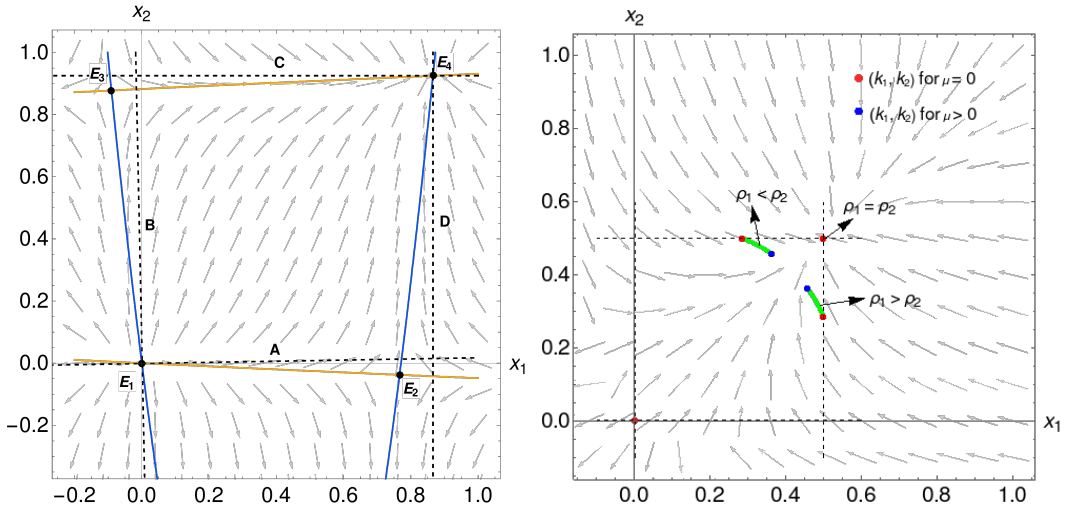

FIGURE 4.3: Graphical view of equilibrium points for system (4.4). Equilibrium points as a result of substitution method. Red lines: trace of intersection points to $x_2(x_1)$ curve. (left) Vector fields around the four equilibrium points; two with non-negative coordinates (E_1 and E_4) and two with negative components (E_2 and E_3). (right) Dependence of E_4 on parameters. Red dots represent the value of E_4 for $\mu = 0$ and blue dots for $\mu > 0$. The green lines show the translation of equilibrium point (k_1, k_2) from $\mu = 0$ to $\mu > 0$. If $\rho_1 = \rho_2$, E_4 is unchanged for both $\mu = 0$ and $\mu > 0$.

$H(x_1)$ and $x_2(x_1)$ are plotted on the same axis. The intersection of $H(x_1)$ with the abscissa gives the x_1-components of the equilibrium points. The coordinates of these intersection points to the curve $x_2(x_1)$ give the corresponding x_2-components and hence characterize the equilibrium points. This is illustrated in Figure 4.3(a), which shows four equilibrium points: the trivial equilibrium point $E_1(0,0)$, where both populations are zero, two others E_2, E_3 and a coexistence equilibrium at $E_4(k_1, k_2)$, where both populations are positive.

Depending on the parameter values, only two or all four equilibrium points are admissible: the origin (which always exists) and (under certain conditions) a coexistence equilibrium in the positive orthant. The points (E_2 and E_3) are not admissible because the values of x_1 and x_2 are negative at E_2 and E_3 respectively. Hence, the only biologically meaningful equilibrium points are the origin E_1 and the positive coexistence equilibrium at E_4.

A vector field plot of system (4.4) depicts these equilibrium points and gives a hint of the nature of their stability. This is shown in Figure 4.3 which also illustrates the dependence of E_4 on parameter values.

Stability

The origin, $E_1(0,0)$ is a common equilibrium point which always exists independent of the parameters thus, making it the point of interest from the stability point of view. Since $E_1(0,0)$ is a common equilibrium point, once its stability is addressed, the stability of E_4 can be inferred. The Jacobian matrix for eq (4.4) is

$$J_{(x_1,x_2)} = \begin{pmatrix} -\delta - \mu + \rho_1 - 2\rho_1 x_1 & \mu \\ \mu & -\delta - \mu + \rho_2 - 2\rho_2 x_2 \end{pmatrix}$$

with eigenvalues

$$\lambda_{1,2} \quad = \tfrac{1}{2}\left[-2\delta - 2\mu + G(x_1,x_2)\right] \pm \sqrt{4\mu^2 - G(x_1,x_2)^2} \tag{4.5}$$

where $G(x_1,x_2) = 2\rho_1 x_1 + \rho_1 - 2\rho_2 x_2 + \rho_2$

At the origin, the trace and determinant of the Jacobian matrix are:

$\text{tr} = -2(\delta + \mu) + \rho_1 + \rho_2$,

$\det = \delta^2 + \mu(-\rho_1 - \rho_2) + \delta(2\mu - \rho_1 - \rho_2) + \rho_1\rho_2$.

Thus, for stability of $E_1(0,0)$, the restriction of $\tau < 0$ and $\Delta > 0$ is satisfied by the conditions:

$$\text{C1} : \mu > \frac{(\delta - \rho_1)(\delta - \rho_2)}{-2\delta + \rho_1 + \rho_2} = \mu_c \text{ and C2} : 2\delta > \rho_1 + \rho_2 \tag{4.6}$$

where μ_c is a critical mutation rate.

It follows that whenever both $\rho_1 > \delta$ and $\rho_2 > \delta$, then $\mu_c > 0$ and $-2\delta + \rho_1 + \rho_2 > 0$. The former is a contradiction to C2 and consequently E_1 is not stable. However, when both $\rho_1 < \delta$ and $\rho_2 < \delta$, then $-2\delta + \rho_1 + \rho_2 < 0$ and $\mu_c < 0$. Thus E_1 is stable for any value of $\mu > 0$. Furthermore, if either $\rho_1 > \delta$ and $\rho_2 \leq \delta$ or $\rho_1 \leq \delta$ and $\rho_2 > \delta$ but their sum $(\rho_1 + \rho_2)$ still satisfies C2, then $(\delta - \rho_1)(\delta - \rho_2) < 0$ and $-2\delta + \rho_1 + \rho_2 < 0$ so $\mu_c > 0$. The origin is not always stable in this case and there exist some values of μ which make E_1 stable.

Proposition 4.1. *The stability of E_4 is complementary to that of E_1 in that when E_1 is stable, E_4 does not exist but whenever E_4 exists, E_1 is unstable. In addition, the points E_2 and E_3 are saddles if they exist.*

Note that the evolution of E_2 and E_3 as a function of changes in μ could lead to the escape of trajectories from the positive orthant and thus, a study of the positivity of the solutions

is necessary. The feasible region of state space is required to be positive since the system is based on populations. The following subsection investigates the positivity of solutions by means of the invariance of the feasible region.

4.3.1.2 Set-theoretic characterisation of behaviour

The notion of positive systems relates to the positivity of solutions of the system. We aim to prove the positivity of the system (4.4) by means of the invariance of the state-space region of biological interest.

Proposition 4.2 (Positivity of solutions)**.** *Solutions of the system with non-negative μ remain non-negative for any positive initial conditions in $\mathbb{R}^2$ and for all time $t > 0$.*

Proof. Let $t > 0$ and assume non-negative values of μ. From system (4.4) we have;

$$\dot{x}_i \geq x_i \left(-\delta - \mu + \rho_i(1 - x_i)\right)$$

with solution

$$x_i(t) \geq \frac{(\rho_i - \delta)}{\rho_i \left(1 + \left(\frac{(\rho_i - \delta)}{x_0} - 1\right) e^{-t(\rho_i - \delta - \mu)}\right)} \tag{4.7}$$

for all $\rho_i \geq 0\,, \delta \geq 0$.

When $\rho_i > \delta$,

$$\lim_{t\to\infty} x_i(t) \quad = \quad \frac{(\rho_i - \delta)}{\rho_i} > 0 \quad \text{since} \quad \rho_i > \delta$$

When $\rho_i \leq \delta$,

$$\lim_{t\to\infty} x_i(t) \quad \longrightarrow \quad \frac{(\rho_i - \delta)}{\rho_i(1 + \infty)} = 0$$

Thus, all components are converging monotonically and $\lim_{t\to\infty} x_i(t) = 0$.

This proves that the solution of the system (4.4) is non-negative for all $t > 0$. □

Let us now consider the region of invariance with respect to system (4.4) .

Proposition 4.3. *Given a set of positive parameters: ρ_i, δ and μ, the set*

$$\Omega = \left\{(x_1, x_2) \in \mathbb{R}^2 \mid 0 \leq x_1 \leq k_1, 0 \leq x_2 \leq k_2\right\} \tag{4.8}$$

is positively invariant with respect to system (4.4) above with the coexistence equilibrium point at (k_1, k_2).

Proof. Consider the general dynamical system

$$\dot{x} = F(x) \tag{4.9}$$

with $F : \mathbb{R}^2 \to \mathbb{R}^2$ and let $\mathcal{X}$ be the set of all initial conditions in $\mathbb{R}^2$. Following Nagumo's theorem (in Chapter 2, Section 2.6), assume that for each initial condition in $\mathcal{X}$, there is a globally unique solution and let $\Omega \subseteq \mathcal{X}$ be a closed and convex set. The boundary of the set Ω is denoted as $\partial\Omega$ and the tangent cone of Ω at x is denoted as $\mathcal{T}_{\Omega(x)}$. Then, the set Ω is positively invariant for the system if and only if

$$F(x) \in \mathcal{T}_{\Omega(x)}, \ \forall \ x \in \partial\Omega,$$

Thus, if for every $x \in \partial\Omega$, the derivative $\dot{x}(t)$ points inside the set Ω, then the trajectory $x(t)$ remains in Ω [33].

In the particular case of Ω in eq (4.8) and $\dot{x}_i$ in eq (4.4) with $F(x) = \begin{bmatrix} f_1(x) \\ f_2(x) \end{bmatrix}$, $\partial\Omega$ is defined by the four line segments (see Figure 4.3);
$A = \{(x_1, x_2) \mid 0 < x_1 < k_1, x_2 = 0\}$,
$B = \{(x_1, x_2) \mid x_1 = 0, 0 < x_2 < k_2\}$,
$C = \{(x_1, x_2) \mid 0 < x_1 < k_1, x_2 = k_2\}$ and
$D = \{(x_1, x_2) \mid x_1 = k_1, 0 < x_2 < k_2\}$.

To show that all points along $\partial\Omega$ point inwards, one has to use normals that point inside Ω by using the dot product. However, we recall Proposition 4.2, where it was shown that the system is positive and hence the points along the boundaries defined by A and B are proved to point inside Ω. Thus, it remains to show that points along C and D also point inside Ω.

For C, x_2 is constant and x_1 changes from 0 to k_1 with the normal vector $\vec{n_C} = (0, -1)$. For any point $p \in [0, k_1]$, let $X = \begin{bmatrix} p \\ k_2 \end{bmatrix}$ be the initial conditions. Then,

$$\begin{aligned} F(X)^T.\vec{n_C} &= F\left(\begin{bmatrix} p \\ k_2 \end{bmatrix}\right)^T . \begin{pmatrix} 0 \\ -1 \end{pmatrix} \\ &= \begin{bmatrix} f_1\left(\begin{bmatrix} p \\ k_2 \end{bmatrix}\right) & f_2\left(\begin{bmatrix} p \\ k_2 \end{bmatrix}\right) \end{bmatrix} . \begin{pmatrix} 0 \\ -1 \end{pmatrix} \\ &= -f_2\left(\begin{bmatrix} p \\ k_2 \end{bmatrix}\right), \forall p. \end{aligned}$$

It remains to show now that

$$F(X)^T.\vec{n_C} = -f_2\left(\begin{bmatrix} p \\ k_2 \end{bmatrix}\right) \geq 0, \forall p \in [0, k_1]. \tag{4.10}$$

From eq (4.4b),

$$\dot{x}_2 = \left[-\delta + \rho_2(1 - x_2)\right] x_2 + \mu(-x_1 + x_2). \tag{4.11}$$

Since (k_1, k_2) are roots of the system (4.4),

$$\dot{x}_2 = \left[-\delta + \rho_2(1 - k_2)\right] k_2 + \mu(-k_1 + k_2) = 0. \tag{4.12}$$

Thus,

$$\begin{aligned} \left[-\delta + \rho_2(1 - k_2) - \mu\right] k_2 + \mu k_1 &= 0 \\ \left[-\delta + \rho_2(1 - k_2) - \mu\right] k_2 &= -\mu k_1 \end{aligned} \tag{4.13}$$

Now from eq (4.10),

$$\begin{aligned} -f_2\left(\begin{bmatrix} p \\ k_2 \end{bmatrix}\right) &= -\left[\rho_2 k_2 (1 - k_2) - \delta k_2 - \mu k_2 + \mu p\right] \\ &= -\left[\rho_2 k_2 (1 - k_2) - \delta k_2 - \mu k_2\right] - \mu p \\ &= -(-\mu k_1) - \mu p \quad \text{from eq (4.13)} \\ &= \mu(k_1 - p) > 0 \quad \text{when } p \in (0, k_1) \end{aligned}$$

The value of the dot product being positive, the vector fields point in the same direction as a normal field (i.e. inside the domain Ω).

For D, x_1 is constant and x_2 changes from 0 to k_2 with the normal vector $\vec{n_D} = (-1, 0)$. Based on the same reasoning, similar results are obtained:

$$F(X)^T.\vec{n_D} = f_1\left(\begin{bmatrix} k_1 \\ p \end{bmatrix}\right) > 0, \forall p \in [0, k_2].$$

and the vector fields point inside the domain.

Eventually, since all points along $\partial\Omega$ point inwards, the set Ω is positively invariant with respect to system (4.4). □

Corollary 4.4. *In the case when there is no mutation, that is when $\mu = 0$, along the boundaries C and D,*

$$f_2\left(\begin{bmatrix} p \\ k_2 \end{bmatrix}\right) = 0 \text{ and } f_1\left(\begin{bmatrix} k_1 \\ p \end{bmatrix}\right) = 0$$

respectively. Therefore the set Ω is positively invariant with respect to system (4.4).

The invariant region Ω bounded by the line segments A, B, C, D is illustrated in Figure 4.3.

4.3.1.3 Lyapunov stability analysis

We have established that all solutions of the system (4.4) with positive initial conditions are positive and remain in the positively invariant region Ω (in eq (4.8)) for all $t > 0$. We have also shown that the system converges to either the origin or the coexistence equilibrium point. However, the convergence of interest is the one at the origin which indicates the eradication of both strains of bacteria. The stability of the origin is analysed in this section using Lyapunov's theory from Theorem 2.3 on stability of dynamical systems. Using a Lyapunov function, we can determine the Lyapunov stability of the equilibrium point, E_1 for system (4.4).

Theorem 4.5. *The system (4.4) under the conditions (4.6) has $\bar{x} = 0$ as stable equilibrium with a domain of attraction $\Omega_D = \{(x_1, x_2) \in \Omega \mid (x_1, x_2) \neq (k_1, k_2)\}$.*

Proof. Starting from the positive invariance of $\Omega \subset \mathbb{R}^2$, we construct a candidate Lyapunov function in the form

$$V(x) = (x_1 - \bar{x}_1)^2 + (x_2 - \bar{x}_2)^2. \tag{4.14}$$

Over the domain Ω_D, $V(x)$ is continuously differentiable, $V(\bar{x}) = 0$ and $V(x) > 0$ for all $x \neq \bar{x}$. Thus $V(x)$ is a valid Lyapunov candidate. The derivative, $\dot{V}(x)$ of the Lyapunov function $V(x)$ is calculated along the trajectories as

$$\dot{V}(x) = 2(x_1 - \bar{x}_1)\dot{x}_1 + 2(x_2 - \bar{x}_2)\dot{x}_2 \tag{4.15}$$

Clearly, $\dot{V}(x) = 0$ for $x = (0, 0)$ and $x = (k_1, k_2)$. Next, we consider the Lyapunov stability of the origin and develop eq (4.14) for $x \in \Omega_D$ and the equilibrium point $\bar{x} = (0, 0)$

$$\begin{aligned}
\dot{V}(x) &= 2x_1\dot{x}_1 + 2x_2\dot{x}_2 \\
&= 2x_1\left[(-\delta + \rho_1(1 - x_1))x_1 + \mu(-x_1 + x_2)\right] \\
&+ 2x_2\left[(-\delta + \rho_2(1 - x_2))x_2 + \mu(x_1 - x_2)\right] \\
&= 2x_1^2(\rho_1 - \delta) + 2x_2^2(\rho_2 - \delta) \\
&- 2(\rho_1 x_1^3 + \rho_2 x_2^3) - 2\mu(x_1 - x_2)^2
\end{aligned}$$

Let μ be expressed in terms of the critical mutation rate μ_c from eq (4.6) as $\mu = \mu_c + \epsilon$. Substituting this into $\dot{V}(x)$ yields:

$$\begin{aligned}
\dot{V} \quad (x) &= 2x_1^2(\rho_1 - \delta) + 2x_2^2(\rho_2 - \delta) - 2\left(\rho_1 x_1^3 + \rho_2 x_2^3\right) \\
&\quad -2(x_1 - x_2)^2 \left(\frac{(\delta - \rho_1)(\delta - \rho_2)}{-2\delta + \rho_1 + \rho_2} + \epsilon\right) \\
&= -2\rho_1 x_1^3 - 2\rho_2 x_2^3 - 2\epsilon x_1^2 - 2\epsilon x_2^2 + 4\epsilon x_1 x_2 \\
&\quad + \frac{2(\delta - \rho_1)^2 x_1^2 + 2(\delta - \rho_2)^2 x_2^2 + 4(\delta - \rho_1)(\delta - \rho_2) x_1 x_2}{-2\delta + \rho_1 + \rho_2} \\
&= -2\rho_1 x_1^3 - 2\rho_2 x_2^3 - 2\epsilon(x_1 - x_2)^2 \\
&\quad + \frac{2((\delta - \rho_1)x_1 + (\delta - \rho_2)x_2)^2}{-2\delta + \rho_1 + \rho_2}
\end{aligned}$$

When C1 is satisfied then $\frac{2((\delta-\rho_1)x_1+(\delta-\rho_2)x_2)^2}{-2\delta+\rho_1+\rho_2} < 0$. When C2 is satisfied then $\epsilon > 0$ and $-2\epsilon(x_1 - x_2)^2 < 0$.

Therefore satisfying both conditions (4.6) ensures that $\dot{V}(x) < 0$, $\forall\, x \in \Omega$. □

When any of the conditions (4.6) are not satisfied, there exists at least one combination of $(x_1, x_2) \in \Omega_D$ which makes the expression (4.15) non-negative, thus invalidating the stability of the origin over this domain.

4.3.2 Model analysis with switching between therapies for two pathogen strains

By considering the switched system (4.4), we introduce here a mechanism for improving the stabilisation and the rate of convergence of the system (4.4) when more than one treatment policy is employed. Two types of switching policies are considered: Periodic switching and Lyapunov switching.

A periodic switching policy is the switching of therapies i in a periodic pattern at regular intervals T_i. The principle of periodic switching of therapies can be described as follows in the case of two therapies. Given two therapies with administration periods T_1 and T_2, we have the switching policies $\sigma(T_1) = 1$ and $\sigma(T_2) = 2$. A periodic cycling policy in this case begins at the initial state with therapy 1, then runs along with the switching policy $\sigma = 1$ for a period T_1, and at the end of T_1, the system turns to the switching policy $\sigma = 2$ for a period T_2. Therefore as time goes, this pattern switches the therapies one by one for the entire duration of time (see Figure 4.4).

A Lyapunov switching policy refers to cycling of therapies based on the Lyapunov function.

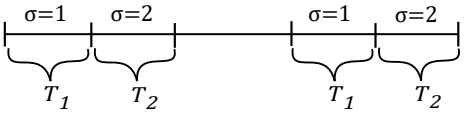

FIGURE 4.4: Illustrating periodic switching of two therapies with periods T_1 and T_2. Treatment begins at the initial state with policy $\sigma = 1$ and continues for a period T_1. At the end of T_1, the system runs with switching policy $\sigma = 2$ for a period T_2. Continuing this way creates a pattern of switching between the two therapies consecutively thus giving rise to a periodic switching policy.

4.3.2.1 Switching based on control Lyapunov function

The use of the Lyapunov function serves as a tool for finding strategies to achieve convergence. Based on the Lyapunov function argument, we can have a switching strategy which ensures the stability of the origin under a given choice of the parameters.

Proposition 4.6. *The system (4.4) has the origin as a stable equilibrium if for every $x \in \Omega_D$ there exists at least one therapy $\sigma_x \in \{\sigma_1, \sigma_2\}$ for which $\dot{V}(x, \sigma_x) < 0$, where $\dot{V}$ is the Lyapunov function derivative in eq (4.15).*

Proof. Let the Lyapunov function derivative $\dot{V}$ defined as in eq (4.15) be with respect to the dynamics of system (4.4) by considering it as a function of x and σ. If for every $x \in \Omega_D$ there is at least one therapy σ_x that yields $\dot{V}(x, \sigma_x) < 0$. We can construct a switching policy by choosing the therapy such that

$$\sigma(t) = \arg\min_{\sigma_i} \dot{V}(x, \sigma_i).$$

This constructive solution proves the existence of a switching policy σ, such that $\dot{V}(x, \sigma) < 0$ and hence following from Theorem 2.3, the system has a stable equilibrium at the origin. □

Thus, given two configurations both with the common equilibrium point $(0, 0)$, a policy based on the Lyapunov function derivative can be used to stabilize the system provided that at least one of the configurations guarantees $\dot{V}(x, \sigma_i) < 0$. In addition, switching based on the Lyapunov function derivative can lead to faster convergence than periodic switching. In the following, some scenarios of these conditions are discussed.

4.3.2.2 Numerical simulation for switching therapies for two strain model

If the switching system (4.4) has a common Lyapunov function, then the system is asymptotically stable at the origin for any switching signal $\sigma(t)$. To illustrate this, we consider three different scenarios with different proliferation rates and under two treatment policies

(see Table 1). For all simulations, an initial condition vector $x = [10^3, 10]$ is chosen and the following parameter values are used: $\delta = 0.25, K = 10^5$, $T = 10$ days and $\mu = 10^{-4}$. In case

TABLE 4.2: Proliferation rates for bacterial strains under therapy combinations

Case	Therapy	x_1	x_2	E_1
1	1	$\rho_{1,1} = 0.2$	$\rho_{2,1} = 0.1$	Stable
	2	$\rho_{1,1} = 0.1$	$\rho_{2,1} = 0.2$	Stable
2	1	$\rho_{1,1} = 0.5$	$\rho_{2,1} = 0.1$	Unstable
	2	$\rho_{1,1} = 0.1$	$\rho_{2,1} = 0.2$	Stable
3	1	$\rho_{1,1} = 0.1$	$\rho_{2,1} = 0.35$	Unstable
	2	$\rho_{1,1} = 0.35$	$\rho_{2,1} = 0.1$	Unstable

1, both subsystems are asymptotically stable at the origin. Therefore, any switching policy leads to eradication of both strains. In case 2, the first subsystem is unstable at the origin but the second is stable. Switching periodically between therapies will not stabilize the entire system unconditionally. In cases 1 and 2, switching based on the Lyapunov function argument not only ensures convergence to the origin but also achieves convergence at a faster rate compared to switching periodically between policies. We can see in Figure 4.5a and 4.5b switching results for cases 1 and 2 respectively. For case 3, the two subsystems are not stable at the origin and thus, using the policies independently does not lead to eradication. However, switching between the two policies periodically leads to a convergence at the origin. Moreover, the Lyapunov switching converges to such a periodic stabilizing sequence implicitly and additionally ensures a better convergence of the closed-loop system (see Figure 4.5c).

For this last case, subsystems a priori unstable at the origin can be brought to convergence under the Lyapunov switching argument based on feedback. Moreover, an analysis of the Lyapunov function derivative shows that a sliding mode can occur at the intersection of the two configuration as shown in Figure 4.6(b). Thus, the feedback switching can be seen as a reaching law to the sliding surface. Once the sliding mode is reached, the control can be completed with a sliding law defined based on periodic switching.

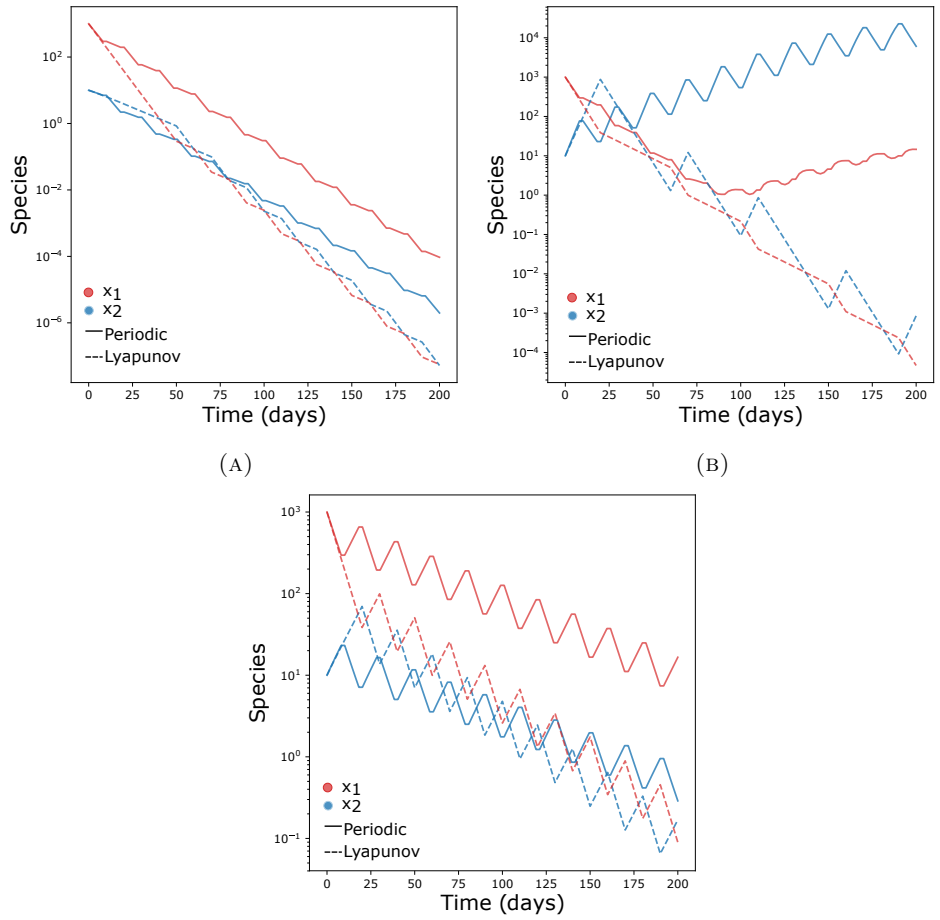

(A) (B)

(C)

FIGURE 4.5: Illustration of therapy switching for all three cases. (a) Case 1; (b) Case 2; (c) Case 3. Solid lines: periodic switching. Dashed lines: Lyapunov based switching. Blue lines: strain x_1. Red lines: strain x_2.

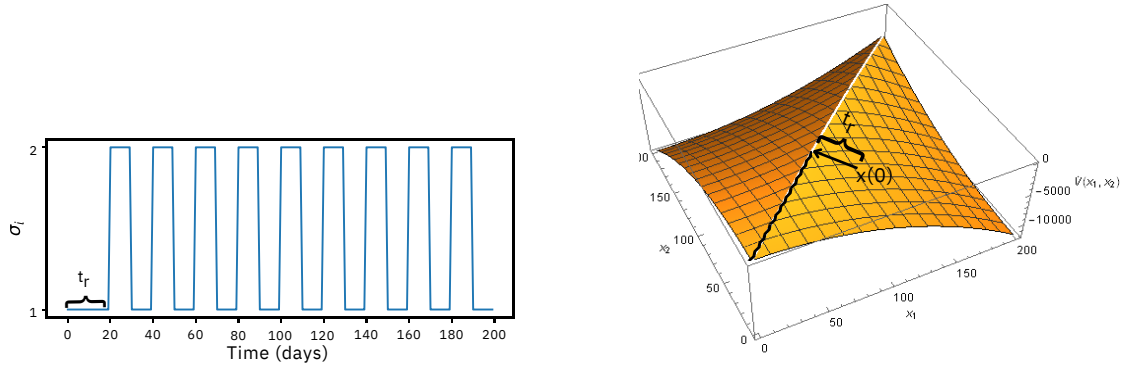

(A) (B)

FIGURE 4.6: A sliding mode for case 3 occurs at the intersection of $\dot{V}(x_1, x_2)$ for therapy 1 and 2 when the minimum of $\dot{V}(x_1, x_2)$ for each pair (x_1, x_2) with respect to both therapies is plotted. The right hand side shows the values of $\dot{V}(x_1, x_2)$ under therapy 1 and the left hand side shows the values of $\dot{V}(x_1, x_2)$ under therapy 2. t_r denotes the time to reach the sliding mode.

Let us now consider a more general case of of the model for antimicrobial resistance.

4.4 General model for antimicrobial resistance

In the following sections, we focus on the qualitative characteristics of the model (4.2). In particular, we examine this generalised model while taking into consideration that the mutation matrices in this case are not constant for all treatment scenarios as in the two strain model discussed above. Instead, these matrices are considered to vary depending on drug use. Additionally, in this case, the mutation process is incorporated as an extra growth factor, resulting in the lack of mass conservation, unlike in the two-strain model.

The following assumptions are made for analysing this model.

Assumption 4.7. Modelling with logistic dynamics It is assumed that the growth rate of the population is proportional to the existing population and the amount of resources available (which is usually in excess in the course of an infection). Thus, for simplicity, we assume the same carrying capacity (K) for the different variants in the presence of antibiotics.

Assumption 4.8. Development of resistance before treatment onset. *In silico* experiments performed by Komarova *et al*[16] suggest that when two or more drugs are used, the phase which plays a dominant role in treatment failure is the period before treatment and that development of resistance during treatment can be ignored. In fact, evidence from experimental studies show that for bacteria isolated from different populations of *P. aeruginosa* selected before the initiation of antibiotic therapy, there were both strains susceptible and resistant to all six antibiotics tested [31]. These observations imply that evolution of resistant strains in a bacteria population can be observed either prior to the use of antibiotics or during the course of treatment. In this study, we assume that resistance to all used antibiotics is developed before the start of treatment.

Assumption 4.9. Proliferation rate as a fitness level. Evolution of mutation in the population results in the progression towards higher fitness levels due to selection pressure. Based on the susceptibility profile (level of sensitivity and/or resistance to a given antibiotic) of each cell, we assume that there are two possible fitness levels under each drug: lowest for most sensitive cells and highest for most resistant cells. The metric used to determine the fitness level in this work is the overall proliferation ability (ability to grow and increase in number) during resistance evolution. This is captured by the proliferation rate $\rho_{i,\sigma}$.

Assumption 4.10. Proliferation rates depend on antibiotic treatment. In the presence of an antibiotic, it is reasonable to assume that the population of sensitive cells decreases whereas that of resistant cells increases. Thus, under each drug, we assign two types of proliferation rates; one for each cellular type. We assume that the sensitive and resistant strains

proliferate at different rates and set the proliferation rates of resistant cells to be higher than that for sensitive cells.

Assumption 4.11. Mutation is based on therapy. With the use of therapy, bacterial cells susceptible to a particular drug, say drug A, can undergo mutations in the course of treatment leading to cells which are resistant to the given drug A but sensitive (collateral sensitivity) or resistant (cross resistance) to another drug, say B. Consequently, the cell dynamics leading to the evolution of mutant strains differs with the use of drug. This is because the genetic connections between cells are defined by their collateral sensitivity profiles which changes depending on the drug in use. Therefore the mutation matrix $M_{\sigma(t)}[M_1, M_2, \ldots, M_n]$ can be seen as a collection of all mutation matrices obtained from n drugs.

Assumption 4.12. Collateral sensitivity or cross resistance is only observed in resistant populations. Experimentally evolved resistant strains of *P. aeruginosa* and *S. aerus* were found to be collaterally sensitive to at least one out of several antibiotics being tested [31]. Therefore, in this model, we assume that collateral sensitivity and cross resistance are accounted for when resistant cells to the current drug are either sensitive or resistant to another drug. Also, a sensitive cell giving rise to other sensitive strains has been excluded from this model.

Assumption 4.13. Mutation rate independent of therapy and strain. For a given drug, the development of resistance within the sensitive population occurs at a rate - the mutation rate, μ. As the mutation rate is increased, the level of resistance also increases thereby generating more resistance cells in the population. This relationship between therapy, cells and the mutation is simplified in this model by assuming a constant mutation rate for all therapy and cells.

Assumption 4.14. Pathogen clearance depends on therapy. Understanding the clearance of bacteria helps to measure the effect of the drug on the population. In this work, we assume that the rate of clearance of bacteria, δ is drug-induced and that the value of this parameter changes with the change of the drug.

4.4.0.1 Mutation matrix $M_{\sigma_{(t)}}$

The process of mutation is assumed to be absolute and irreversible such that a single strain can mutate into several other strains which do not eventually yield the same strain at the start of the mutation process. Thus, it is not possible for two different strains to yield the same mutant upon mutation. In other words, all *backward mutations* are excluded from this model as there exists no sequence of l mutations $x_{j_1} \to x_{j_2} \to \ldots \to x_{j_l} \to x_i$ for any length l when a mutation from strain i to j occurs. In general, it is not possible to come back to strain i starting from strain i.

Let X be a set. We recall that a (homogeneous) relation R on X is a subset of the Cartesian product $X \times X$. Elements $x, y \in X$ are said to be in relation R if $(x, y) \in R$.

The relation "leads to / generates" is defined on the finite set X of all cells in the system such that $X = \{x_1, x_2, \ldots, x_n\}$. This relation holds if and only if x can lead to or generate y. In other words, x acts as a source to y. Thus, when drug A is used, $A_s R A_r$ holds because A_s can lead to or generate A_r. This implies that, cells sensitive to drug A can become resistant to drug A after some time and A_s cells are the source to A_r cells. The entries in the mutation matrix $M_{\sigma(t)}$ are defined by

$$m_{i,j} = \begin{cases} 1 & \text{for } (x, y) \in R \\ 0 & \text{for } (x, y) \notin R \end{cases} \tag{4.16}$$

These are Boolean in nature and are either 0 or 1 depending on whether a relation holds between two strains in X or not.

The mutation matrix $M_{\sigma_{(t)}}$ is a zero diagonal matrix as a cell cannot generate itself and there is no way of going back to strain x_i, not only in one but also in multiple mutation steps starting from strain x_i. Thus, $M_{\sigma_{(t)}}$ can be expressed as the adjacency matrix of a directed acyclic graph (DAG). It follows that there exists a topological ordering of the strains that renders $M_{\sigma_{(t)}}$ upper triangular. In other words, we can relabel the strains so that for every mutation from x_i to x_j, i comes before j. As this DAG is finite, there is a maximum-length path, ν and no other path can be longer than that path. It follows that for $k \geq \nu$, $M^k_{\sigma_{(t)}} = 0$, thus making it nilpotent.

A typical mutation matrix is made up of four main blocks, I, II, III and IV, representing sensitivity (S) and resistance (R) depending on the drug used as seen in Figure 4.7.

$$M_{\sigma(t)} = \begin{array}{c} \\ \text{S} \\ \text{R} \end{array} \begin{array}{c} \begin{array}{cc} \text{S} & \text{R} \end{array} \\ \left[\begin{array}{c|c} \text{I} & \text{II} \\ \hline \text{III} & \text{IV} \end{array}\right] \end{array}$$

FIGURE 4.7: A typical mutation matrix is made up of four main blocks, I, II, III and IV, representing sensitivity (S) and resistance (R) depending on the drug used.

Block I: Entries in this block are 0 as we cannot have cells sensitive to a given drug generating sensitivity to other drugs – this is a direct result of Assumption 4.12. That is, when a particular drug is used, the cells sensitive to that drug are not sensitive to other unused drugs. For instance, when drug A is used, cells sensitive to drug A (A_s) cannot generate cells sensitive to another drug B (B_s). Hence, $(A_s, B_s) \notin R$ and $m_{ij} = 0$.

Block II: When a given drug is used, the cells that developed resistance can give rise to cells sensitive to other drugs - which is the phenomenon of *Collateral sensitivity*. In this case, $(A_r, B_s) \in R$ and $m_{ij} = 1$ else $m_{ij} = 0$. That is, resistant strains of one drug act as sources of sensitive strains to other drugs.

Block III: In this block, cells sensitive to a given drug can become resistant over time. Therefore, when drug A is used for example, $(A_s, A_r) \in R$ and $m_{ij} = 1$.

Block IV: Cells resistant to a given drug can also become resistant to another drug not currently in use. This leads to the phenomenon of *Cross resistance* captured in this block. Here, $(A_r, B_r) \in R$ and $m_{ij} = 1$ else $m_{ij} = 0$. That is, resistant strains of one drug act as sources of resistant strains to other drugs.

4.4.1 Quantitative Analysis for Monotherapy

In this section, we make quantitative analysis of the model by focusing on the use of a single therapy (no switching). Without loss of generality, the model can be simplified with the following change of variables in eq (4.2):

$$\rho_{i,\sigma(t)} \to \rho_i, \delta_{\sigma(t)} \to \delta \text{ and } m_{ij,\sigma(t)} \to m_{ij}.$$

Subsequently, with $K = 1$, eq (4.2) can be rewritten as follows:

$$\dot{x}_i(t) = x_i(t)\left(\rho_i - \delta\right) - \rho_i x_i(t)^2 + \mu \sum_{j=1}^{n} m_{ij} x_j(t), \quad 1 \leq i \leq n. \tag{4.17}$$

The region of biological interest is given as the set

$$\Omega_2 = \left\{(x_1, x_2, \ldots, x_n) \in \mathbb{R}^n \mid x_i \geq 0, i = 1, 2, \ldots, n\right\}. \tag{4.18}$$

Proposition 4.15 (Positivity of solutions)**.** *Solutions of the system (4.17) with non-negative μ are non-negative for any positive initial condition in $\mathbb{R}^n$ and for all times $t > 0$.*

Proof. The proof follows from the proof of Proposition 4.2 above. □

4.4.1.1 Equilibrium points and stability analysis

Solving for $\dot{x}_i = 0$, for any i, the equilibrium points of the system (4.17), which we denote by $E = (x_1^*, x_2^*, \ldots, x_n^*)$, are of the form

$$\begin{cases} x_i^* \in \left\{0, \max\left(\dfrac{\lambda_i}{\rho_i}, 0\right)\right\}, & c_i^* = 0 \\ \\ x_i^* = \dfrac{\lambda_i \pm \sqrt{\lambda_i^2 + 4\mu\rho_i c_i^*}}{2\rho_i}, & c_i^* > 0 \end{cases} \tag{4.19}$$

where c_i^* corresponds to the equilibrium value of the strain that acts as a source of x_i. In other words, if the source of x_i is x_k, then $c_i^* = x_k^*$.

We denote by λ_i, the i-th eigenvalue of the Jacobian matrix of the system evaluated at the origin given by

$$\lambda_i = \rho_i - \delta. \tag{4.20}$$

Remark. If $c_i^* > 0$, x_i^* yields positive values when $x_i^* = \dfrac{\lambda_i + \sqrt{\lambda_i^2 + 4\mu\rho_i c_i^*}}{2\rho_i}$ and negative values when $x_i^* = \dfrac{\lambda_i - \sqrt{\lambda_i^2 + 4\mu\rho_i c_i^*}}{2\rho_i}$. However, for the biological system under study, the only admissible equilibrium points are those with positive values as seen in eq (4.19).

Remark. System (4.17) always has an infection-free equilibrium point $E(0)$ at the origin with $x_i^* = 0$ for all $i = 1, \ldots, n$. This equilibrium is locally asymptotically stable if $\lambda_i < 0$ for $i = 1, \ldots, n$ and unstable if $\lambda_i > 0$ for some i.

The Jacobian matrix of the system evaluated at any given equilibrium point can be written as a sum of two matrices M and D such that

$$J(E) = D(E) + \mu M, \tag{4.21}$$

where M is the mutation matrix and $D \in \mathbb{R}^{n\times n}$ is diagonal with entries

$$d_{ii}(E) = \rho_i - \delta - 2\rho_i x_i^* \tag{4.22}$$

We have established in Proposition 4.4.0.1 that the mutation matrix M has a zero diagonal of and its off-diagonal entries encode the pattern of mutation between strains. Due to the properties of the matrix M, the resulting eigenvalues of J are given by its diagonal entries, d_{ii}. At the origin, we recover the eigenvalue in eq (4.20). Therefore, for all i, the point $E(0)$ is locally asymptotically stable if $\lambda_i < 0$ and unstable if $\lambda_i > 0$.

The trace and determinant of the Jacobian matrix $J(E(0))$ can be expressed as:

$$\text{tr} = \sum_{i=1}^{n}(\rho_i - \delta) \quad \text{and} \quad \det = \prod_{i=1}^{n}(\rho_i - \delta) \tag{4.23}$$

When $\lambda_i < 0$ (that is $\rho_i < \delta$) for all i, the eigenvalues have negative real part and thus, $E(0)$ is locally aysmptotically stable. Moreover, there exists at least one $k \neq i$ such that $\lambda_k > 0$ and $\lambda_i < 0$, thus the trace and the determinant are negative and hence, the point $E(0)$ is a saddle (and consequently contain an unstable point).

Theorem 4.16. *Let $i \in \{1, \ldots, n\}$ with $\{1, \ldots, n\} = \mathcal{J}_1 \cup \mathcal{J}_2 \cup \{i\}$ where $\mathcal{J}_1$ is the subset of indices corresponding to the strains that can be reached from the strain x_i and $\mathcal{J}_1 \cap \mathcal{J}_2 = \emptyset$ and assume $\lambda_i > 0$. Then there exists an equilibrium with $x_k^* > 0$ for all $k \in \mathcal{J}_1 \cup \{i\}$ and $x_j^* = 0$ for all $j \in \mathcal{J}_2$.*

This equilibrium will be linearly stable if, additionally, $\lambda_j < 0$ for all $j \in \mathcal{J}_2$.

Proof. Recall the Jacobian of the system given by eq (4.21) and the corresponding eigenvalues, λ_i in eq (4.20). Since we assumed that $\lambda_i > 0$, $J_{ii}(E) = \Delta_i = -\sqrt{\lambda_i^2 + 4\mu\rho_i c_i^*}$ therefore yielding an eigenvalue which is always negative. Hence, the eigenvalues of the Jacobian corresponding to x_i^* are of the form

$$\Lambda_i = \begin{cases} \lambda_i & x_i^* = 0 \\ \Delta_i, & x_i^* > 0 \end{cases} \tag{4.24}$$

Whenever strain x_i persists (that is, $\lambda_i > 0$), then all strains x_k, $k \in \mathcal{J}_1$, will also persist. On the other hand, all other strains, x_j for $j \in \mathcal{J}_2$, in the system are unable to persist in isolation, $x_j^* = 0$ and the eigenvalues corresponding to $x_i^* > 0$ with $x_k^* > 0$ will satisfy:

$$\begin{aligned} \Delta_k &< 0 \quad \text{if } c_k^* = x_i^* \\ \lambda_k &< 0 \quad \text{if } c_k^* \neq x_i^* \end{aligned}$$

Consequently, the equilibrium point is linearly stable. □

To ensure the depletion of resistant strains, the equilibrium point of interest is the infection-free equilibrium at the origin. We have already established the linear stability of this point in Theorem 4.4.1.1. Next, the stability of the origin is further analysed using Lyapunov's theory on stability of dynamical systems (see Theorem 2.3). For this, we define the domain of attraction, Ω_{2D} as $\Omega_{2D} = \Omega_2 \setminus \mathbb{S}$, where $\mathbb{S} = \{(x_1, \ldots, x_n) \in E | x_i > 0\}$, for all $i \in \{1, \ldots, n\}$.

Theorem 4.17. *In the absence of mutations (that is when $\mu = 0$), the system (4.17) admits the origin to be globally asymptotically stable whenever $\rho_i < \delta$ for all $i \in \{1, \ldots, n\}$.*

Proof. To ensure the global stability of the origin, let us construct a Lyapunov function in the form

$$V(x) = \sum_{i}^{n} x_i^2. \tag{4.25}$$

Over the domain Ω_{2D}, $V(x)$ is continuously differentiable, $V(x^*) = 0$ and $V(x) > 0$ for all $x \neq 0$. Thus $V(x)$ is a valid Lyapunov candidate.

The derivative, $\dot{V}(x)$ of the Lyapunov function $V(x)$ is calculated as

$$\dot{V}(x) = 2\sum_{i}^{n} x_i \dot{x}_i. \tag{4.26}$$

From eq (4.26), $\dot{V}(x) = 0$ for all $x = 0$.

Next, we consider the Lyapunov stability of the origin. Here,

$$\begin{aligned}
\dot{V}(x) &= 2\sum_{i}^{n} x_i \dot{x}_i \\
&= 2\sum_{i}^{n} x_i \left[x_i(t)\left(\rho_i - \delta\right) - \rho_i x_i(t)^2 + \mu \sum_{j=1}^{n} m_{ij} x_j(t) \right] \\
&= 2\sum_{i}^{n} x_i \left[x_i(\rho_i - \delta) - x_i^2 \rho_i + \mu \sum_{j=1}^{n} m_{ij} x_j(t) \right] \\
&= 2\left[\sum_{i}^{n} x_i^2(\rho_i - \delta) - \sum_{i}^{n} x_i^3 \rho_1 + \mu \sum_{j=1}^{n} m_{ij} x_j(t) \right]
\end{aligned}$$

In the absence of mutation (that is when $\mu = 0$),

$$\dot{V}(x) = 2\left[\sum_{i}^{n} x_i^2(\rho_i - \delta) - \sum_{i}^{n} x_i^3 \rho_1 \right] \leq 0 \quad \text{when} \quad \rho_i < \delta \quad \text{for all } i \in \{1, \ldots, n\} \tag{4.27}$$

Therefore, the origin is globally stable under this condition. □

4.4.2 Switching control for therapy scheduling

We aim to design switching strategies which can be used to eliminate bacterial strains within the host on the long term base. In mathematical terms, our main objective is to stabilize the infection-free equilibrium of the system at the origin whilst switching therapies in a given time period. Based on the general model (4.2), we consider a mechanism for improving the stabilisation and the rate of convergence of the system when more than one treatment policy is applied.

4.4.2.1 Choice of a Lyapunov function

Similar to the two strain model, the Lyapunov function can be used as a tool to improve the convergence of the system. A switching strategy which ensures the stability of the origin can be found based on a Lyapunov function argument.

Proposition 4.18. *The system (4.2) has the origin as a stable equilibrium if for every* $x \in \Omega_{2D}$ *there exists at least one therapy* $\sigma_x \in \{\sigma_1, \cdots, \sigma_N\}$ *for which* $\dot{V}(x, \sigma_x) < 0$, *where* $\dot{V}$ *is the Lyapunov function derivative in eq (4.26).*

Proof. The proof follows from the proof of Proposition 4.6 for every $x \in \Omega_{2D}$, $\dot{V}$ as in eq (4.26) and again, by choosing the therapy such that

$$\sigma(t) = \arg\min_{\sigma_i} \dot{V}(x(t), \sigma_i). \tag{4.28}$$

□

Thus, given the subsystems of a class of switched systems with the common equilibrium point at the origin, a policy based on the Lyapunov function derivative can be used to stabilize the system provided that at least one of the configurations guarantees $\dot{V}(x(t), \sigma(t)) < 0$.

4.5 Collateral sensitivity cycling numerical example

Collateral sensitivity cycling of drugs can be implemented to treat infections by cycling antibiotics based on their collateral sensitivities. Here, we examine the sequential application of drugs for an infection as clinically studied by Immamovic *et al* [31]. The modelling approach is to switch or cycle drugs based on the susceptibility profile of resistant cells. At every switching time, a new drug is selected and the corresponding network of collaterally sensitive drugs is applied. As an example, we consider the use of $N = 5$ drugs with collateral interactions as shown in the susceptibility network in Figure 4.8. This network is particularly representative of the collateral interactions among drugs commonly administered to cystic fibrosis patients during treatment of *Pseudomonas aeruginosa* infection [31] – A: Tobramycin, B: Azithromycin, C: Aztreonam, D: Ciprofloxacin, E: Colistin. In Figure 4.8, each directed edge represents CS (blue) or CR (red). From this network, four drug pairs are seen to exhibit mutual collateral sensitivities: drugs A and B, drugs C and E, drugs B and E and drugs A and C. In addition, drugs B and D exhibit mutual cross resistance. These collateral interactions can be summarized in Table 4.3. Based on this network and from the principles of CS above, with the use of drug A as the current therapy, for example, there are four potential therapies, B,C,D and E, that can be used as the next treatment.

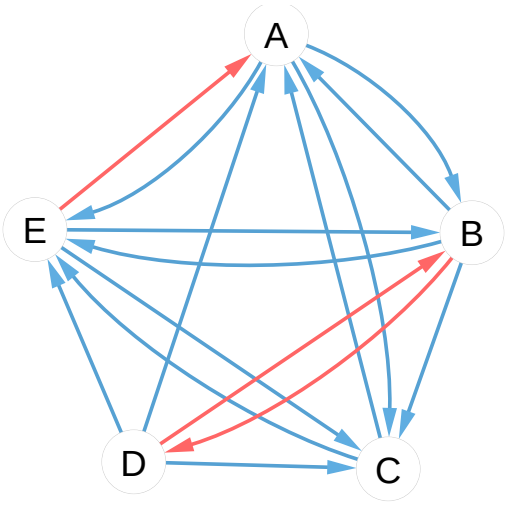

FIGURE 4.8: Network of collateral interactions among five drugs derived from Figure 4.1. A: Tobramycin, B: Azithromycin, C: Aztreonam, D: Ciprofloxacin, E: Colistin. Blue arrows represent CS and red arrows represent CR. The directed path of each arrow represents the collateral susceptibility (blue arrows) or cross resistance (red arrows) of a drug-resistant strain on another drug [31].

Drug	Collateral sensitivity	Cross resistance
A	B, C, D	E
B	A, E	D
C	A, B, D, E	-
D	-	B
E	A, B, C, D	-

TABLE 4.3: Table of collateral interactions from Figure 4.8.

Before the onset of treatment, it is assumed that strains sensitive to and resistant to each drug being considered are present in the system. For example, with ongoing treatment with drug A, some strains initially sensitive to drug A (A_s) which are not affected by the drug, mutate into strains which are resistant to drug A, A_r. These resistant strains develop sensitivity to the potential therapies, B, C and D as seen in (Table 4.3), thus yielding strains B_s, C_s, D_s. These dynamics are illustrated in Figure 4.9 where directed arrows show the mutations from one strain to another: solid arrows represent mutations originating from A_s and dashed arrows represent mutations from A_r.

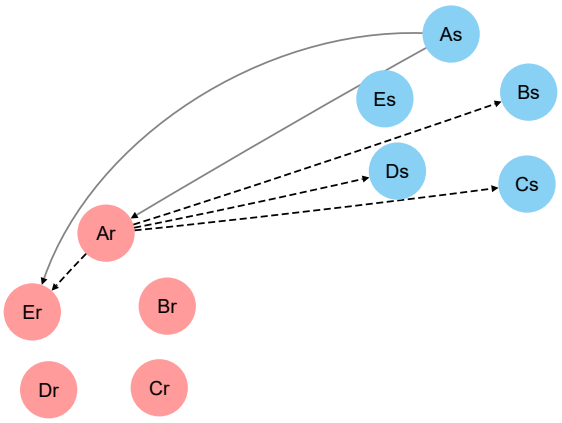

FIGURE 4.9: Mutation network for therapy A. Arrows indicate mutations between strains represented as nodes. Sensitive strains, A_s evolve resistance, A_r, - solid line. Resistant strains A_s are sensitive to drugs B, C, D and resistant to drug E - dashed lines.

The corresponding mutation matrix obtained when drug A is used then is:

$$M_{\sigma(t)} = \begin{array}{c} \\ A_s \\ B_s \\ C_s \\ D_s \\ E_s \\ A_r \\ B_r \\ C_r \\ D_r \\ E_r \end{array} \begin{array}{c} \begin{array}{cccccccccc} A_s & B_s & C_s & D_s & E_s & A_r & B_r & C_r & D_r & E_r \end{array} \\ \left[\begin{array}{cccccccccc} 0 & 0 & 0 & 0 & 0 & 0 & 0 & 0 & 0 & 0 \\ 0 & 0 & 0 & 0 & 0 & 1 & 0 & 0 & 0 & 0 \\ 0 & 0 & 0 & 0 & 0 & 1 & 0 & 0 & 0 & 0 \\ 0 & 0 & 0 & 0 & 0 & 1 & 0 & 0 & 0 & 0 \\ 0 & 0 & 0 & 0 & 0 & 0 & 0 & 0 & 0 & 0 \\ \hline 1 & 0 & 0 & 0 & 0 & 0 & 0 & 0 & 0 & 0 \\ 0 & 0 & 0 & 0 & 0 & 0 & 0 & 0 & 0 & 0 \\ 0 & 0 & 0 & 0 & 0 & 0 & 0 & 0 & 0 & 0 \\ 0 & 0 & 0 & 0 & 0 & 0 & 0 & 0 & 0 & 0 \\ 1 & 0 & 0 & 0 & 0 & 1 & 0 & 0 & 0 & 0 \end{array}\right] \end{array}$$

4.5.1 Numerical simulations

As already established in section 4.4.2.1, if the switching system (4.17) has a common Lyapunov function, then the system is asymptotically stable at the origin for any switching signal $\sigma(t)$. To illustrate this, we make use of examples based on the collateral susceptibility network in Figure 4.8. Here, $(A_s, B_s, C_s, D_s, E_s, A_r, B_r, C_r, D_r, E_r)$ is equivalent to $(x_1, x_2, x_3, x_4, x_5, x_6, x_7, x_8, x_9, x_{10}) \in \mathbb{R}^{10}$ and therapies A, B, C, D, E are denoted as therapies $1, 2, 3, 4, 5$ respectively.

For all simulations, an initial condition vector $x = [10^3, 0, 0, 0, 0, 10, 0, 0, 0, 0]$ is chosen and the carrying capacity $K = 10^6$ is used. The mutation rate μ is fixed at 10^{-4} and the pathogen

clearance rate δ_σ is fixed at 0.25 day^{-1} for each therapy. Four different scenarios are explored using the following strategies:

S1) Periodic switching: For this switching sequence, we consider a three drug switching sequences made up of drugs 1,3 and 5 (that is, A,C and E). Thus, the sequence is as follows, $A, C, E, A, C, E, \cdots$.

S2) Sub-optimal switching type 1: This is based on the Lyapunov function in eq (4.28) having a restricted number of drugs such as 1, 3 and 5 (that is, A,C and E).

S3) Sub-optimal switching type 2: This is also based on the Lyapunov function in eq (4.28) but with more freedom to select any of the available drugs such as 1, 2, 3, 4 and 5 (that is A, B, C, D and E).

The proliferation rates $\rho_{i,\sigma}$ for these scenarios are captured in Table 4.4. In all scenarios, therapies 1 to 5 inhibit respectively strains x_1, x_2, x_3, x_4, x_5 (that is $\rho_{1,1} < \delta, \rho_{2,2} < \delta, \rho_{3,3} < \delta, \rho_{4,4} < \delta, \rho_{5,5} < \delta$) but promote strains $x_6, x_7, x_8, x_9, x_{10}$ (that is $\rho_{1,1} > \delta, \rho_{2,2} > \delta, \rho_{3,3} > \delta, \rho_{4,4} > \delta, \rho_{5,5} > \delta$) respectively. Thus, without any feedback control, all systems are not stabilizable at the origin.

Scenario	Therapy	x_1	x_2	x_3	x_4	x_5	x_6	x_7	x_8	x_9	x_{10}
1	1	0.1	0.15	0.16	0.3	0.18	0.29	0.216	0.217	0.218	0.219
	2	0.15	0.1	0.16	0.17	0.18	0.1	0.29	0.217	0.218	0.219
	3	0.15	0.16	0.1	0.17	0.18	0.2	0.215	0.29	0.216	0.219
	4	0.15	0.16	0.17	0.1	0.18	0.216	0.217	0.218	0.29	0.219
	5	0.15	0.16	0.17	0.18	0.1	0.1	0.217	0.218	0.219	0.29
2	1	0.1	0.3	0.16	0.3	0.18	0.29	0.216	0.217	0.218	0.219
	2	0.3	0.1	0.16	0.17	0.3	0.1	0.29	0.217	0.218	0.219
	3	0.15	0.16	0.1	0.3	0.18	0.2	0.215	0.29	0.216	0.219
	4	0.15	0.3	0.3	0.1	0.18	0.216	0.217	0.218	0.29	0.219
	5	0.3	0.3	0.17	0.18	0.1	0.253	0.217	0.218	0.219	0.29
3	1	0.1	0.15	0.16	0.3	0.18	0.29	0.3	0.217	0.3	0.219
	2	0.15	0.1	0.16	0.17	0.18	0.3	0.29	0.217	0.218	0.3
	3	0.15	0.16	0.1	0.17	0.18	0.2	0.215	0.3	0.3	0.219
	4	0.15	0.16	0.17	0.1	0.18	0.216	0.3	0.3	0.29	0.219
	5	0.15	0.16	0.17	0.18	0.1	0.3	0.3	0.218	0.219	0.29
4	1	0.1	0.15	0.16	0.3	0.18	0.29	0.26	0.217	0.3	0.219
	2	0.15	0.1	0.3	0.17	0.18	0.1	0.29	0.27	0.278	0.219
	3	0.15	0.16	0.1	0.3	0.18	0.27	0.215	0.29	0.26	0.219
	4	0.3	0.16	0.17	0.1	0.18	0.256	0.217	0.218	0.29	0.279
	5	0.15	0.16	0.3	0.18	0.1	0.251	0.217	0.3	0.219	0.29

TABLE 4.4: The proliferation rates $\rho_{i,\sigma}$ for the illustrative scenarios for drug resistance based on eq (4.17). Each value in the table denotes the value of $\rho_{i,\sigma}$ for each strain x_i with $i = 1, 2, \ldots, 10$ and under each therapy, σ with $\sigma = 1, 2, \ldots, 5$. For example, $\rho_{1,1} = 0.1$ and $\rho_{10,5} = 0.29$.

In scenario 1, we assume populations susceptible to different drugs. In addition to the general assumptions for all scenarios stated above, in this scenario, we also assume that strain x_4 is promoted by therapy one (that is, $\rho_{4,1} > \delta$). Hence, without any control policy, the strain x_4 together with strains x_5 to x_{10} are expected to proliferate in the system. With the introduction of switching in the system, any switching policy leads to eradication of strains in the long run. However, the switching based on the Lyapunov function ensures a faster rate of convergence to eradication. In particular, the sub-optimal switching type 2 achieves this faster than any other drug switching approach (see Figure 4.10) and it is also interesting to note from that this is obtained without the use of therapy 5 in the switching sequence.

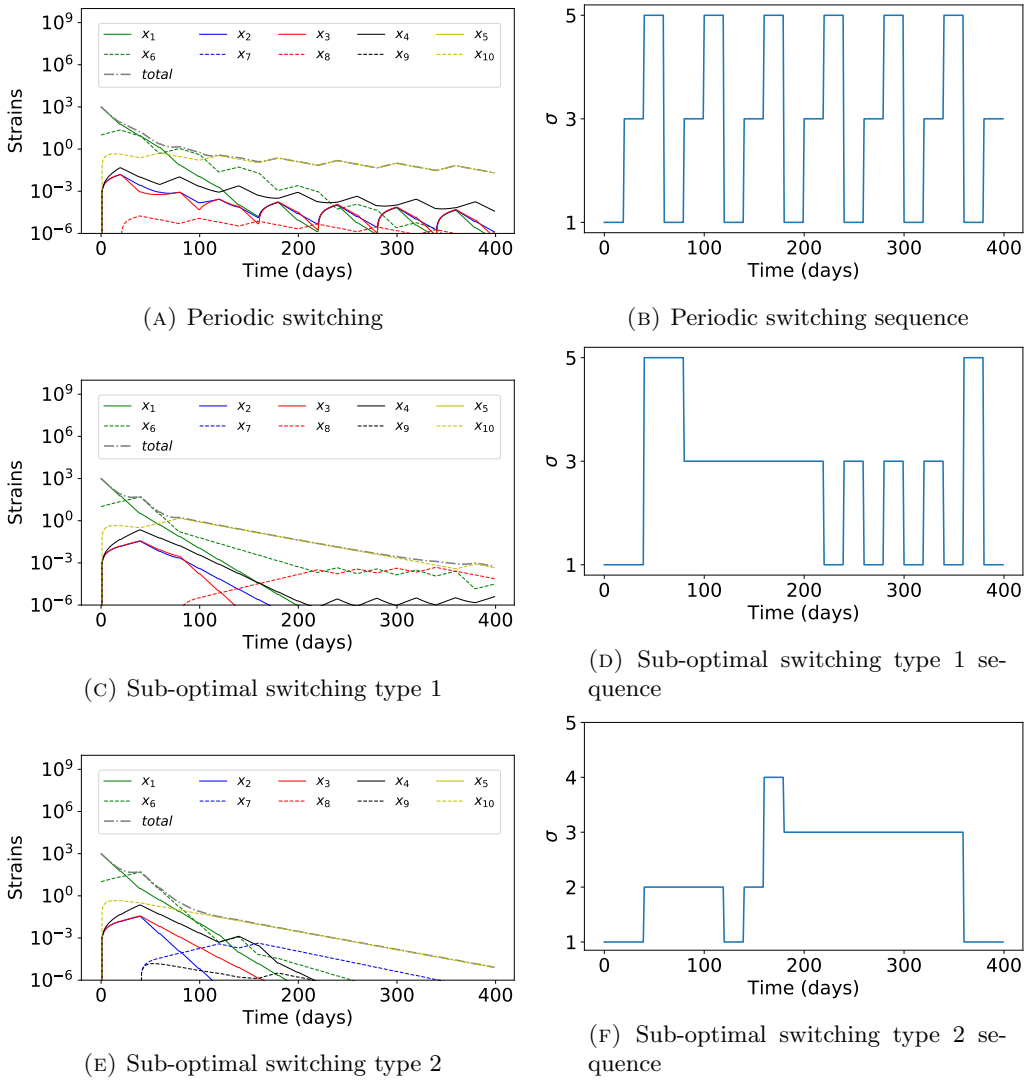

(A) Periodic switching

(B) Periodic switching sequence

(C) Sub-optimal switching type 1

(D) Sub-optimal switching type 1 sequence

(E) Sub-optimal switching type 2

(F) Sub-optimal switching type 2 sequence

FIGURE 4.10: Periodic, sub-optimal types 1 and 2 switching policies for Scenario 1.

In scenario 2, we have that there are more strains being inhibited in the susceptible class (that is strains x_1 to x_5) with only x_6 in the resistance class being inhibited by therapy 5. Therefore without switching, these strains are going to proliferate in the system thus making

the system unstable. Due to these proliferations, even with switching control, the system cannot be stabilised in the origin by a periodic switching as these strains still persist (see Figure 4.11). However, both types of the Lyapunov-based switching (sub-optimal switching types 1 and 2) ensures eradication, that is the convergence at the origin, with the sub-optimal switching type 2 achieving this even faster and with the lowest pathogen load at the end of treatment days.

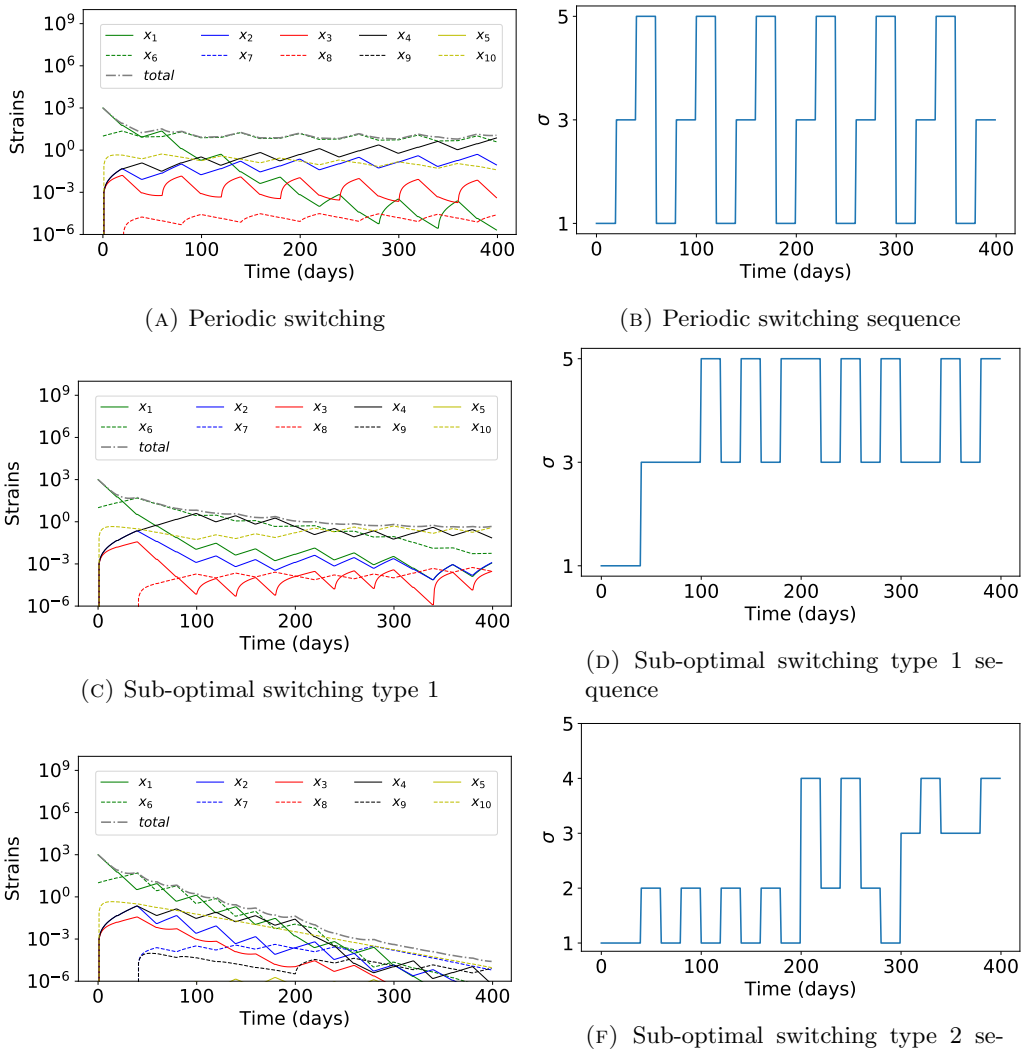

(A) Periodic switching

(B) Periodic switching sequence

(C) Sub-optimal switching type 1

(D) Sub-optimal switching type 1 sequence

(E) Sub-optimal switching type 2

(F) Sub-optimal switching type 2 sequence

FIGURE 4.11: Periodic, sub-optimal types 1 and 2 switching policies for Scenario 2.

In sharp contrast to scenario 2, in scenario 3, there are more strains being inhibited in the resistance class (that is strains x_6 to x_{10}) with only x_4 in the susceptible class being inhibited by therapy 1. This results in an ever-growing resistant population rendering the system unstable. Introducing switching control into the system still makes it unstabilsable at the origin with either periodic switching or any of the two Lyapunov switching types. We observe that there is no change in switching sequence and total pathogen load at the end

of treatment for both types of Lyapunov-based switching policies as seen in Table 4.5 and Figure 4.12. Furthermore, the switching sequences for both types of the Lyapunov switching also remain the same.

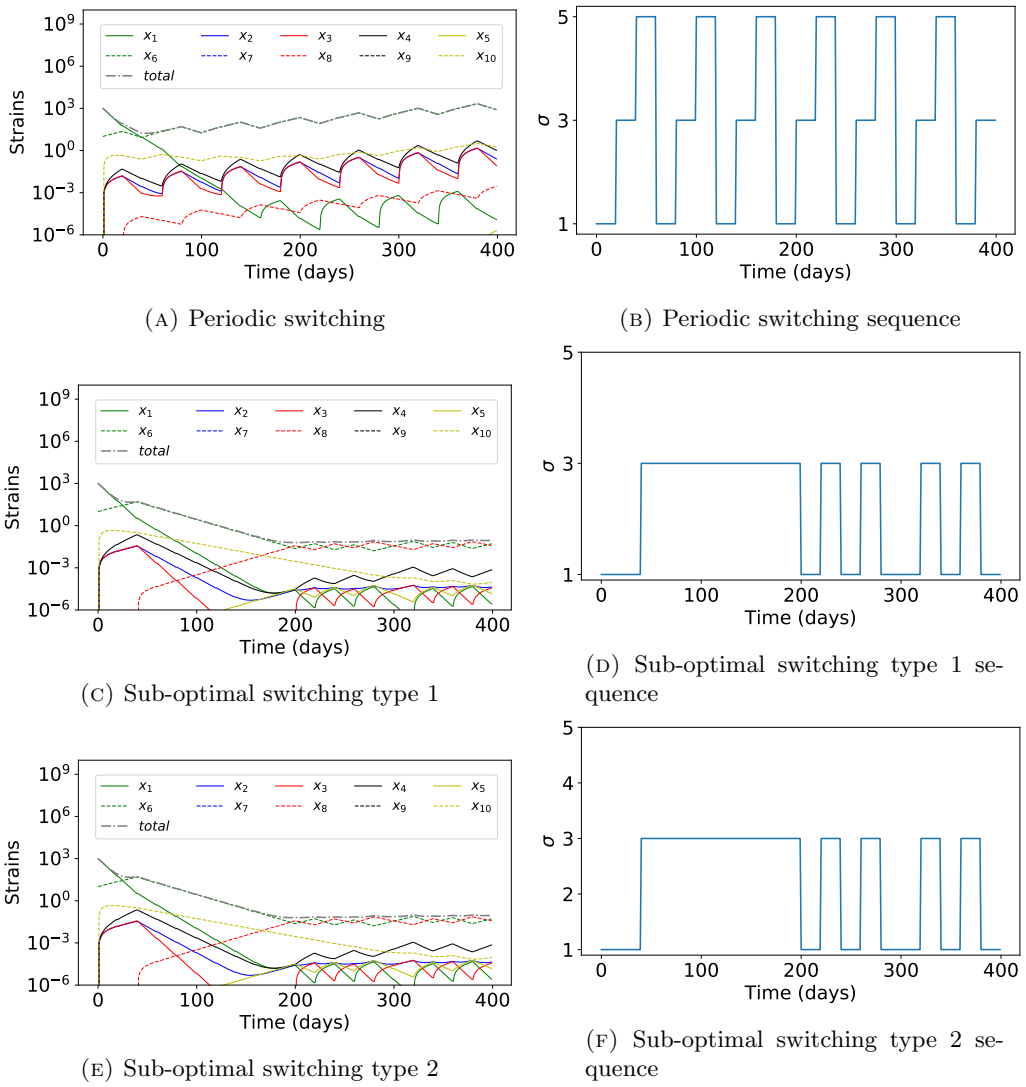

(A) Periodic switching

(B) Periodic switching sequence

(C) Sub-optimal switching type 1

(D) Sub-optimal switching type 1 sequence

(E) Sub-optimal switching type 2

(F) Sub-optimal switching type 2 sequence

FIGURE 4.12: Periodic, sub-optimal types 1 and 2 switching policies for Scenario 3.

In scenario 4, however, all therapies promote the growth of strains in both susceptible and resistant classes (see Table 4.4). Without any control policy, this system is not stable at the origin. However, sub-optimal switching type 2 gives a better control to the origin and lowest pathogen load at the end of the treatment period (see Figure 4.13).

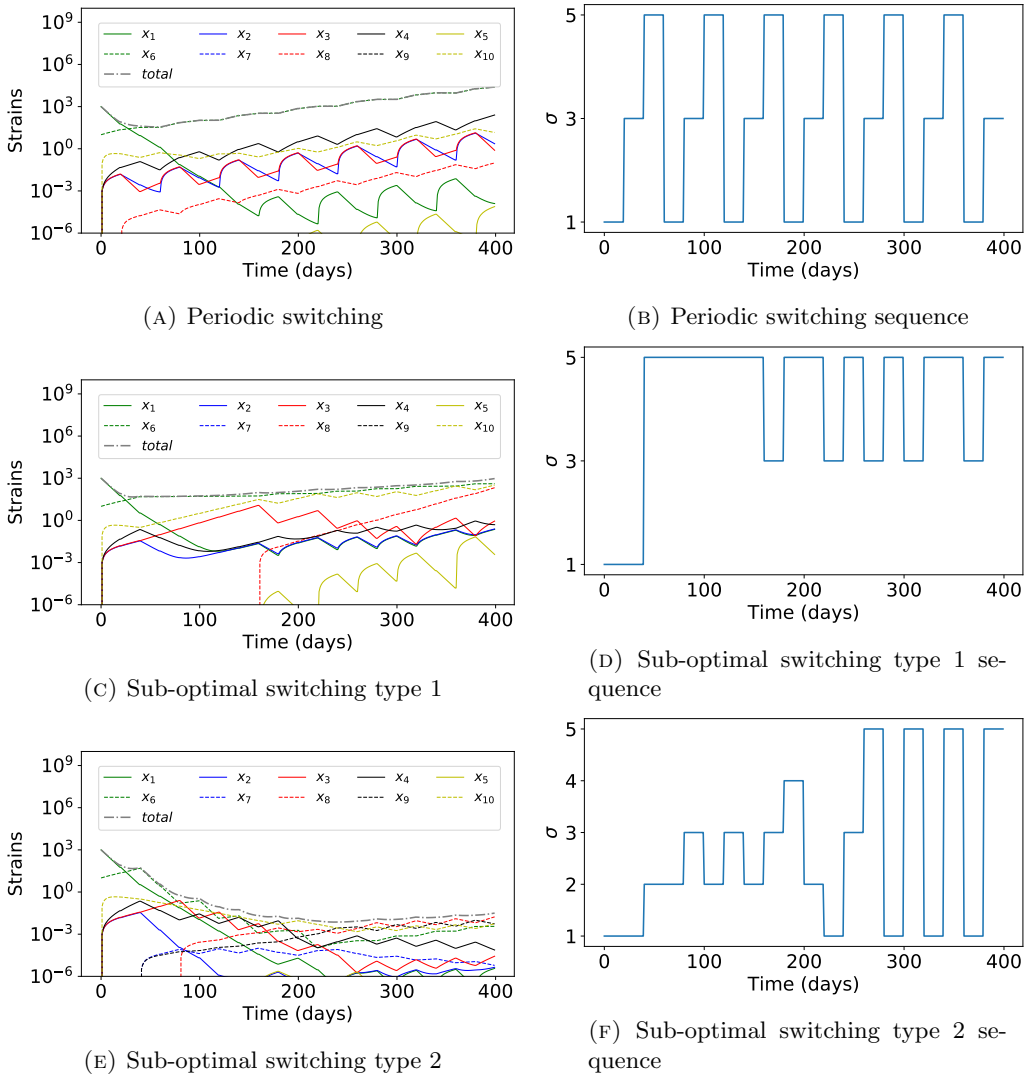

(A) Periodic switching

(B) Periodic switching sequence

(C) Sub-optimal switching type 1

(D) Sub-optimal switching type 1 sequence

(E) Sub-optimal switching type 2

(F) Sub-optimal switching type 2 sequence

FIGURE 4.13: Periodic, sub-optimal types 1 and 2 switching policies for Scenario 4.

Table 4.5 summarises the treatment scenarios of 400 days with a decision to switch therapy every 20 days. As seen in Table 4.5, the Lyapunov type 2 switching approach yields the best alternative for all the scenarios considered.

Scenario	Periodic	Sup-optimal type 1	Sub-optimal type 2
1	0.02	5.63×10^{-4}	8.16×10^{-6}
2	11.39	0.46	2.55×10^{-5}
3	808.14	0.09	0.09
4	24476.55	945.80	0.03

TABLE 4.5: Total pathogen load at the end of treatment of 400 days with a 20 day drug switching interval.

4.6 Chapter summary

The aim of any drug treatment during an infection is the complete eradication of the pathogen by exposing disease-causing cells to adequate concentrations of drug within the host. The current clinical principle of drug cycling relies on the reduction of resistant strains in the absence of resistance selection [111]. However, collateral sensitivity cycling allows for selection against resistance with a primary basis on an increase in drug sensitivity as a result of rational selection of drugs with reciprocal collateral sensitivities [31, 30]. In principle, drug treatment based on collateral sensitivity cycling should exhibit superior efficacy in patients infected with both the fully susceptible pathogens population and resistant mutants compared to cycling of drugs without compatible collateral sensitivity profiles. However, designing effective drug protocols for clinical use is a challenging problem.

In this chapter, we presented a generalised switching logistic model with the potential to be the basis for scheduling antimicrobials to mitigate resistance. We analysed this model by considering two pathogen strains and two therapies as well as a more general form of the model which can take several strains and several therapies. In the former, the mutation matrix was held constant for both therapies but in the later, this condition is relaxed and the mutation matrix is allowed to vary with the drug used.

As discussed in section Section 4.3, in the scenario involving two strains, the mutation process can lead to the loss of strain x_1 or the gain of strain x_2, while keeping the total mass of bacterial cells constant over time. Here, the matrix M represents the mutation scenario, with -1 on the main diagonals and 1 elsewhere. Positive values of μ are required because a negative value of μ leads to a positive coefficient for x_1 in eq (4.4a) and a positive coefficient for x_2 in eq (4.4b), which is not possible since a strain cannot mutate into itself.

Furthermore, in the two-strain model, conditions for which the unstable zero-equilibrium of the logistic equations can be stabilized through a periodic switching signal are derived, assuming there is no mutation. For the case with mutations, switching strategies based on Lyapunov functions prove to be a fast and practical computational approach. Numerical results highlighted that the strategy with Lyapunov functions will perform better than periodic therapies, and in certain conditions will be able to eradicate pathogenic populations. Numerical results also show that cycling strategies are not intuitive and bacterial dynamics under different treatments are central for infection eradication.

A key biological aspect of this proposed control-theoretical approach for the two strain model is that, in a first stage one needs to identify the distribution of the bacterial population. Based on this initial information, a switching trajectory (see Figure 4.6(a)) can be computed to indirectly define a sliding mode (see Figure 4.6(b)). Once on the sliding mode, a periodic switching between therapies can be utilised to eradicate the bacterial colony. In conclusion,

this approach can be used as an instrument in the future to guide therapies to tackle bacterial resistance with a minimal collection of information.

In the more general model, the implications of different types of cycling strategies as well as the use of cross sensitivity of cell strains to treatment in a general setting and not for specific antibiotics and/or pathogens was explored. We implemented drug cycling by changing drug dependent parameters which consequently leads to changes in cell mutations and hence varying mutation matrices for each drug used. Cell mutations are assumed to be absolute and irreversible events which depend on the drug used. Therefore, the use of different drugs gives rise to different mutations due to the varying collateral susceptible profiles of pathogens.

It is important to note that this general formulation includes the mutation process as an additional growth factor, resulting in the absence of mass conservation. The main diagonal of $M_{\sigma(t)}$ is neglected, implying that there will be more growth than with a mutation process that does not produce extra bacteria. Thus, if the zero fixed point can be stabilised for this general case as shown in Section 4.4, then its analysis is sufficient for the other cases to hold.

We used three types of drug switching strategies with different switching orders. In the first switching type, periodic switching, the order of drug sequence is periodic. In our two sub-optimal switching strategies, the effect of drug measured at a specific time point is defined by the instantaneous rate of change in total pathogen size under the Lyapunov function in eq (4.25) and the switching law defined by eq (4.28). Hence, these depend on the pathogen load at a given moment and the effect of the drug towards cells. Thus, if the cell composition and/or drug parameters are unknown, we cannot measure the drug effect. This therefore poses a challenge to capturing the switching sequence leading to the eradication of resistant strains.

In most microbial infections it is difficult to obtain detailed information about heterogeneity of cell population. Thus, although we have derived sub-optimal therapeutic protocols for therapy scheduling based on collateral sensitivity profiles of drugs and pathogen strains, their application in a clinical setting would require knowledge of drug and pathogen parameters. One important aspect for the clinical implementation of our sub-optimal switching strategies lies in fast quantification of pathogen population as well as drug parameters as defined in our algorithm. Recent advances [215] provide robust techniques to obtain this information in a clinically relevant setting. In [215] plasma cell-free DNA is sampled from a patient with relatively high temporal frequency and used to resolve the corresponding evolutionary dynamics.

Several studies have identified many collateral sensitivity relationships among various antibiotics as well as anticancer drugs [31, 203, 193, 216]. Our numerical simulations are made up

of three and five drug cycles. From our results in Figures 4.10-4.13, we observe that the application of more than three-drug cycles in our sub-optimal switching type 2 strategy leads to low pathogen loads compared to the other methods considered, indicating that this method can improve the efficacy of therapies when designed suitably and taking into consideration the susceptibility profiles of pathogens.

To sum up, switching therapies can be considered as a mechanism for improving the stabilisation and rate of convergence of a positive system when more than one treatment policy is used. For the particular case of antibiotic resistance infections, switching can be applied for the gradual eradication of resistant strains on the long term based on a feedback decision. Our numerical simulations suggest that switching between therapies based on the switching rule from the Lyapunov function leads to a better convergence at the origin than an open-loop periodic switching.

Chapter 5

Between-host resistance

In this chapter, we present a between-host model of the novel coronavirus, SARS-CoV-2, epidemic using network theory. We consider the progression of the epidemic amidst vaccination and non-pharmaceutical interventions such as lockdowns. We also investigate the effect of vaccine resistant strains on the transmission dynamics of the disease. Using stochastic simulations, we analyse and highlight the need for strengthening vaccination efforts so as to curb further spread of the virus. This project is coded in Python v.3 and the simulation codes can be found in this Github repository

5.1 Introduction

Between-host transmission generally refers to the transmission of infection between individuals in a population. The general framework underlying models at the between-host level is usually classic compartmental modelling. This involves dividing a given population into different compartments based on disease or infection symptoms. Typically, the population under study is divided into three classes which represent the interactions between susceptible individuals S, infected individuals I, and recovered individuals R. Susceptible individuals include all in the population who are not yet infected with the disease but are prone to infection. Infected individuals are all those assumed to have been infected and capable of transmitting the disease causing agents to susceptibles. Individuals in the recovered compartment are those individuals who have either been infected and recovered from the disease and have therefore become immune or vaccinated against infection or isolated from the rest of the population. Depending on the disease under study, more compartments can be created.

The earliest basic compartmental model to describe the transmission of infectious diseases was formulated by W.O. Kermack and A.G. McKendrick in 1927 [170]. These models are

deterministic in nature and predict similar behaviours observed in numerous diseases that pose a threat to a population. They have been used over the years to predict the spread of infectious diseases between individuals in a given population. To mention a few, such models have been instrumental in the study of malaria, measles and the SARS epidemic of 2002-2003.

In the rest of this chapter, we focus on the disease transmission dynamics of the novel coronavirus, SARS-CoV-2 using a social network model based on a Susceptible-Asymptomatic-Infected-Recovered disease dynamic. We shall discuss the epidemic process of the disease with and without vaccination in the population and highlight the importance of vaccination efforts during disease outbreaks, especially during the SARS-CoV-2 pandemic. We shall also discuss the impacts of vaccine-resistant strains on the disease dynamics of SARS-CoV-2.

5.2 Network modelling of SARS-CoV-2

To curb the spread of SARS-CoV-2, governments across the world have implemented measures ranging from quarantining, social distancing, wearing of face masks, among others. Amidst this crisis, national health care systems such as in Italy and the United States of America have been overwhelmed by the ever-increasing number of infection cases [163].

SARS-CoV-2 epidemiological models have been formulated to understand and curb the spread of the disease. Many of these models follow an SIR framework [169, 170] either in the deterministic or stochastic form or both [171, 172, 173, 174, 175, 176]. Other variations and modifications to this general model have been considered including SEIR [177, 178, 179] and SIRD [180] compartmental models. Some models also include parameters such as age-heterogeneity [181], guiding the flow of users in supermarkets [182] and governmental policies [179, 183, 184]. However, only a few of these models, consider the structure of the population and the underlying interactions between individuals [187, 188, 189].

The assumption of random homogeneous mixing in epidemiological models has been documented to be unrealistic in nature as populations have underlying structural properties and individuals tend to interact with each other [217]. Increasingly, network theory is being used in epidemiology [218, 219, 220, 221]. In particular, social networks have gained popularity in conceptualising the effects of social interaction during epidemics in a given population [222, 223, 224]. Contacts between individuals can be captured in a network where nodes represent individuals and the edges represent the connections between them [27]. Social networks are thus important determinants of infectious disease transmission as for example, infections transmitted by close contact can easily spread along the paths of a network. Figure 5.1 illustrates infection spread on a social network.

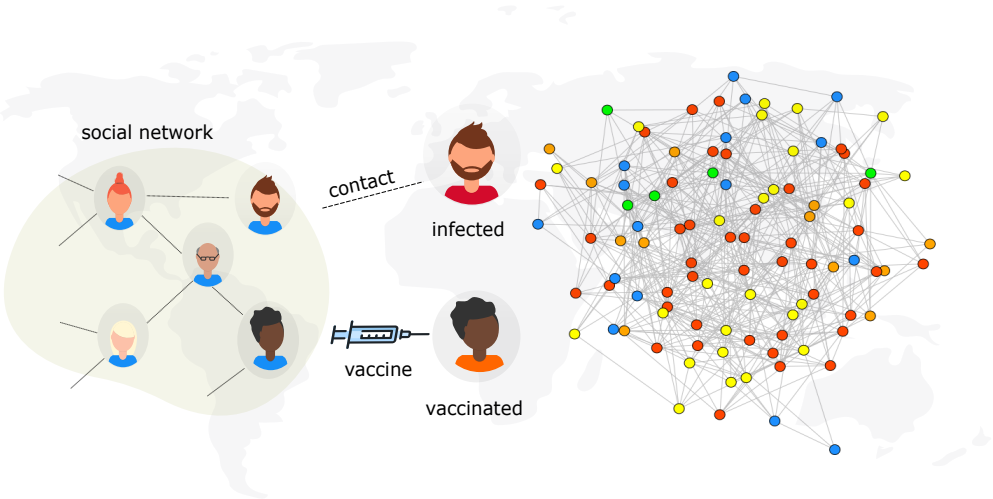

FIGURE 5.1: Illustration of infection spread with vaccination on a social network. Individuals in the social network are considered as nodes. Contact between nodes exposed to the virus and those who do not have the virus can potentially lead to a transmission. Persons who are vaccinated are considered to be immune to infection. The epidemic state of each node is represented by a colour: Susceptible, S, (•), Asymptomatic, A, (•), infectious, I, (•), Vaccinated, V, (•) and Recovered, R, (•).

Many studies in network theory have found that networks may display varying connectivity properties such as randomness and regularity. Some well-known network models include random networks, scale-free networks and small-world networks. Random networks such as the Erdos-Renyi network, are characterised by a Poisson distribution of nodes whereby there is equal distribution of nodes. Such models do not have hubs and there is absence of clustering effect. However, scale-free networks such as the Barabási and Albert model, follow a power-law distribution and have an inhomogeneous degree distribution of nodes [225] (that is, the number of connections a node has to other nodes). In small-world networks such as the Watts and Strogatz model, the pattern of connectivity between nodes is more localized [226] and the average path length is comparable with a homogeneous random network, without any regard to clustering.

During a disease outbreak, it is less likely for the disease to reach epidemic proportions in the power-law network than it is in random networks [227, 228]. This is because power-law networks are made up of vertices with few contacts and a very small proportion of hubs (or superspreaders) whereas vertices in random networks are fairly homogeneous. Thus, while it is possible to reach an epidemic in power-law networks with a high enough transmissibility, a random network reaches an epidemic threshold only when the outbreak leads to an epidemic [229, 218].

Since the declaration of SARS-CoV-2 as a pandemic, initial control efforts relied heavily on the use of non-pharmaceutical interventions (NPIs), including physical distancing, wearing of masks and hand hygeine. In many countries across the globe, school closures and national

lockdowns have been implemented as part of NPIs to mitigate infection [230, 231, 232]. However, with the continuation of SARS-CoV-2 worldwide, the push for a vaccine became highly necessary. Pharmaceutical companies have been in a race to develop suitable vaccines as there is a lack of other alternatives. As of October 2020, there were 17 candidate vaccines undergoing trial at various stages. Owing to the fact that it is a novel viral disease, it is still unclear what levels of vaccine efficacies will be sufficient to curb the spread of the virus. Identifying such efficacies earlier can direct vaccine development and administration in the population [233]. Previous studies suggest that vaccination would be effective for protecting the host against SARS-CoV-2 [140], however, few studies to evaluate the potential effects of different vaccination programs over a network model.

Although some vaccines (Pfizer-BioNtech and Modern) have showed high efficacy for the original strain of the virus, these clinical trials were done before the emergence of SARS-CoV-2 variants of concern. Variants of concern, especially delta, alpha, gamma and omicron are the main reason for continued infections globally. Consequently, even though mass vaccination campaigns have been launched in many countries including Israel, Germany, the United Kingdom and the United States with more than 50% of the population fully vaccinated [234], the continued evolution of SARS-CoV-2 could eventually give rise to a fully vaccine-resistant variant [235]. Such a variant has the potential to spread quickly due to its ability to infect vaccinated and recovered people in addition to fully susceptible individuals and consequently reducing the efficacy of current SARS-CoV-2 vaccines.

A key question to be answered is, how much vaccine is required to create herd immunity to block SARS-CoV-2 transmission? [236]. In other words, how many people need to be vaccinated in order to reach herd immunity?

Here, we employ a network-based approach to explore the potentials of two vaccination schemes, classical mass vaccination and ring vaccination, in minimizing the spread of SARS-CoV-2. Furthermore, we also study the potential impacts of vaccine resistant strains of the virus on the transmission dynamics of the disease.

Our analysis uses stochastic network simulation models of SARS-CoV-2 transmission to examine its control by different vaccination strategies with varying vaccine efficacy in the presence of non-pharmaceutical disease control interventions. Given that vaccinating millions of people will require a lot of time, this study implements a lockdown period as a further control measure. It is important to note that the roll out of vaccines play an increasing role in reducing the number of infections - thereby causing governments to ease lockdown measures. However, in order to keep our model mathematically tractable, we assume that social contacts follow lockdown-period patterns throughout the vaccination campaign.

5.2.1 Model Setup

Network Generation. To study the impact of vaccination on the epidemic dynamics of SARS-CoV-2, the underlying structure of human interactions is represented by a typical complex network. As heterogeneous networks are often used to explore epidemic spread, we consider the infection dynamics on a random Erdos-Renyi (ER) network and a scale-free Barabási–Albert (BA) network due to their tractability and practicability [237, 225] (see also Chapter 2). The ER network is based on the $G(n, M)$ random graph model characterized by two parameters; the network size n and the number of edges M which assigns exactly M edges to each graph. In the ER networks used for this study, $n = N, M = 5N$, that is $G(N, 5N)$, which yields an average degree $\langle k \rangle = 10$. On the other hand, the BA network is created using $G(N, m, p)$ consisting of N vertices and m outgoing edges for each vertex with a power constant p of the nonlinear model equal to one. For the simulations using the BA network, $m = 5$ and $p = 1$ which ensures an average degree of $\langle k \rangle = 10$ as in the ER network. Table 5.1 summarizes all the key terms and parameters used in the rest of this chapter.

TABLE 5.1: Definition of key terms and parameters

Key term	**Definition**	**Value**
N	number of nodes in the network	10^6
$\langle k \rangle$	average degree of nodes in the network	10
transmission probability β	the probability that infection is spread due to contact between an infectious node and a susceptible node	eq (5.7)
incubation period	the interval between exposure to virus and initial occurrence of symptoms	$1-5$ days [238]
infection period	interval between symptom onset to recovery	$6-19$ days [239]
vaccine efficacy η	efficacy of vaccine	varies [240]
$\%vac$	percentage of population vaccinated prior to infection (before case zero)	varies
T	epidemic duration	360 days
$\%asymptomatic$	percentage of population asymptomatic to virus before onset of vaccination	varies
symptomatic probability, δ	the probability that a person in the A class moves to the I class	0.2 [241]

Epidemic Spread. SARS-CoV-2 is a disease which spreads primarily through close contact with an infected person. Following the exposure to the SARS-CoV-2 virus and before symptom onset, individuals go through an incubation period of about $2-14$ days with the average being about $5-6$ days [239, 242, 238]. After this incubation period, infectious individuals become symptomatic and are able to transmit to others through respiratory droplets or by direct contact [239].

Model formulation. Let $W = \{1, \ldots, n\}$ be the set of all virus variants circulating in the population. For each $j \in W$ and time $t \geq 0$, let $S(t), A_j(t), I_j(t), R_j(t)$ and $V(t)$ respectively denote the number of Susceptible, Asymptomatic due to strain j, Infectious due to strain j, Recovered from strain j and Vaccinated individuals in the population at time t.

At any time t during the infection process, individuals in the susceptible class $S(t)$ are not infected but are prone to infection with the virus. The Asymptomatic population $A_j(t)$ consists of individuals who are infectious with variant j, may not show symptoms and can transmit to others. Individuals making up the Infectious population $I_j(t)$ are infectious with variant j, symptomatic and capable of transmission to others. In the Recovered population $R_j(t)$, individuals are recovered and immune to variant j (but can be susceptible to another variant, $v \neq j$) and the Vaccinated population $V(t)$ consists of individuals who have been vaccinated. In addition, we assume that there is no co-infection and hence individuals can only be infected by one variant at any given time. Therefore, at any time, t, in the infection process, $N(t) = S(t) + A(t) + I(t) + R(t) + V(t)$.

The main goal of vaccination is to prevent transmission. At the beginning of each epidemic simulation, a fraction of the population ($\%vac$) is given a vaccine. Due to delayed immunity of the vaccine, these vaccinated individuals remain in the S state for a period of 14 days. Within this 14 day window, these individuals, which we denote as V_s, are still prone to interaction with asymptomatic and infectious individuals which can lead to more infections with a probability β. After 14 days, individuals in V_s who do not have the virus, move to V state. Individuals in V that become exposed to the virus due to contact with an exposed individual move into the A state with probability $(1 - \eta)\beta(t)$, where η is the efficacy of the vaccine. Individuals for whom the vaccine is effective remain in the V state whilst those for whom the vaccine is not effective move into the A state. Furthermore, depending on the vaccination strategy being modelled, the time of vaccination as well as population coverage varies.

We denote by X_t the set of nodes with state $x_{it} = X$ at time t. The model proceeds in discrete one-day time steps for a given period to determine the dynamics of the disease. Each node $i = 1, \ldots, N$ has an individual state x_{it} at time t. We initialize the model simulation by randomly assigning a number of nodes (seed nodes) to the asymptomatic state (A_1), that is setting $x_{i0} = A_1$ and the rest of the nodes to the susceptible state. Conditional on the current state x_{it}, the next state $x_{it'}$ for node i is determined as follows.

- Susceptible nodes

$$x_{it'}|(x_{it} = S) = \begin{cases} A_j & \text{with binomial trial} \quad B(1, \beta(t)) \\ S & otherwise \end{cases} \tag{5.1}$$

- Asymptomatic nodes

$$x_{it'}|(x_{it} = A_j) = \begin{cases} I_j & \text{after incubation period} \\ R_j & otherwise \end{cases} \tag{5.2}$$

- Infectious nodes

$$x_{it'}|(x_{it} = I_j) = \begin{cases} R_j & \text{after infectious period} \\ I_j & otherwise \end{cases} \tag{5.3}$$

- Recovered nodes

$$x_{it'}|(x_{it} = R_j) = R_j \quad \text{with probability} \quad 1 \tag{5.4}$$

- Vaccinated nodes

$$x_{it'}|(x_{it} = V_s) = \begin{cases} S & \text{within 14 days post vaccination} \\ V & \text{after 14 days post vaccination} \end{cases} \tag{5.5}$$

$$x_{it'}|(x_{it} = V) = \begin{cases} A_j & \text{with binomial trial} \quad B(1, (1-\eta) \times \beta(t)) \\ V & otherwise \end{cases} \tag{5.6}$$

This mathematical model and general methodology can be extrapolated to more variants, increasing the number of equations and parameters. Figure 5.2 illustrates an example of the model described above, specific for two viral strains.

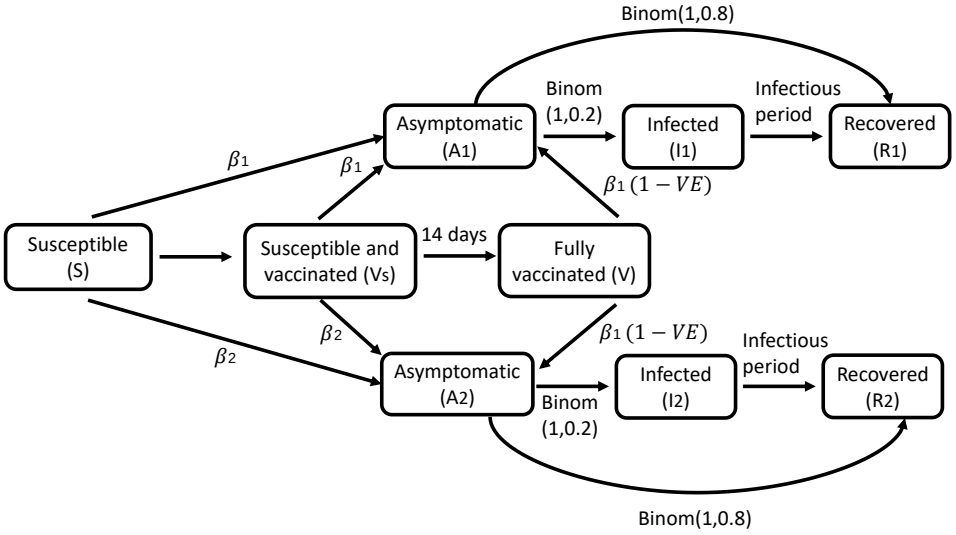

FIGURE 5.2: Schematic illustration of double strain network model with for SARS-CoV-2. S: susceptible, V: vaccinated, A_1: asymptomatic with strain one, I_1: infected with strain one, A_2: asymptomatic with strain two, I_2: infected with strain two, R: Recovered from infection.

5.3 High-Performance Computing

Implementations of the models used in this Chapter were computationally demanding and challenging using conventional resources. For instance, one simulation can take up to several hours or days to complete in a modern desktop computer. Thus, due to these limitations, we employed a High-Performance Computing (HPC) cluster for our simulations. The cluster used is FUCHS-CSC from the Center for Scientific Computing (CSC, Frankfurt, Germany). It is based on 72 dual-socket AMD Magny-Cours CPU compute nodes with 64 GB of RAM, 250 dual-socket AMD Istanbul compute nodes with 32 GB of RAM and 36 quad-socket AMD Magny-Cours compute nodes with 128 GB of RAM each. A simulation in the HPC takes about 5 hours to complete for the classical vaccination scenarios and about $5-8$ days for the ring vaccination scenarios for the single strain model. In the double strain model, a single scenario takes about 24 hours to complete in the cluster.

In the subsequent sections, we will explore these dynamics using a single strain of the virus, with a double strain and further with a vaccine resistant strain of the virus.

5.4 Single strain network modelling of SARS-CoV-2

5.4.1 Epidemic Process

For a single strain (where $n = 1$ and $W = \{1\}$), the model proceeds for a period of 360 days. At the initial state of the epidemic process, all individuals in the network are susceptible except one (patient zero) which is in the asymptomatic state. On each day during the epidemic process, there is interaction between individuals and infected persons can potentially transmit to their susceptible contacts. If a susceptible individual comes into contact with someone who has the virus (that is, a person in the A or I state), a Binomial trial is used to determine if the contact results in an infection. If yes, the newly infected susceptible individual moves from the S state to the A state. Any individual exposed to the disease remains in the A state for the duration of the incubation period. After the incubation period, infected nodes either move to the I state with a probability δ or to the R state with a probability $(1 - \delta)$. When infectious individuals come into contact with their neighbours, they can transmit to their neighbours in a Binomial trial with a given probability, $\beta(t)$ and then move into the R state after the infectious period.

In the course of an epidemic, the rate of infection is never constant. As interventions are being executed, the per-capita transmission rate of infection decreases, and when these interventions cease, this rate will increase towards its pre-intervention level. To model this response, we utilise a double logistic function to model the various phases of the infection dynamics leading to a decline in cases when interventions are initiated and a resurgence in cases when interventions cease. The double logistic function used to define a time dependent probability of infection, $\beta(t)$ is as follows:

$$\beta(t) = b_1 + (b_2 - b_1)\left(-1 + \frac{1}{1 + e^{-r_1(t-m_1)}} + 1 + e^{-r_2(t-m_2)}\right) \tag{5.7}$$

where b_1 is the first boundary (i.e. function value at time zero), b_2 is the second boundary, r_1 is the rate of change of first period, r_2 is rate of change of second period, m_1 is the midpoint of the first period (start of interventions), m_2 is the midpoint of the second period (end of interventions) and t is time. Note that if $b_1 > b_2$ the function increases first and then decreases, and vice versa. To get a good set of parameters for $\beta(t)$, we applied eq (5.7) to emulate infection data (from February 22 to September 1 2020) from Italy, one of the worst hit countries during the SARS-CoV-2 pandemic (see Figure 5.3).

For the first strategy which we refer to as the **classical mass vaccination** strategy, a fraction of individuals start in the V state (denoted $\%vac$) with one index case (patient zero) and the rest in the S state. The population coverage in this case ranges from $10\%, 20\%, \cdots, 100\%$. The modelling process follows as in Algorithm 1.

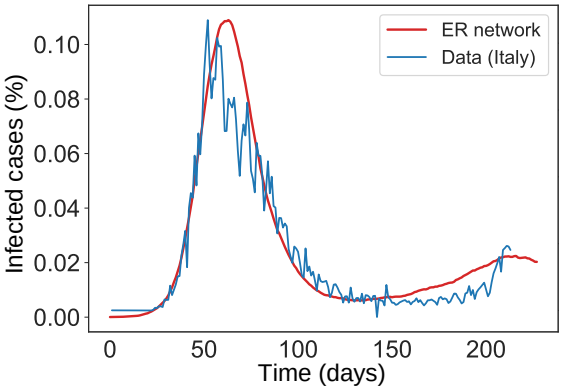

FIGURE 5.3: Infection cases between the network model simulation using $\beta(t)$ and Italian SARS-CoV-2 data from February 22 2020 to September 1 2020. The y-axis shows the infection cases. Parameter values used are $b_1 = 0.028$,$b_2 = 0.001$, $r_1 = 0.09$, $r_2 = 0.04$, $m_1 = 50$, $m_2 = 126$.

Algorithm 1: Epidemic process on social network

Input: Network, $\beta(t)$, epidemic duration, $T = 360$ days

Output: Number of nodes in each state after each simulation

Initialize: Choose an index case at random, and set state to be A. Set

$$V_s = \%vac, V(0) = 0, S(0) = N, A(0) = 1, I(0) = 0, R(0) = 0, State(\%vac) = V_s$$

for $t \in T$ **do**
  for $i \in \{\%vac\}$ **do**
    if *14 days is reached and* $State(i) = V_s$ **then**
      $State(i) = V$
  for $n \in \{e|State(e) = A\}$ **do**
    if *incubation period is reached* **then**
      $State(n) = R$ with binomial trial $B(1, \delta$
    else
      $State(n) = I$
    for *each neighbour, nb of* n **do**
      if $State(nb) = S$ **then**
        $State(nb) = A$ with a binomial trial $B(1, \beta(t))$
      if $State(nb) = V$ **then**
        $State(nb) = A$ with a binomial trial $B(1, (1 - \eta) \times \beta(t))$
      if *before 14 days is reached and* $State(nb) = V_s$ **then**
        $State(nb) = A$ with a binomial trial $B(1, (\beta(t))$
  for $m \in \{i|State(i) = I\}$ **do**
    for *each neighbour, mnb of* m **do**
      if $State(mnb) = S$ **then**
        $State(mnb) = A$ with a binomial trial $B(1, \beta(t))$
    If the infectious period is reached, $State(m) = R$
  Stop the simulation when there is no infectious node and update the number of nodes in all states.

Result: Updated number of nodes in all states

For the second strategy which we refer to as **ring vaccination**, vaccination occurs after a percentage (1% or 3%) of the population has been exposed to the virus during the epidemic and is in the asymptomatic state. In this case, we simulate the epidemics as described above (in Algorithm 1) with no vaccination and only begin vaccine administration after a proportion of the population ($\%asymptomatic$) is asymptomatic (See Algorithm 2 for more details).

Algorithm 2: Ring vaccination model on social network

Input: Network, $\beta(t)$, epidemic duration, $T = 360$ days,$\%asymptomatic$

Output: Number of nodes in each state after each simulation

Initialize: Choose an index case (i) at random, and set state to be A. Set

$$V(0) = 0, S(0) = N, A(0) = 1, I(0) = 0, R(0) = 0$$

```
for t ∈ T do
    if #{ e|State(e) = A} < %asymptomatic then
        proceed using Algorithm 1
    else
        for n ∈ {e|State(e) = A} do
            if incubation period is reached then
                State(n) = I
            for each neighbour, nb of n do
                if State(nb) = S then
                    State(nb) = A with a binomial trial, B(1, β(t))
                    select and store susceptible neighbours not exposed in previous step and
                     label as first contacts
                if State(nb) = V then
                    State(nb) = A with a binomial trial, B(1, β(t))
                    for each node in first contacts do
                        vaccinate
                        select and store susceptible neighbours and label as second contacts
                    for each node in second contacts do
                        vaccinate
    for m ∈ {i|State(i) = I} do
        for  each neighbour, mnb of m do
            if State(mnb) = S then
                State(mnb) = A with a binomial trial, B(1, β(t))
        If the infectious period is reached, State(m) = R
    Stop the simulation when there is no infectious node and update the number of nodes in all
     states.
```

Result: Updated number of nodes in all states

We assume that once a case is diagnosed, all the contacts or neighbours are traceable and vaccinated. To initiate the ring vaccination, susceptible contacts of exposed individuals can be vaccinated in a binomial trial with probability $(1-\eta)\beta(t)$. This vaccination is further extended to susceptible contacts of these first contacts with the assumption that contacts are identified through contact tracing. Contacts of contacts are also vaccinated with the same probability. In our model, we also assume that traced and identified susceptible contacts and contacts of contacts are vaccinated. This process is described in Algorithm 2. In both strategies, we assume that the vaccine does not have an effect on infectious or asymptomatic individuals.

5.4.2 Simulation Scenarios

Several scenarios are explored here. First, we consider an epidemic implemented with no vaccination. This scenario is evident of the epidemic outcome without the discovery of a vaccine. Subsequent scenarios consist of the overall performance of the vaccine by considering its efficacy in preventing transmission and symptomatic infection using either the classical mass vaccination or the ring vaccination strategy. In our simulations, vaccine efficacy varied between $40\% - 100\%$ whereas population coverage for classical vaccination varied between $10\% - 100\%$. For ring vaccination, the proportion of asymptomatic individuals ($\%asymptomatic$) varied as 1% and 3% (see Table 5.2). For ER simulations: $N = 10^6$, $b_1 = 0.028$, $b_2 = 0.001$, $r_1 = 0.09$, $r_2 = 0.04$, $m_1 =$ day 50, $m_2 =$ day 126 and $T = 360$ days. For BA simulations: $N = 10^6$, $b_1 = 0.013$, $b_2 = 0.001$, $r_1 = 0.09$, $r_2 = 0.04$, $m_1 =$ day 50, $m_2 =$ day 126 and $T = 360$ days. Each scenario is repeated 100 times and the mean of infection cases taken for analysis.

TABLE 5.2: Vaccination scenarios with corresponding population coverage and vaccine efficacy.

Scenario	**Coverage**	**Time of vaccination**	**Effect of vaccine (%)**
No vaccination	0%	-	-
Mass vaccination	$10\%, 20\%, \cdots, 100\%$	Before case zero	$40, 60, 80, 100$
Ring vaccination	1st order and identified contacts AND contacts of contacts	After percentage of population infectious (varies between $1\%, 3\%$)	$40, 60, 80, 100$

5.4.3 Results

Our parameter fitting for $\beta(t)$ shows infection peaks at comparable time points with varying population percentages but essentially a qualitative fit of the data (see Figure 5.3). The parameter values used to fit $\beta(t)$ are: $b_1 = 0.028$, $b_2 = 0.001$, $r_1 = 0.09$, $r_2 = 0.04$, $m_1 = 50$, $m_2 = 126$.

Control Scenario

In a completely susceptible population, the introduction of one asymptomatic individual leads to the spread of the infection with more than one peak of cases of infection after some months. In Figure 5.4, the mean number of infectious cases peaks at 0.83% for ER network and 0.07% for BA network.

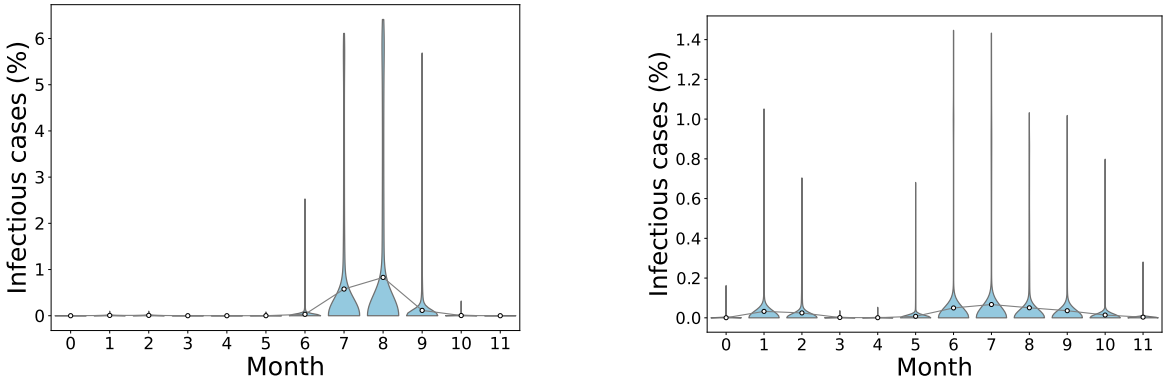

(A) (B)

FIGURE 5.4: Distribution of the final infectious cases in different timing for scenarios without vaccination in both networks. A population of N= 10^6 individuals was generated and 100 simulations were run to simulate the epidemic in the course of one year. An individual was chosen randomly as patient zero for each run. Circles represent mean infection cases for each month connected by lines. (a): Erdos-Renyi network, (b): Barabasi-Albert network.

Mass Vaccination Scenarios

These scenarios determine the outcome of vaccination at the initial stages of the epidemic before infectious cases peak in both networks. From Figure 5.5 we observe that generally, infection peaks are much lower in Barabasi-Albert network than in the Erdos-Renyi network.

In the Erdos-Renyi network, when vaccine efficacy is 40%, a population coverage of 40% or more is needed to achieve infection peak with less than 1% infection cases in the population. Figure 5.5 reveals that with vaccine efficacy of 60%, a coverage more than 60% keeps mean infection cases on the low with elimination of the peak occurring when coverage is more than 80%. Furthermore, low cases of infection are observed when 70% or more of the population is vaccinated and vaccine efficacy is 80%. On the other hand, a vaccine which is 100%

efficacious requires just 20% or more of the population to be vaccinated to ensure there is no peak of infections.

In the Barabasi-Albert network, with a vaccine efficacy of 40%, a population coverage of more than 60% ensures elimination of infection peaks whereas when vaccine efficacy is 60%, a coverage more than 70% achieves elimination. In addition, when 70% or more of the population is vaccinated with an 80% efficacious vaccine, infection cases are almost negligible. In the case when a 100% efficacious vaccine is administered, a population coverage more than 20% keeps infection peaks at bay.

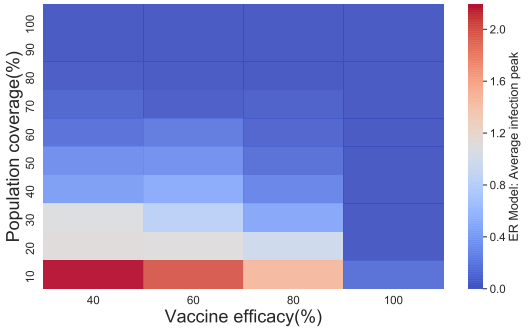

(A) Erdos-Renyi Model: Heatmap illustrating average infection peaks considering vaccine efficacy and population coverage.

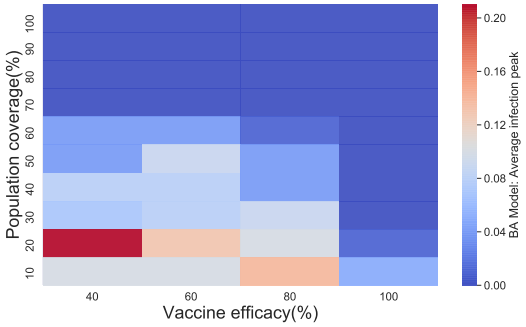

(B) Barabasi Albert Model: Heatmap illustrating average infection peaks considering vaccine efficacy and population coverage.

FIGURE 5.5: Comparing infection peaks in both networks.

As seen in Figures 5.6 and 5.7 (see also Figures A.1 - A.4 and Figures A.7 - A.10 in the appendix), peak(s) of infection cases are observed when a small percentage of the population is vaccinated in both networks with double infection peaks more frequent in the Barabasi-Albert network. For instance, in both networks, there is at least one peak of infection for vaccine coverage between 20% and 60% even when η varies. Therefore, vaccinating a small proportion of the population is not useful in these instances as cases can still peak even with a vaccine with 100% efficacy. Thus, the key to eliminating infection peaks is to administer very efficacious vaccines to many individuals.

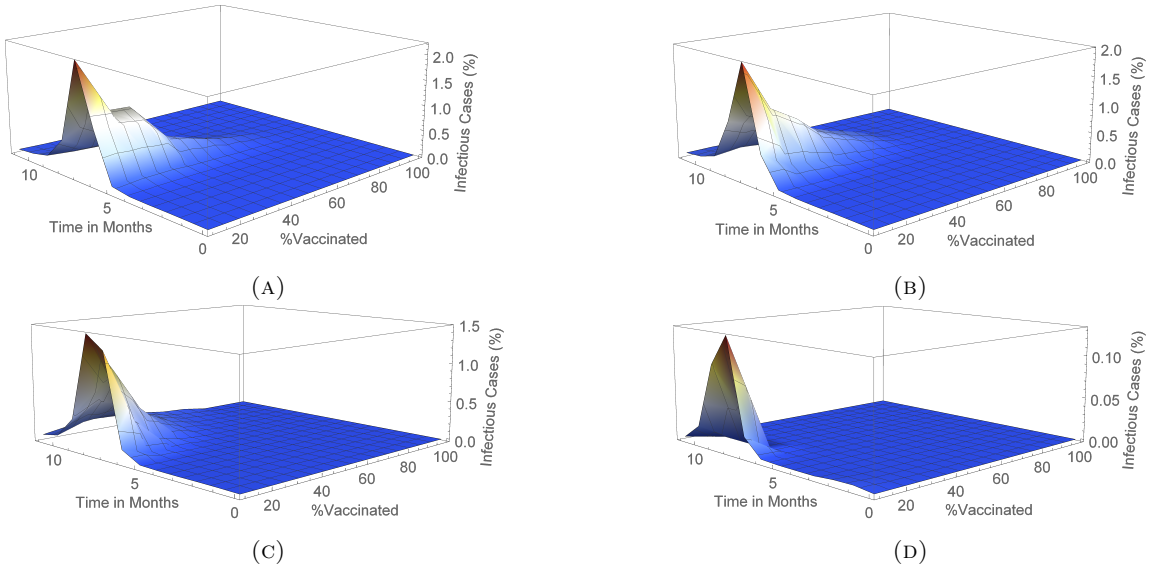

FIGURE 5.6: Outcome for mass vaccination scenarios for each vaccine efficacy percentage on an Erdos-Renyi network. This shows the changes in mean infected cases over time under the different vaccine efficacies. In (a), (b), (c) and (d) vaccine efficacies are $40\%, 60\%, 80\%$ and 100% respectively.

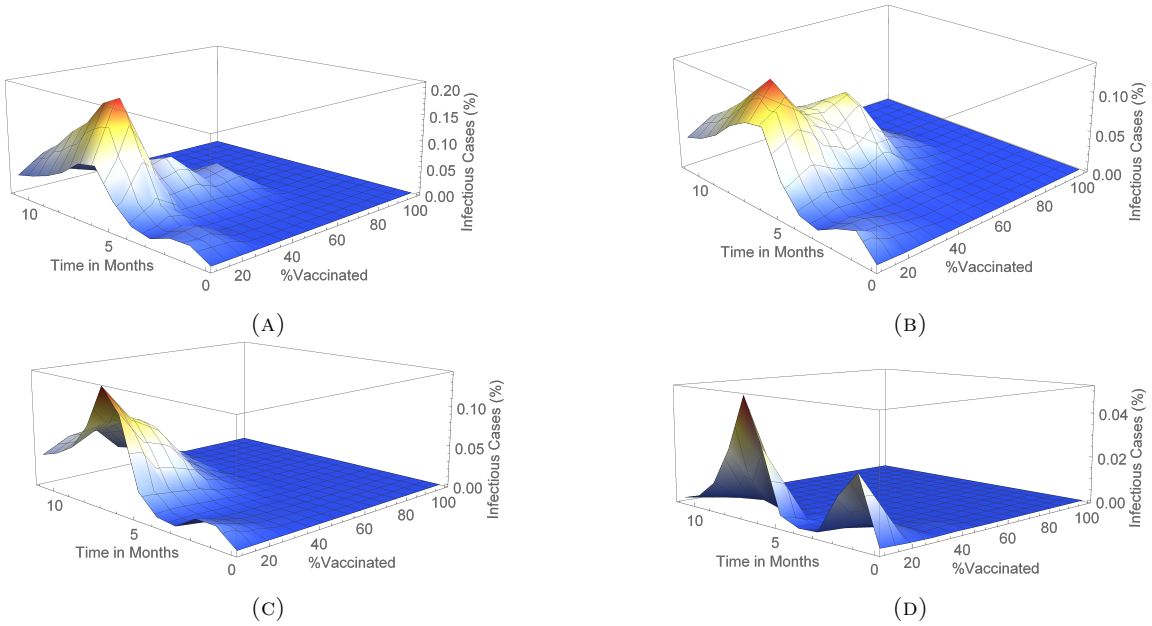

FIGURE 5.7: Outcome for mass vaccination scenarios for each vaccine efficacy percentage on a Barabasi Albert network. This shows the changes in mean infected cases over time under the different vaccine efficacies. In (a), (b), (c) and (d) vaccine efficacies are $40\%, 60\%, 80\%$ and 100% respectively.

Furthermore, infection cases in vaccinated and unvaccinated individuals is much higher in the ER model than in the BA model (see Figures 5.8a, 5.9a, 5.8b, 5.9b. and Tables A.6, A.5, A.3, A.2). In both networks, a 100% efficacious vaccine ensures that no susceptible (unvaccinated) individual gets exposed to the disease and is asymptomatic (Figure 5.8).

Similar results are observed in the proportion of vaccinated individuals who later become asymptomatic (Figure 5.9). For the ER network, the highest infection cases occur when vaccine efficacy is 40% and only 10% of the population is vaccinated. In the BA network however, this is seen at vaccine efficacy of 40% and 20% population coverage.

In the population of unvaccinated individuals for the ER network, higher cases of infection are observed with vaccine efficacy of 80% or less and population coverage less than 40% (Figure 5.8a). However, for the BA network, observed cases of infection are usually low in comparison with the ER network (Figure 5.8b). In the population of vaccinated individuals for the ER network, higher cases of infection are observed with vaccine efficacy of 60% or less and population coverage less than 40% (Figure 5.9a). Again, for the BA network, observed cases of infection are usually low in comparison with the ER network (Figure 5.9b).

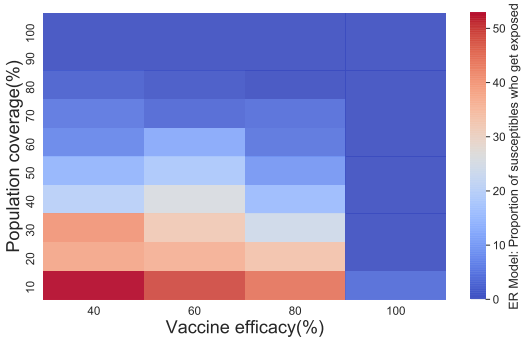

(A) Erdos-Renyi Model: Heatmap illustrating average proportion of unvaccinated (susceptible) individuals who got exposed and moved to the asymptomatic state in the course of the infection. Derived from Table A.3.

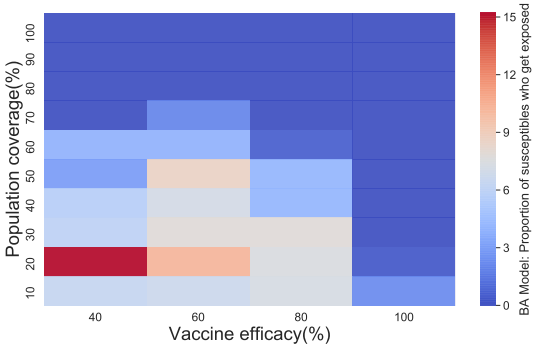

(B) Barabasi-Albert Model: Heatmap illustrating average proportion of unvaccinated (susceptible) individuals who got exposed and moved to the asymptomatic state in the course of the infection. Derived from Table A.6.

FIGURE 5.8: Comparing average proportion of unvaccinated individuals who got exposed and moved to the asymptomatic state in the course of the infection in both networks.

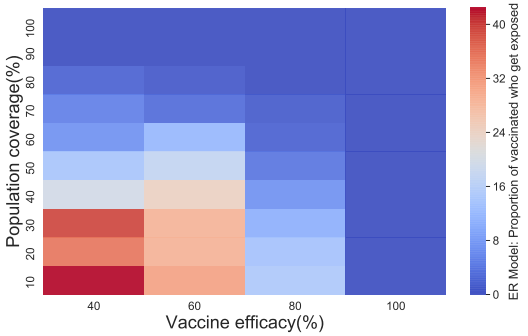

(A) Erdos-Renyi Model: Heatmap illustrating average proportion of vaccinated individuals who got exposed and moved to the asymptomatic state in the course of the infection. Derived from Table A.2.

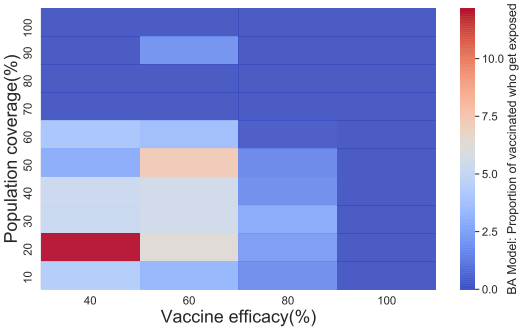

(B) Barabasi Albert Model: Heatmap illustrating average proportion of vaccinated individuals who got exposed and moved to the asymptomatic state in the course of the infection. Derived from Table A.5.

FIGURE 5.9: Comparing average proportion of vaccinated individuals who got exposed and moved to the asymptomatic state in the course of the infection in both networks.

Ring vaccination scenarios

We carried out simulations using Algorithm 2 to determine the infection outcome when ring vaccination is used in both networks. In Figures 5.10 and 5.11 (see also Figures A.5, A.6, A.11, A.12 and Table 5.3), we show these outcomes with varying scenarios of vaccine efficacy and when 1% or 3% of the population is already exposed (and in the asymptomatic state) to the disease before the onset of vaccination.

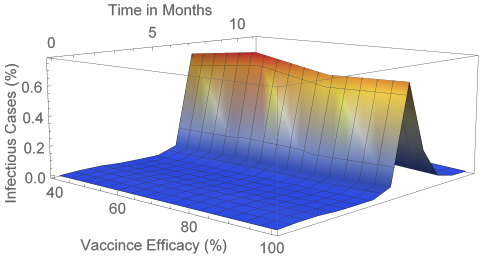

(A)

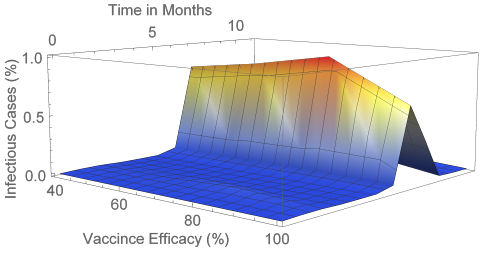

(B)

FIGURE 5.10: Outcome for ring vaccination scenarios for each vaccine efficacy percentage on a Erdos-Renyi network. This shows the changes in mean infected cases over time when there is 1% and 3% prior exposed population in (a) and (b) respectively.

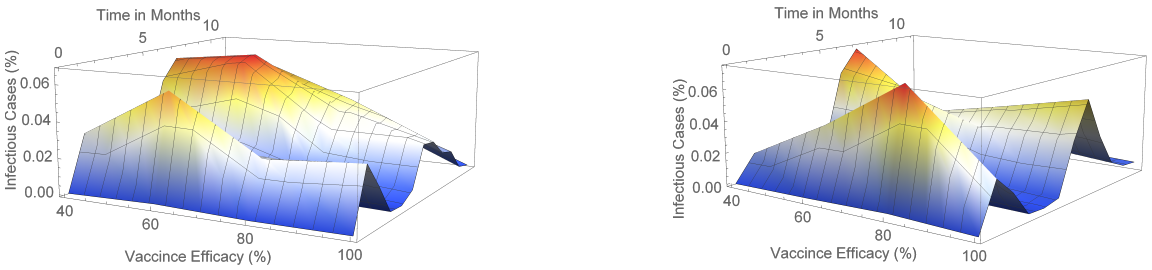

(A) (B)

FIGURE 5.11: Outcome for ring vaccination scenarios for each vaccine efficacy percentage on a Barabasi Albert network. This shows the changes in mean infected cases over time when there is 1% and 3% prior exposed population in (a) and (b) respectively.

We see that in both networks, there are less cases realised with a 1% exposed population before the start of vaccination as compared to a 3% exposed population. In addition, the number of infected cases in these scenarios are considerably lower than that of the classical vaccination method. Also, even with a 100% efficacious vaccine, total eradication of the peak is not achieved irrespective of the exposed population prior to vaccination and regardless of the network.

In comparison to mass vaccination, a lower percentage of the population has to be vaccinated when using a ring vaccination protocol in order to attain low infection cases (see Table 5.3). This is especially so as with effective contract tracing, more individuals can be vaccinated and thus decreasing the number of infections. It is worth noting also that even with the above results, the percentage of vaccinated individuals is lesser when only 1% of the population is exposed prior to vaccination than when the prior exposed population is 3%. Also, from Table 5.3 we see that for each network, the vaccinated populations are very similar in both scenarios (that is when 1% or 3% of the population is exposed) respectively irrespective of the efficacy of the vaccine.

TABLE 5.3: Average population coverage (in %) for ring vaccination scenarios in both ER and BA networks considering vaccine efficacy.

	Vaccine Efficacy			
	40%	60%	80%	100%
(ER Network)				
(1% of population exposed before vaccination)				
	0.71 ± 0.20	0.77 ± 0.23	0.67 ± 0.20	0.68 ± 0.19
(3% of population exposed before vaccination)				
	0.81 ± 0.23	0.89 ± 0.26	1.00 ± 0.29	0.65 ± 0.19
(BA Network)				
(1% of population exposed before vaccination)				
	0.062 ± 0.02	0.068 ± 0.02	0.043 ± 0.01	0.032 ± 0.01
(3% of population exposed before vaccination)				
	0.073 ± 0.02	0.049 ± 0.02	0.057 ± 0.02	0.65 ± 0.19

Table 5.4 shows the average proportion of unvaccinated (susceptible) individuals who got exposed in the course of the infection in both ER and BA networks under ring vaccination. Similar to the average infection peaks, there are less cases in unvaccinated individuals in the BA network than in the ER network. In addition, more cases are seen when 3% of the population is exposed than when 1% is exposed. From our simulations for ring vaccination in both networks, vaccinated individuals remain vaccinated and do not get exposed during the course of the infection process.

TABLE 5.4: Average proportion (in %) of unvaccinated (susceptible) individuals who got exposed in the course of the infection in both ER and BA networks under ring vaccination.

	Vaccine Efficacy			
	40%	60%	80%	100%
(ER Network)				
(1% of population exposed before vaccination)				
	0.71 ± 1.00	0.82 ± 1.01	0.77 ± 1.04	0.71 ± 0.99
(3% of population exposed before vaccination)				
	1.85 ± 2.68	2.26 ± 2.81	2.56 ± 2.90	1.72 ± 2.63
(BA Network)				
(1% of population exposed before vaccination)				
	0.40 ± 1.00	0.65 ± 1.27	0.66 ± 1.78	0.41 ± 1.04
(3% of population exposed before vaccination)				
	1.98 ± 4.95	1.57 ± 4.12	2.17 ± 4.59	1.52 ± 4.38

5.5 Double strain network modelling of SARS-CoV-2

5.5.1 Epidemic process

In this section, we describe the dynamics of two strains of the SARS–CoV–2 virus under one vaccination regime - mass vaccination. We assume a situation that models the competition between the original SARS–CoV–2 virus and one of its mutated variants (such as alpha, delta and omicron), that have been observed in many countries. We also assume that a stable social behaviour has been reached in some countries and hence the transmission rates can be maintained relatively constant. In this case, the two competing variants are assumed to have different transmission rates $\beta_1, \beta_2 > 0$ which are fixed throughout the epidemic process. The mutated variant has a higher infection rate, that is $\beta_2 > \beta_1$.

Though initially developed for the original SARS-CoV-2 virus, some vaccines have been said to be effective against other variants of the virus which have occurred due to mutations. As there are no variant specific vaccines, we assume only one vaccinated group. We also assume that there is no possibility of coinfection, hence, a node may only be infected by one variant at any given time. This makes it possible to divide individuals into two groups - those infected

with strain 1 and those infected with strain 2 as in Figure 5.1. Here, since we consider two strains of the virus, $W = \{1, 2\}$. For each $j \in W$, the epidemic transmission model used here follows from that of the single variant model in Section 5.4. Considering vaccination, our aim is to provide a qualitative analysis regarding the effect of the introduction of a new more transmissible SARS-CoV-2 variant.

The infection process starts by selecting a node uniformly at random and exposing it with variant 1 at which time the second variant is not yet introduced in the population (it can also be considered as being dormant) and hence $A_1(0) = 1$, $A_2(0) = 0$. Variant 1 circulates in the population until day τ when variant 2 is introduced into the population with α number of nodes set to the state $A_2(\tau)$. Therefore, $A_1(0) > A_2(0)$ and $A_2(\tau) = \alpha$. As interventions change, transmission rates also change accordingly. For instance, individuals are likely to avoid face-to-face interactions and hence have fewer contacts during lockdowns. To account for this, we remove edges from the network who have more than l connections during the time at which lockdown is implemented in the model. l in our model is taken as the average node degree in the network.

5.5.2 Simulation scenarios

Similar to the single strain model above, we consider two main simulation scenarios: (1) model without vaccination (control scenario) and (2) model with vaccination. However, for the double variant model, we only consider mass vaccination as that is the most widely used vaccination strategy since immunizations towards the epidemic started. This is mainly due to the fact that tracking individuals throughout the infection period is a challenging task and has not been a success. Here, the vaccine efficacy levels and population coverage levels considered are the same as in the single strain model. That is vaccine efficacy varied between $40\% - 100\%$ whereas population coverage varied between $10\% - 100\%$. In all simulations, we consider that lockdown begins on day 50 and ends on day 140. For ER simulations: $N = 10^5$, $\beta_1 = 0.022$, $\beta_2 = 0.025$, $\tau =$ day 220 and $T = 539$ days. For BA simulations: $N = 10^5$, $\beta_1 = 0.014$, $\beta_2 = 0.017$, $\tau =$ day 220 and $T = 539$ days. Each scenario is repeated 100 times and the outputs are taken for analysis.

5.5.3 Results

5.5.3.1 Scenario without vaccination

Figure 5.12, shows the simulation results for epidemic spread when there is no vaccination in the population. Here, we observe that at the onset of the second strain, there is a drastic reduction in total infectious cases in the first strain which then causes the infection levels of

the second strain to rise steadily before reaching peak values. The number of cases for strain 1 begin to decline when strain 2 is introduced and eventually die out when strain 2 peaks. In Figure 5.12, the mean number of infectious cases peaks at 1.07% for strain 1 and 0.97% strain 2 in the ER network. In the BA network, infection peaks are observed at 0.33 and 0.92 for strain 1 and strain 2 respectively. Similar to the single strain model, epidemic peaks in the BA network are lesser than that in the ER network.

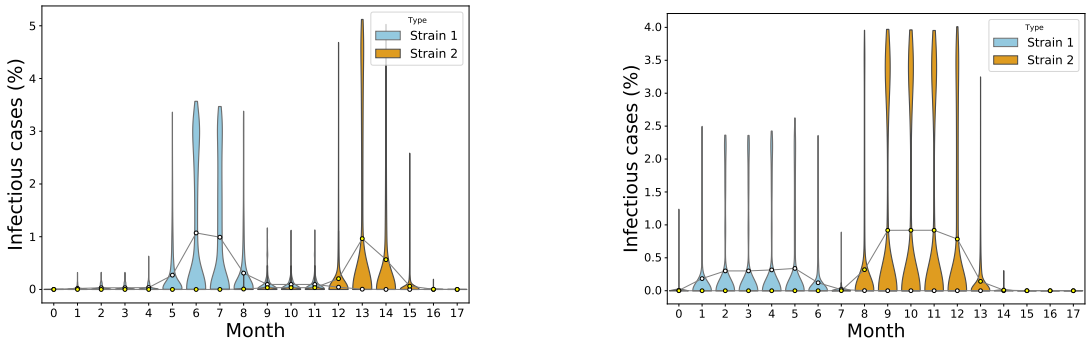

(A) (B)

FIGURE 5.12: Distribution of the final infectious cases for no vaccination scenario in both networks. A population of N= 10^5 individuals was generated and 100 simulations were run for 539 days. Circles represent mean infection cases for each month connected by lines. (A): Erdos-Renyi network, (B): Barabasi-Albert network.

5.5.3.2 Mass vaccination assuming equal vaccine efficacy

In this section, we evaluated how mass vaccination with similar vaccine efficacy levels in both strains affect the spread of both strains of the virus. In general, we observe that the peak values in these cases are lower than in the single strain model scenarios. However, the disease dynamics are quite similar for both models. See Appendix B.

In the **ER network**, for vaccine efficacy levels of $40\%, 60\%$ and 80%, infectious cases are much high for strain one than for strain 2, when strain 2 exists (that is, for population coverage levels of $10\%, 20\%$ and 30%). This also means that the average infection peaks for strain 1 are higher than that for strain 2 as can be observed in Figure 5.13. When vaccine efficacy is 100% however, a different trend is observed. Infectious cases for strain 2 are on average higher than for strain 1 when there is low vaccination coverage. Both strains become extinguished when population coverage is 40% and above as seen in Figure 5.13d.

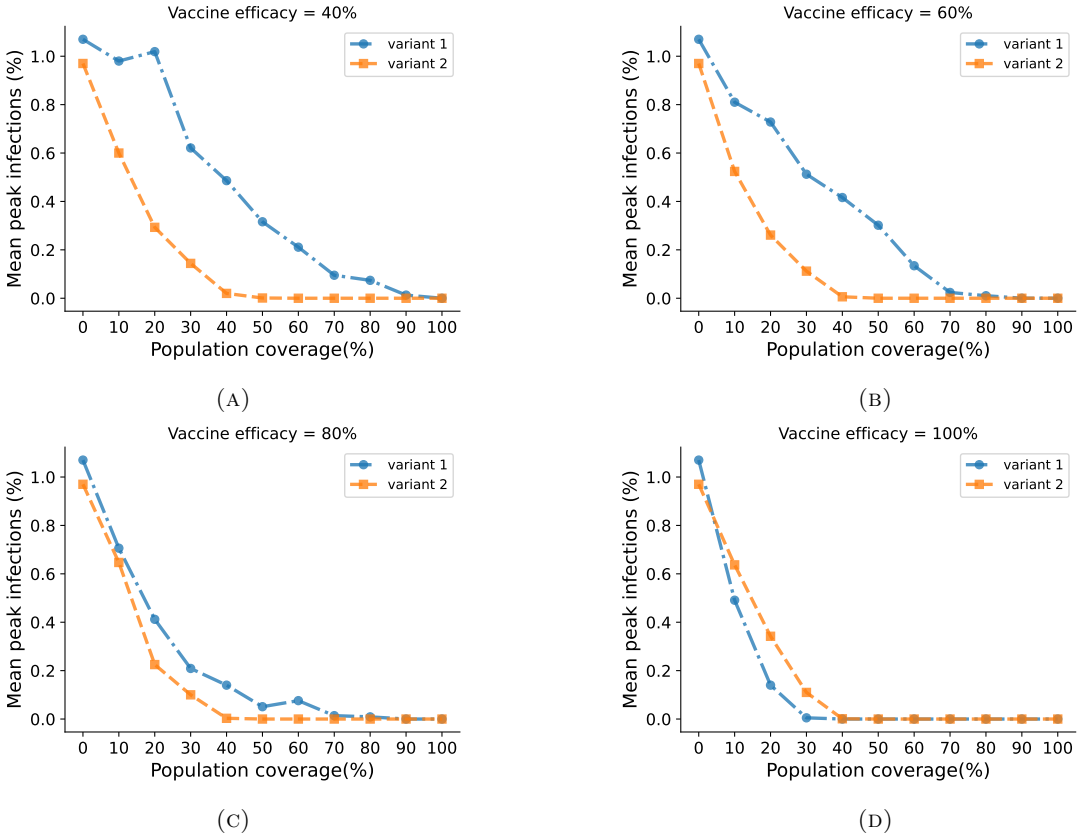

(A) (B)

(C) (D)

FIGURE 5.13: Erdos-Renyi Model: Comparing average infection peak values for both strains and for different levels of vaccine efficacy. A population of N= 10^5 individuals was generated and 100 simulations were run to simulate the epidemic in the course of one year. In (A), (B), (C) and (D) vaccine efficacies are $40\%, 60\%, 80\%$ and 100% respectively. Population coverage of zero corresponds to the control scenario (ie. no vaccination). Dots and squares represent the average peak infection values for 100 simulations of each pair of vaccine efficacy level and population coverage level.

There is also an observed plateau of infections with increasing population coverage when vaccine efficacy is $60\%, 80\%$ and 100% as seen in Figure 5.13. This plateau of infections occur when mean peak of infections is 0% and signifies infection eradication. For 60% vaccine efficacy, this plateau of infections is observed from 40% to 80% population coverage. For 80% vaccine efficacy, this plateau of infections is observed from 50% to 80% population coverage. For 100% vaccine efficacy, this plateau of infections is observed from 40% to 80% population coverage but at notably extremely low values.

From Figure 5.14, we see a general decline in average infectious cases as vaccine efficacy and population coverage levels increase. Also, irrespective of the vaccine efficacy, average infectious cases for each strain indicate that when population coverage is from 40% to 100%, the only strain circulating in the population is strain 1 (strain 2 is dormant) as seen in Figure 5.14b.

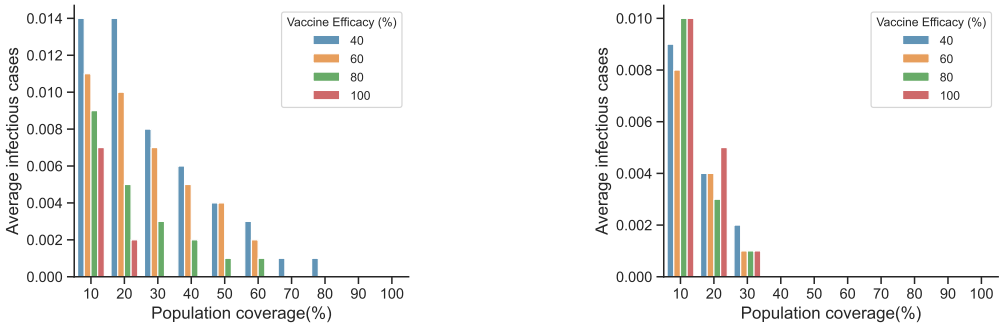

(A) Average infected cases for different vaccine efficacies and for strain 1.

(B) Average infected cases for different vaccine efficacies and for strain 2.

FIGURE 5.14: Erdos-Renyi Model: Comparing average infected cases for different vaccine efficacy levels and for each strain. (A) is for strain 1 and (B) is for strain 2. A population of N= 10^5 individuals was generated and 100 simulations were run to simulate the epidemic in the course of one year

In all scenarios for the ER model, 100% efficacious vaccine and 100% population coverage ensure that there are no vaccinated or unvaccinated individuals who get exposed as seen in Figures 5.16 and 5.15. This finding is similar in the single strain model above (see also Figures 5.8a and 5.8b).

For strain 1, the average number of vaccinated individuals who later get exposed are higher when vaccine efficacy is 40% which are also higher than that when vaccine efficacy is 60% which is also higher than when vaccine efficacy is 80%. This observation is true only for all population coverage levels except $30\%, 40\%$ and 50% where we find that the mean number of vaccinated who get exposed are higher for 60% vaccine efficacy, which is also higher for 40% vaccine efficacy which is also higher than 80% vaccine efficacy.

The findings for strain 2 are slightly different. Here, vaccinated individuals who got exposed were only found when only 10% to 40% of the population is vaccinated. Similar to strain 1, there are no vaccinated individuals who were exposed when vaccine efficacy is 100%. Also, we find that average values for vaccinated individuals is highest when vaccine efficacy is 40% and population coverage is also 20%. Also, this numbers decrease when vaccine efficacy and population coverage increases with more observations for lower population coverage thereby yielding a right-skewed distribution as seen in Figure 5.15b.

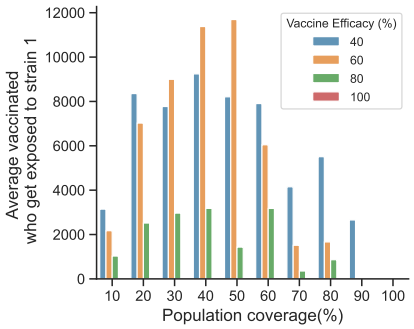

(A) Proportion of vaccinated individuals who got became asymptomatic to strain 1.

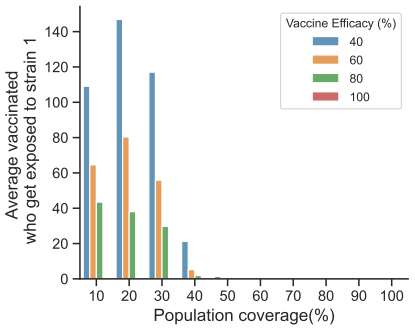

(B) Proportion of vaccinated individuals who became asymptomatic to strain 2.

FIGURE 5.15: ER Model: Comparing average proportion of vaccinated individuals who became asymptomatic in the course of the infection in both strains. A population of N= 10^5 individuals was generated and 100 simulations were run to simulate the epidemic in the course of 539 days.

In the results for unvaccinated individuals who are exposed to the virus, we find that in general, as vaccination efficacy increases and population coverage also increases, we have less unvaccinated individuals being exposed as seen in Figure 5.8. Also, we observe that for strain 1, there are no unvaccinated exposed individuals when vaccine efficacy is 100% and population coverage ranges from 40%. A similar observation is made for strain 2.

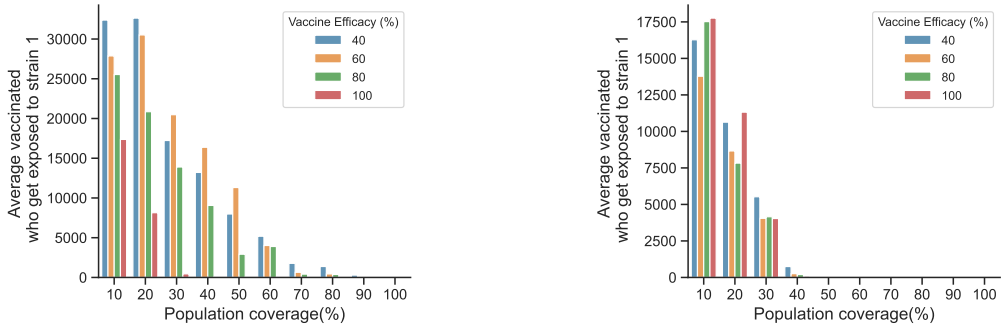

(A) Proportion of unvaccinated individuals who got exposed to strain 1.

(B) Proportion of unvaccinated individuals who got exposed to strain 2.

FIGURE 5.16: ER Model: Comparing average proportion of unvaccinated individuals who got exposed in the course of the infection for both strains. A population of N= 10^5 individuals was generated and 100 simulations were run to simulate the epidemic in the course of 539 days.

For the **BA network**, we have a slightly different observation (see Figure 5.17 and also Figure B.1.2 in the appendix). The infection peaks for no vaccination appear to be much higher in comparison to the vaccination scenarios. When vaccine efficacy is $40\%, 60\%$ and 80% (see Figure 5.17a, 5.17b, 5.17c), strain 2 dominates at lower population coverage whereas strain 1 dominates at high population coverage levels and both strains coexist at very low levels. However, when vaccine efficacy is 100%, in Figure 5.17d, strain 2 dominates at all population coverage levels until a point (when population coverage $> 50\%$) where both strains are extinguished.

Furthermore, we observe that with increasing vaccine efficacy, the less population coverage required to eradicate both strains of the virus. For instance, when vaccine efficacy is 40%, eradicating both strains will require everyone in the population to be vaccinated whereas for efficacy of 60%, more than a 90% coverage is needed. For efficacy of 80%, more than an 80% coverage is needed and for efficacy of 100%, more than 40% coverage is needed to achieve this. See Figure 5.17.

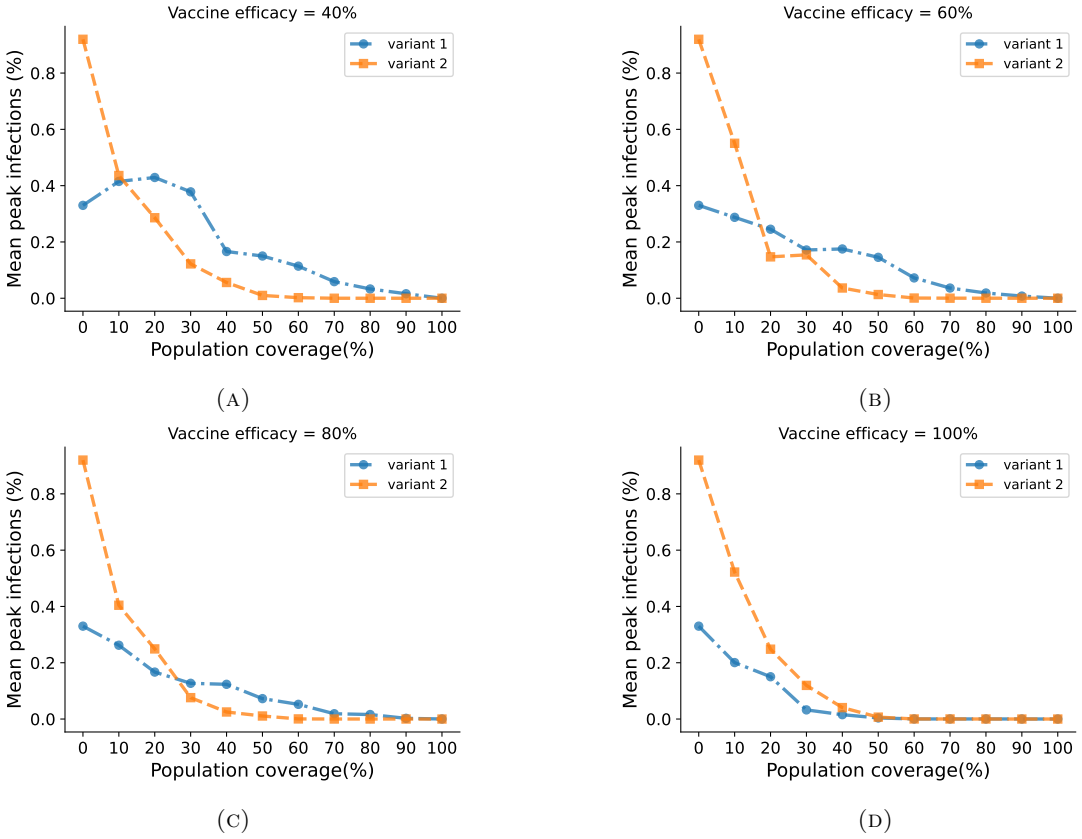

(A) (B)

(C) (D)

FIGURE 5.17: Barabasi-Albert Model: Comparing average infection peak values for both strains and for different levels of vaccine efficacy. A population of N= 10^5 individuals was generated and 100 simulations were run to simulate the epidemic in the course of one year. In (A), (B), (C) and (D) vaccine efficacies are 40%, 60%, 80% and 100% respectively. Population coverage of zero corresponds to the control scenario (ie. no vaccination). Dots and squares represent the average peak infection values for 100 simulations of each pair of vaccine efficacy level and population coverage level.

In addition, the average infectious cases for the BA network model for both strains are relatively lower compared to those observed in the ER network model but we can see a similar declining trend as population coverage and vaccine efficacy increases, see Figure 5.18. For both strains, a vaccine efficacy of 100% ensures eradication when population coverage is more than 40% (Figure 5.18a and 5.18b). For strain 2, this coverage level increases to 50% for the remaining efficacy levels whilst for strain 1, 80% population coverage ensures eradication for all vaccine efficacy levels.

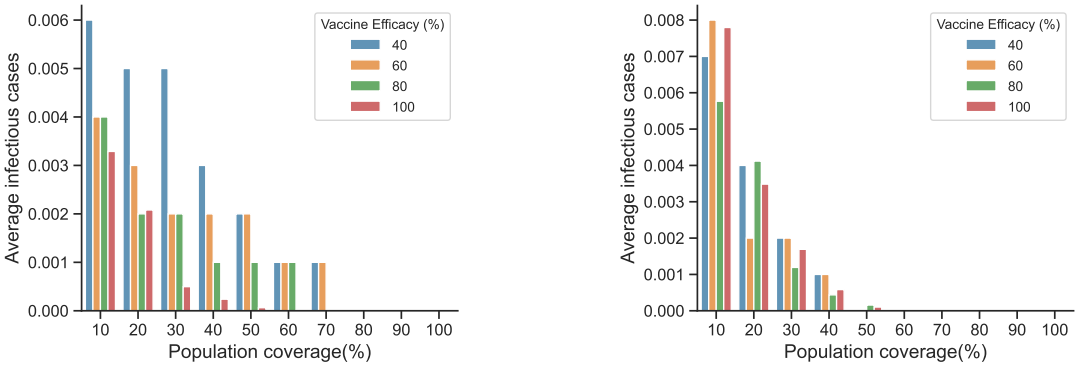

(A) Average infected cases for different vaccine efficacies and for strain 1.

(B) Average infected cases for different vaccine efficacies and for strain 2.

FIGURE 5.18: Barabasi-Albert Model: Comparing average infected cases for different vaccine efficacy levels and for each strain. (A) is for strain 1 and (B) is for strain 2. A population of N= 10^5 individuals was generated and 100 simulations were run to simulate the epidemic in the course of 539 days.

In the case of vaccinated individuals who later on became exposed and asymptomatic, there are less of such cases in general for strain 2 than for strain 1. To add to that, we observe that similar to the ER model, with a vaccine efficacy of 100%, there are no vaccinated individuals who later get exposed to either strain of the virus, Figure 5.19. Instead, for strain 1, we observe a general increase of vaccinated individuals who get exposed as population coverage increases, reaching a peak and then tapering off as more people are vaccinated. When population coverage is 100%, there are no cases of vaccinated individuals being exposed to either strain. For strain 2 however, peak values of average vaccinated who get exposed are higher for lower population coverage levels thereby achieving a right-skewed distribution as seen in Figure 5.19b. These observations are similar to those observed for the ER network.

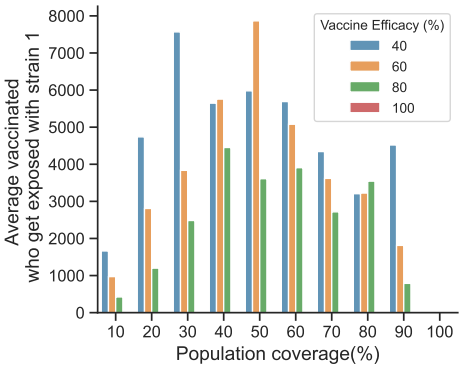

(A) Proportion of vaccinated individuals who got became asymptomatic to strain 1.

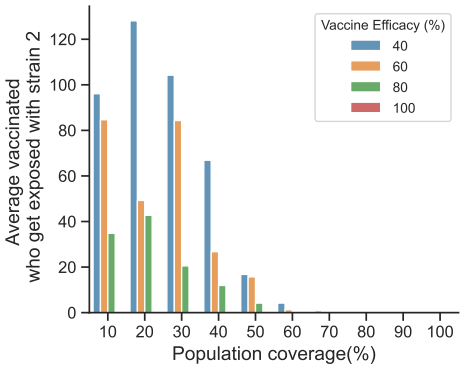

(B) Proportion of vaccinated individuals who became asymptomatic to strain 2.

FIGURE 5.19: Barabasi-Albert Model: Comparing average proportion of vaccinated individuals who became asymptomatic in the course of the infection in both strains. A population of N= 10^5 individuals was generated and 100 simulations were run to simulate the epidemic in the course of 539 days.

In the case of unvaccinateds, there are more individuals becoming exposed and asymptomatic to strain 1 than to strain 2. Also, there is a general declining trend in such cases, for both strains, as vaccine efficacy and population coverage increase. Except for when vaccine efficacy and population coverage are both 100%, there are many unvaccinated individuals who become asymptomatic to strain 1 of the virus (see Figure 5.20). However, a population coverage of 60% and more ensures that there are no unvaccinated who are later asymptomatic to strain 2 for all vaccine efficacy levels. A vaccine efficacy of 100% and population coverage $\geq$ 60% ensures that there are no unvaccinated individuals who become asymptomatic to either strain of the virus.

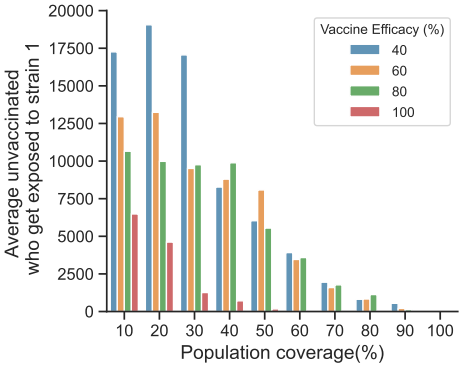

(A) Proportion of unvaccinated individuals who got exposed to strain 1.

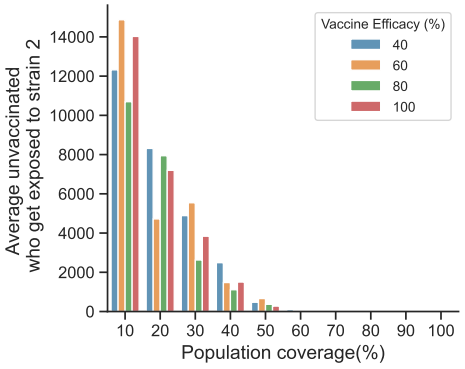

(B) Proportion of unvaccinated individuals who got exposed to strain 2.

FIGURE 5.20: Barabasi-Albert Model: Comparing average proportion of unvaccinated individuals who got exposed in the course of the infection for both strains.

5.6 Modelling Vaccine Resistance

In this section, we distinguish between a wild-type virus and a vaccine-resistant mutant virus. The vaccine is effective against the wild-type strain, while the mutant strain evades immunity induced by the vaccine. We assume here that individuals who have recovered from the wild-type infection are still prone to infection with the vaccine resistant variant of the virus. We carry out simulations that mimic immunity acquired by two doses of the Pfizer-BioNTech (BNT162b2) vaccine (the first FDA-approved COVID-19 vaccine) against the original SARS-CoV-2 virus. We use this vaccine because it is the most widely used vaccine worldwide. In particular, we are interested in the disease dynamics when the wild-type strain is in circulation with the omicron variant. Experimental observations highlight that vaccine effectiveness for the wild-type variant within two to four weeks after two doses of vaccine for the prevention of symptomatic COVID-19 is 95% and that for the omicron variant is 65% [4]. However, vaccine efficacy drops in the omicron variant, reaching as low as 8.8% at 25 weeks or more after the second dose [4] (see also Figure 5.21).

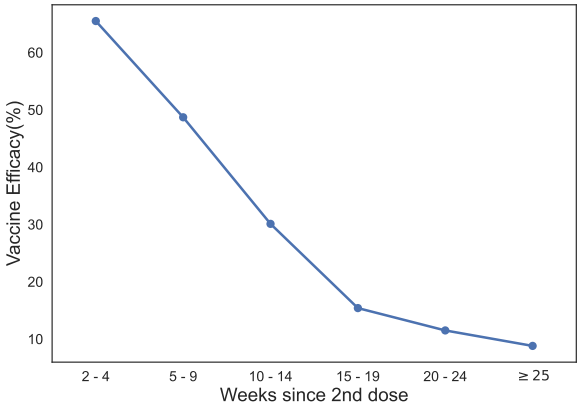

FIGURE 5.21: Vaccine effectiveness for omicron variant after second dose of Pfizer-BioNTech vaccine from Table 5.5.

To determine the fold change in vaccine efficacy between the wild-type and the mutant strain, we can find a parameter k such that k is the fold change of vaccine efficacy between the wild-type and the mutant strain. That is, k is the ratio of the vaccine efficacy (η) of the mutant strain to the wild-type given by

$$\eta(strain) = k * \eta(WT) \tag{5.8}$$

For our study, we assume the vaccine efficacy for the wild-type is 95%. In order to mimic the experimental data in [4], we find a k (from eq (5.8)) for each week interval presented in Table 5.5. Following from the preceding sections, for our simulations, we hypothesize that the vaccine efficacy for the wild-type ranges from $\{40\%, 60\%, 80\%, 100\%\}$. Therefore,

using eq (5.8), we obtain a value for k as $k = 0.655$ within $2-4$ weeks post second vaccine dose. Consequently, we have that vaccine efficacy for the resistant variant will be $\{40\%, 60\%, 80\%, 100\%\}$ each multiplied by 0.655 as per eq (5.8). Hence, the vaccine efficacy values of the mutant omicron variant becomes $\{26.2\%, 39.3\%, 52.4\%, 65.5\%\}$ respectively. Similar processes can be used to obtain the vaccine efficacy values for the remaining week intervals shown in Table 5.5

TABLE 5.5: Vaccine efficacy of Pfizer-BioNTech vaccine (BNT162b2) for the omicron variant of SARS-CoV-2 and corresponding k-values from eq (5.8). Adapted from [4].

Week after vaccination	Vaccine efficacy (%)	k-values
$2-4$	65.5	0.655
$5-9$	48.7	0.0195
$10-14$	30.1	0.0316
$15-19$	15.4	0.0617
$20-24$	11.5	0.0826
≥ 25	8.8	0.108

In the subsequent subsections, we shall analyse the model with the above mentioned considerations. All numerical scenarios hereafter follow from the above reasoning.

5.6.1 Scenario without vaccination

Analysing the scenario without vaccination, we observe high infection cases overall but higher in strain 1 (with an average peak value of 1.32) than strain 2 (with an average peak value of 1.12), see Figure 5.22. These values are considerably high in comparison to the previous examples of no vaccination in the preceding sections. These high values are attributed to the increase in transmissibility of the mutant strain and its reduced response to the effect of the vaccine.

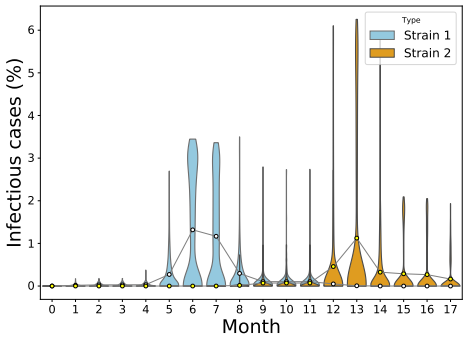

FIGURE 5.22: Erdos-Renyi vaccine resistance model: Distribution of the final infectious cases for no vaccination scenario in an Erdos-Renyi network. A population of N= 10^5 individuals was generated and 100 simulations were run for 539 days. Circles represent mean infection cases for each month connected by lines.

5.6.2 Mass Vaccination Scenarios

Comparing average infection peak values, we observe that there are higher infection peaks in strain 2 relative to strain 1 for all vaccine efficacy levels as seen in Figure 5.23 (see also Figures B.9 - B.12 in Appendix B.2.1). For vaccine efficacy of 100%, a plateau of very low peak infections is reached from population coverage of 30% and above in strain 1 and 90% and above in strain 2 (see Figure 5.23d). It is also important to note here that even with vaccination campaigns, it is possible to have infection cases higher in strain 2 than the control scenario when there is no vaccination. This is more evident at low population coverage levels. This observation relates with the reduced effect of vaccine in the resistant strain 2.

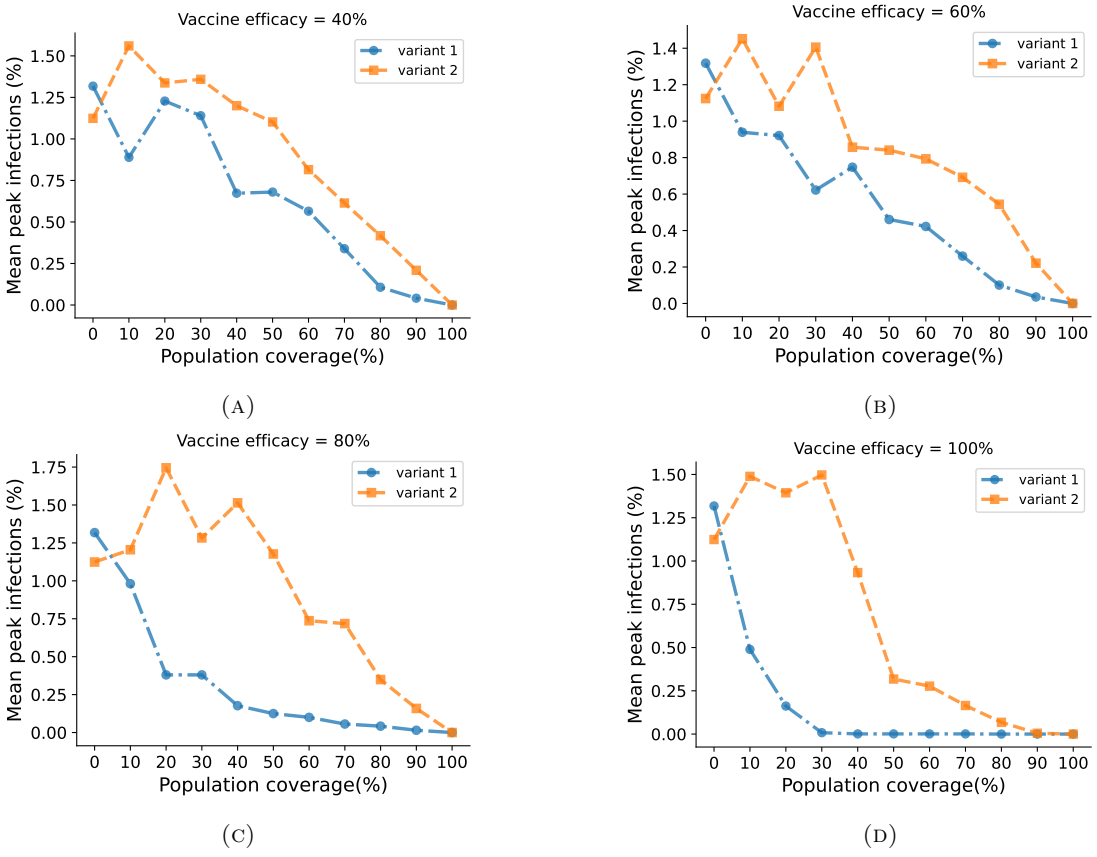

FIGURE 5.23: Erdos-Renyi vaccine resistance model: Comparing average infection peak values for both strains and for different levels of vaccine efficacy. A population of N= 10^5 individuals was generated and 100 simulations were run to simulate the epidemic in the course of one year. In (A), (B), (C) and (D) vaccine efficacies are $40\%, 60\%, 80\%$ and 100% respectively. Population coverage of zero corresponds to the control scenario (ie. no vaccination). Dots and squares represent the average peak infection values for 100 simulations of each pair of vaccine efficacy level and population coverage level.

In terms of average infected cases, there is a general decline in the number of infected cases as more people are vaccinated for both strains, see Figure 5.24. Thus, less people are infected on average when more people in the population are vaccinated against the virus. With strain 1, vaccine efficacy of 100% ensures negligible infection cases when 30% or more of the population is vaccinated. For strain 2, more infection cases are observed irrespective of population coverage and vaccine efficacy levels (see Figure 5.24b). In addition, higher infection values are obtained due to strain 2 than strain 1 as seen in Figure 5.24b.

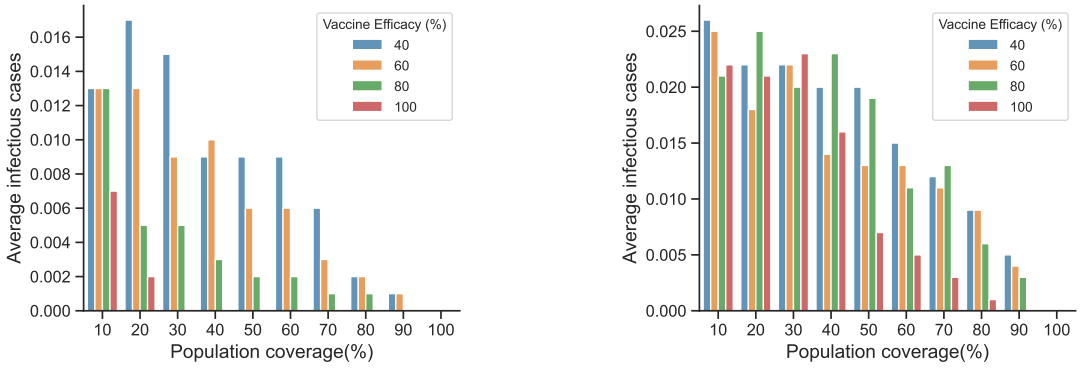

(A) Average infected cases for different vaccine efficacies and for strain 1.

(B) Average infected cases for different vaccine efficacies and for strain 2.

FIGURE 5.24: Erdos-Renyi vaccine resistance model: Comparing average infected cases for different vaccine efficacy levels and for each strain. (A) is for strain 1 and (B) is for strain 2. A population of N= 10^5 individuals was generated and 100 simulations were run to simulate the epidemic in the course of 539 days.

In Figure 5.25, we see a comparison of the number of vaccinated individuals who got exposed and became asymptomatic to either strain of the virus in the course of the epidemic. We observe that in general, this number is lower for strain 1 than for strain 2. In addition, a vaccine efficacy of 100% yields no infection cases irrespective of the population coverage in strain 1. Furthermore, the number of vaccinated individuals who become asymptomatic rise steadily at low population coverage levels reaching a peak at about population coverage $(60\%, 70\%)$ before decreasing at higher population coverage levels (see Figure 5.25a). On the other hand, for strain 2, the number of vaccinated who got exposed increases steadily for vaccine efficacy of $40\%, 60\%$ and 80%. For vaccine efficacy of 100%, this number increases at low population coverage, reaching a peak at 40% population coverage before tapering down at higher population coverage.

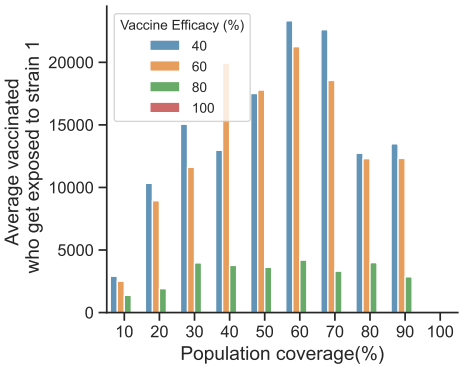

(A) Proportion of vaccinated individuals who became asymptomatic to strain 1.

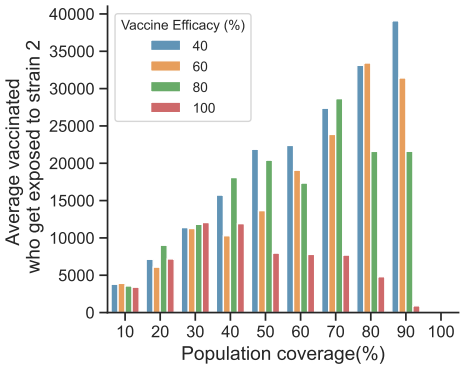

(B) Proportion of vaccinated individuals who became asymptomatic to strain 2.

FIGURE 5.25: Erdos-Renyi vaccine resistance model: Comparing average proportion of vaccinated individuals who became asymptomatic in the course of the infection in both strains. A population of N= 10^5 individuals was generated and 100 simulations were run to simulate the epidemic in the course of 539 days.

In terms of unvaccinated individuals who get exposed in the course of the epidemic, we observe a general decline in both strains with increasing population coverage (see Figure 5.26) but with considerably much higher values for strain 2 than for strain 1. For unvaccinated individuals exposed to strain 1, population coverage of 30% or more yields low to no exposure to the virus (see 5.26a).

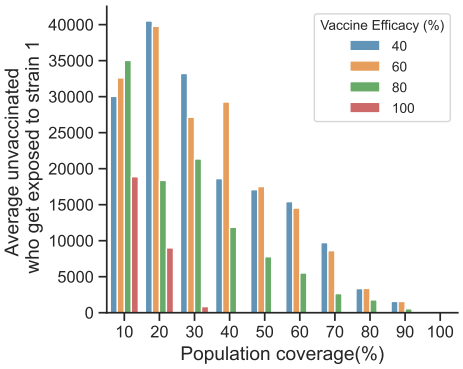

(A) Proportion of unvaccinated individuals who got exposed to strain 1.

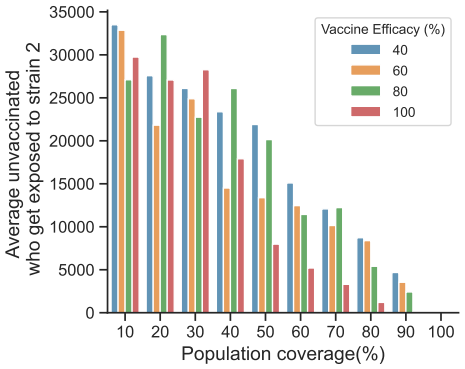

(B) Proportion of unvaccinated individuals who got exposed to strain 2.

FIGURE 5.26: Erdos-Renyi vaccine resistance model: Comparing average proportion of unvaccinated individuals who got exposed in the course of the infection for both strains.

5.7 Chapter summary

In this chapter, we modelled the spread of SARS-CoV-2 infection using an SAIRV model structure social networks for both single variant and double variant models. We carried out

stochastic simulations to determine vaccine efficacy and population coverage limits capable of extinguishing the disease in a given time period. We considered two vaccination strategies for the single variant case, each with varying scenarios regarding vaccine efficacy and population coverage and one vaccination strategy for the double variant models. We found that, the introduction of a single infectious person into a completely susceptible population leads to the spread of infection giving rise to more infectious cases and subsequently more than one infection peak in all models.

In addition, the introduction of vaccination lowered the number of infectious cases irrespective of the type of vaccination and contact network for the single strain model. Our simulations and analysis show that when using a mass vaccination strategy, the lower the efficacy of the vaccine, the more people needed to be vaccinated against the disease in order to eliminate infection peak(s). This is true for both ER and BA networks. For instance, in an ER network, a vaccine with an efficacy of 40% will require more than 40% of the entire population to be vaccinated in order to reach low infection peak values less than 1% whereas in a BA network, a population coverage more than 70% with a vaccine efficacy of 80% achieves negligible infection cases. In both networks, a 100% effective vaccine will require just about 20% of the population to be vaccinated.

Furthermore, in the presence of two circulating variants of the virus, vaccination plays a major role in achieving eradication. A vaccine efficacy of 100% ensures extremely low average infection values even with population coverage levels for both strain of the virus. In addition, with good enough vaccines (with efficacy more than 30%), our simulations tell us that we can achieve zero infectious cases when more than 40% of the population is vaccinated with a vaccine which has efficacy of 40% or more. Moreover, the more people are vaccinated, the less exposure vaccinated individuals have to the virus and hence low number of vaccinated individuals become exposed to the second strain of the virus. Similarly, increasing population coverage and vaccine efficacy leads to less number of unvaccinated individuals being exposed to either strain of the virus.

To add to that, when a vaccine resistant strain is in circulation with the wild-type of the virus in the population, our numerical simulations indicate that even with vaccination campaigns, it is possible to have infections greater than when there is no vaccination. In addition, more people are infected with the resistant strain than the wild-type irrespective of the efficacy of the vaccine and the population coverage. A 100% efficacious vaccine however, yields low to no infections with the wild-type strain when 30% or more of the population is vaccinated.

Even though there are some vaccines which require a single dose regimen to achieve acclaimed efficacy levels (from Table 3.4), it can be seen easily that majority of vaccines require more than one dose to achieve the levels of efficacy claimed by manufacturers. Given that this is a simplified model to explore the effects of vaccination strategies in general, it is worth

pointing out that our model is limited when considering a two-dose vaccine regimen and hence results from our model can likely be influenced under such circumstances.

Given the experimental nature and limited initial supply of vaccines, a classical mass vaccination campaign might not be feasible in many countries. However, ring vaccination of likely case contacts and contacts of cases could provide an effective alternative in distributing the vaccine to ensure low levels of infection and subsequently preventing infection peaks. This is with the assumption of effective contract tracing of infectious people.

Researchers, policy makers and the general public are of the opinion that the discovery of a vaccine will allow the return to normality of life before the SARS-CoV-2 pandemic. It is worth noting that, the discovery of a proven-to-be effective vaccine however, might not reduce transmission completely. This is due to the fact that a vaccine which effectively reduces the severity of transmission does not necessarily reduce virus transmission to a comparable degree [243].

It is also important to consider the potential impact of voluntary mass vaccination in the efforts of clearing the epidemic [244, 245, 246, 247]. In years past, the roll-out of vaccination has been faced with declining vaccine confidence in the general public which could possibly lead to hesitancy in getting vaccinated [248]. Such instances could easily lead to a disruption of people receiving a vaccine voluntarily thus, having a detrimental effect on efforts to eradicate the disease and hence such situations should not be underestimated.

Chapter 6

Conclusions and Future Work

In the absence of adequate epidemiological data, mathematical models produce some evidence for the efficacy of disease interventions through simulation. Knowledge of the transmission characteristics of infections can be incorporated into mathematical models to make better inferences about infections. In this thesis, we have used mathematical modelling techniques to explore the problem of drug resistance at two levels: between-host and within-host. We have described the importance of mathematical models as a cost effective approach to understanding infection progression dynamics as well as control and interventions at both levels. Studying biological problems of this nature with mathematical approaches can be a useful predictive tool to explore some uncertain scenarios during a disease outbreak and most importantly, predict the plausible effects of control and interventions.

In Chapter 3, we presented a general introduction to drug resistance evolution both within the host and in a given population. We described in depth the biological underpinnings of the problem of drug resistant infections that can be found in the existing literature. We also explored various mathematical approaches which have been used in the study of resistant infections such as deterministic, stochastic and statistical methods. These models are often times limited to the dynamics of the spread of resistance while neglecting resistance evolution and are often deterministic in nature. They present hypothetical situations for the spread of drug resistance infections in hospitals and in the community and also indicate some commonly used treatment strategies.

A common practice for modellers is to use deterministic models since simulating such models is often easier than stochastic models. Stochastic models are effective for capturing complex heterogeneous processes in a biological system. They can be used to unveil certain complexities of resistance that deterministic models do not. Such models can be used to explore complex interactions that may affect resistance such as dosing effect and immune response.

While these approaches are all good steps in the direction of understanding resistant infections, tackling resistance, however, will stem from understanding the mechanisms leading to the evolution of resistance. Therefore, it is important for models addressing this problem to include specific evolutionary mechanisms of resistance such as mutations and interactions between resistant genes. This will aid for understanding of the interaction between genetic strains of pathogens and help tailor appropriate interventions.

To this end, in Chapter 4, we used mathematical modelling techniques to explore the evolution and spread of resistant infections within the host and to analyze some treatment strategies to combat resistance. We presented logistic based mathematical models to describe the dynamics of different pathogen strains during drug therapy and also capture the process of cell mutation which lead to resistance within the host. In drug therapy for eliminating resistance, treatment scheduling remains an important area of research as there is no consensus on the best treatment protocols.

Motivated by studies which have shown that sequential administration of drugs tend to be superior in eradicating resistant strains in the long term, we used notions from control engineering and switched positive systems to tailor drug cycling strategies with the aim of eradicating drug-resistance within the host. In particular, we analysed scheduling and sequential use of drugs for treatment within a host using the principle of collateral sensitivity in bacteria and compared different therapy switching approaches to determine their performance in eradicating resistance in the host on the long term. We compared switching under two different types of drug switching approaches: periodic switching and lyapunov switching and studied these systems both in the presence and absence of mutation. When mutation is considered to be present, asymptotic stability of the origin is achieved if the switching system has a common Lyapunov function.

Beginning with a simple two strain system with two therapies, we investigated suitable drug scheduling protocols on a small scale. We showed using numerical simulations that any switching strategy ensured eradication of resistance when both subsystems are asymptotically stable at the origin. However, when only one subsystem is unstable, periodic switching does not guarantee that resistance will die out but lyapunov based switching does and is even much faster. And when all subsystems are unstable at the origin, only a lyapunov based switching ensures eradication. However, a sliding mode occurs at the intersection of the two configurations in which case feedback switching can be used to reach the sliding surface and the control can be completed with a sliding law defined based on periodic switching.

We then extended this model to a more generalised system with more than two strains and with many therapies. We obtained similar results for the general model as well. Our numerical simulations showed that switching strategies based on Lyapunov functions have better performance. The cases considered in this chapter, yielded faster and computationally

practical outcomes and in certain conditions were able to eradicate pathogenic populations. Simulation results emphasise that drug cycling protocols are not intuitive and therefore, pathogen dynamics under different treatments are central for infection eradication. Despite this good performance, it will be interesting to check Model Predictive Control (MPC) approaches as well since MPC has been shown to work well for nonlinear models especially in control theory.

In Chapter 5, our overarching goal was to use mathematical and computational approaches to describe antimicrobial infections between hosts. We used the novel coronavirus as a case study and modelled it's transmission dynamics on a social network amidst vaccination campaigns and other non-pharmaceutical interventions. We described the general dynamics of the disease while investigating the impact of vaccination protocols on the spread of this virus. Using numerical simulations, we also studied the potential qualitative impact that a new and more transmissible mutant vaccine-resistant variant could have on the population.

Our results for the single strain model indicate that regardless of the vaccination protocol and network model, the number of infectious cases reduced whenever there was vaccination. In addition, the number of people needed to be vaccinated in order to reach low infection values and peaks depended heavily on the efficacy of the vaccine. For instance, with a low efficacy vaccine, more people would have to be vaccinated in order to prevent infection peaks.

However, with the introduction of a more vaccine resistant variant in circulation with the wild type virus, more individuals are infected with the vaccine resistant strain than with the wild type and with all vaccine efficacy levels except for 100%. With a 100% efficacious vaccine on the other hand, there is low to no infection when more than 30% of the population is vaccinated. In addition, we found that in the vaccinated population, less people are infected with the wild type strain than the mutant strain. This observation is due to the increased transmissibility and reduced efficacy of vaccine towards the mutant strain.

Though exploring the effects of SARS-CoV-2 transmission on social networks, we limited our analysis to two types of social network which is the Erdos-Renyi network and the Barabasi-Albert network models. To proceed towards increasing practicality, the analysis performed in this thesis can be extended to consider disease spread and vaccination on other social networks and small-world network models such as the Watts-Strogatz network, using similar scenarios and protocols. Such network models can be compared with each other and the outcomes analysed. Data on known social networks such as contact matrices and mixing patterns can also be used for further analysis and evaluation.

In our numerical simulations, we assumed an optimistic condition in which all infectious individuals are identified. In reality, contact tracing is especially difficult in the course of an ongoing epidemic. In the particular case of SARS-CoV-2, traditional interview based

approaches as well as recent digital contact-tracing apps have proven to be less effective. Thus, identifying all infectious contacts and their secondary contacts (especially for the ring vaccination strategy) becomes difficult and comes at a higher cost. In effect, these challenges can potentially reduce the impact of vaccination efforts. Also, the model used here assumes there is equal mixing of individuals and their neighbours in the network whereas in reality this is not the case. Consequently, this could lead to lower infection cases and lower population coverage.

The focus of this thesis has principally been on modelling techniques for resistant infections between-host and within-host. However, the problem of resistance is complex and hence further adaptation of these models can be formulated as knowledge and technology improves.

Control strategies from the model presented in Chapter 4 provide the theoretical road map to alleviating resistant strains. However, knowledge of how to implement different typical model parameters and how these relate to reality is crucial in validating these strategies for real-world use. For instance, what is the carrying capacity of a human patient for different types of resistant strains, and how can this be measured? This emphasizes the need for future research to provide ample data (experimental and observational) to develop model simulations and support model validation. In addition, many multiscale models have been used to understand the dynamics of infectious diseases across multiple scales such as between-host and within-host processes. Such models describe the dependence of each scale on the other and can provide understanding of interactions at different scales. However, such models are lacking for the problem of antibiotic resistance and thus, remain open areas for future research.

To add to that, although the model presented in Chapter 5 is simplistic in itself, it allows to study the basic effect of vaccination as well as vaccine-resistant viral strains on the course of an epidemic and the proportion of the population to be vaccinated to stop the epidemic. With this model, we are able to gain some insights into the qualitative behaviour of the transmission process of the virus but it can be extended to study some quantitative features such as the potential number of individuals in the population carrying the virus. The model can also be expanded to capture some of the finer details of the disease such as the differentiation of recovered and dead individuals, inclusion of hospitalized and quarantined compartments, and healthcare workers. Furthermore, the ring vaccination intervention strategy has potential to yield desirable results when infectious cases can be rightly targeted and tracked. As this strategy relies on infected individuals and their neighbours, developing methods and technology tools to identify and trace infectious individuals and their neighbours can aid in containing the infection. These should be instrumental in future models.

Appendices

Appendix A

Single strain SARS-CoV-2 model results

Here, we present the simulation plots for the single strain model in Chapter 5. The set of figures presented here represent the model in Section 5.4 where the vaccine efficacy levels and population coverage levels considered are the same as in the single strain model. As mentioned in the main text, vaccine efficacy varied between $40\% - 100\%$ whereas population coverage for classical vaccination varied between $10\% - 100\%$. For ring vaccination, the proportion of asymptomatic individuals ($\%asymptomatic$) varied as 1% and 3% (see Table 5.2). For ER simulations: $N = 10^6$, $b_1 = 0.028$, $b_2 = 0.001$, $r_1 = 0.09$, $r_2 = 0.04$, $m_1 =$ day 50, $m_2 =$ day 126 and $T = 360$ days. For BA simulations: $N = 10^6$, $b_1 = 0.013$, $b_2 = 0.001$, $r_1 = 0.09$, $r_2 = 0.04$, $m_1 =$ day 50, $m_2 =$ day 126 and $T = 360$ days. Each scenario is repeated 100 times and the mean of infection cases taken for analysis.

A.1 Erdos-Renyi network results

Mass vaccination

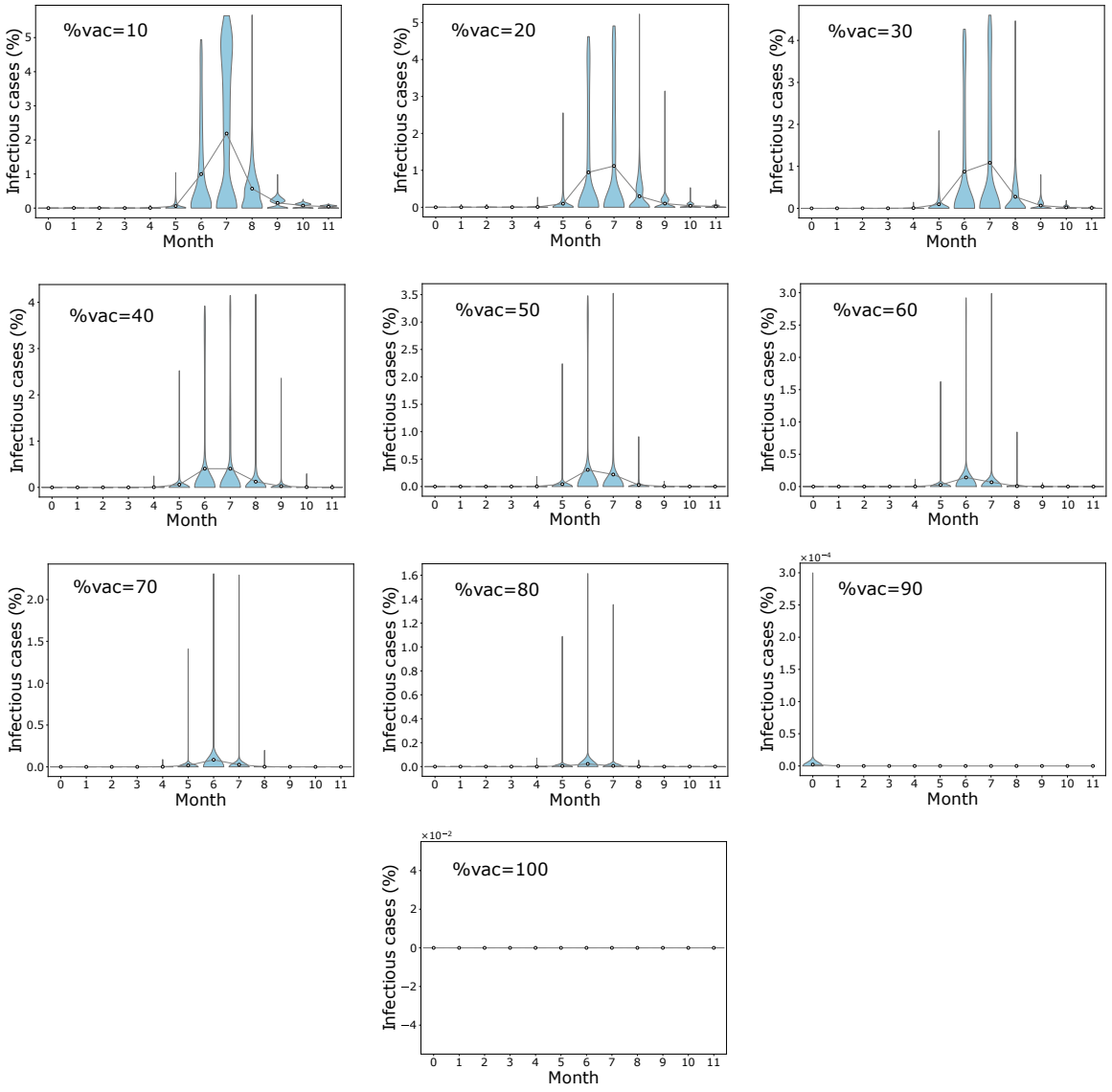

FIGURE A.1: Erdos-Renyi network: Distribution of final infectious cases in different timing for mass vaccination scenario when $\eta = 40\%$. Population coverage varies from $10\% - 100\%$. Circles represent mean infection cases for each month connected by lines.

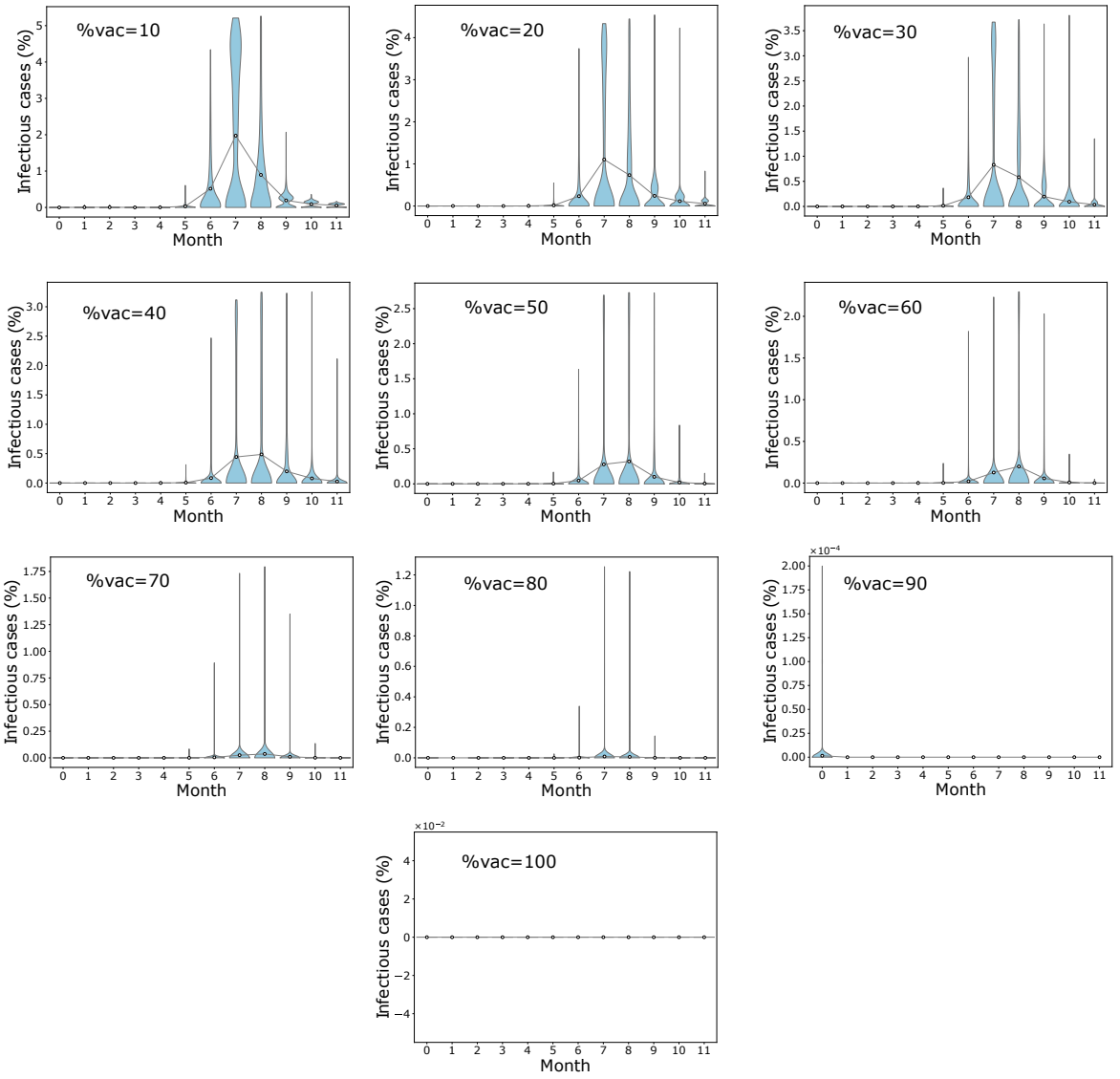

FIGURE A.2: Erdos-Renyi network: Distribution of final infectious cases in different timing for mass vaccination scenario when $\eta = 60\%$. Population coverage varies from $10\% - 100\%$. Circles represent mean infection cases for each month connected by lines.

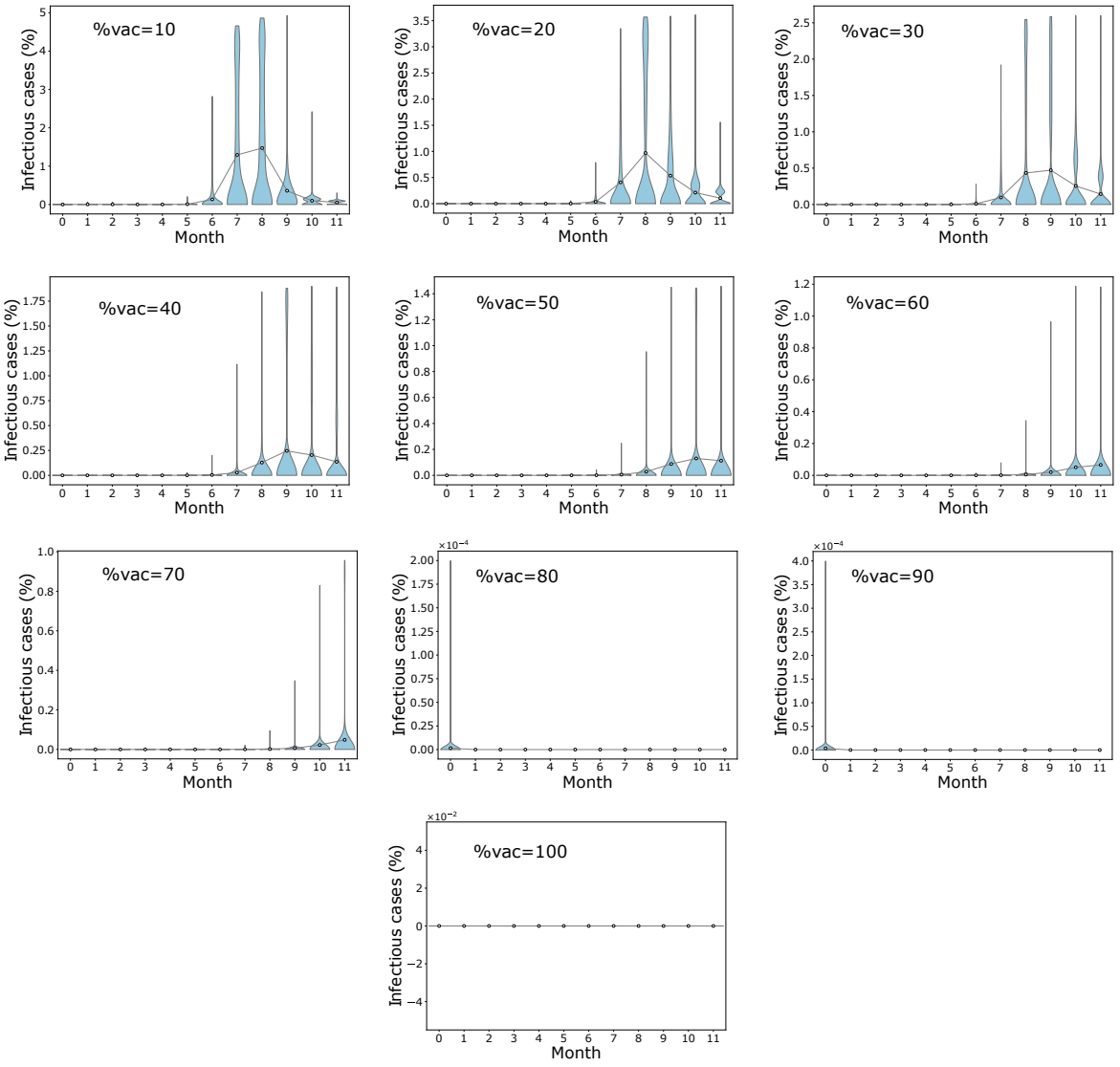

FIGURE A.3: Erdos-Renyi network: Distribution of final infectious cases in different timing for mass vaccination scenario when $\eta = 80\%$. Population coverage varies from $10\% - 100\%$. Circles represent mean infection cases for each month connected by lines.

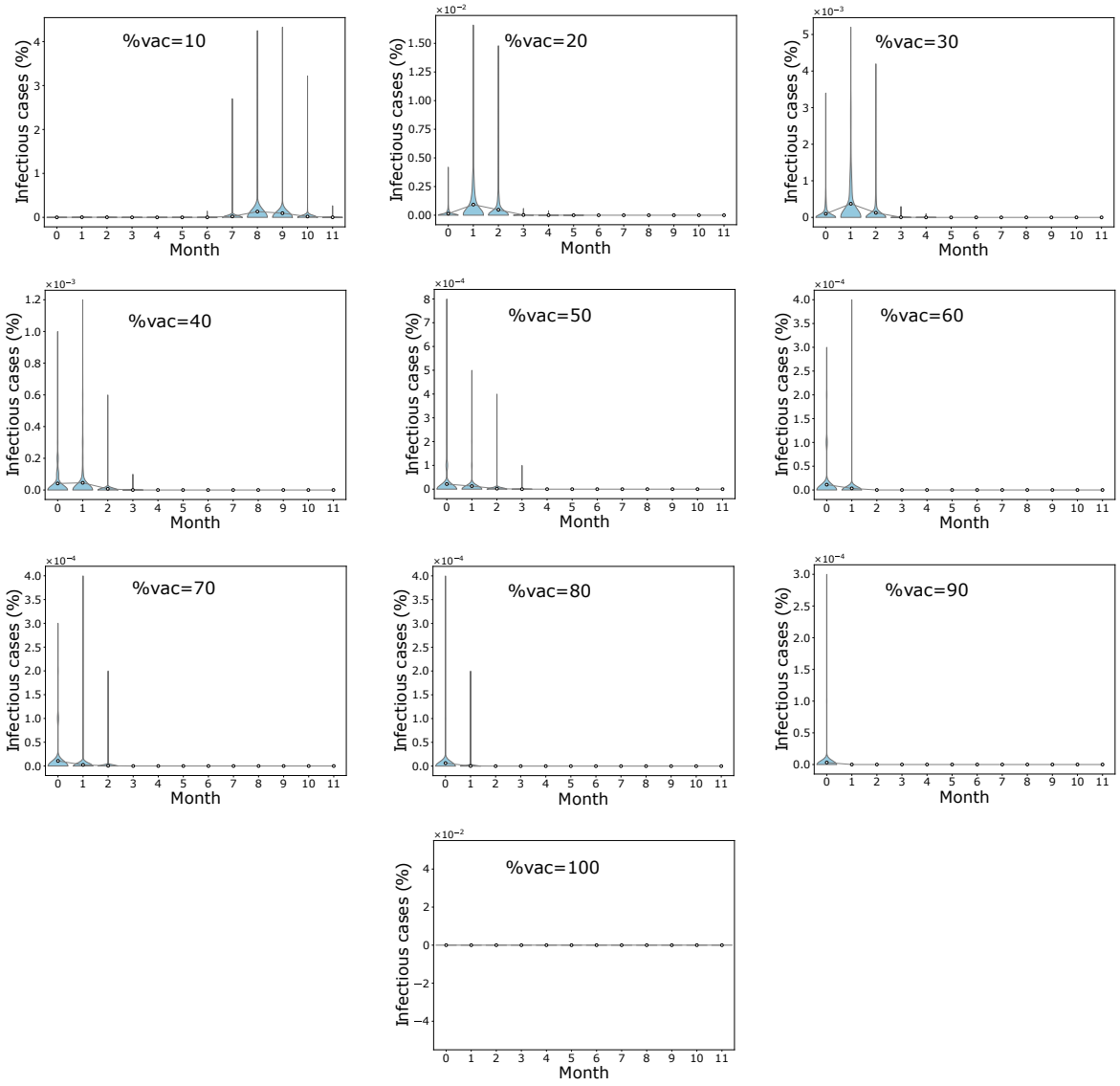

FIGURE A.4: Erdos-Renyi network: Distribution of final infectious cases in different timing for mass vaccination scenario when $\eta = 100\%$. Population coverage varies from $10\% - 100\%$. Circles represent mean infection cases for each month connected by lines.

TABLE A.1: Erdos-Renyi Model: Average infection peak values considering vaccine efficacy and population coverage.

Mass vaccination scenarios (vaccination before case zero)				
Population	**Vaccine Efficacy**			
Coverage	40%	60%	80%	100%
10%	2.19 ± 0.63	1.98 ± 0.57	1.47 ± 0.50	0.13 ± 0.04
20%	1.12 ± 0.37	1.11 ± 0.34	0.97 ± 0.29	0 ± 0
30%	1.09 ± 0.36	0.83 ± 0.26	0.47 ± 0.17	0 ± 0
40%	0.41 ± 0.15	0.49 ± 0.17	0.25 ± 0.09	0 ± 0
50%	0.3 ± 0.1	0.32 ± 0.1	0.13 ± 0.05	0.0 ± 0
60%	0.14 ± 0.04	0.20 ± 0.06	0.07 ± 0.02	0.0 ± 0
70%	0.08 ± 0.02	0.04 ± 0.01	0.05 ± 0.01	0 ± 0
80%	0.02 ± 0	0.01 ± 0	0 ± 0	0 ± 0
90%	0 ± 0	0 ± 0	0 ± 0	0 ± 0
100%	0 ± 0	0 ± 0	0 ± 0	0 ± 0

TABLE A.2: Erdos-Renyi Model: Average proportion and standard deviation of vaccinated individuals who got exposed in the course of the infection.

Mass vaccination scenarios (vaccination before case zero)				
Population	**Vaccine Efficacy**			
Coverage	40%	60%	80%	100%
10%	42.33 ± 34.56	30.9 ± 26.84	14.64 ± 12.98	0 ± 0
20%	35.13 ± 43.02	28.78 ± 36.03	13.43 ± 16.53	0 ± 0
30%	39.04 ± 46.84	28.61 ± 40.82	10.69 ± 17.39	0 ± 0
40%	19.61 ± 39.23	24.02 ± 40.59	6.97 ± 15.5	0 ± 0
50%	13.93 ± 34.44	17.43 ± 37.21	4.03 ± 11.78	0.0 ± 0
60%	6.98 ± 25.44	11.81 ± 31.99	1.9 ± 7.62	0.0 ± 0
70%	4.99 ± 21.77	2.98 ± 16.93	1.36 ± 5.45	0 ± 0
80%	2 ± 13.99	1.0 ± 9.92	0 ± 0	0 ± 0
90%	0 ± 0	0 ± 0	0 ± 0	0 ± 0
100%	0 ± 0	0 ± 0	0 ± 0	0 ± 0

TABLE A.3: Erdos-Renyi Model: Average proportion and standard deviation of unvaccinated(susceptibles) individuals who got exposed in the course of the infection.

Mass vaccination scenarios (vaccination before case zero)				
Population	**Vaccine Efficacy**			
Coverage	40%	60%	80%	100%
10%	52.75 ± 43.07	48.52 ± 42.14	44.12 ± 39.11	3.5 ± 14.98
20%	38.1 ± 46.66	36.3 ± 45.4	33.18 ± 40.65	0.02 ± 0.04
30%	40.24 ± 48.27	32.04 ± 45.66	23.86 ± 38.31	0.01 ± 0.02
40%	19.85 ± 39.69	25.64 ± 43.26	15.05 ± 32.42	0 ± 0
50%	13.96 ± 34.59	17.91 ± 38.23	9.15 ± 25.7	0.0 ± 0
60%	6.99 ± 25.48	11.97 ± 32.43	4.72 ± 18.14	0.0 ± 0
70%	5 ± 21.78	3 ± 17.04	3.86 ± 14.83	0 ± 0
80%	2 ± 14.00	1 ± 9.95	0 ± 0	0 ± 0
90%	0 ± 0	0 ± 0	0 ± 0	0 ± 0
100%	0 ± 0	0 ± 0	0 ± 0	0 ± 0

Ring Vaccination

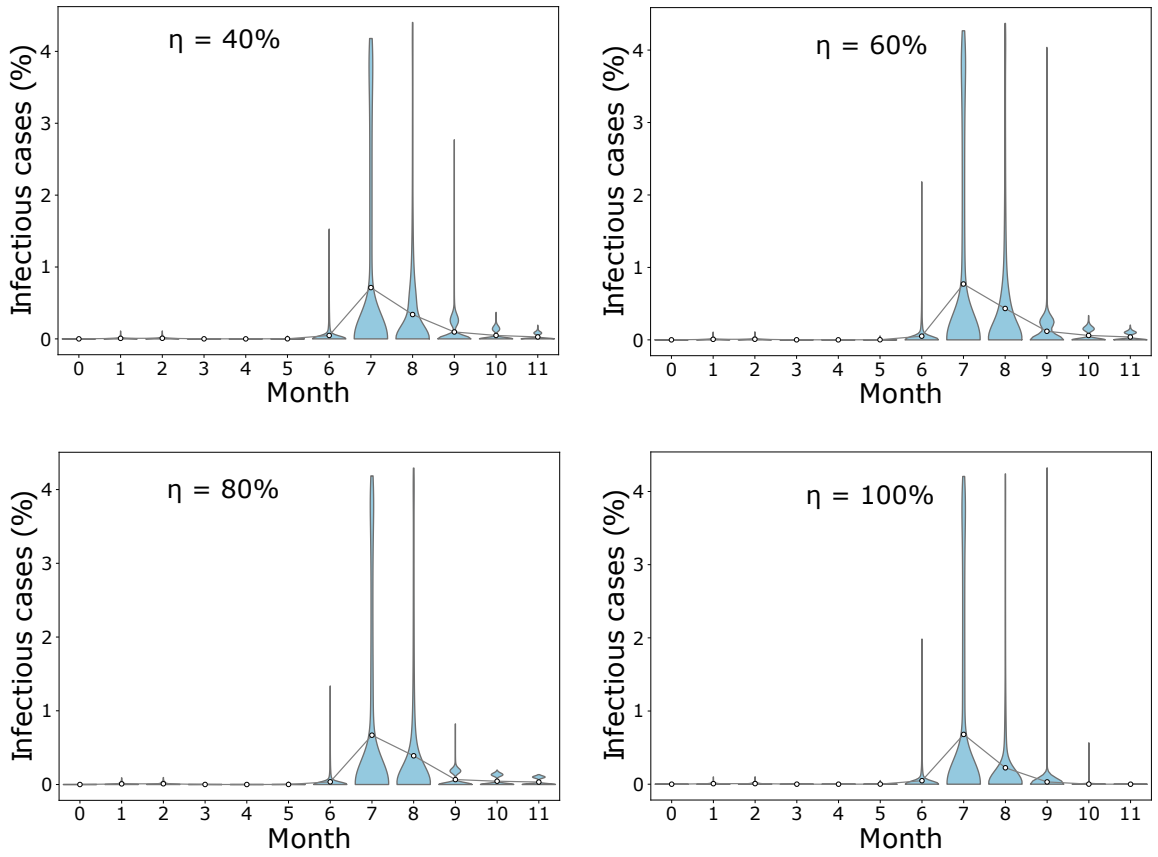

FIGURE A.5: Erdos-Renyi network: Distribution of final infectious cases in different timing for ring vaccination scenario when 1% of the population is exposed prior to vaccination. Circles represent mean infection cases for each month connected by lines.

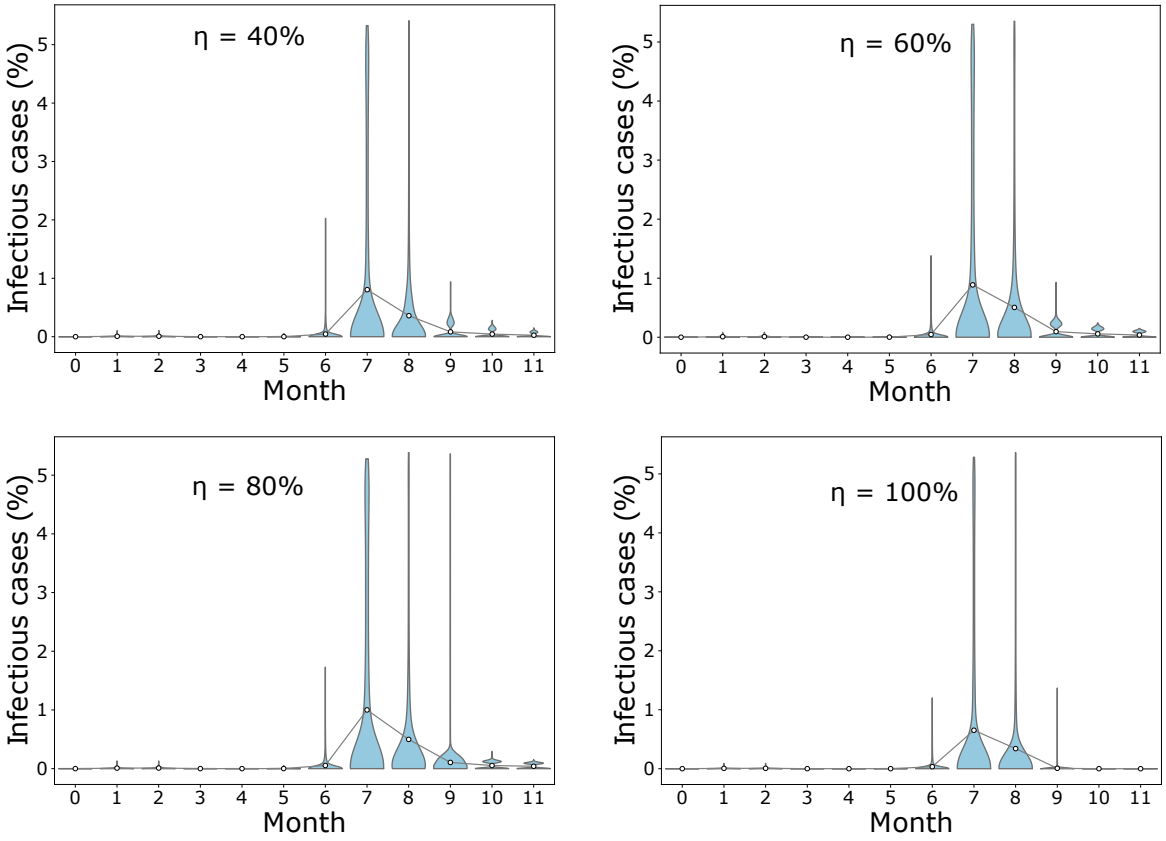

FIGURE A.6: Erdos-Renyi network: Distribution of final infectious cases in different timing for ring vaccination scenario when 3% of the population is exposed prior to vaccination. Circles represent mean infection cases for each month connected by lines.

Barabasi-Albert network results

Mass vaccination

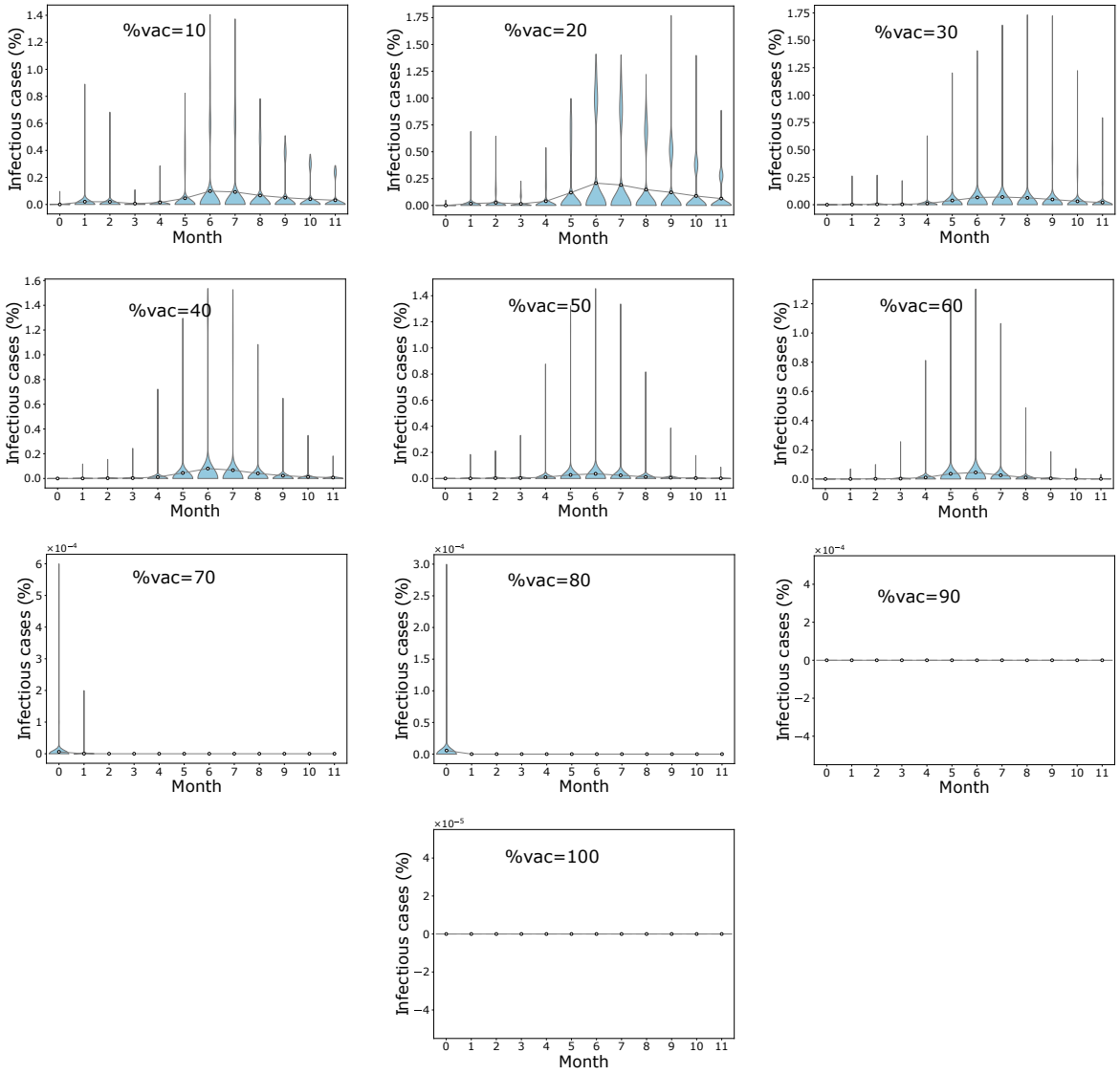

FIGURE A.7: Barabasi-Albert network: Distribution of final infectious cases in different timing for mass vaccination scenario when $\eta = 40\%$. Population coverage varies from $10\% - 100\%$. Circles represent mean infection cases for each month connected by lines.

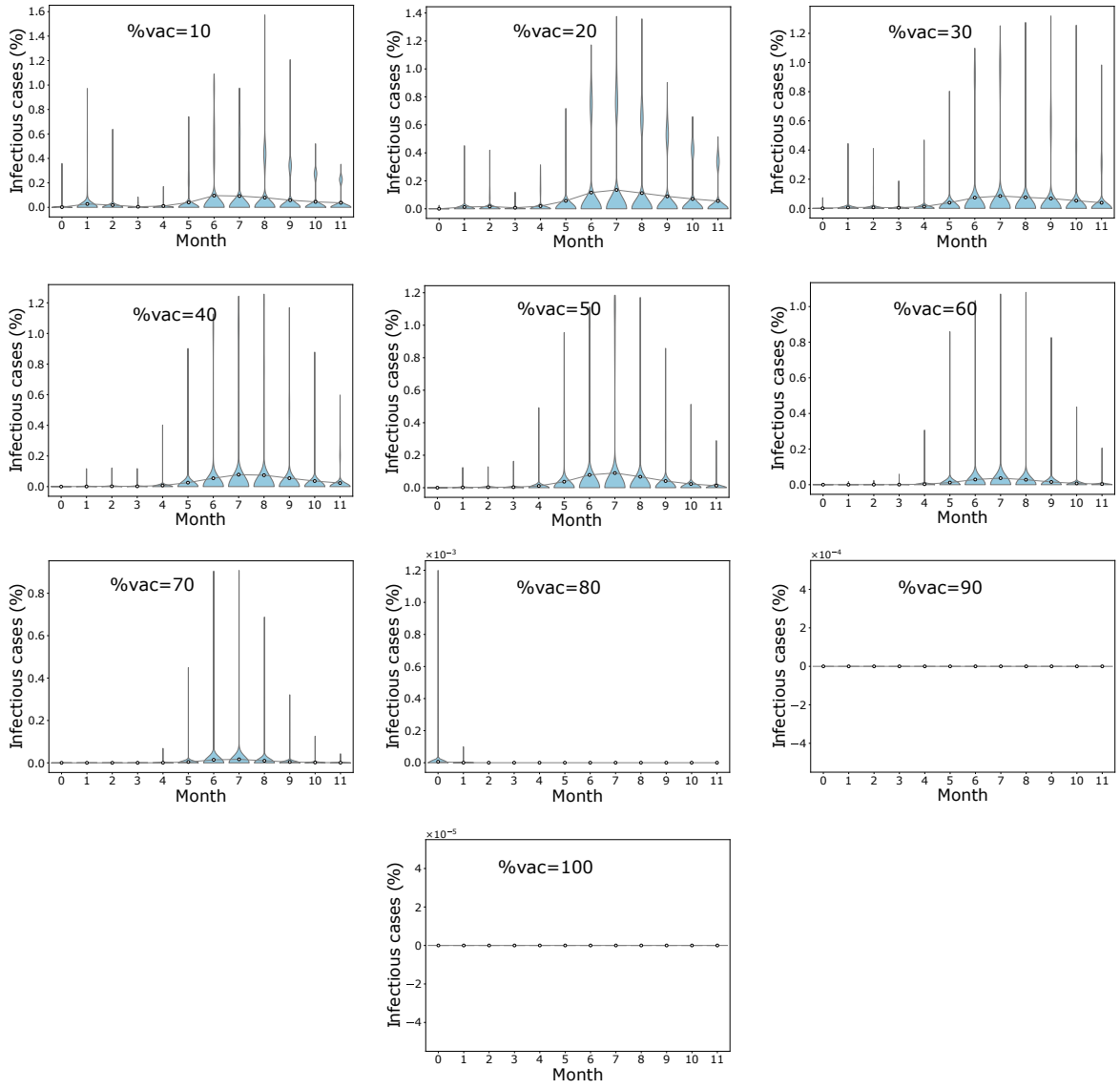

FIGURE A.8: Barabasi-Albert network: Distribution of final infectious cases in different timing for mass vaccination scenario when $\eta = 60\%$. Population coverage varies from $10\% - 100\%$. Circles represent mean infection cases for each month connected by lines.

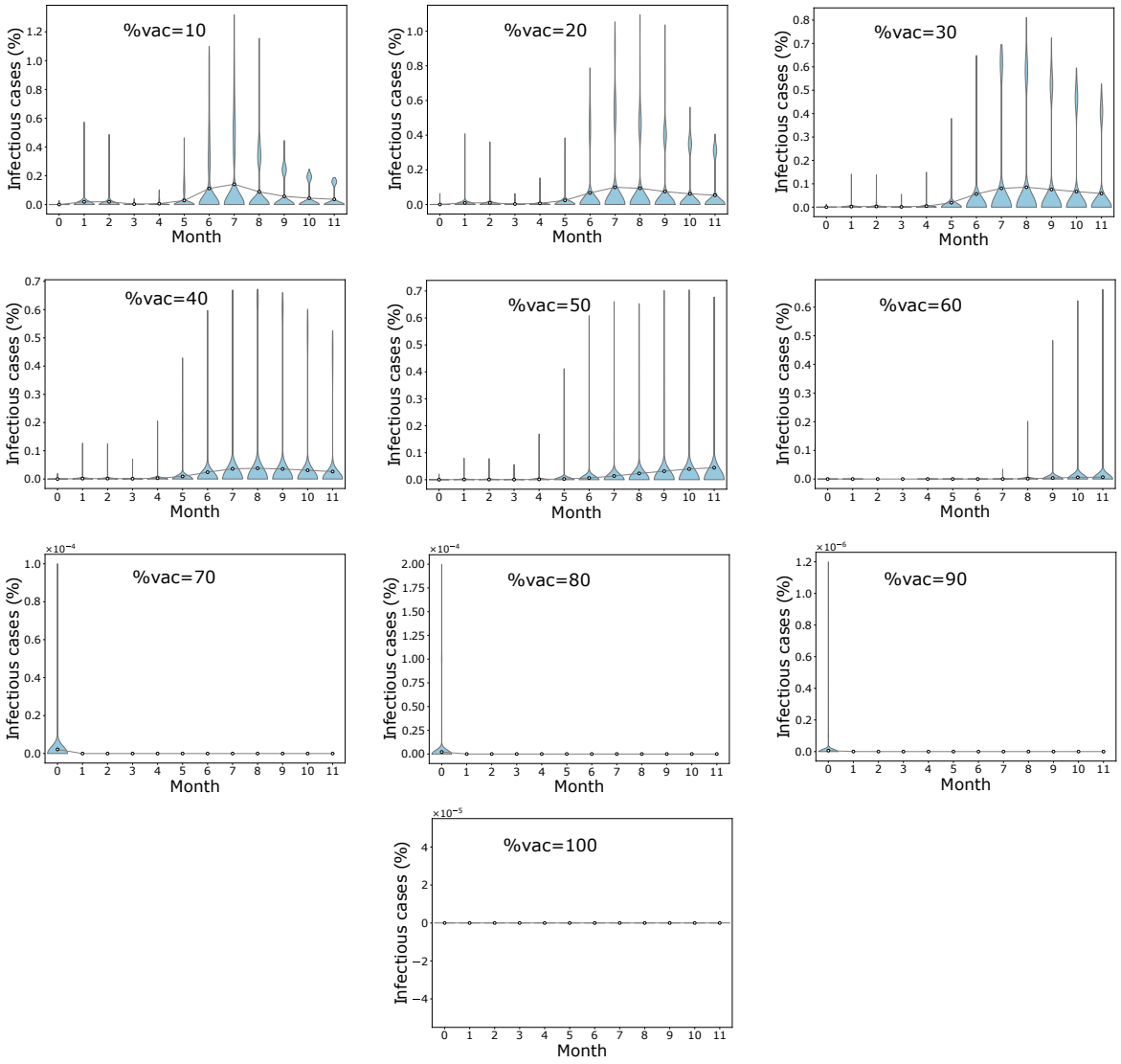

FIGURE A.9: Barabasi-Albert network: Distribution of final infectious cases in different timing for mass vaccination scenario when $\eta = 80\%$. Population coverage varies from $10\% - 100\%$. Circles represent mean infection cases for each month connected by lines.

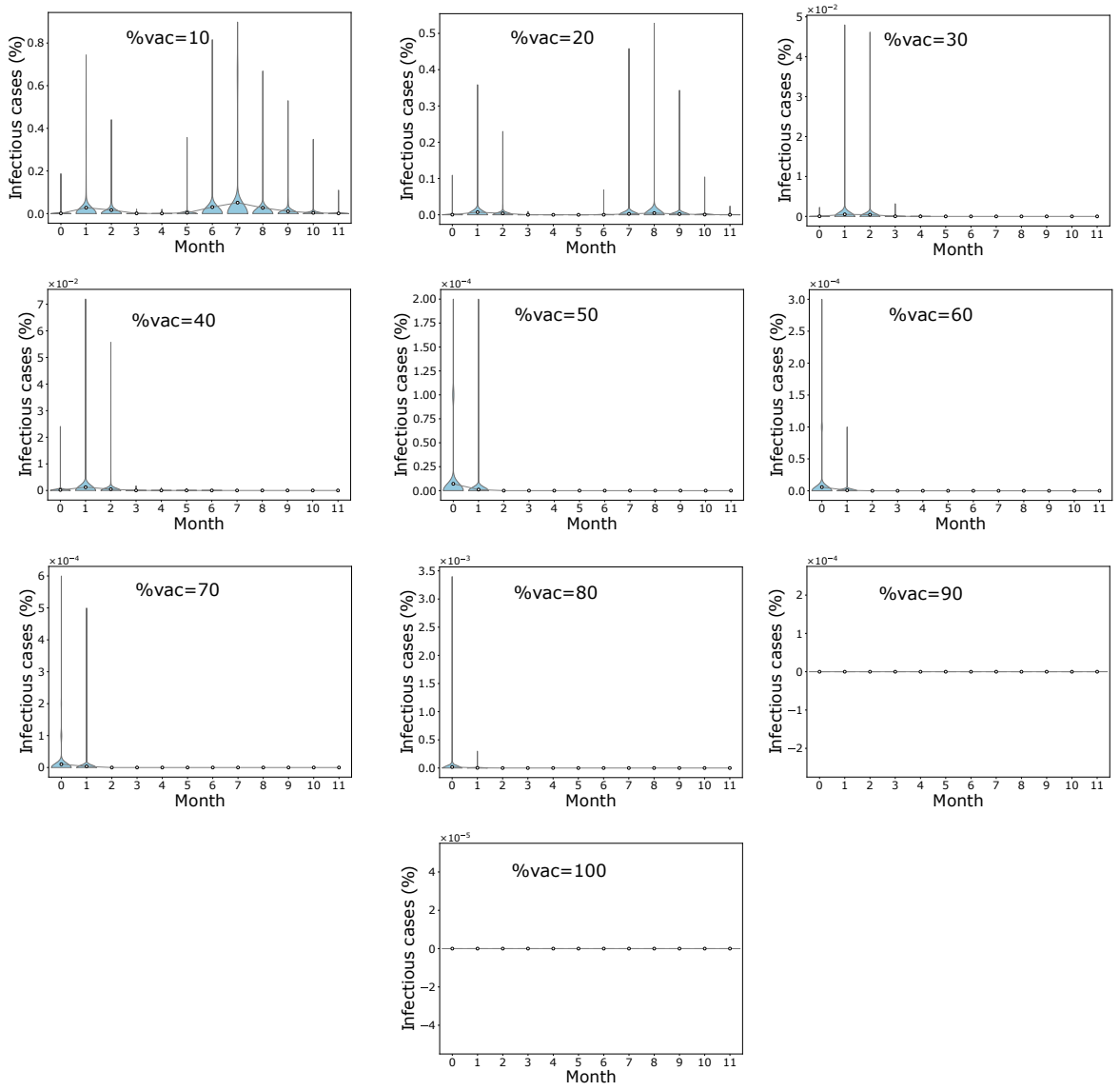

FIGURE A.10: Barabasi-Albert network: Distribution of final infectious cases in different timing for mass vaccination scenario when $\eta = 100\%$. Population coverage varies from $10\% - 100\%$. Circles represent mean infection cases for each month connected by lines.

TABLE A.4: Barabasi Albert Model: Average infection peak values considering vaccine efficacy and population coverage.

Mass vaccination scenarios (vaccination before case zero)				
Population	**Vaccine Efficacy**			
Coverage	40%	60%	80%	100%
10%	0.1 ± 0.03	0.1 ± 0.03	0.14 ± 0.04	0.05 ± 0.01
20%	0.21 ± 0.07	0.13 ± 0.05	0.10 ± 0.04	0.01 ± 0
30%	0.07 ± 0.03	0.08 ± 0.03	0.09 ± 0.03	0 ± 0
40%	0.08 ± 0.03	0.08 ± 0.03	0.04 ± 0.02	0 ± 0
50%	0.04 ± 0.01	0.09 ± 0.03	0.04 ± 0.02	0.0 ± 0
60%	0.04 ± 0.01	0.04 ± 0.01	0.01 ± 0	0.0 ± 0
70%	0 ± 0	0 ± 0	0 ± 0	0 ± 0
80%	0 ± 0	0 ± 0	0 ± 0	0 ± 0
90%	0 ± 0	0 ± 0	0 ± 0	0 ± 0
100%	0 ± 0	0 ± 0	0 ± 0	0 ± 0

TABLE A.5: Barabasi Albert Model:Average proportion and standard deviation of vaccinated individuals who got exposed in the course of the infection.

Mass vaccination scenarios (vaccination before case zero)				
Population	**Vaccine Efficacy**			
Coverage	40%	60%	80%	100%
10%	4.29 ± 11.09	3.22 ± 7.38	1.7 ± 3.11	0.0 ± 0
20%	12.17 ± 23.67	6.29 ± 14.44	2.22 ± 4.93	0.0 ± 0
30%	5.18 ± 18.94	5.48 ± 16.65	2.73 ± 6.83	0 ± 0
40%	± 20.86	5.5 ± 18.72	1.75 ± 6.98	0 ± 0
50%	2.84 ± 16.12	7.39 ± 23.53	1.56 ± 6.39	0.0 ± 0
60%	3.9 ± 19.1	3.52 ± 17.24	0.18 ± 1.81	0.0 ± 0
70%	$0.0\pm$	1.87 ± 13.07	0 ± 0	0 ± 0
80%	0 ± 0	0 ± 0	0 ± 0	0 ± 0
90%	0 ± 0	0 ± 0	0 ± 0	0 ± 0
100%	0 ± 0	0 ± 0	0 ± 0	0 ± 0

TABLE A.6: Barabasi Albert Model:Average proportion and standard deviation of unvaccinated(susceptibles) individuals who got exposed in the course of the infection.

Mass vaccination scenarios (vaccination before case zero)				
Population	**Vaccine Efficacy**			
Coverage	40%	60%	80%	100%
10%	6.36 ± 16.47	6.69 ± 15.34	7.27 ± 13.34	2.24 ± 5.57
20%	15.2 ± 29.50	10.23 ± 23.44	7.48 ± 16.54	0.32 ± 1.67
30%	5.97 ± 21.79	7.79 ± 23.46	7.8 ± 19.37	0.02 ± 0.09
40%	5.66 ± 22.4	7.08 ± 24.01	4.15 ± 16.44	0.04 ± 0.19
50%	2.94 ± 16.69	8.59 ± 27.33	4.15 ± 15.26	0.0 ± 0
60%	3.97 ± 19.44	3.92 ± 19.18	0.55 ± 5.45	0.0 ± 0
70%	0 ± 0	1.99 ± 13.91	0 ± 0	0 ± 0
80%	0 ± 0	0 ± 0	0 ± 0	0 ± 0
90%	0 ± 0	0 ± 0	0 ± 0	0 ± 0
100%	0 ± 0	0 ± 0	0 ± 0	0 ± 0

Ring vaccination

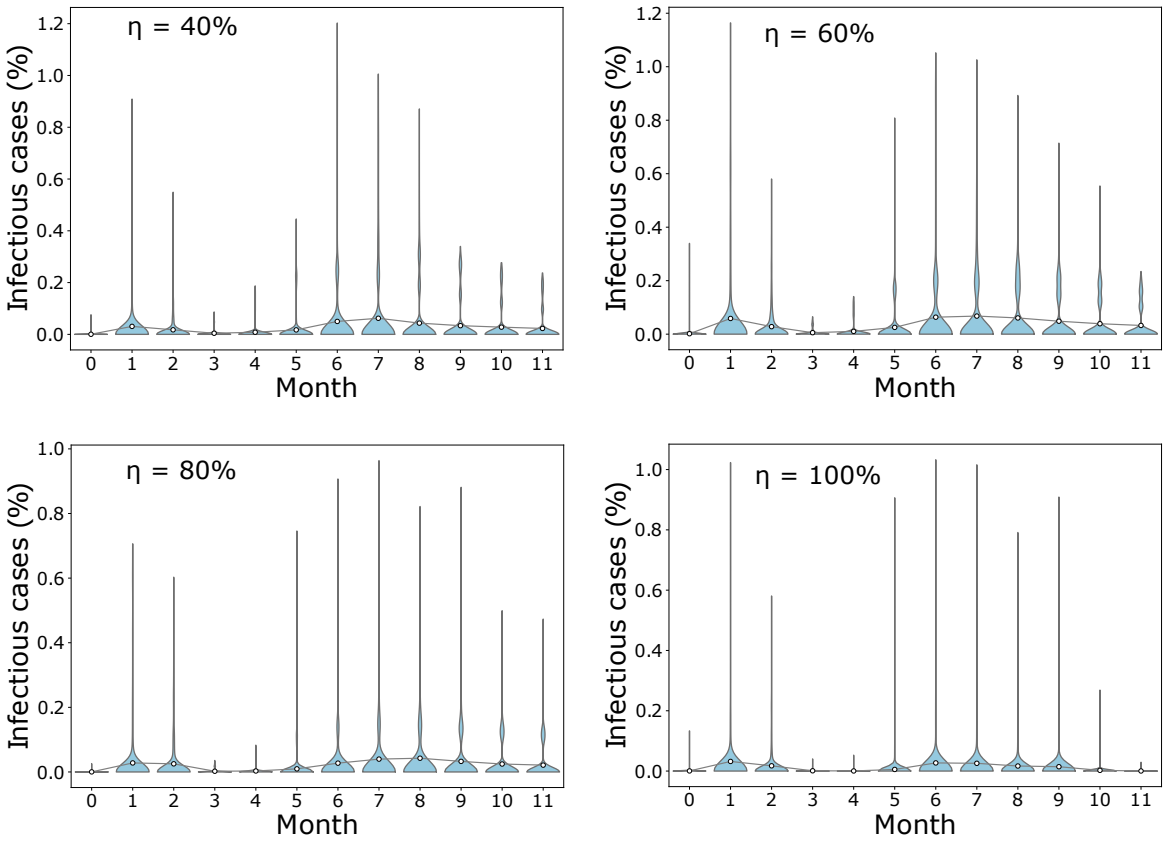

FIGURE A.11: Barabasi-Albert network: Distribution of final infectious cases in different timing for ring vaccination scenario when 1% of the population is exposed prior to vaccination. Circles represent mean infection cases for each month connected by lines.

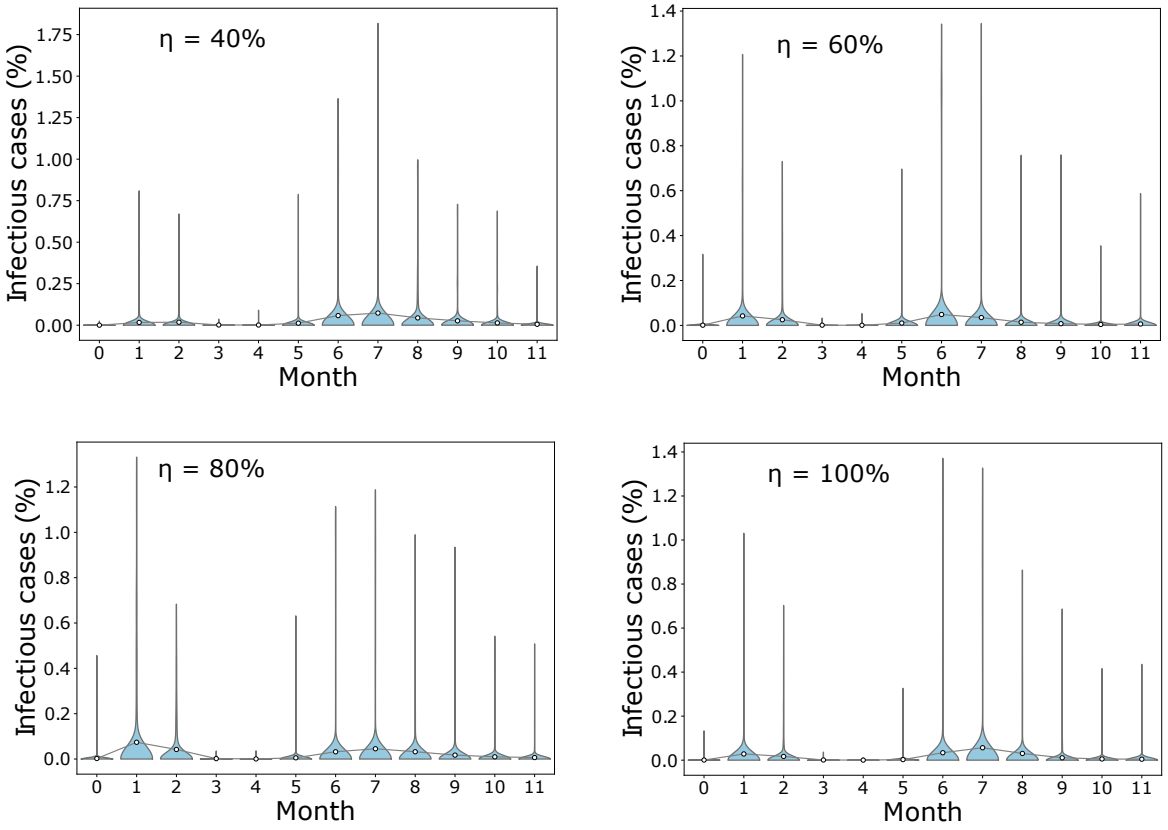

FIGURE A.12: Barabasi-Albert network: Distribution of final infectious cases in different timing for ring vaccination scenario when 3% of the population is exposed prior to vaccination. Circles represent mean infection cases for each month connected by lines.

Appendix B

Double strain SARS-CoV-2 model results

Here, we present the simulation plots for the double strain model in Chapter 5 and considering only mass vaccination.

B.1 Model assuming equal vaccine efficacy levels

The set of figures presented here represent the model in Section 5.5.3.2 where the vaccine efficacy levels and population coverage levels considered are the same as in the single strain model. As mentioned in the main text, vaccine efficacy varied between $40\% - 100\%$ whereas population coverage varied between $10\% - 100\%$. In all simulations, we consider that lock-down begins on day 50 and ends on day 140. For ER simulations: $N = 10^5$, $\beta_1 = 0.022$, $\beta_2 = 0.025$, $\tau =$ day 220 and $T = 539$ days. For BA simulations: $N = 10^5$, $\beta_1 = 0.014$, $\beta_2 = 0.017$, $\tau =$ day 220 and $T = 539$ days. Each scenario is repeated 100 times and the outputs are taken for analysis.

B.1.1 Erdos-Renyi network

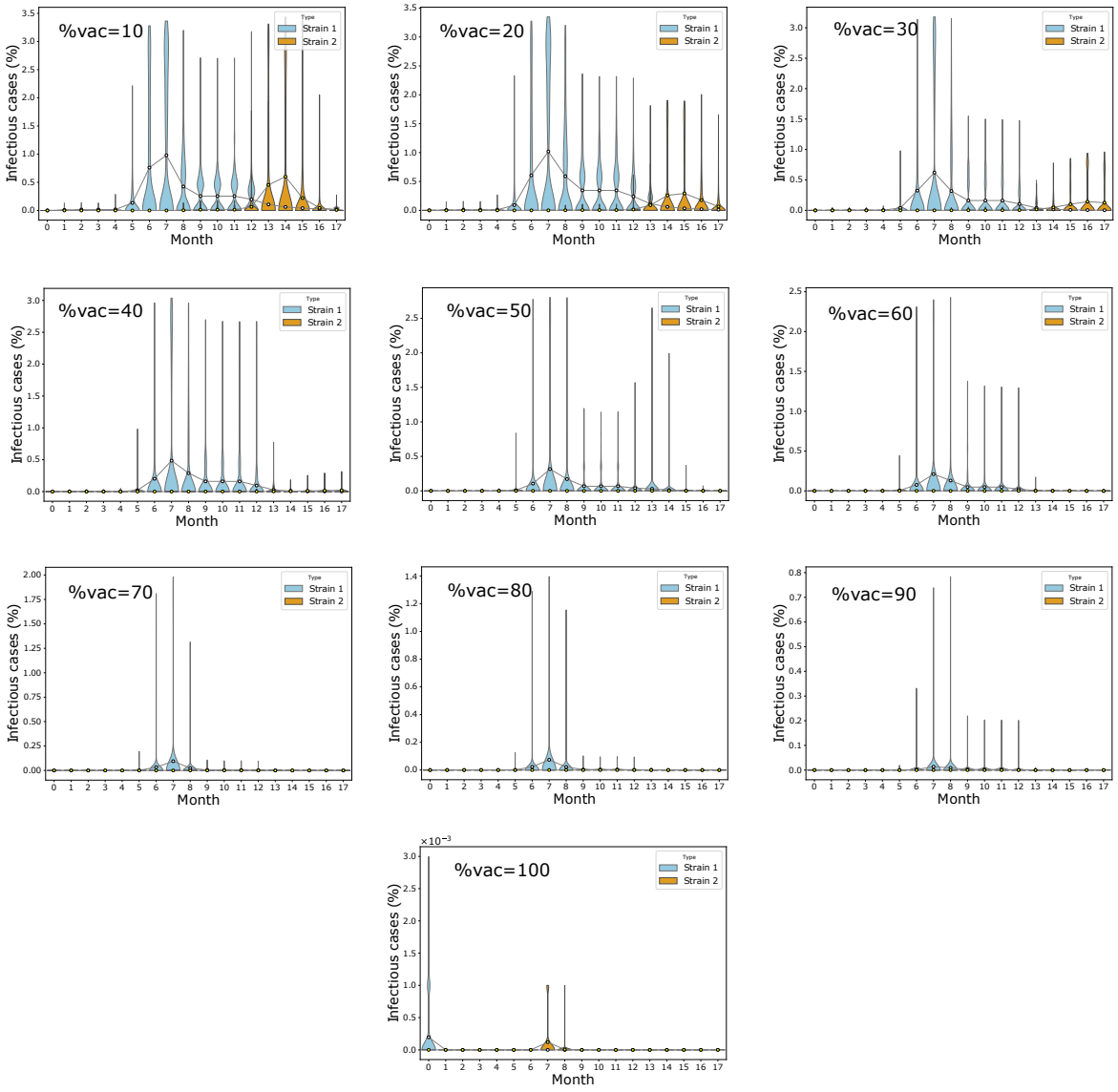

FIGURE B.1: Erdos-Renyi network: Distribution of final infectious cases in different timing for mass vaccination scenario when $\eta = 40\%$. Population coverage varies from $10\% - 100\%$. Circles represent mean infection cases for each month connected by lines.

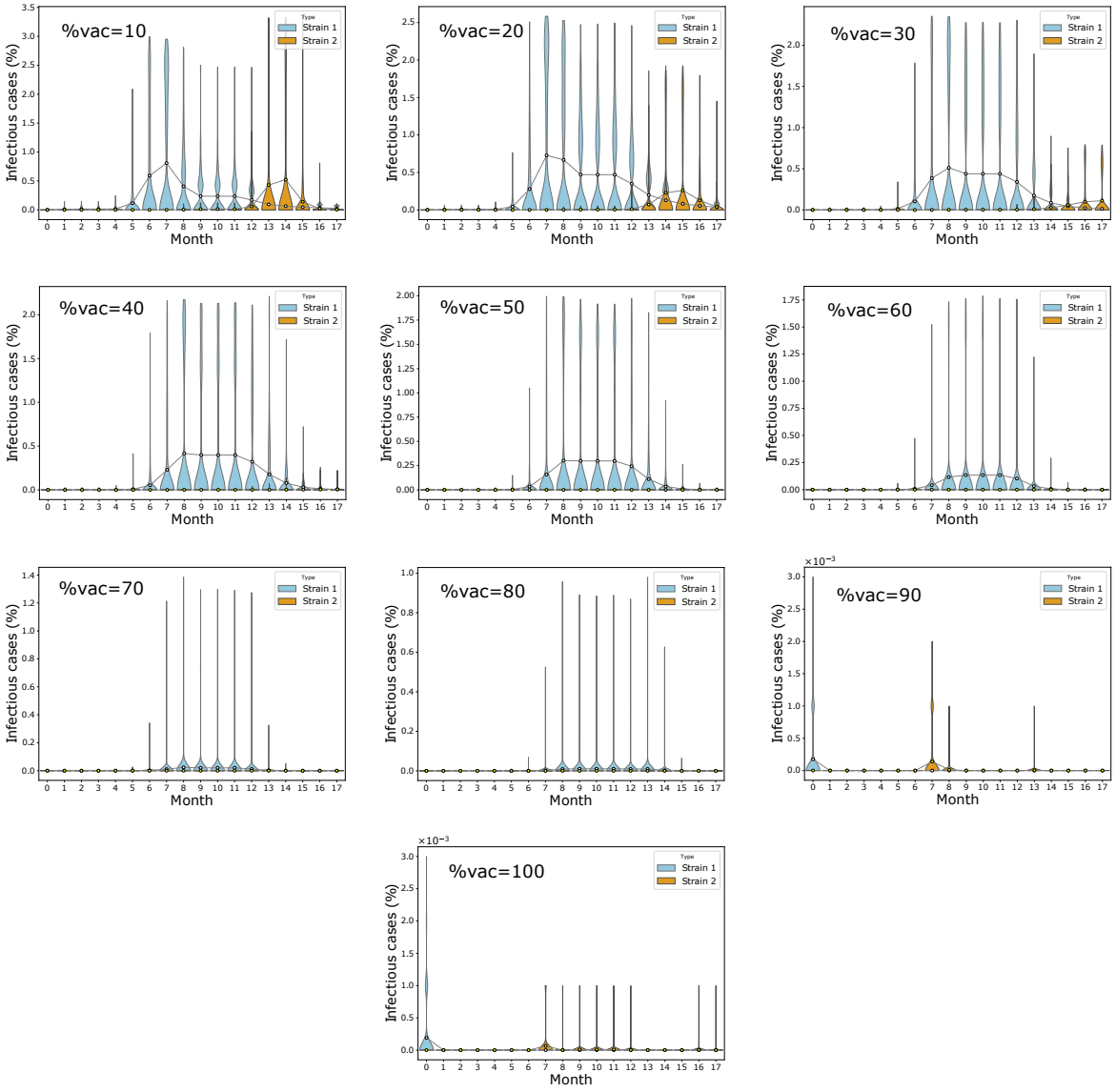

FIGURE B.2: Erdos-Renyi network: Distribution of final infectious cases in different timing for mass vaccination scenario when $\eta = 60\%$. Population coverage varies from $10\% - 100\%$. Circles represent mean infection cases for each month connected by lines.

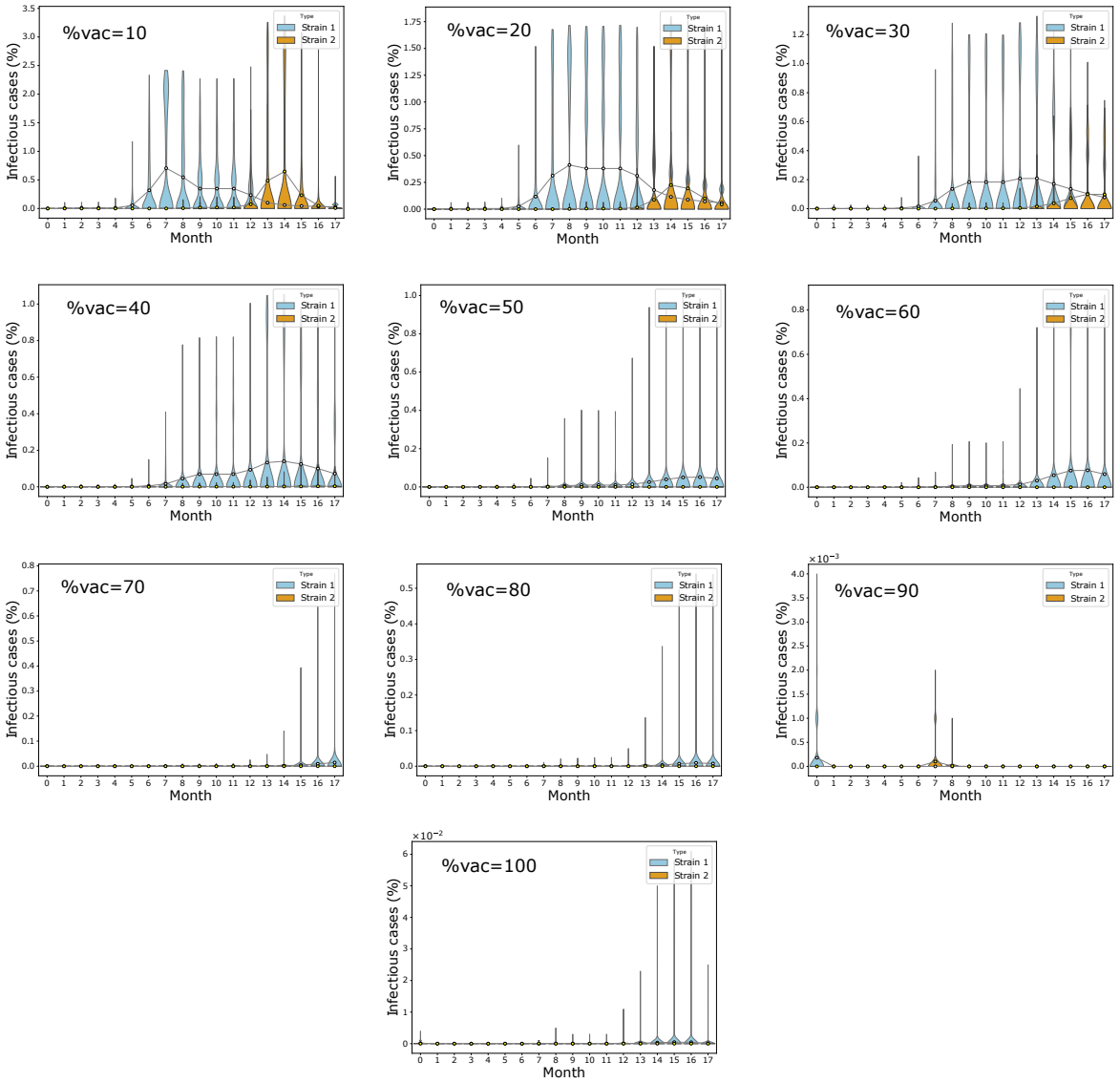

FIGURE B.3: Erdos-Renyi network: Distribution of final infectious cases in different timing for mass vaccination scenario when $\eta = 80\%$. Population coverage varies from $10\% - 100\%$. Circles represent mean infection cases for each month connected by lines.

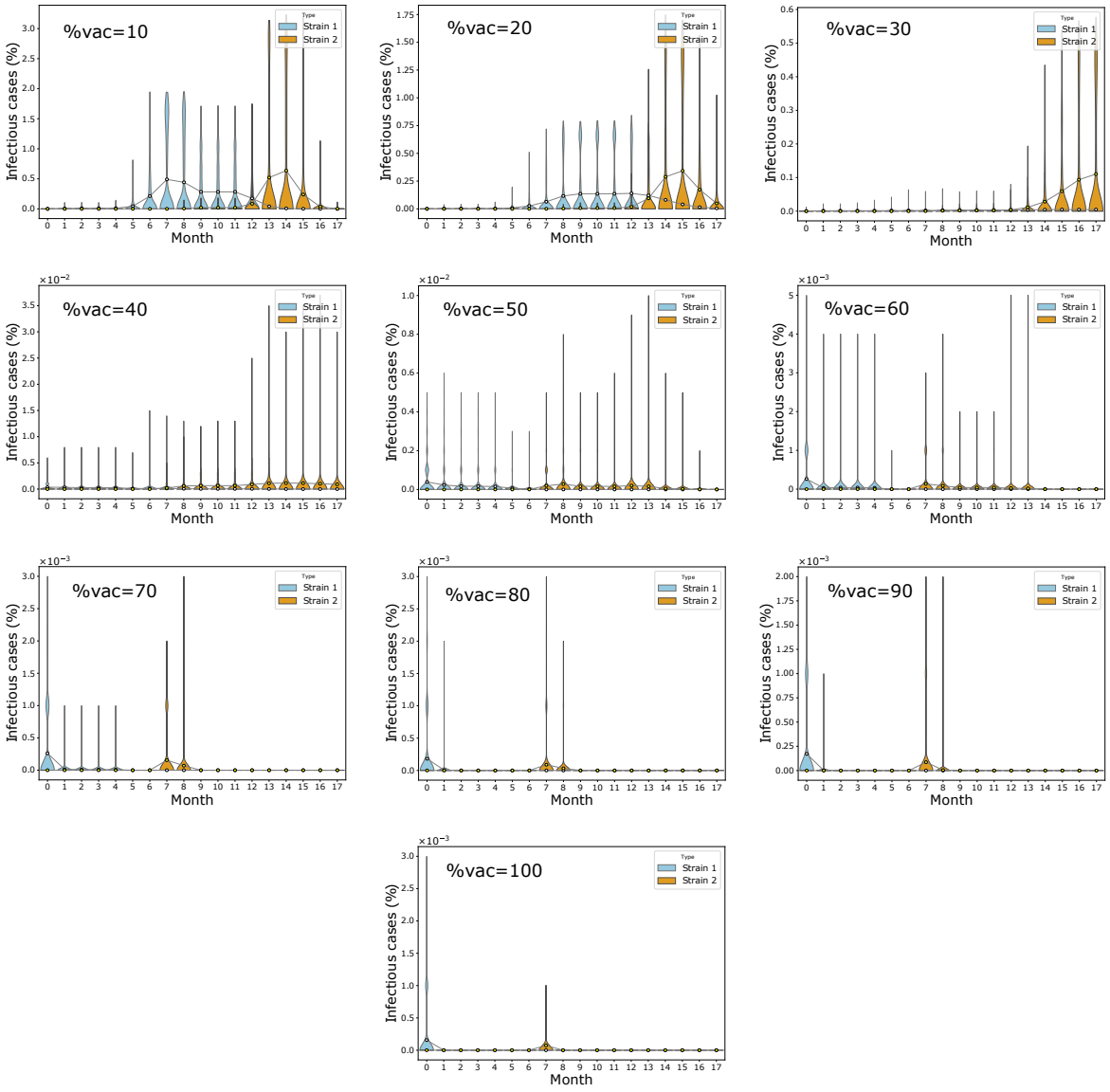

FIGURE B.4: Erdos-Renyi network: Distribution of final infectious cases in different timing for mass vaccination scenario when $\eta = 100\%$. Population coverage varies from $10\% - 100\%$. Circles represent mean infection cases for each month connected by lines.

B.1.2 Barabasi-Albert network

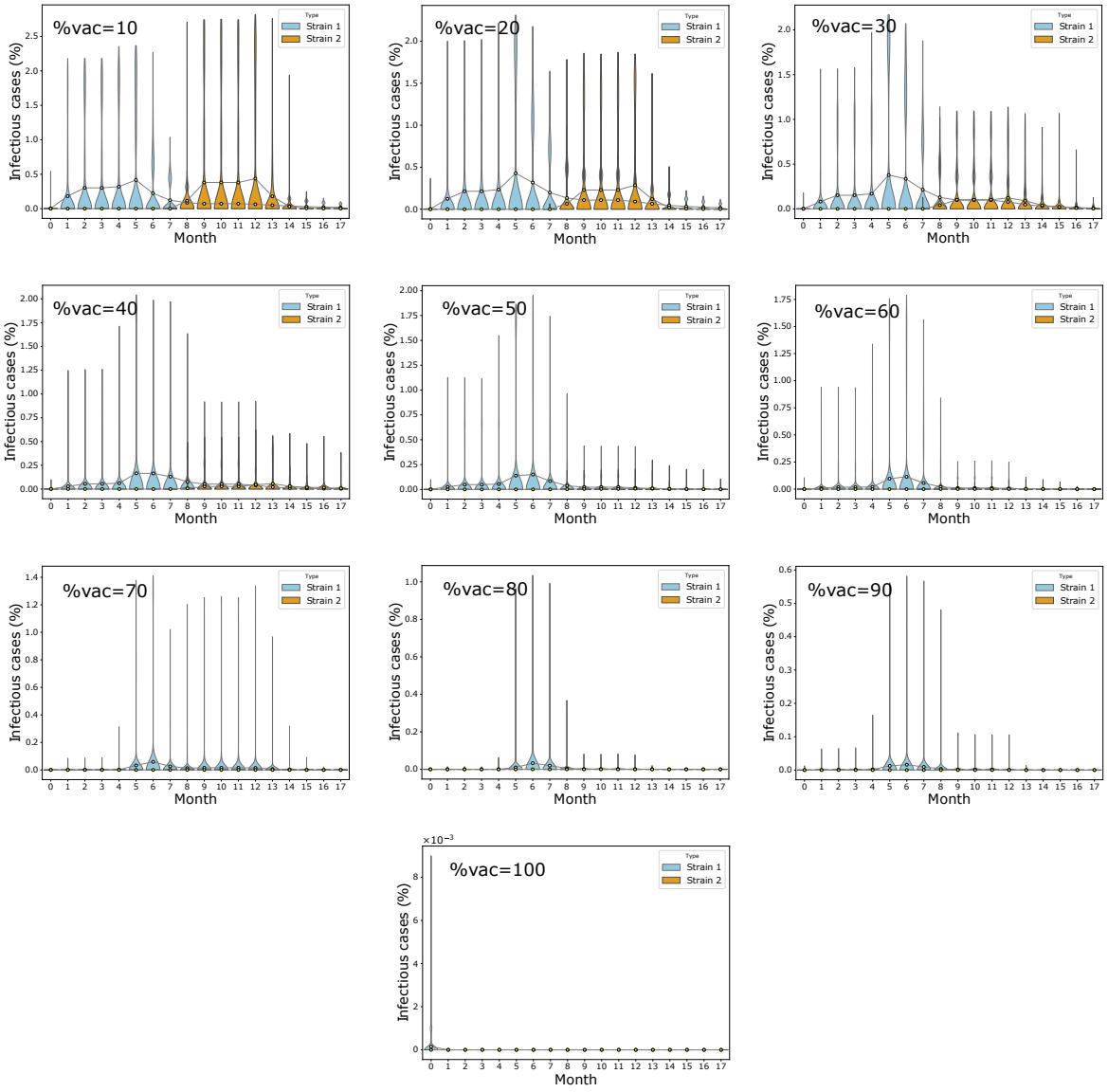

FIGURE B.5: BA network: Distribution of final infectious cases in different timing for mass vaccination scenario when $\eta = 40\%$. Population coverage varies from $10\% - 100\%$. Circles represent mean infection cases for each month connected by lines.

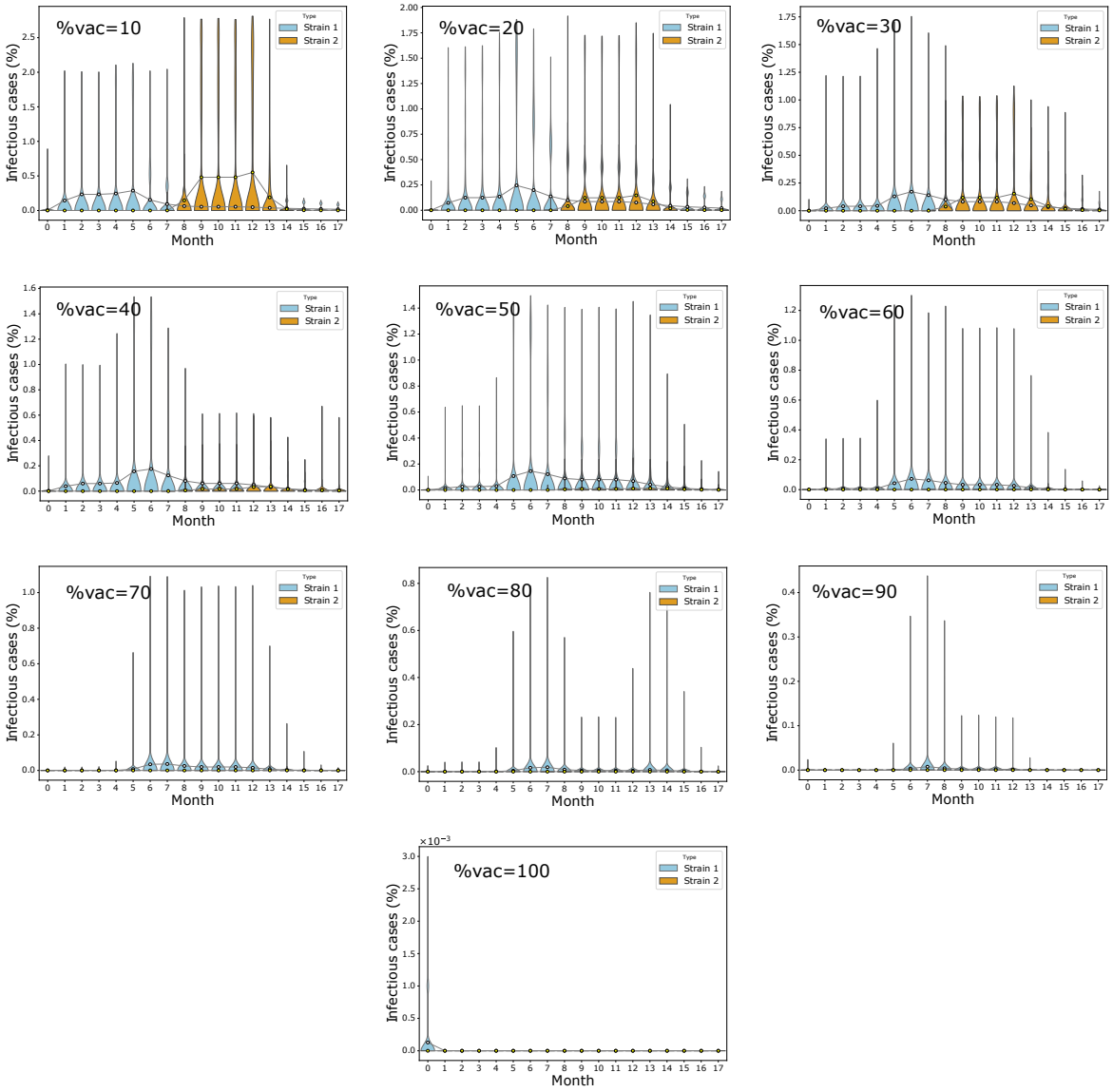

FIGURE B.6: BA network: Distribution of final infectious cases in different timing for mass vaccination scenario when $\eta = 60\%$. Population coverage varies from $10\% - 100\%$. Circles represent mean infection cases for each month connected by lines.

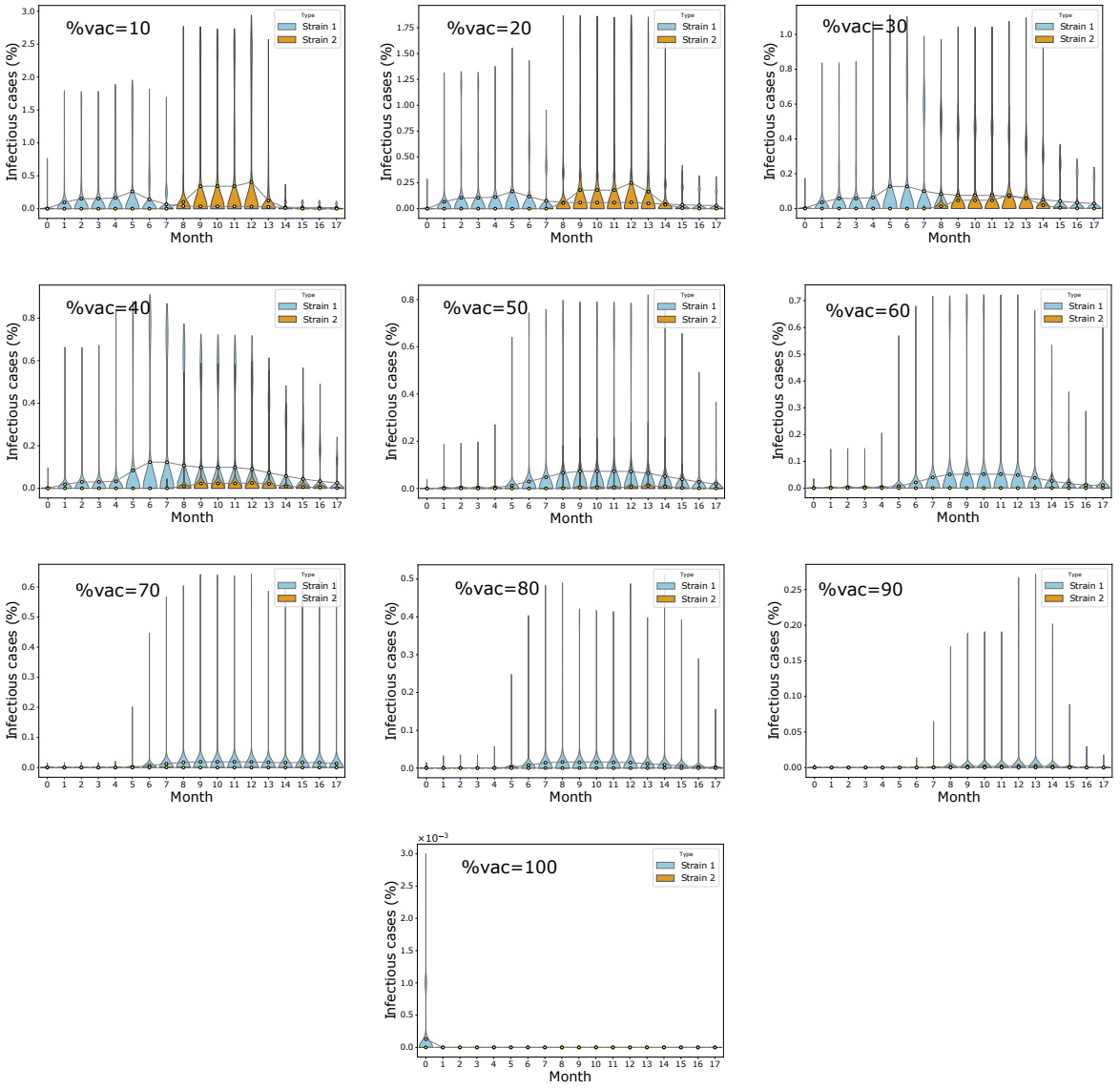

FIGURE B.7: BA network: Distribution of final infectious cases in different timing for mass vaccination scenario when $\eta = 80\%$. Population coverage varies from $10\% - 100\%$. Circles represent mean infection cases for each month connected by lines.

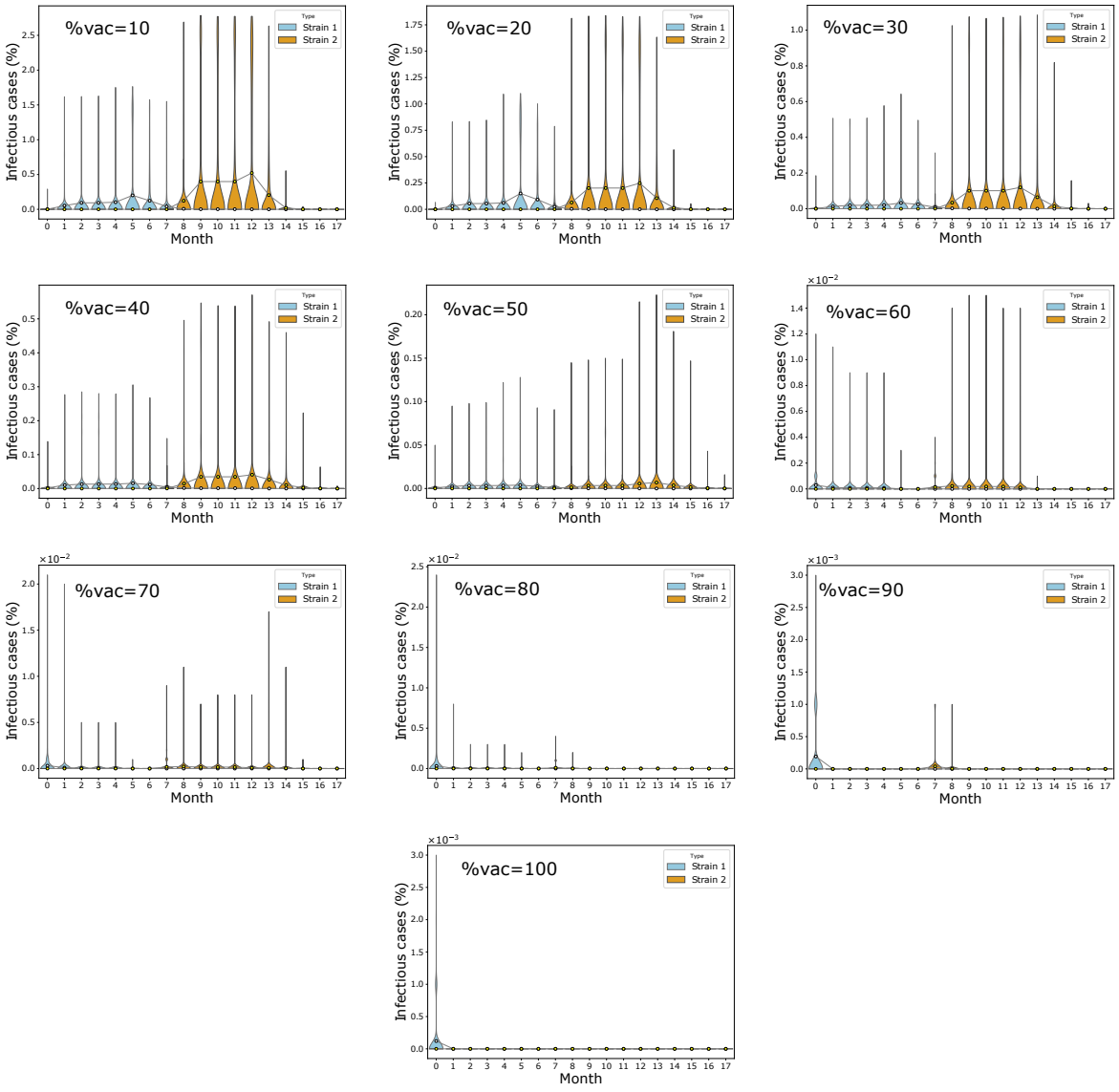

FIGURE B.8: BA network: Distribution of final infectious cases in different timing for mass vaccination scenario when $\eta = 100\%$. Population coverage varies from $10\% - 100\%$. Circles represent mean infection cases for each month connected by lines.

B.2 Model assuming vaccine resistance

The set of figures presented here represent the model in Section 5.6 where the vaccine efficacy levels and population coverage levels considered are the same as in the single strain model. As mentioned in the main text, vaccine efficacy varied between $40\% - 100\%$ whereas population coverage varied between $10\% - 100\%$. In all simulations, we consider that lockdown begins on day 50 and ends on day 140. For ER simulations: $N = 10^5$, $\beta_1 = 0.022$, $\beta_2 = 0.025$, $\tau =$ day 220 and $T = 539$ days. For BA simulations: $N = 10^5$, $\beta_1 = 0.014$, $\beta_2 = 0.017$, $\tau =$ day 220 and $T = 539$ days. Each scenario is repeated 100 times and the outputs are taken for analysis.

B.2.1 Erdos-Renyi network

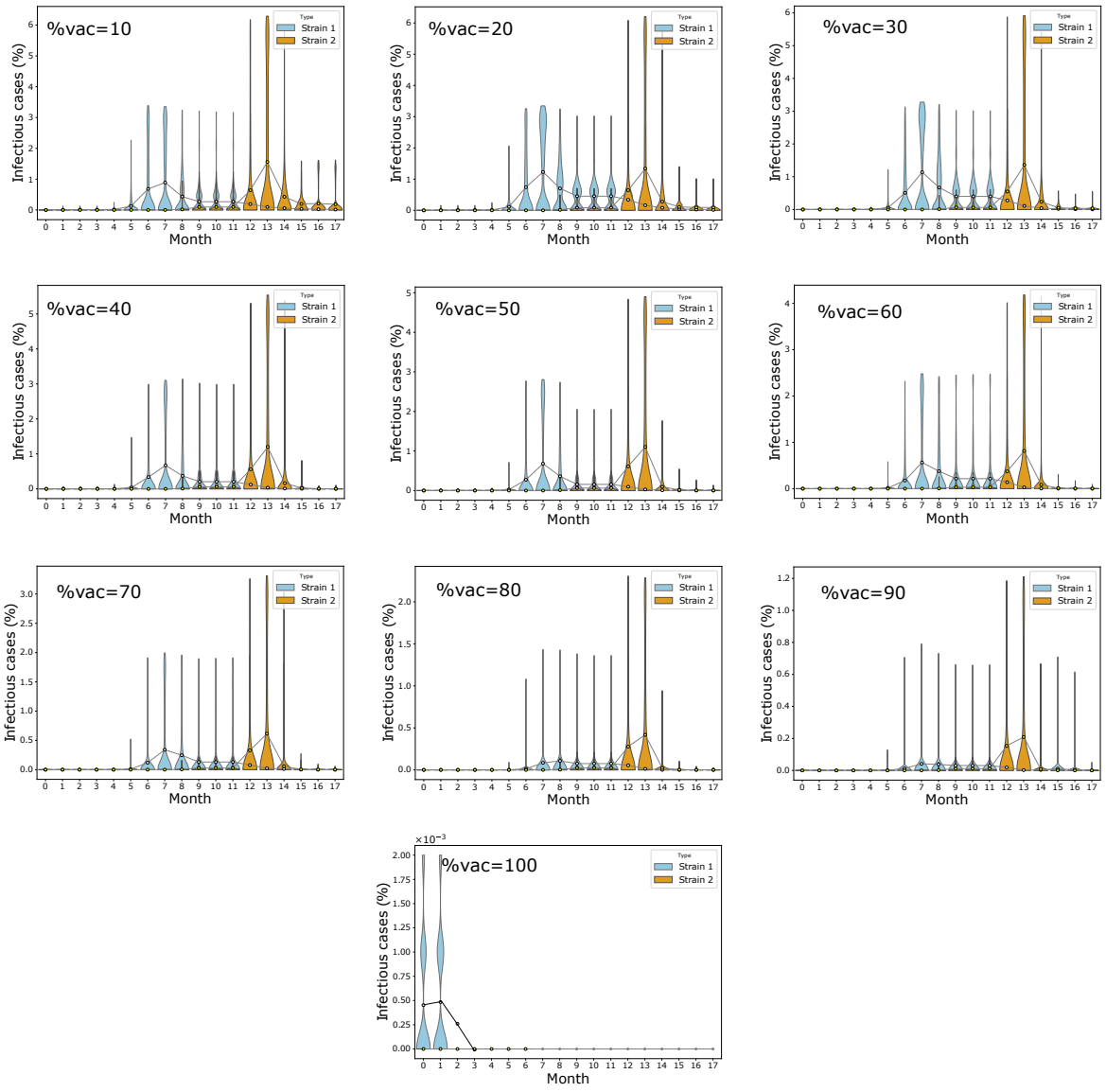

FIGURE B.9: Erdos-Renyi vaccine resistance model: Distribution of final infectious cases in different timing for mass vaccination scenario when $\eta = 40\%$. Population coverage varies from $10\% - 100\%$. Circles represent mean infection cases for each month connected by lines.

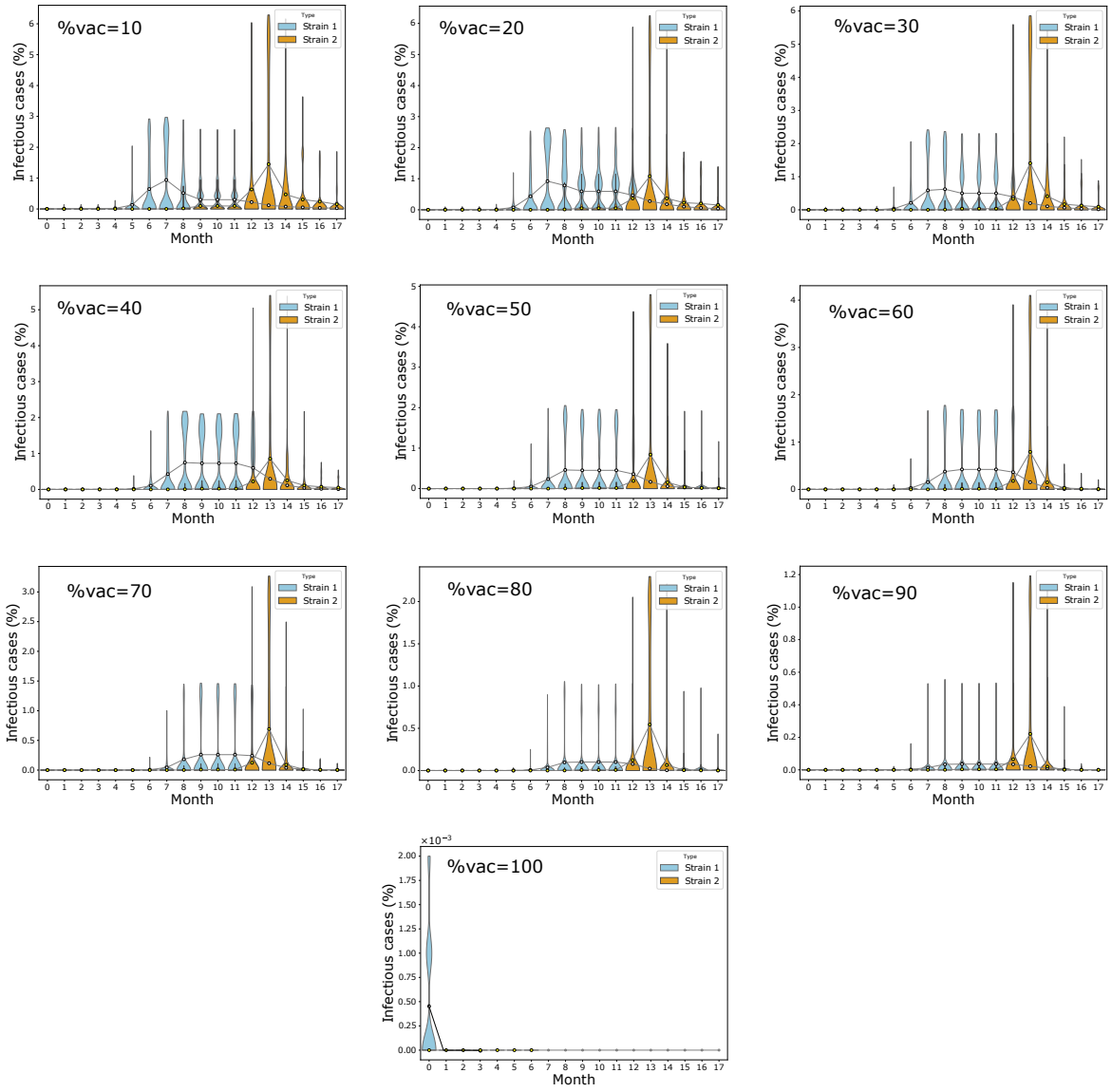

FIGURE B.10: Erdos-Renyi vaccine resistance model: Distribution of final infectious cases in different timing for mass vaccination scenario when $\eta = 60\%$. Population coverage varies from $10\% - 100\%$. Circles represent mean infection cases for each month connected by lines.

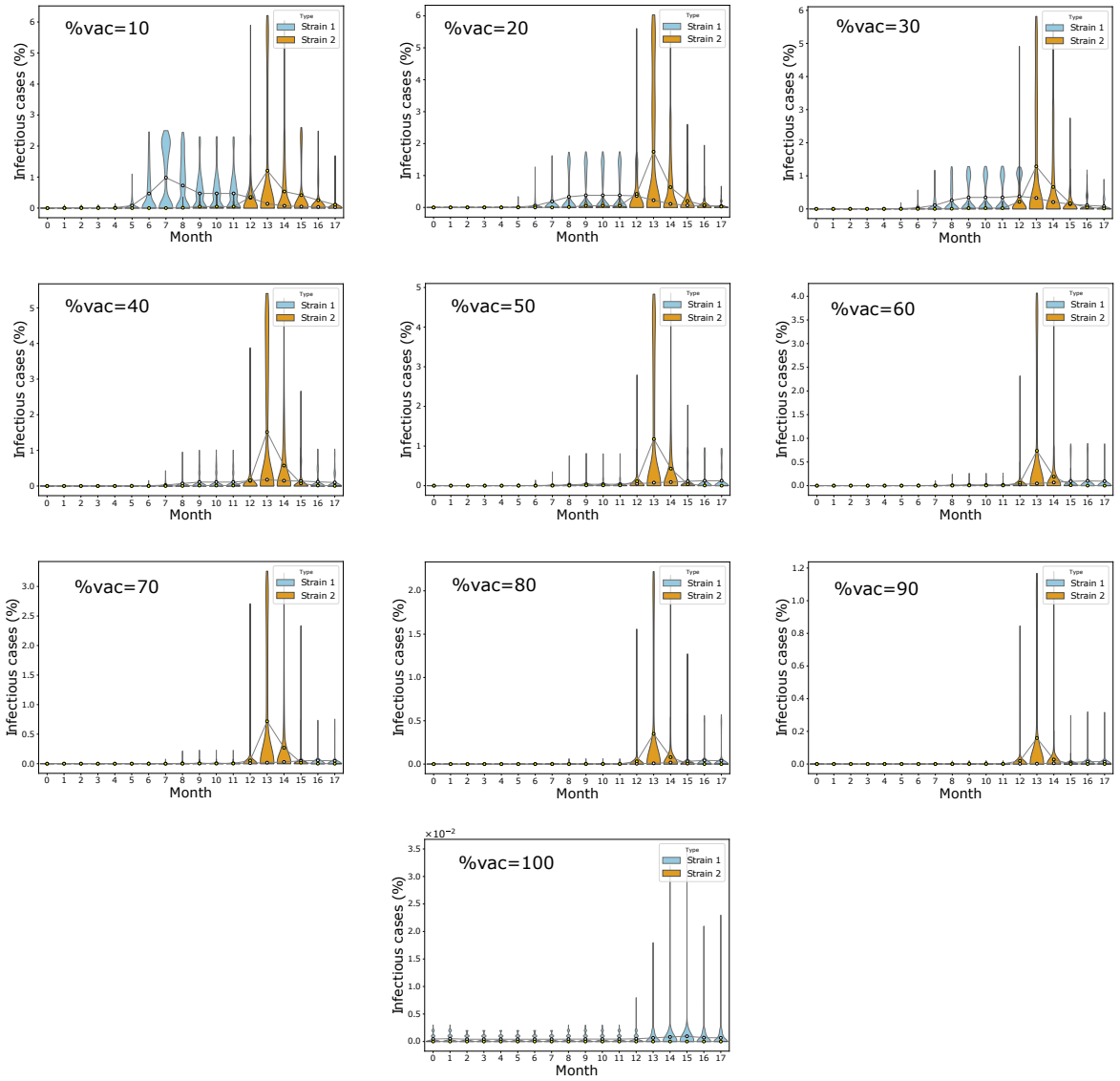

FIGURE B.11: Erdos-Renyi vaccine resistance model: Distribution of final infectious cases in different timing for mass vaccination scenario when $\eta = 80\%$. Population coverage varies from $10\% - 100\%$. Circles represent mean infection cases for each month connected by lines.

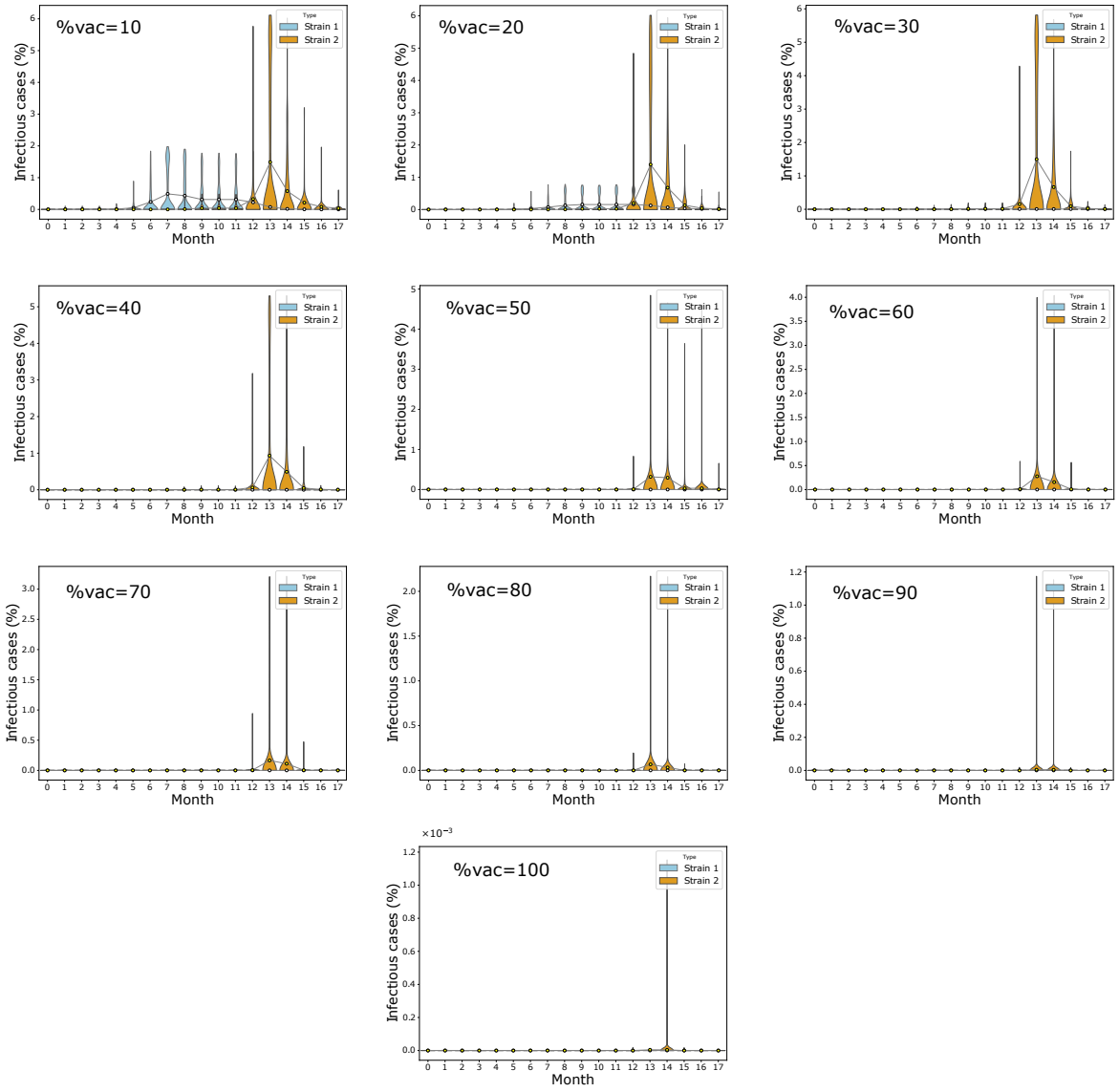

FIGURE B.12: Erdos-Renyi vaccine resistance model: Distribution of final infectious cases in different timing for mass vaccination scenario when $\eta = 100\%$. Population coverage varies from $10\% - 100\%$. Circles represent mean infection cases for each month connected by lines.

Deutsche Zusammenfassung

Aufgrund des Mangels an geeigneter epidemiologischer Daten liefern mathematische Modelle durch Simulation einen gewissen Anhaltspunkt für die Wirksamkeit von Krankheitsbekaempfungsinterventionen. Kenntnisse über die Übertragungseigenschaften von Infektionen können in mathematische Modelle einbezogen werden, um bessere Rückschlüsse auf Infektionen zu ziehen. In dieser Arbeit haben wir mathematische Modellierungstechniken eingesetzt, um das Problem der Arzneimittelresistenz auf zwei Ebenen zu untersuchen: zwischen den Wirten und innerhalb der Wirte. Wir haben die Bedeutung mathematischer Modelle als kosteneffizienten Ansatz zum Verständnis der Dynamik des Infektionsverlaufs sowie der Kontrolle und der Interventionen auf beiden Ebenen beschrieben. Die Untersuchung biologischer Probleme dieser Art mit mathematischen Ansätzen ist ein nützliches Vorhersageinstrument, um einige ungewisse Szenarien während eines Krankheitsausbruchs zu erforschen und, was am wichtigsten ist, die plausiblen Auswirkungen von Kontrollmaßnahmen und Interventionen vorherzusagen.

In Kapitel 2, haben wir eine allgemeine Einführung in die Entwicklung der Arzneimittelresistenz sowohl innerhalb des Wirts als auch in einer bestimmten Population gegeben. Wir haben die biologischen Grundlagen des Problems der arzneimittelresistenten Infektionen, die in der vorhandenen Literatur zu finden sind, eingehend beschrieben. Wir haben auch verschiedene mathematische Ansätze erforscht, die bei der Untersuchung resistenter Infektionen verwendet wurden, zum Beispiel deterministische, stochastische und statistische Methoden. Diese Modelle beschränken sich häufig auf die Dynamik der Resistenzausbreitung, vernachlässigen aber die Resistenzevolution und sind häufig deterministischer Natur. Sie stellen hypothetische Situationen für die Ausbreitung von Infektionen mit Arzneimittelresistenzen in Krankenhäusern und in der Bevölkerung dar und zeigen auch einige häufig verwendete Behandlungsstrategien auf.

Eine gängige Praxis für Modellierer ist die Verwendung deterministischer Modelle, da die Simulation solcher Modelle oft einfacher ist als die stochastischer Modelle. Stochastische Modelle eignen sich gut zur Erfassung komplexer heterogener Prozesse in einem biolo-gischen System. Sie können dazu verwendet werden, bestimmte Komplexitäten der Widerstandsfähigkeit

aufzudecken, was deterministische Modelle nicht können. Mit solchen Modellen lassen sich komplexe Wechselwirkungen erforschen, die sich auf die Resistenz auswirken können, wie z.B. die Dosierungswirkung und die Immunantwort.

Diese Ansätze sind zwar alle ein guter Schritt in Richtung eines besseren Verständnisses resistenter Infektionen, doch die Bekämpfung der Resistenz hängt vom Verständnis der Mechanismen ab, die zur Entstehung der Resistenz führen. Daher ist es wichtig, dass Modelle, die sich mit diesem Problem befassen, spezifische evolutionäre Mechanismen der Resistenz wie Mutationen und Interaktionen zwischen resistenten Genen einbeziehen. Dies wird zum Verständnis der Interaktion zwischen genetischen Stämmen von Krankheitserregern beitragen und helfen, geeignete Maßnahmen zu entwickeln.

Zu diesem Zweck haben wir in Kapitel 3 mathematische Modellierungstechniken eingesetzt, um die Entwicklung und Ausbreitung resistenter Infektionen im Wirt zu untersuchen und einige Behandlungsstrategien zur Bekämpfung der Resistenz zu analysieren. Wir haben logistisch basierte mathematische Modelle vorgestellt, um die Dynamik verschiedener Erregerstämme während der Arzneimitteltherapie zu beschreiben und auch den Prozess der Zellmutation zu erfassen, der zur Resistenz im Wirt führt.

Die Dynamik der Antibiotikaresistenz lässt sich mit dem folgenden, von [214] vorgeschlagenen allgemeinen, geschalteten logistischen System beschreiben. Dieses Modell beschreibt die Interaktion zwischen genetischen Bakterienstämmen und hilft dabei, geeignete Maßnahmen festzulegen. Die Modellgleichung lautet

$$\dot{x}_i(t) = \rho_{i,\sigma(t)} x_i(t) \left(1 - \frac{x_i(t)}{K}\right) - \delta_{\sigma(t)} x_i(t) + \mu \sum_{j=1}^{n} m_{ij,\sigma(t)} x_j(t)$$

und ist definiert für alle $t \geq 0$ und wobei $x_i : i = 1, 2, 3, ..., n$ mit n verschiedene Bakterienstämme repräsentieren. Jeder Zustand x_i bezeichnet einen Bakterienstamm, der ent-weder empfindlich oder resistent gegen ein bestimmtes verwendetes Medikament ist. μ ist die Mutationsrate. $\delta_{\sigma(t)}$ ist die bakterielle Clearance in Abhängigkeit von dem verwendeten Medikament. $\rho_{i,\sigma(t)}$ ist die Proliferationsrate des Stammes i unter der Therapie σ zu einem beliebigen Zeitpunkt t. $m_{ij,\sigma(t)}$ ist die Mutation von Stamm i zu Stamm j unter Therapie σ zu jedem Zeitpunkt t. K definiert die maximale Belastbarkeit und $\sigma(t)$ bezeichnet das Umschaltsignal (siehe 2.2.2.1) auf der Grundlage der Behandlungspolitik, so dass $\sigma(t)$ Werte in $\{\sigma_1, \sigma_2, \ldots, \sigma_N\}$ annimmt, wobei N die Anzahl der Medikamente darstellt. Alle Parameter und Anfangsbedingungen werden als nicht-negativ angenommen, so dass $x_i(0) \geq 0$ für $i \in \{1, 2, \ldots, n\}$.

Ohne Beschraenkung der Allgemeingültigkeit kann das Modell durch die folgende Änderung der Variablen in Gleichung (4.2) vereinfacht werden:

$$\rho_{i,\sigma(t)} \to \rho_i, \delta_{\sigma(t)} \to \delta \text{ und } m_{ij,\sigma(t)} \to m_{ij}.$$

Somit mit $K = 1$ laesst sich die Gleichung (4.2) umschreiben als

$$\dot{x}_i(t) = x_i(t)\,(\rho_i - \delta) - \rho_i x_i(t)^2 + \mu \sum_{j=1}^{n} m_{ij} x_j(t), \quad 1 \leq i \leq n.$$

Die Region von biologischen Interesse ist gegeben als die Menge

$$\Omega_2 = \{(x_1, x_2, \ldots, x_n) \in \mathbb{R}^n \mid x_i \geq 0, i = 1, 2, \ldots, n\}\,.$$

Bei der medikamentösen Therapie zur Beseitigung von Resistenzen ist die Behandlungsplanung nach wie vor ein wichtiges Forschungsgebiet, da es keinen Konsens über die besten Behandlungsprotokolle gibt.

Angeregt durch Studien, die gezeigt haben, dass die sequenzielle Verabreichung von Medikamenten langfristig besser geeignet ist, resistente Stämme auszurotten, haben wir Begriffe aus der Steuerungstechnik und aus positiv geschalteten Systemen verwendet, um Stra-tegien für die zyklische Verabreichung von Medikamenten mit dem Ziel zu entwickeln, die Medikamentenresistenz im Wirt auszurotten. Insbesondere analysierten wir die zeitliche Planung und den sequenziellen Einsatz von Arzneimitteln für die Behandlung innerhalb eines Wirts unter Anwendung des Prinzips der kollateralen Empfindlichkeit bei Bakterien und verglichen verschiedene Therapiewechselansätze, um ihre Leistung bei der langfristigen Ausrottung von Resistenzen im Wirt zu bestimmen. Wir verglichen die Umschaltung bei zwei verschiedenen Arten von Arzneimittelumschaltungen: periodische Umschaltung und Lyapunov-Umschaltung und untersuchten diese Systeme sowohl bei Vorhandensein als auch bei Abwesenheit einer Mutation. Wenn Mutation als vorhanden betrachtet wird, wird asymptotische Stabilität des Ursprungs erreicht, wenn das Schaltsystem eine gemeinsame Lyapunov-Funktion hat.

Um die Verarmung der resistenten Stämme zu gewährleisten ist der Gleichgewichtspunkt von Interesse das infektionsfreie Gleichgewicht am Ursprung. Die lineare Stabilität dieses Punktes haben wir bereits in Theorem 4.4.1.1 nachgewiesen. Als Nächstes wird die Stabilität des Ursprungs mit Hilfe der Lyapunov-Theorie über die Stabilität dynamischer Systeme (siehe Theorem 2.3) weiter analysiert. Dazu definieren wir den Anziehungsbereich Ω_{2D} als $\Omega_{2D} = \Omega_2 \setminus \mathbb{S}$, wobei $\mathbb{S} = \{(x_1, \ldots, x_n) \in E | x_i > 0 \text{ for all } i = 1, \ldots, n\}$.

Theorem 4.17 In Abwesenheit von Mutationen (d.h. wenn $\mu = 0$), lässt das System (4.17) zu, dass der Ursprung global asymptotisch stabil ist, wenn $\rho_i < \delta$ für alle $i \in \{1, \ldots, n\}$.

Ausgehend von einem einfachen Zweistamm-System mit zwei Therapien untersuchten wir in kleinem Maßstab geeignete Protokolle für die Medikamentenplanung. Anhand numerischer Simulationen konnten wir zeigen, dass jede Umschaltstrategie die Ausrottung der Resistenz gewährleistet, wenn beide Teilsysteme am Ursprung asymptotisch stabil sind. Wenn jedoch nur ein Teilsystem instabil ist, garantiert das periodische Schalten nicht, dass die Resistenz verschwindet, aber das Lyapunov-basierte Schalten tut es und ist sogar viel schneller. Wenn alle Teilsysteme am Ursprung instabil sind, gewährleistet nur eine lyapunov-basierte Umschaltung die Auslöschung. In diesem Fall kann die Rückkopplungsschaltung verwendet werden, um die Gleitfläche zu erreichen, und die Steuerung kann mit einem Gleitgesetz vervollständigt werden, das auf periodischer Schaltung basiert.

Anschließend haben wir dieses Modell auf ein allgemeineres System mit mehr als zwei Stämmen und vielen Therapien ausgedehnt. Auch für das allgemeine Modell erhielten wir ähnliche Ergebnisse.

Proposition 4.18 Das System (4.2) hat den Ursprung als stabiles Gleichgewicht, wenn es für jedes $x \in \Omega_{2D}$ mindestens eine Therapie $\sigma_x \in \{\sigma_1, \cdots, \sigma_N\}$, für die $\dot{V}(x, \sigma_x) < 0$, wobei $\dot{V}$ die Ableitung der Lyapunov-Funktion in eq (4.26) ist.

Unsere numerischen Simulationen zeigten, dass Umschaltstrategien auf der Grundlage von Lyapunov-Funktionen eine bessere Leistung aufweisen. Die in diesem Kapitel betrachteten Fälle lieferten schnellere und rechnerisch praktikable Ergebnisse und waren unter bestimmten Bedingungen in der Lage, die pathogenen Populationen auszurotten. Die Simulationsergebnisse machen deutlich, dass die Protokolle für den Medikamentenzyklus nicht intuitiv sind und daher die Erregerdynamik unter verschiedenen Behandlungen für die Ausrottung der Infektion von zentraler Bedeutung ist. Trotz dieser guten Leistung wird es interessant sein, auch Ansätze der Model Predictive Control (MPC) zu prüfen, da sich MPC insbesondere in der Kontrolltheorie als gut für nichtlineare Modelle erwiesen hat.

In Kapitel 4 war es unser übergeordnetes Ziel, mathematische und rechnerische Ansätze zu verwenden, um antimikrobielle Infektionen zwischen Wirten zu beschreiben. Wir verwendeten das neuartige Coronavirus als Fallstudie und modellierten seine Übertragungsdynamik in einem sozialen Netzwerk inmitten von Impfkampagnen und anderen nicht-pharmazeutischen Interventionen. Wir beschrieben die allgemeine Dynamik der Krankheit und untersuchten die Auswirkungen von Impfprotokollen auf die Ausbreitung dieses Virus. Mit hilfe numerischer Simulationen haben wir auch die potenziellen qualitativen Auswirkungen untersucht, die eine neue und besser übertragbare mutierte, impfstoffresistente Variante auf die Bevölkerung haben könnte.

Unsere Ergebnisse für das Modell mit einem einzigen Stamm zeigen, dass unabhängig vom Impfprotokoll und vom Netzwerkmodell die Zahl der Infektionsfälle immer dann zurückging, wenn geimpft wurde. Darüber hinaus hing die Zahl der Personen, die geimpft werden mussten, um niedrige Infektionswerte und Spitzenwerte zu erreichen, stark von der Wirksamkeit des Impfstoffs ab. Bei einem Impfstoff mit geringer Wirksamkeit müssten beispielsweise mehr Menschen geimpft werden, um Infektionsspitzen zu vermeiden.

Wird jedoch eine impfstoffresistentere Variante zusammen mit dem Wildtypvirus in den Verkehr gebracht, so werden mit dem impfstoffresistenten Stamm mehr Personen infiziert als mit dem Wildtyp und zwar bei allen Impfstoffwirkungsgraden außer bei 100%. Bei einem wirksamen 100%-Impfstoff hingegen kommt es nur zu einer geringen oder gar keiner Infektion, wenn mehr als 30% der Bevölkerung geimpft sind. Darüber hinaus haben wir festgestellt, dass in der geimpften Bevölkerung weniger Menschen mit dem Wildtyp-Stamm infiziert sind als mit dem mutierten Stamm. Diese Beobachtung ist auf die erhöhte Übertragbarkeit und die geringere Wirksamkeit des Impfstoffs gegenüber dem mutierten Stamm zurückzuführen.

Bei der Untersuchung der Auswirkungen der SARS-CoV-2-Übertragung auf soziale Netzwerke haben wir unsere Analyse auf zwei Arten von sozialen Netzwerken beschränkt, nämlich das Erdos-Renyi-Netzwerk und das Barabasi-Albert-Netzwerkmodell. Im Hinblick auf eine größere Praxisnähe kann die in dieser Arbeit durchgeführte Analyse erweitert werden, um die Krankheitsausbreitung und Impfung in anderen sozialen Netzwerken und Small-World-Netzwerkmodellen wie dem Watts-Strogatz-Netzwerk unter Verwendung ähnlicher Szena-rien und Protokolle zu untersuchen. Solche Netzwerkmodelle können miteinander verglichen und die Ergebnisse analysiert werden. Daten über bekannte soziale Netzwerke wie Kontaktmatrizen und Mischungsmuster können ebenfalls für weitere Analysen und Bewertungen herangezogen werden.

In unseren numerischen Simulationen sind wir von einem optimistischen Zustand ausgegangen, in dem alle infektiösen Personen identifiziert werden. In der Realität ist die Rückverfolgung von Kontakten im Verlauf einer laufenden Epidemie besonders schwierig. Im speziellen Fall von SARS-CoV-2 haben sich sowohl herkömmliche, auf Befragungen basierende Ansätze als auch neuere digitale Anwendungen zur Kontaktverfolgung als weniger effektiv erwiesen. Die Identifizierung aller infektiösen Kontakte und ihrer Sekundärkontakte (insbesondere für die Ringimpfungsstrategie) ist daher schwierig und mit höheren Kosten verbunden. In der Tat können diese Herausforderungen die Wirkung der Impfbemühungen potenziell verringern. Außerdem geht das hier verwendete Modell von einer gleichmäßigen Durchmischung der Individuen und ihrer Nachbarn im Netzwerk aus, während dies in der Realität nicht der Fall ist. Folglich könnte dies zu einer geringeren Zahl von Infektionsfällen und einer geringeren Durchimpfung der Bevölkerung führen.

Bibliography

[1] Anthony Vere Hodge and Hugh J Field. General mechanisms of antiviral resistance. In *Genetics and Evolution of Infectious Disease*, pages 339–362. Elsevier, 2011. [Cited on pages viii, 2, 30, and 32.]

[2] World Health Organisation. Draft landscape of covid-19 candidate vaccines, 2020. Accessed: 2020-12-10. [Cited on pages viii, 39, and 40.]

[3] BioSpace. Comparing covid-19 vaccines: Timelines, types and prices, 2021. Accessed: 2021-22-06. [Cited on pages viii, 32, and 40.]

[4] Nick Andrews, Julia Stowe, Freja Kirsebom, Samuel Toffa, Tim Rickeard, Eileen Gallagher, Charlotte Gower, Meaghan Kall, Natalie Groves, Anne-Marie O'Connell, et al. Covid-19 vaccine effectiveness against the omicron (b. 1.1. 529) variant. *New England Journal of Medicine*, 2022. [Cited on pages viii, 105, and 106.]

[5] Fred Brauer, Carlos Castillo-Chavez, and Carlos Castillo-Chavez. *Mathematical models in population biology and epidemiology*, volume 2. Springer, 2012. [Cited on page 1.]

[6] Edwin O Jordan et al. Epidemic influenza. a survey. *Epidemic Influenza. A Survey.*, 1927. [Cited on page 1.]

[7] Coronavirus disease (covid-19) pandemic, . Accessed: 2019-03-05. [Cited on page 1.]

[8] Stuart B Levy and Bonnie Marshall. Antibacterial resistance worldwide: causes, challenges and responses. *Nature medicine*, 10(12s):S122, 2004. [Cited on pages 1, 12, and 14.]

[9] Anne Mai-Prochnow, Maryse Clauson, Jungmi Hong, and Anthony B Murphy. Gram positive and gram negative bacteria differ in their sensitivity to cold plasma. *Scientific reports*, 6:38610, 2016. [Cited on pages 1 and 13.]

[10] DAC Heesterbeek, NI Martin, A Velthuizen, M Duijst, M Ruyken, R Wubbolts, SHM Rooijakkers, and BW Bardoel. Complement-dependent outer membrane perturbation sensitizes gram-negative bacteria to gram-positive specific antibiotics. *Scientific reports*, 9(1):3074, 2019. [Cited on pages 1, 2, 13, and 14.]

[11] Mya Breitbart and Forest Rohwer. Here a virus, there a virus, everywhere the same virus? *Trends in microbiology*, 13(6):278–284, 2005. [Cited on pages 1 and 30.]

[12] Eugene V Koonin, Tatiana G Senkevich, and Valerian V Dolja. The ancient virus world and evolution of cells. *Biology direct*, 1(1):1–27, 2006. [Cited on pages 1 and 30.]

[13] Andrew F Read, Troy Day, and Silvie Huijben. The evolution of drug resistance and the curious orthodoxy of aggressive chemotherapy. *Proceedings of the National Academy of Sciences*, 108(Supplement 2):10871–10877, 2011. [Cited on pages 2 and 22.]

[14] Pleuni S Pennings. Hiv drug resistance: problems and perspectives. *Infectious disease reports*, 5(11):21–25, 2013. [Cited on page 2.]

[15] Mazhar Hussain, Henry D Galvin, Tatt Y Haw, Ashley N Nutsford, and Matloob Husain. Drug resistance in influenza a virus: the epidemiology and management. *Infection and drug resistance*, 10:121, 2017. [Cited on page 2.]

[16] Natalia L Komarova and Dominik Wodarz. Drug resistance in cancer: principles of emergence and prevention. *Proceedings of the National Academy of Sciences*, 102(27): 9714–9719, 2005. [Cited on pages 2, 35, 43, 45, and 59.]

[17] Erica C Pehrsson, Pablo Tsukayama, Sanket Patel, Melissa Mejía-Bautista, Giordano Sosa-Soto, Karla M Navarrete, Maritza Calderon, Lilia Cabrera, William Hoyos-Arango, M Teresita Bertoli, et al. Interconnected microbiomes and resistomes in low-income human habitats. *Nature*, 533(7602):212, 2016. [Cited on page 2.]

[18] Ramanan Laxminarayan, Adriano Duse, Chand Wattal, Anita KM Zaidi, Heiman FL Wertheim, Nithima Sumpradit, Erika Vlieghe, Gabriel Levy Hara, Ian M Gould, Herman Goossens, et al. Antibiotic resistance-the need for global solutions. *The Lancet infectious diseases*, 13(12):1057–1098, 2013. [Cited on page 2.]

[19] World Health Organization. Risk management and healthcare policy. 2014. [Cited on page 2.]

[20] Alison H Holmes, Luke SP Moore, Arnfinn Sundsfjord, Martin Steinbakk, Sadie Regmi, Abhilasha Karkey, Philippe J Guerin, and Laura JV Piddock. Understanding the mechanisms and drivers of antimicrobial resistance. *The Lancet*, 387(10014):176–187, 2016. [Cited on pages 2 and 15.]

[21] World Health Organization. Global tuberculosis report 2016. 2016. [Cited on page 2.]

[22] Hana M Dobrovolny and Catherine AA Beauchemin. Modelling the emergence of influenza drug resistance: The roles of surface proteins, the immune response and antiviral mechanisms. *PLoS One*, 12(7):e0180582, 2017. [Cited on pages 2, 34, and 35.]

[23] Margaret Okomo-Adhiambo, Ha T Nguyen, Katrina Sleeman, Tiffany G Sheu, Varough M Deyde, Rebecca J Garten, Xiyan Xu, Michael W Shaw, Alexander I Klimov, and Larisa V Gubareva. Host cell selection of influenza neuraminidase variants: implications for drug resistance monitoring in a (h1n1) viruses. *Antiviral research*, 85(2): 381–388, 2010. [Cited on page 2.]

[24] Markus A Rose, Oliver Damm, Wolfgang Greiner, Markus Knuf, Peter Wutzler, Johannes G Liese, Hagen Krüger, Ulrich Wahn, Tom Schaberg, Markus Schwehm, et al. The epidemiological impact of childhood influenza vaccination using live-attenuated influenza vaccine (laiv) in germany: predictions of a simulation study. *BMC infectious diseases*, 14(1):1–13, 2014. [Cited on page 2.]

[25] Neil M Ferguson, Derek AT Cummings, Simon Cauchemez, Christophe Fraser, Steven Riley, Aronrag Meeyai, Sopon Iamsirithaworn, and Donald S Burke. Strategies for containing an emerging influenza pandemic in southeast asia. *Nature*, 437(7056):209–214, 2005. [Cited on page 3.]

[26] Frank Tanser, Till Bärnighausen, Erofili Grapsa, Jaffer Zaidi, and Marie-Louise Newell. High coverage of art associated with decline in risk of hiv acquisition in rural kwazulu-natal, south africa. *Science*, 339(6122):966–971, 2013. [Cited on page 3.]

[27] Esteban A Hernandez-Vargas, Alma Y Alanis, and Josephine Tetteh. A new view of multiscale stochastic impulsive systems for modeling and control of epidemics. *Annual Reviews in Control*, 2019. [Cited on pages 3 and 78.]

[28] Lejla Imamovic and Morten OA Sommer. Use of collateral sensitivity networks to design drug cycling protocols that avoid resistance development. *Science translational medicine*, 5(204):204ra132–204ra132, 2013. [Cited on page 3.]

[29] Viktória Lázár, István Nagy, Réka Spohn, Bálint Csörgő, Ádám Györkei, Ákos Nyerges, Balázs Horváth, Andrea Vörös, Róbert Busa-Fekete, Mónika Hrtyan, et al. Genome-wide analysis captures the determinants of the antibiotic cross-resistance interaction network. *Nature communications*, 5:4352, 2014. [Cited on pages 3 and 44.]

[30] Csaba Pál, Balázs Papp, and Viktória Lázár. Collateral sensitivity of antibiotic-resistant microbes. *Trends in microbiology*, 23(7):401–407, 2015. [Cited on pages 3, 44, 47, and 74.]

[31] Lejla Imamovic, Mostafa Mostafa Hashim Ellabaan, Ana Manuel Dantas Machado, Linda Citterio, Tune Wulff, Soren Molin, Helle Krogh Johansen, and Morten Otto Alexander Sommer. Drug-driven phenotypic convergence supports rational treatment strategies of chronic infections. *Cell*, 172(1-2):121–134, 2018. [Cited on pages 3, 14, 44, 45, 59, 60, 66, 67, 74, and 75.]

[32] Hassan K Khalil. Nonlinear systems. *Upper Saddle River*, 2002. [Cited on page 6.]

[33] Franco Blanchini. Set invariance in control. *Automatica*, 35(11):1747–1767, 1999. [Cited on pages 7 and 52.]

[34] Daniel Liberzon. *Switching in systems and control*. Springer Science & Business Media, 2003. [Cited on pages 8 and 45.]

[35] Sirijan Santajit and Nitaya Indrawattana. Mechanisms of antimicrobial resistance in eskape pathogens. *BioMed research international*, 2016, 2016. [Cited on pages 12 and 14.]

[36] Parjit Kaur and Elizabeth Peterson. Antibiotic resistance mechanisms in bacteria: Relationships between resistance determinants of antibiotic producers, environmental bacteria, and clinical pathogens. *Frontiers in Microbiology*, 9:2928, 2018. [Cited on page 12.]

[37] M May. Drug development: time for teamwork. nature 509, 2014. [Cited on page 12.]

[38] SJ Projan and DM Shlaes. Antibacterial drug discovery: is it all downhill from here? *Clinical Microbiology and Infection*, 10:18–22, 2004. [Cited on page 12.]

[39] Suzanne Edwards, Chantal Morel, Reinhard Busse, and Stephan Harbarth. Combatting antibiotic resistance together: How can we enlist the help of industry? *Antibiotics*, 7 (4):111, 2018. [Cited on page 12.]

[40] Thomas U Berendonk, Célia M Manaia, Christophe Merlin, Despo Fatta-Kassinos, Eddie Cytryn, Fiona Walsh, Helmut Bürgmann, Henning Sørum, Madelaine Norström, Marie-Noelle Pons, et al. Tackling antibiotic resistance: the environmental framework. *Nature Reviews Microbiology*, 13(5):310, 2015. [Cited on page 12.]

[41] Global action plan on antimicrobial resistance, . Accessed: 2019-03-18. [Cited on page 12.]

[42] World Health Organization. Global framework for development & stewardship to combat antimicrobial resistance. 2017. [Cited on page 12.]

[43] Karen L Tang, Niamh P Caffrey, Diego B Nóbrega, Susan C Cork, Paul E Ronksley, Herman W Barkema, Alicia J Polachek, Heather Ganshorn, Nishan Sharma, James D Kellner, et al. Restricting the use of antibiotics in food-producing animals and its associations with antibiotic resistance in food-producing animals and human beings: a systematic review and meta-analysis. *The Lancet Planetary Health*, 1(8):e316–e327, 2017. [Cited on page 13.]

[44] Sam Millet and Luc Maertens. The european ban on antibiotic growth promoters in animal feed: from challenges to opportunities., 2011. [Cited on page 13.]

[45] Brad Spellberg, Gail R Hansen, Avinash Kar, Carmen D Cordova, Lance B Price, and James R Johnson. Antibiotic resistance in humans and animals. *NAM Perspectives*, 2016. [Cited on page 13.]

[46] Bonnie M Marshall and Stuart B Levy. Food animals and antimicrobials: impacts on human health. *Clinical microbiology reviews*, 24(4):718–733, 2011. [Cited on page 13.]

[47] Yue Ma, Estrella Frutos-Beltrán, Dongwei Kang, Christophe Pannecouque, Erik De Clercq, Luis Menéndez-Arias, Xinyong Liu, and Peng Zhan. Medicinal chemistry strategies for discovering antivirals effective against drug-resistant viruses. *Chemical Society Reviews*, 50(7):4514–4540, 2021. [Cited on page 13.]

[48] Laura Temime, Gilles Hejblum, Michel Setbon, and Alain-Jacques Valleron. The rising impact of mathematical modelling in epidemiology: antibiotic resistance research as a case study. *Epidemiology & Infection*, 136(3):289–298, 2008. [Cited on pages 13, 15, and 45.]

[49] Josephine NA Tetteh, Franziska Matthäus, and Esteban A Hernandez-Vargas. A survey of within-host and between-hosts modelling for antibiotic resistance. *Biosystems*, page 104182, 2020. [Cited on page 13.]

[50] Murray E Alexander, Christopher S Bowman, Zhilan Feng, Michael Gardam, Seyed M Moghadas, Gergely Röst, Jianhong Wu, and Ping Yan. Emergence of drug resistance: implications for antiviral control of pandemic influenza. *Proceedings of the Royal Society B: Biological Sciences*, 274(1619):1675–1684, 2007. [Cited on page 13.]

[51] Florence Débarre, Sebastian Bonhoeffer, and Roland R Regoes. The effect of population structure on the emergence of drug resistance during influenza pandemics. *Journal of the Royal Society Interface*, 4(16):893–906, 2007. [Cited on page 13.]

[52] Yanyu Xiao, Fred Brauer, and Seyed M Moghadas. Can treatment increase the epidemic size? *Journal of Mathematical Biology*, 72(1):343–361, 2016. [Cited on page 13.]

[53] Marguerite Robinson and Nikolaos I Stilianakis. A model for the emergence of drug resistance in the presence of asymptomatic infections. *Mathematical biosciences*, 243 (2):163–177, 2013. [Cited on page 13.]

[54] Anna Camilla Birkegård, Tariq Halasa, Nils Toft, Anders Folkesson, and Kaare Græsbøll. Send more data: a systematic review of mathematical models of antimicrobial resistance. *Antimicrobial Resistance & Infection Control*, 7(1):117, 2018. [Cited on page 13.]

[55] Heather K Allen, Justin Donato, Helena Huimi Wang, Karen A Cloud-Hansen, Julian Davies, and Jo Handelsman. Call of the wild: antibiotic resistance genes in natural environments. *Nature Reviews Microbiology*, 8(4):251, 2010. [Cited on page 13.]

[56] Joseph AH Romaniuk and Lynette Cegelski. Bacterial cell wall composition and the influence of antibiotics by cell-wall and whole-cell nmr. *Philosophical Transactions of the Royal Society B: Biological Sciences*, 370(1679):20150024, 2015. [Cited on page 13.]

[57] Julian Davies and Dorothy Davies. Origins and evolution of antibiotic resistance. *Microbiol. Mol. Biol. Rev.*, 74(3):417–433, 2010. [Cited on pages 13 and 14.]

[58] Karen Bush and George A Jacoby. Updated functional classification of β-lactamases. *Antimicrobial agents and chemotherapy*, 54(3):969–976, 2010. [Cited on page 14.]

[59] C Lee Ventola. The antibiotic resistance crisis: part 1: causes and threats. *Pharmacy and therapeutics*, 40(4):277, 2015. [Cited on page 14.]

[60] Gleice Cristina Leite, Maura Salaroli Oliveira, Lauro Vieira Perdigão-Neto, Cristiana Kamia Dias Rocha, Thais Guimarães, Camila Rizek, Anna Sara Levin, and Silvia Figueiredo Costa. Antimicrobial combinations against pan-resistant acinetobacter baumannii isolates with different resistance mechanisms. *PLoS One*, 11(3):e0151270, 2016. [Cited on page 14.]

[61] Edward Geisinger and Ralph R Isberg. Interplay between antibiotic resistance and virulence during disease promoted by multidrug-resistant bacteria. *The Journal of infectious diseases*, 215(suppl_1):S9–S17, 2017. [Cited on page 14.]

[62] Louis B Rice. Federal funding for the study of antimicrobial resistance in nosocomial pathogens: no eskape, 2008. [Cited on page 14.]

[63] Gabriel Cabot, Alain A Ocampo-Sosa, M Angeles Domínguez, Juan F Gago, Carlos Juan, Fe Tubau, Cristina Rodríguez, Bartolomé Moyà, Carmen Peña, Luis Martínez-Martínez, et al. Genetic markers of widespread extensively drug-resistant pseudomonas aeruginosa high-risk clones. *Antimicrobial agents and chemotherapy*, 56(12):6349–6357, 2012. [Cited on page 14.]

[64] Helen W Boucher, George H Talbot, Daniel K Benjamin Jr, John Bradley, Robert J Guidos, Ronald N Jones, Barbara E Murray, Robert A Bonomo, David Gilbert, and Infectious Diseases Society of America. 10×'20 progress-development of new drugs active against gram-negative bacilli: an update from the infectious diseases society of america. *Clinical infectious diseases*, 56(12):1685–1694, 2013. [Cited on page 14.]

[65] Kfir B Steinbuch and Micha Fridman. Mechanisms of resistance to membrane-disrupting antibiotics in gram-positive and gram-negative bacteria. *MedChemComm*, 7(1):86–102, 2016. [Cited on page 14.]

[66] José Luis Martínez and Fernando Baquero. Emergence and spread of antibiotic resistance: setting a parameter space. *Upsala journal of medical sciences*, 119(2):68–77, 2014. [Cited on page 14.]

[67] Julian Davies. Inactivation of antibiotics and the dissemination of resistance genes. *Science*, 264(5157):375–382, 1994. [Cited on page 14.]

[68] Jeffrey D Fuller and Donald E Low. A review of streptococcus pneumoniae infection treatment failures associated with fluoroquinolone resistance. *Clinical infectious diseases*, 41(1):118–121, 2005. [Cited on page 14.]

[69] Gill Erin E., Octavio L. Franco, and Robert E. W. Hancock. Antibiotic adjuvants: diverse strategies for controlling drug-resistant pathogens. *Chemical & biology drug design*, 85(1):56, 2015. [Cited on page 15.]

[70] Ashley A DeNegre, Martial L Ndeffo Mbah, Kellen Myers, and Nina H Fefferman. Emergence of antibiotic resistance in immunocompromised host populations: A case study of emerging antibiotic resistant tuberculosis in aids patients. *PloS one*, 14(2): e0212969, 2019. [Cited on page 15.]

[71] Sebastian Bonhoeffer, Marc Lipsitch, and Bruce R Levin. Evaluating treatment protocols to prevent antibiotic resistance. *Proceedings of the National Academy of Sciences*, 94(22):12106–12111, 1997. [Cited on pages 15, 16, 17, 19, 20, 21, and 29.]

[72] Lipsitch M. Blanquart F., Lehtinen S. and Fraser C. The evolution of antibiotic resistance in a structured host population. *Journal of The Royal Society Interface*, 15 (143):20180040, 2018. [Cited on pages 15, 23, and 42.]

[73] Roca I., Akova M., Baquero F., Carlet J., Cavaleri M., Coenen S., Cohen J., Findlay D., Gyssens I., Heure O.E., and Kahlmeter G. The global threat of antimicrobial resistance: science for intervention. *New microbes and new infections*, 6:22–29, 2015. [Cited on page 15.]

[74] Stone L.K. Baym M. and Kishony R. Multidrug evolutionary strategies to reverse antibiotic resistance. *Science*, page 6268, 2016. [Cited on page 15.]

[75] Portia M Mira, Kristina Crona, Devin Greene, Juan C Meza, Bernd Sturmfels, and Miriam Barlow. Rational design of antibiotic treatment plans: a treatment strategy for managing evolution and reversing resistance. *PloS one*, 10(5):e0122283, 2015. [Cited on page 15.]

[76] BR Levin, M Lipsitch, V Perrot, S Schrag, R Antia, Lone Simonsen, N Moore Walker, and FM Stewart. The population genetics of antibiotic resistance. *Clinical infectious diseases*, 24(Supplement_1):S9–S16, 1997. [Cited on pages 15 and 16.]

[77] Bruce R Levin and Daniel E Rozen. Non-inherited antibiotic resistance. *Nature Reviews Microbiology*, 4(7):556, 2006. [Cited on page 15.]

[78] Michael D LaFleur, Qingguo Qi, and Kim Lewis. Patients with long-term oral carriage harbor high-persister mutants of candida albicans. *Antimicrobial agents and chemotherapy*, 54(1):39–44, 2010. [Cited on page 15.]

[79] Kristine Stepanyan, Tom Wenseleers, Edgar A Duéñez-Guzmán, Frédéric Muratori, Bram Van den Bergh, Natalie Verstraeten, Luc De Meester, Kevin J Verstrepen, Maarten Fauvart, and Jan Michiels. Fitness trade-offs explain low levels of persister cells in the opportunistic pathogen pseudomonas aeruginosa. *Molecular ecology*, 24 (7):1572–1583, 2015. [Cited on page 15.]

[80] Timothy C Reluga. Simple models of antibiotic cycling. *Mathematical medicine and biology: a journal of the IMA*, 22(2):187–208, 2005. [Cited on pages 15 and 16.]

[81] Carl T Bergstrom, Monique Lo, and Marc Lipsitch. Ecological theory suggests that antimicrobial cycling will not reduce antimicrobial resistance in hospitals. *Proceedings of the National Academy of Sciences*, 101(36):13285–13290, 2004. [Cited on pages 15, 16, 19, 20, 21, and 29.]

[82] Marc Lipsitch, Carl T Bergstrom, and Bruce R Levin. The epidemiology of antibiotic resistance in hospitals: paradoxes and prescriptions. *Proceedings of the National Academy of Sciences*, 97(4):1938–1943, 2000. [Cited on pages 16, 18, and 19.]

[83] Michael Haber, Bruce R Levin, and Piotr Kramarz. Antibiotic control of antibiotic resistance in hospitals: a simulation study. *BMC infectious diseases*, 10(1):254, 2010. [Cited on page 16.]

[84] DJ Austin and RM Anderson. Transmission dynamics of epidemic methicillin-resistant staphylococcus aureus and vancomycin-resistant enterococci in england and wales. *The Journal of infectious diseases*, 179(4):883–891, 1999. [Cited on page 16.]

[85] Hong-Rui Sun, Xinxin Lu, and Shigui Ruan. Qualitative analysis of models with different treatment protocols to prevent antibiotic resistance. *Mathematical biosciences*, 227(1):56–67, 2010. [Cited on pages 16, 17, and 18.]

[86] Xia Wang, Shengqiang Liu, and Hongjian Guo. A nosocomial-pathogens-infections model with impulsive antibiotics treatment on multiple bacteria. *Applied Mathematics and Computation*, 296:64–87, 2017. [Cited on page 16.]

[87] ML Joyner, CC Manning, and BN Canter. Modeling the effects of introducing a new antibiotic in a hospital setting: A case study. *Mathematical biosciences and engineering: MBE*, 9(3):601, 2012. [Cited on page 16.]

[88] Michele L Joyner. Modeling the differences in the development of a new antibiotic class versus the development of a next generation antibiotic on the total resistance in a hospital setting. *Journal of Biological Systems*, 20(01):109–132, 2012. [Cited on page 16.]

[89] Karen Chow, Xiaohong Wang, R Curtiss III, and Carlos Castillo-Chavez. Evaluating the efficacy of antimicrobial cycling programmes and patient isolation on dual resistance in hospitals. *Journal of biological dynamics*, 5(1):27–43, 2011. [Cited on page 16.]

[90] Xiuli Cen, Zhilan Feng, Yiqiang Zheng, and Yulin Zhao. Bifurcation analysis and global dynamics of a mathematical model of antibiotic resistance in hospitals. *Journal of mathematical biology*, 75(6-7):1463–1485, 2017. [Cited on page 16.]

[91] Marc Lipsitch and Carl T Bergstrom. Modeling of antibiotic resistance in the icu - us slant. Kluwer, 2002. [Cited on pages 16, 17, 18, and 19.]

[92] Robert Eric Beardmore, Rafael Peña-Miller, Fabio Gori, and Jonathan Iredell. Antibiotic cycling and antibiotic mixing: which one best mitigates antibiotic resistance? *Molecular biology and evolution*, 34(4):802–817, 2017. [Cited on pages 20 and 21.]

[93] Hildegard Uecker and Sebastian Bonhoeffer. Modeling antimicrobial cycling and mixing: Differences arising from an individual-based versus a population-based perspective. *Mathematical biosciences*, 294:85–91, 2017. [Cited on page 21.]

[94] Burcu Tepekule, Hildegard Uecker, Isabel Derungs, Antoine Frenoy, and Sebastian Bonhoeffer. Modeling antibiotic treatment in hospitals: A systematic approach shows benefits of combination therapy over cycling, mixing, and mono-drug therapies. *PLoS computational biology*, 13(9):e1005745, 2017. [Cited on page 21.]

[95] DJ Austin and RM Anderson. Studies of antibiotic resistance within the patient, hospitals and the community using simple mathematical models. *Philosophical Transactions of the Royal Society of London. Series B: Biological Sciences*, 354(1384):721–738, 1999. [Cited on pages 21 and 30.]

[96] Nicholas G Davies, Stefan Flasche, Mark Jit, and Katherine E Atkins. Within-host dynamics shape antibiotic resistance in commensal bacteria. *Nature ecology & evolution*, 3(3):440, 2019. [Cited on pages 21, 22, 23, and 30.]

[97] Pratik R Bhagunde, Michael Nikolaou, and Vincent H Tam. Modeling heterogeneous bacterial populations exposed to antibiotics: The logistic-dynamics case. *AIChE Journal*, 61(8):2385–2393, 2015. [Cited on page 21.]

[98] Eugene A Yurtsev, Hui Xiao Chao, Manoshi S Datta, Tatiana Artemova, and Jeff Gore. Bacterial cheating drives the population dynamics of cooperative antibiotic resistance plasmids. *Molecular systems biology*, 9(1):683, 2013. [Cited on pages 21 and 30.]

[99] Andreas Handel, Elisa Margolis, and Bruce R Levin. Exploring the role of the immune response in preventing antibiotic resistance. *Journal of theoretical biology*, 256(4):655–662, 2009. [Cited on pages 21, 23, 26, and 30.]

[100] Erida Gjini and Patricia H Brito. Integrating antimicrobial therapy with host immunity to fight drug-resistant infections: classical vs. adaptive treatment. *PLoS computational biology*, 12(4):e1004857, 2016. [Cited on pages 21, 23, 24, 25, and 30.]

[101] Peter Ankomah and Bruce R Levin. Exploring the collaboration between antibiotics and the immune response in the treatment of acute, self-limiting infections. *Proceedings of the National Academy of Sciences*, 111(23):8331–8338, 2014. [Cited on pages 21, 23, and 30.]

[102] Troy Day and Andrew F Read. Does high-dose antimicrobial chemotherapy prevent the evolution of resistance? *PLoS computational biology*, 12(1):e1004689, 2016. [Cited on pages 21 and 30.]

[103] Patricia Geli, Ramanan Laxminarayan, Michael Dunne, and David L Smith. "one-size-fits-all"? optimizing treatment duration for bacterial infections. *PloS one*, 7(1):e29838, 2012. [Cited on pages 21, 25, 26, and 30.]

[104] Iona K Paterson, Andy Hoyle, Gabriela Ochoa, Craig Baker-Austin, and Nick GH Taylor. Optimising antibiotic usage to treat bacterial infections. *Scientific reports*, 6: 37853, 2016. [Cited on pages 21 and 26.]

[105] Caroline Colijn and Ted Cohen. How competition governs whether moderate or aggressive treatment minimizes antibiotic resistance. *Elife*, 4:e10559, 2015. [Cited on page 22.]

[106] Caroline Colijn, Ted Cohen, Christophe Fraser, William Hanage, Edward Goldstein, Noga Givon-Lavi, Ron Dagan, and Marc Lipsitch. What is the mechanism for persistent coexistence of drug-susceptible and drug-resistant strains of streptococcus pneumoniae? *Journal of The Royal Society Interface*, 7(47):905–919, 2010. [Cited on page 22.]

[107] Isabel Frost, William PJ Smith, Sara Mitri, Alvaro San Millan, Yohan Davit, James M Osborne, Joe M Pitt-Francis, R Craig MacLean, and Kevin R Foster. Cooperation, competition and antibiotic resistance in bacterial colonies. *The ISME journal*, 12(6): 1582–1593, 2018. [Cited on page 22.]

[108] Sylvie Estrela and Sam P Brown. Community interactions and spatial structure shape selection on antibiotic resistant lineages. *PLoS computational biology*, 14(6), 2018. [Cited on page 22.]

[109] Nina Wale, Derek G Sim, Matthew J Jones, Rahel Salathe, Troy Day, and Andrew F Read. Resource limitation prevents the emergence of drug resistance by intensifying within-host competition. *Proceedings of the National Academy of Sciences*, 114(52): 13774–13779, 2017. [Cited on page 22.]

[110] Alan M Garber. Antibiotic exposure and resistance in mixed bacterial populations. *Theoretical population biology*, 32(3):326–346, 1987. [Cited on pages 22 and 30.]

[111] François Blanquart. Evolutionary epidemiology models to predict the dynamics of antibiotic resistance. *Evolutionary Applications*, 12(3):365–383, 2019. [Cited on pages 23, 45, and 74.]

[112] Justino Alavez-Ramirez, J Rogelio Avendano Castellanos, Lourdes Esteva, José Antonio Flores, José Luis Fuentes-Allen, Gisela García-Ramos, Guillermo Gómez, and Jesús López-Estrada. Within-host population dynamics of antibiotic-resistant m. tuberculosis. *Mathematical Medicine and Biology*, 24(1):35–56, 2007. [Cited on pages 25 and 30.]

[113] Roland R Regoes, Camilla Wiuff, Renata M Zappala, Kim N Garner, Fernando Baquero, and Bruce R Levin. Pharmacodynamic functions: a multiparameter approach to the design of antibiotic treatment regimens. *Antimicrobial agents and chemotherapy*, 48(10):3670–3676, 2004. [Cited on pages 25, 27, 28, and 30.]

[114] Klas I Udekwu and Howard Weiss. Pharmacodynamic considerations of collateral sensitivity in design of antibiotic treatment regimen. *Drug design, development and therapy*, 12:2249, 2018. [Cited on pages 25, 28, 30, and 44.]

[115] Femke de Velde, Johan W Mouton, Brenda CM de Winter, Teun van Gelder, and Birgit CP Koch. Clinical applications of population pharmacokinetic models of antibiotics: Challenges and perspectives. *Pharmacological research*, 2018. [Cited on page 25.]

[116] Joseph L Kuti. Optimizing antimicrobial pharmacodynamics: a guide for your stewardship program. *Revista Médica Clínica Las Condes*, 27(5):615–624, 2016. [Cited on page 25.]

[117] Tan N Doan, Pengxing Cao, Theophilus I Emeto, James M McCaw, and Emma S McBryde. Predicting the outcomes of new short-course regimens for multidrug-resistant tuberculosis using intrahost and pharmacokinetic-pharmacodynamic modeling. *Antimicrobial agents and chemotherapy*, 62(12):e01487–18, 2018. [Cited on page 25.]

[118] Miao Zhao, Alexander J Lepak, and David R Andes. Animal models in the pharmacokinetic/pharmacodynamic evaluation of antimicrobial agents. *Bioorganic & medicinal chemistry*, 24(24):6390–6400, 2016. [Cited on page 25.]

[119] Eduardo Asín-Prieto, Alicia Rodríguez-Gascón, and Arantxazu Isla. Applications of the pharmacokinetic/pharmacodynamic (pk/pd) analysis of antimicrobial agents. *Journal of Infection and Chemotherapy*, 21(5):319–329, 2015. [Cited on page 25.]

[120] Anne E Clatworthy, Emily Pierson, and Deborah T Hung. Targeting virulence: a new paradigm for antimicrobial therapy. *Nature chemical biology*, 3(9):541, 2007. [Cited on page 28.]

[121] Thu Thuy Nguyen, Jeremie Guedj, Elisabeth Chachaty, Jean de Gunzburg, Antoine Andremont, and France Mentré. Mathematical modeling of bacterial kinetics to predict the impact of antibiotic colonic exposure and treatment duration on the amount of resistant enterobacteria excreted. *PLoS computational biology*, 10(9):e1003840, 2014. [Cited on page 30.]

[122] Eduardo Ibargüen-Mondragón, Saulo Mosquera, Miller Cerón, Edith Mariela Burbano-Rosero, Sandra P Hidalgo-Bonilla, Lourdes Esteva, and Jhoana P Romero-Leitón. Mathematical modeling on bacterial resistance to multiple antibiotics caused by spontaneous mutations. *Biosystems*, 117:60–67, 2014. [Cited on page 30.]

[123] Bahatdin Daşbaşı and İlhan Öztürk. Mathematical modelling of bacterial resistance to multiple antibiotics and immune system response. *SpringerPlus*, 5(1):408, 2016. [Cited on page 30.]

[124] Hui-Xing Song, Yuan-Ying Peng, and Zhi-Fu Zhu. Competition between plasmid-bearing and plasmid-free organisms in the host: population dynamics and antibiotic resistance. *Medical Principles and Practice*, 15(6):436–442, 2006. [Cited on page 30.]

[125] Lawrence S Schulman. Bacterial resistance to antibodies: a model evolutionary study. *Journal of theoretical biology*, 417:61–67, 2017. [Cited on page 30.]

[126] Michael Nikolaou and Vincent H Tam. A new modeling approach to the effect of antimicrobial agents on heterogeneous microbial populations. *Journal of mathematical biology*, 52(2):154–182, 2006. [Cited on page 30.]

[127] Neeraj Suthar, Sandip Roy, Douglas R Call, Thomas E Besser, and Margaret A Davis. An individual-based model of transmission of resistant bacteria in a veterinary teaching hospital. *PloS one*, 9(6):e98589, 2014. [Cited on page 30.]

[128] Jeffrey J Campion, Patrick J McNamara, and Martin E Evans. Pharmacodynamic modeling of ciprofloxacin resistance in staphylococcus aureus. *Antimicrobial agents and chemotherapy*, 49(1):209–219, 2005. [Cited on page 30.]

[129] Patrick Forterre. Defining life: the virus viewpoint. *Origins of Life and Evolution of Biospheres*, 40(2):151–160, 2010. [Cited on page 30.]

[130] Claudiu I Baˆndea. A new theory on the origin and the nature of viruses. *Journal of Theoretical Biology*, 105(4):591–602, 1983. [Cited on page 30.]

[131] Carlos Enrique Catalano. Viral genome packaging machines. *Viral genome packaging machines: Genetics, structure, and mechanism*, pages 1–4, 2005. [Cited on page 30.]

[132] Gertrude B Elion, Phillip A Furman, James A Fyfe, Paulo De Miranda, Lilia Beauchamp, and Howard J Schaeffer. Selectivity of action of an antiherpetic agent, 9-(2-hydroxyethoxymethyl) guanine. *Proceedings of the National Academy of Sciences*, 74(12):5716–5720, 1977. [Cited on page 30.]

[133] Naveen Kumar, Shalini Sharma, Ram Kumar, Bhupendra N Tripathi, Sanjay Barua, Hinh Ly, and Barry T Rouse. Host-directed antiviral therapy. *Clinical microbiology reviews*, 33(3):e00168–19, 2020. [Cited on page 31.]

[134] Guido Antonelli and Ombretta Turriziani. Antiviral therapy: old and current issues. *International journal of antimicrobial agents*, 40(2):95–102, 2012. [Cited on page 31.]

[135] Robert L Gottlieb, Carlos E Vaca, Roger Paredes, Jorge Mera, Brandon J Webb, Gilberto Perez, Godson Oguchi, Pablo Ryan, Bibi U Nielsen, Michael Brown, et al. Early remdesivir to prevent progression to severe covid-19 in outpatients. *New England Journal of Medicine*, 386(4):305–315, 2022. [Cited on page 31.]

[136] Douglas D Richman. Antiviral drug resistance. *Antiviral research*, 71(2-3):117–121, 2006. [Cited on page 32.]

[137] EC Herrmann Jr and JA Herrmann. A working hypothesis—virus resistance development as an indicator of specific antiviral activity. *Annals of the New York Academy of Sciences*, 284(1):632–637, 1977. [Cited on page 32.]

[138] Kristen K Irwin, Nicholas Renzette, Timothy F Kowalik, and Jeffrey D Jensen. Antiviral drug resistance as an adaptive process. *Virus evolution*, 2(1), 2016. [Cited on page 32.]

[139] Rui Wang, Jiahui Chen, and Guo-Wei Wei. Mechanisms of sars-cov-2 evolution revealing vaccine-resistant mutations in europe and america. *The journal of physical chemistry letters*, 12(49):11850–11857, 2021. [Cited on pages 32 and 33.]

[140] Florian Krammer. SARS-CoV-2 vaccines in development. *Nature*, 586(7830):516–527, 2020. ISSN 14764687. doi: 10.1038/s41586-020-2798-3. [Cited on pages 32 and 80.]

[141] World Health Organisation. Coronavirus disease (covid-19): Vaccines, 2020. Accessed: 2020-12-12. [Cited on page 32.]

[142] Nature Reviews Drug Discovery. Covid-19 vaccines buoy hope, 2020. Accessed: 2020-12-12. [Cited on pages 32 and 39.]

[143] Nikolaos I Stilianakis, Alan S Perelson, and Frederick G Hayden. Emergence of drug resistance during an influenza epidemic: insights from a mathematical model. *Journal of Infectious Diseases*, 177(4):863–873, 1998. [Cited on pages 33 and 35.]

[144] Sally Blower and Paul Volberding. What can modeling tell us about the threat of antiviral drug resistance? *Current Opinion in Infectious Diseases*, 15(6):609–614, 2002. [Cited on page 33.]

[145] Sally M Blower, Hayley B Gershengorn, and RM Grant. A tale of two futures: Hiv and antiretroviral therapy in san francisco. *Science*, 287(5453):650–654, 2000. [Cited on pages 33 and 34.]

[146] Sally M Blower, AN Aschenbach, HB Gershengorn, and JO Kahn. Predicting the unpredictable: transmission of drug-resistant hiv. *Nature medicine*, 7(9):1016–1020, 2001. [Cited on page 33.]

[147] World Health Organization et al. Coronavirus disease 2019 (covid-19): situation report, 73. 2020. [Cited on pages 37 and 38.]

[148] Domenico Cucinotta and Maurizio Vanelli. Who declares covid-19 a pandemic. *Acta Bio Medica: Atenei Parmensis*, 91(1):157, 2020. [Cited on page 37.]

[149] Stanley Perlman. Another decade, another coronavirus, 2020. [Cited on pages 37 and 38.]

[150] Peng Zhou, Xing-Lou Yang, Xian-Guang Wang, Ben Hu, Lei Zhang, Wei Zhang, Hao-Rui Si, Yan Zhu, Bei Li, Chao-Lin Huang, et al. Discovery of a novel coronavirus associated with the recent pneumonia outbreak in humans and its potential bat origin. *BioRxiv*, 2020. [Cited on pages 37 and 38.]

[151] Na Zhu, Dingyu Zhang, Wenling Wang, Xingwang Li, Bo Yang, Jingdong Song, Xiang Zhao, Baoying Huang, Weifeng Shi, Roujian Lu, et al. A novel coronavirus from patients with pneumonia in china, 2019. *New England journal of medicine*, 2020. [Cited on page 38.]

[152] Tanu Singhal. A review of coronavirus disease-2019 (covid-19). *The indian journal of pediatrics*, 87(4):281–286, 2020. [Cited on page 38.]

[153] Thirumalaisamy P Velavan and Christian G Meyer. The covid-19 epidemic. *Tropical medicine & international health*, 25(3):278, 2020. [Cited on pages 38 and 39.]

[154] Ensheng Dong, Hongru Du, and Lauren Gardner. An interactive web-based dashboard to track covid-19 in real time. *The Lancet infectious diseases*, 20(5):533–534, 2020. [Cited on page 38.]

[155] Haiyan Qiu, Junhua Wu, Liang Hong, Yunling Luo, Qifa Song, and Dong Chen. Clinical and epidemiological features of 36 children with coronavirus disease 2019 (covid-19) in zhejiang, china: an observational cohort study. *The Lancet infectious diseases*, 20(6): 689–696, 2020. [Cited on page 38.]

[156] Xiaoxia Lu, Liqiong Zhang, Hui Du, Jingjing Zhang, Yuan Y Li, Jingyu Qu, Wenxin Zhang, Youjie Wang, Shuangshuang Bao, Ying Li, et al. Sars-cov-2 infection in children. *New England Journal of Medicine*, 382(17):1663–1665, 2020. [Cited on page 38.]

[157] Yuanyuan Dong, Xi Mo, Yabin Hu, Xin Qi, Fan Jiang, Zhongyi Jiang, and Shilu Tong. Epidemiology of covid-19 among children in china. *Pediatrics*, 145(6), 2020. [Cited on page 38.]

[158] Chaolin Huang, Yeming Wang, Xingwang Li, Lili Ren, Jianping Zhao, Yi Hu, Li Zhang, Guohui Fan, Jiuyang Xu, Xiaoying Gu, et al. Clinical features of patients infected with 2019 novel coronavirus in wuhan, china. *The lancet*, 395(10223):497–506, 2020. [Cited on pages 38 and 39.]

[159] Heshui Shi, Xiaoyu Han, Nanchuan Jiang, Yukun Cao, Osamah Alwalid, Jin Gu, Yanqing Fan, and Chuansheng Zheng. Radiological findings from 81 patients with covid-19 pneumonia in wuhan, china: a descriptive study. *The Lancet infectious diseases*, 20(4): 425–434, 2020. [Cited on page 38.]

[160] Fei Zhou, Ting Yu, Ronghui Du, Guohui Fan, Ying Liu, Zhibo Liu, Jie Xiang, Yeming Wang, Bin Song, Xiaoying Gu, et al. Clinical course and risk factors for mortality of adult inpatients with covid-19 in wuhan, china: a retrospective cohort study. *The lancet*, 395(10229):1054–1062, 2020. [Cited on page 38.]

[161] Dawei Wang, Bo Hu, Chang Hu, Fangfang Zhu, Xing Liu, Jing Zhang, Binbin Wang, Hui Xiang, Zhenshun Cheng, Yong Xiong, et al. Clinical characteristics of 138 hospitalized patients with 2019 novel coronavirus-infected pneumonia in wuhan, china. *Jama*, 323(11):1061–1069, 2020. [Cited on page 38.]

[162] Nanshan Chen, Min Zhou, Xuan Dong, Jieming Qu, Fengyun Gong, Yang Han, Yang Qiu, Jingli Wang, Ying Liu, Yuan Wei, et al. Epidemiological and clinical characteristics of 99 cases of 2019 novel coronavirus pneumonia in wuhan, china: a descriptive study. *The lancet*, 395(10223):507–513, 2020. [Cited on page 38.]

[163] Ian F Miller, Alexander D Becker, Bryan T Grenfell, and C Jessica E Metcalf. Disease and healthcare burden of covid-19 in the united states. *Nature Medicine*, pages 1–6, 2020. [Cited on pages 39 and 78.]

[164] Oxford University. Oxford university breakthrough on global covid-19 vaccine, 2020. Accessed: 2020-12-10. [Cited on page 39.]

[165] Pfizer Inc. Pfizer and biontech announce vaccine candidate against covid-19 achieved success in first interim analysis from phase 3 study, 2020. Accessed: 2020-12-10. [Cited on page 39.]

[166] Moderna. Moderna's covid-19 vaccine candidate meets its primary efficacy endpoint in the first interim analysis of the phase 3 cove study, 2020. Accessed: 2020-12-10. [Cited on page 39.]

[167] United States Food and Drug Authority. Emergency use authorization, 2020. Accessed: 2020-12-10. [Cited on page 39.]

[168] Hayley K Charlton Hume and Linda HL Lua. Platform technologies for modern vaccine manufacturing. *Vaccine*, 35(35):4480–4485, 2017. [Cited on page 39.]

[169] Norman TJ Bailey et al. *The mathematical theory of infectious diseases and its applications*. Charles Griffin & Company Ltd, 5a Crendon Street, High Wycombe, Bucks HP13 6LE., 1975. [Cited on pages 39 and 78.]

[170] William Ogilvy Kermack and Anderson G McKendrick. A contribution to the mathematical theory of epidemics. *Proceedings of the royal society of london. Series A, Containing papers of a mathematical and physical character*, 115(772):700–721, 1927. [Cited on pages 39, 77, and 78.]

[171] Roy M Anderson, Hans Heesterbeek, Don Klinkenberg, and T Déirdre Hollingsworth. How will country-based mitigation measures influence the course of the COVID-19 epidemic? *The Lancet*, mar 2020. ISSN 0140-6736. doi: 10.1016/S0140-6736(20)30567-5. [Cited on pages 39 and 78.]

[172] Joshua S Weitz, Stephen J Beckett, Ashley R Coenen, David Demory, Marian Dominguez-mirazo, Jonathan Dushoff, Chung-yin Leung, Guanlin Li, Andreea Măgălie, Sang Woo Park, Rogelio Rodriguez-gonzalez, Shashwat Shivam, and Conan Y Zhao. Modeling shield immunity to reduce COVID-19 epidemic spread. *Nature Medicine*, 2020. doi: 10.1038/s41591-020-0895-3. [Cited on pages 39 and 78.]

[173] Reza Sameni. Mathematical modeling of epidemic diseases; a case study of the covid-19 coronavirus. *arXiv preprint arXiv:2003.11371*, 2020. [Cited on pages 39 and 78.]

[174] Ashutosh Simha, R Venkatesha Prasad, and Sujay Narayana. A simple stochastic sir model for covid 19 infection dynamics for karnataka: Learning from europe. *arXiv preprint arXiv:2003.11920*, 2020. [Cited on pages 39 and 78.]

[175] Giuseppe C Calafiore, Carlo Novara, and Corrado Possieri. A modified sirr model for the covid-19 contagion in italy. *arXiv preprint arXiv:2003.14391*, 2020. [Cited on pages 39 and 78.]

[176] Kaustuv Chatterjee, Kaushik Chatterjee, Arun Kumar, and Subramanian Shankar. Healthcare impact of covid-19 epidemic in india: A stochastic mathematical model. *Medical Journal Armed Forces India*, 2020. [Cited on pages 39 and 78.]

[177] Liangrong Peng, Wuyue Yang, Dongyan Zhang, Changjing Zhuge, and Liu Hong. Epidemic analysis of COVID-19 in China by dynamical modeling. *arXiv*, feb 2020. [Cited on pages 39 and 78.]

[178] Adam J Kucharski, Timothy W Russell, Charlie Diamond, Yang Liu, John Edmunds, Sebastian Funk, Rosalind M Eggo, Fiona Sun, Mark Jit, James D Munday, et al. Early dynamics of transmission and control of covid-19: a mathematical modelling study. *The lancet infectious diseases*, 2020. [Cited on pages 39, 40, and 78.]

[179] Cristy Leonor Ricardo-Azanza and Esteban Abelardo Vargas-Hernandez. The Risk of Lifting COVID-19 Confinement in Mexico. *medRxiv*, page 2020.05.28.20115063, jun 2020. doi: 10.1101/2020.05.28.20115063. [Cited on pages 39, 40, and 78.]

[180] Duccio Fanelli and Francesco Piazza. Analysis and forecast of covid-19 spreading in china, italy and france. *Chaos, Solitons & Fractals*, 134:109761, 2020. [Cited on pages 40 and 78.]

[181] Rajesh Singh and R Adhikari. Age-structured impact of social distancing on the covid-19 epidemic in india. *arXiv preprint arXiv:2003.12055*, 2020. [Cited on pages 40 and 78.]

[182] Gustavo Hernandez-Mejia and Esteban A. Hernandez-Vargas. When is sars-cov-2 in your shopping list? *Mathematical Biosciences*, 328:108434, 2020. ISSN 0025-5564. doi: https://doi.org/10.1016/j.mbs.2020.108434. [Cited on pages 40 and 78.]

[183] Alex Arenas, Wesley Cota, Jesús Gómez-Gardenes, Sergio Gómez, Clara Granell, Joan T Matamalas, David Soriano-Panos, and Benjamin Steinegger. A mathematical model for the spatiotemporal epidemic spreading of covid19. *medRxiv*, 2020. [Cited on pages 40 and 78.]

[184] Qianying Lin, Shi Zhao, Daozhou Gao, Yijun Lou, Shu Yang, Salihu S Musa, Maggie H Wang, Yongli Cai, Weiming Wang, Lin Yang, et al. A conceptual model for the outbreak of coronavirus disease 2019 (covid-19) in wuhan, china with individual reaction and governmental action. *International journal of infectious diseases*, 2020. [Cited on pages 40 and 78.]

[185] Esteban A Hernandez-Vargas and Jorge X Velasco-Hernandez. In-host mathematical modelling of covid-19 in humans. *Annual reviews in control*, 2020. [Cited on pages 40 and 41.]

[186] Alexis Erich S. Almocera, Griselda Quiroz, and Esteban A. Hernandez-Vargas. Stability analysis in covid-19 within-host model with immune response. *Communications in Nonlinear Science and Numerical Simulation*, page 105584, 2020. ISSN 1007-5704. doi: https://doi.org/10.1016/j.cnsns.2020.105584. [Cited on page 40.]

[187] Josh A Firth, Joel Hellewell, Petra Klepac, Stephen Kissler, Adam J Kucharski, and Lewis G Spurgin. Using a real-world network to model localized covid-19 control strategies. *Nature medicine*, 26(10):1616–1622, 2020. [Cited on pages 40 and 78.]

[188] Ziga Zaplotnik, Aleksandar Gavric, and Luka Medic. Simulation of the covid-19 pandemic on the social network of slovenia: estimating the intrinsic forecast uncertainty. *arXiv preprint arXiv:2005.13282*, 2020. [Cited on pages 40 and 78.]

[189] Helena A Herrmann and Jean-Marc Schwartz. Why covid-19 models should incorporate the network of social interactions. *Physical Biology*, 17(6):065008, 2020. [Cited on pages 40 and 78.]

[190] Takaaki Horinouchi, Shingo Suzuki, Takashi Hirasawa, Naoaki Ono, Tetsuya Yomo, Hiroshi Shimizu, and Chikara Furusawa. Phenotypic convergence in bacterial adaptive evolution to ethanol stress. *BMC evolutionary biology*, 15(1):1–14, 2015. [Cited on page 43.]

[191] AJ Coldman and JH Goldie. A stochastic model for the origin and treatment of tumors containing drug-resistant cells. *Bulletin of mathematical biology*, 48(3-4):279–292, 1986. [Cited on pages 43 and 45.]

[192] Nara Yoon, Nikhil Krishnan, and Jacob Scott. Modeling of collaterally sensitive drug cycles, and optimization of the drug effect in the spirit of adaptive therapy. *bioRxiv*, 2020. [Cited on pages 43 and 44.]

[193] Daniel Nichol, Joseph Rutter, Christopher Bryant, Andrea M Hujer, Sai Lek, Mark D Adams, Peter Jeavons, Alexander RA Anderson, Robert A Bonomo, and Jacob G Scott. Antibiotic collateral sensitivity is contingent on the repeatability of evolution. *Nature communications*, 10(1):334, 2019. [Cited on pages 44 and 75.]

[194] Viktória Lázár, Gajinder Pal Singh, Réka Spohn, István Nagy, Balázs Horváth, Mónika Hrtyan, Róbert Busa-Fekete, Balázs Bogos, Orsolya Méhi, Bálint Csörgő, et al. Bacterial evolution of antibiotic hypersensitivity. *Molecular systems biology*, 9(1):700, 2013. [Cited on page 44.]

[195] Esteban A. Hernandez-Vargas, Alma Y. Alanis, and Josephine Tetteh. A new view of multiscale stochastic impulsive systems for modeling and control of epidemics. *Annual Reviews in Control*, 48:242–249, jan 2019. ISSN 13675788. doi: 10.1016/j.arcontrol.2019.06.002. [Cited on page 44.]

[196] Leonardo López and Xavier Rodó. The end of social confinement and COVID-19 re-emergence risk. *Nature Human Behaviour*, 4(7):746–755, 2020. ISSN 23973374. doi: 10.1038/s41562-020-0908-8. [Cited on page 44.]

[197] Josephine N.A. Tetteh, Van Kinh Nguyen, and Esteban A. Hernandez-Vargas. Network models to evaluate vaccine strategies towards herd immunity in covid-19. *Journal of Theoretical Biology*, 531:1–13, 9 2021. ISSN 0022-5193. doi: 10.1016/J.JTBI.2021.110894. [Cited on page 44.]

[198] Roy M. Anderson. *Population Dynamics of Infectious Diseases: Theory and Applications*, volume 53. Springer, 1982. ISBN 9780412216107. doi: 10.2307/4361. [Cited on page 45.]

[199] Pablo S Rivadeneira, Juan E Sereno, Nicolas Magdelaine, and Claude H Moog. Blood glycemia reconstruction from discrete measurements using an impulsive observer. *IFAC-PapersOnLine*, 50(1):14723–14728, 2017. [Cited on page 45.]

[200] Esteban A. Hernandez-Vargas. *Modeling and Control of Infectious Diseases: with MATLAB and R*. ELSEVIER Academic Press, London, 1st editio edition, 2019. ISBN 9780128130520. [Cited on page 45.]

[201] John A. Adam and Nicola Bellomo, editors. *A Survey of Models for Tumor-Immune System Dynamics*. Number 59 in Modeling and Simulation in Science, Engineering, & Technology. Birkhäuser Boston, Boston, MA, 1997. ISBN 978-1-4612-6408-8. doi: 10.1007/978-0-8176-8119-7. [Cited on page 45.]

[202] Alfonsas Juška, Genovaite Gedminiene, and Ruta Ivanec. Growth of microbial populations: Mathematical modeling, laboratory exercises, and model-based data analysis. *Biochemistry and Molecular Biology Education*, 34(6):417–422, nov 2006. ISSN 14708175. doi: 10.1002/bmb.2006.494034062669. [Cited on page 45.]

[203] Nara Yoon, Robert Vander Velde, Andriy Marusyk, and Jacob G Scott. Optimal therapy scheduling based on a pair of collaterally sensitive drugs. *Bulletin of mathematical biology*, 80(7):1776–1809, 2018. [Cited on pages 45 and 75.]

[204] James H Goldie and Andrew J Coldman. *Drug resistance in cancer: mechanisms and models*. Cambridge University Press, 2009. [Cited on page 45.]

[205] A. Tsoularis and J. Wallace. Analysis of logistic growth models. *Mathematical Biosciences*, 179(1):21–55, jul 2002. ISSN 00255564. doi: 10.1016/S0025-5564(02)00096-2. [Cited on page 45.]

[206] Paolo Di Giamberardino and Daniela Iacoviello. Hiv infection control: a constructive algorithm for a state-based switching control. *International Journal of Control, Automation and Systems*, 16(3):1469–1473, 2018. [Cited on page 45.]

[207] Esteban Hernandez-Vargas, Patrizio Colaneri, Richard Middleton, and Franco Blanchini. Discrete-time control for switched positive systems with application to mitigating

viral escape. *International journal of robust and nonlinear control*, 21(10):1093–1111, 2011. [Cited on page 45.]

[208] Baltazar Aguirre-Hernández, Eric Campos-Cantón, Jorge Antonio López-Renteria, and EC Díaz González. A polynomial approach for generating a monoparametric family of chaotic attractors via switched linear systems. *Chaos, Solitons & Fractals*, 71:100–106, 2015. [Cited on page 45.]

[209] Baltazar Aguirre-Hernández, Francisco A Carrillo, Jesús F Espinoza, and Horacio Leyva. Global product structure for a space of special matrices. *Boletin de la Sociedad Matemática Mexicana*, 25(1):77–85, 2019. [Cited on page 45.]

[210] Edgar C Díaz-González, Jorge-Antonio López-Rentería, Eric Campos-Cantón, and Baltazar Aguirre-Hernández. Maximal unstable dissipative interval to preserve multi-scroll attractors via multi-saturated functions. *Journal of Nonlinear Science*, 26(6):1833–1850, 2016. [Cited on page 45.]

[211] Xudong Zhao, Lixian Zhang, Peng Shi, and Ming Liu. Stability of switched positive linear systems with average dwell time switching. *Automatica*, 48(6):1132–1137, 2012. [Cited on page 45.]

[212] Nael H El-Farra, Prashant Mhaskar, and Panagiotis D Christofides. Output feedback control of switched nonlinear systems using multiple lyapunov functions. *Systems & Control Letters*, 54(12):1163–1182, 2005. [Cited on page 45.]

[213] Franco Blanchini, Patrizio Colaneri, Maria Elena Valcher, et al. Switched positive linear systems. *Foundations and Trends® in Systems and Control*, 2(2):101–273, 2015. [Cited on page 45.]

[214] Esteban Hernandez-Vargas and Sorin Olaru. Switching logistic to design cycling approaches against drug resistance. *BioRxiv*, 2019. doi: https://doi.org/10.1101/2020.03.17.995928. [Cited on pages 46 and 149.]

[215] Khurum H Khan, David Cunningham, Benjamin Werner, Georgios Vlachogiannis, Inmaculada Spiteri, Timon Heide, Javier Fernandez Mateos, Alexandra Vatsiou, Andrea Lampis, Mahnaz Darvish Damavandi, et al. Longitudinal liquid biopsy and mathematical modeling of clonal evolution forecast time to treatment failure in the prospect-c phase ii colorectal cancer clinical trial. *Cancer discovery*, 8(10):1270–1285, 2018. [Cited on page 75.]

[216] Jeff Maltas and Kevin B Wood. Pervasive and diverse collateral sensitivity profiles inform optimal strategies to limit antibiotic resistance. *bioRxiv*, page 241075, 2019. [Cited on page 75.]

[217] Luca Ferretti, Michele Cortelezzi, Bin Yang, Giacomo Marmorini, and Ginestra Bianconi. Features and heterogeneities in growing network models. *Physical Review E*, 85 (6):066110, 2012. [Cited on page 78.]

[218] Lauren Ancel Meyers, Babak Pourbohloul, Mark EJ Newman, Danuta M Skowronski, and Robert C Brunham. Network theory and sars: predicting outbreak diversity. *Journal of theoretical biology*, 232(1):71–81, 2005. [Cited on pages 78 and 79.]

[219] Matt J Keeling and Ken TD Eames. Networks and epidemic models. *Journal of the Royal Society Interface*, 2(4):295–307, 2005. [Cited on page 78.]

[220] Alessandro Rizzo, Biagio Pedalino, and Maurizio Porfiri. A network model for ebola spreading. *Journal of theoretical biology*, 394:212–222, 2016. [Cited on page 78.]

[221] Wayne M Getz, Richard Salter, and Whitney Mgbara. Adequacy of seir models when epidemics have spatial structure: Ebola in sierra leone. *Philosophical Transactions of the Royal Society B*, 374(1775):20180282, 2019. [Cited on page 78.]

[222] Antoine Moinet, Romualdo Pastor-Satorras, and Alain Barrat. Effect of risk perception on epidemic spreading in temporal networks. *Physical Review E*, 97(1):012313, 2018. [Cited on page 78.]

[223] KM Ariful Kabir, Kazuki Kuga, and Jun Tanimoto. Effect of information spreading to suppress the disease contagion on the epidemic vaccination game. *Chaos, Solitons & Fractals*, 119:180–187, 2019. [Cited on page 78.]

[224] Anupama Sharma, Shakti N Menon, V Sasidevan, and Sitabhra Sinha. Epidemic prevalence information on social networks mediates emergent collective outcomes in voluntary vaccine schemes. *arXiv preprint arXiv:1709.07674*, 2017. [Cited on page 78.]

[225] Albert-László Barabási. Linked: The new science of networks, 2003. [Cited on pages 79 and 81.]

[226] Duncan J Watts and Steven H Strogatz. Collective dynamics of 'small-world'networks. *nature*, 393(6684):440–442, 1998. [Cited on page 79.]

[227] Zoltán Dezső and Albert-László Barabási. Halting viruses in scale-free networks. *Physical Review E*, 65(5):055103, 2002. [Cited on page 79.]

[228] Erik Volz. Sir dynamics in random networks with heterogeneous connectivity. *Journal of mathematical biology*, 56(3):293–310, 2008. [Cited on page 79.]

[229] Victor M Eguiluz and Konstantin Klemm. Epidemic threshold in structured scale-free networks. *Physical Review Letters*, 89(10):108701, 2002. [Cited on page 79.]

[230] Seth Flaxman, Swapnil Mishra, Axel Gandy, H Juliette T Unwin, Thomas A Mellan, Helen Coupland, Charles Whittaker, Harrison Zhu, Tresnia Berah, Jeffrey W Eaton, et al. Estimating the effects of non-pharmaceutical interventions on covid-19 in europe. *Nature*, 584(7820):257–261, 2020. [Cited on page 80.]

[231] Russell M Viner, Simon J Russell, Helen Croker, Jessica Packer, Joseph Ward, Claire Stansfield, Oliver Mytton, Chris Bonell, and Robert Booy. School closure and management practices during coronavirus outbreaks including covid-19: a rapid systematic review. *The Lancet Child & Adolescent Health*, 4(5):397–404, 2020. [Cited on page 80.]

[232] Enrico Lavezzo, Elisa Franchin, Constanze Ciavarella, Gina Cuomo-Dannenburg, Luisa Barzon, Claudia Del Vecchio, Lucia Rossi, Riccardo Manganelli, Arianna Loregian, Nicolò Navarin, et al. Suppression of a sars-cov-2 outbreak in the italian municipality of vo'. *Nature*, 584(7821):425–429, 2020. [Cited on page 80.]

[233] Susanne H Hodgson, Kushal Mansatta, Garry Mallett, Victoria Harris, Katherine RW Emary, and Andrew J Pollard. What defines an efficacious covid-19 vaccine? a review of the challenges assessing the clinical efficacy of vaccines against sars-cov-2. *The Lancet Infectious Diseases*, 2020. [Cited on page 80.]

[234] Ugo Avila-Ponce de León, Eric Avila-Vales, and Kuan-lin Huang. Modeling covid-19 dynamic using a two-strain model with vaccination. *Chaos, Solitons & Fractals*, page 111927, 2022. [Cited on page 80.]

[235] Pragya D Yadav and Sanjay Kumar. Global emergence of sars-cov-2 variants: new foresight needed for improved vaccine efficacy. *The Lancet. Infectious Diseases*, 2021. [Cited on page 80.]

[236] Roy M. Anderson, Carolin Vegvari, James Truscott, and Benjamin S. Collyer. Challenges in creating herd immunity to SARS-CoV-2 infection by mass vaccination. *The Lancet*, 396(10263):1614–1616, 2020. ISSN 1474547X. doi: 10.1016/S0140-6736(20)32318-7. [Cited on page 80.]

[237] Francois Kepes. *Biological networks*, volume 3. World Scientific, 2007. [Cited on page 81.]

[238] Rachel M Burke. Active monitoring of persons exposed to patients with confirmed covid-19—united states, january–february 2020. *MMWR. Morbidity and mortality weekly report*, 69, 2020. [Cited on page 81.]

[239] Jiaye Liu, Xuejiao Liao, Shen Qian, Jing Yuan, Fuxiang Wang, Yingxia Liu, Zhaoqin Wang, Fu-Sheng Wang, Lei Liu, and Zheng Zhang. Community transmission of severe acute respiratory syndrome coronavirus 2, shenzhen, china, 2020. *Emerging infectious diseases*, 26(6), 2020. [Cited on page 81.]

[240] Ewen Callaway and Smriti Mallapaty. Novavax covid vaccine protects people against variants. *Nature*, 590:17, 2021. [Cited on page 81.]

[241] Roy M Anderson, Hans Heesterbeek, Don Klinkenberg, and T Déirdre Hollingsworth. How will country-based mitigation measures influence the course of the covid-19 epidemic? *The lancet*, 395(10228):931–934, 2020. [Cited on page 81.]

[242] Clark D Russell, Jonathan E Millar, and J Kenneth Baillie. Clinical evidence does not support corticosteroid treatment for 2019-ncov lung injury. *The Lancet*, 395(10223): 473–475, 2020. [Cited on page 81.]

[243] Stephen M Kissler, Christine Tedijanto, Edward Goldstein, Yonatan H Grad, and Marc Lipsitch. Projecting the transmission dynamics of sars-cov-2 through the postpandemic period. *Science*, 368(6493):860–868, 2020. [Cited on page 111.]

[244] Saad B Omer, Daniel A Salmon, Walter A Orenstein, M Patricia Dehart, and Neal Halsey. Vaccine refusal, mandatory immunization, and the risks of vaccine-preventable diseases. *New England Journal of Medicine*, 360(19):1981–1988, 2009. [Cited on page 111.]

[245] Varun K Phadke, Robert A Bednarczyk, Daniel A Salmon, and Saad B Omer. Association between vaccine refusal and vaccine-preventable diseases in the united states: a review of measles and pertussis. *Jama*, 315(11):1149–1158, 2016. [Cited on page 111.]

[246] Heidi J Larson, Caitlin Jarrett, Elisabeth Eckersberger, David MD Smith, and Pauline Paterson. Understanding vaccine hesitancy around vaccines and vaccination from a global perspective: a systematic review of published literature, 2007–2012. *Vaccine*, 32 (19):2150–2159, 2014. [Cited on page 111.]

[247] Louis Z Cooper, Heidi J Larson, and Samuel L Katz. Protecting public trust in immunization. *Pediatrics*, 122(1):149–153, 2008. [Cited on page 111.]

[248] Alexandre de Figueiredo, Clarissa Simas, Emilie Karafillakis, Pauline Paterson, and Heidi J Larson. Mapping global trends in vaccine confidence and investigating barriers to vaccine uptake: a large-scale retrospective temporal modelling study. *The Lancet*, 396(10255):898–908, 2020. [Cited on page 111.]

List of Publications

1. Tetteh, J. N., & Hernandez-Vargas, E. A. (2021). Network models to evaluate vaccine strategies towards herd immunity in COVID-19. Journal of Theoretical Biology, 531, 110894.

2. Tetteh, J. N., Matthäus, F., & Hernandez-Vargas, E. A. (2020). A survey of within-host and between-hosts modelling for antibiotic resistance. Biosystems, 196, 104182.

3. Tetteh, J. N., Olaru, S., Parra-Rojas, C., & Hernandez-Vargas, E. A. (2020). Lyapunov-based Switching to Mitigate Antimicrobial Resistance. IFAC-PapersOnLine, 53(2), 16049-16054.

4. Hernandez-Vargas, E. A., Alanis, A. Y., & Tetteh, J. (2019). A new view of multiscale stochastic impulsive systems for modeling and control of epidemics. Annual Reviews in Control, 48, 242-249.